

This electronic thesis or dissertation has been downloaded from the King's Research Portal at <https://kclpure.kcl.ac.uk/portal/>



An optical proteomic profile of the HER2 family in breast tumours and the effect of exposure to tyrosine kinase inhibitors

Patel, Gargi

Awarding institution:
King's College London

The copyright of this thesis rests with the author and no quotation from it or information derived from it may be published without proper acknowledgement.

END USER LICENCE AGREEMENT



Unless another licence is stated on the immediately following page this work is licensed

under a Creative Commons Attribution-NonCommercial-NoDerivatives 4.0 International

licence. <https://creativecommons.org/licenses/by-nc-nd/4.0/>

You are free to copy, distribute and transmit the work

Under the following conditions:

- Attribution: You must attribute the work in the manner specified by the author (but not in any way that suggests that they endorse you or your use of the work).
- Non Commercial: You may not use this work for commercial purposes.
- No Derivative Works - You may not alter, transform, or build upon this work.

Any of these conditions can be waived if you receive permission from the author. Your fair dealings and other rights are in no way affected by the above.

Take down policy

If you believe that this document breaches copyright please contact librarypure@kcl.ac.uk providing details, and we will remove access to the work immediately and investigate your claim.

This electronic theses or dissertation has been downloaded from the King's Research Portal at <https://kclpure.kcl.ac.uk/portal/>

Title:An optical proteomic profile of the HER2 family in breast tumours and the effect of exposure to tyrosine kinase inhibitors

Author:Gargi Patel

The copyright of this thesis rests with the author and no quotation from it or information derived from it may be published without proper acknowledgement.

END USER LICENSE AGREEMENT



This work is licensed under a Creative Commons Attribution-NonCommercial-NoDerivs 3.0 Unported License. <http://creativecommons.org/licenses/by-nc-nd/3.0/>

You are free to:

- Share: to copy, distribute and transmit the work

Under the following conditions:

- Attribution: You must attribute the work in the manner specified by the author (but not in any way that suggests that they endorse you or your use of the work).
- Non Commercial: You may not use this work for commercial purposes.
- No Derivative Works - You may not alter, transform, or build upon this work.

Any of these conditions can be waived if you receive permission from the author. Your fair dealings and other rights are in no way affected by the above.

Take down policy

If you believe that this document breaches copyright please contact librarypure@kcl.ac.uk providing details, and we will remove access to the work immediately and investigate your claim.

*An optical proteomic profile of the
HER2 family in breast tumours and
the effect of exposure to tyrosine
kinase inhibitors*

*A thesis submitted to the Kings College London for the
degree of Doctor of Philosophy*

By

Gargi Patel

The Richard Dimbleby Laboratory

*Division of Cancer Studies and the Randall Division of
Cell and Molecular Biophysics*

Kings College London

2012

*This thesis is dedicated to Surendra, Bharti, Heena, Abhi,
Helen and Dawn for their unfailing support, patience,
telephone calls and provisions of sustenance,
and to Toby for being the light to my shadow.*

Acknowledgements

This project received generous funding from Cancer Research UK and the NIHR Biomedical Research Centre (BRC) at Kings College London.

I wish to thank my supervisors, Professors Tony Ng and Paul Ellis, and Dr Cheryl Gillett without whom this work would not have existed. I especially wish to thank Professor Tony Ng for his inspiration, perseverance, support and never ending optimism. He has truly introduced me to the world of academic medicine and has helped me understand clinical disease in an entirely new context. Thanks to Cheryl for my histopathological training and for encouraging me to persist through all my failed antibody experiments. I also wish to thank Professor Ellis for maintaining a clinical slant to this work, for all his help in commencing the set up for our clinical study and in obtaining valuable patient samples for the eventual validation of our biomarker assay. These individuals have helped shaped the work described herein and more importantly, inspired me for the future.

I also wish to thank my collaborators, Dr Franca Fraternali and Dr Flavia Autore, who helped me greatly with the structural chemistry, and Professor Peter Parker, Dr Angus Cameron and Mr. Jeroen Claus, who contributed greatly to the preparation of my work for publication. Within the group I have benefited from advice from many individuals from many different disciplines. I would like to thank Dr Simon Ameer-beg and Dr Dan Matthews for introducing me to the technical side of FRET/FLIM work and for their patience throughout. Thanks also, to Dr Paul Barber who has unassumingly supported me through all the analytical and practical mishaps. I am grateful for Professor Ton Coolen and Dr Katherine Lawler for all their wealth of knowledge of statistics and bio-informatics, of which I could only skim the surface. Last but definitely not least, I would like to thank all the members of Tony's lab both past and present who have helped me indefinitely with my work here and beyond in too many ways to recount: Dr Melanie Keppler, Dr Tai Kiuchi, Dr Gilbert Fruhwirth, Mr. Adrian Brock, Dr Gregory Weitsman, Dr Elena Ortiz-Zapater, Dr James Monypeny, and Mr. Anthony Khong. Thanks to Dr Muireann Kelleher and Mr. Enyi Ofo who paved the way for me in this lab and who have completed excellent pieces of research, and thanks to Dr Sheeba Irshad for her enthusiasm and moral support.

A special thanks to Toby Radcliffe for his lay reading of this thesis and for his never-ending optimism and support throughout.

Abstract

My hypothesis is that delineation of the effects of HER2-targeted therapy with the tyrosine kinase inhibitor (TKI) lapatinib, *in vitro*, and elucidation of the ensuing conformational changes may help understand the molecular activity of lapatinib and elucidate mechanisms of resistance. Clinical translation of this knowledge may help to improve performance of current biopsy-derived biomarkers, bringing real patient benefits.

HER2-targeted treatments such as the monoclonal antibody, trastuzumab and the tyrosine kinase inhibitor (TKI) lapatinib, were developed for HER2-positive breast cancer patients; a group with a poor prognosis. However trastuzumab induces response in only 40% of patients and resistance inevitably develops to both drugs. HER2:HER3 dimerisation is vital to the translation of extracellular signals, via intracellular signaling cascades, to promote cancer cell proliferation, invasion and metastasis, and is studied herein. Regulation of the amplitude and kinetics of signal transduction from the HER family is reliant upon receptor endocytosis, and sorting to recycling or degradation. As these processes are likely to play a key role in treatment of HER2-positive breast cancer and the development of resistance, they are investigated in this project.

Within the context of this work, optical proteomics quantifies post-translational modifications and protein-protein interactions by measuring Förster resonance energy transfer (FRET). Where fluorophores are located within nanometer proximity, FRET occurs, thus allowing quantification of protein-protein interactions. This novel technology is used alongside traditional biochemical methods, to demonstrate HER2/3 dimerisation, and the effect of perturbation of this system by lapatinib.

Treatment with lapatinib abolishes HER2 phosphorylation but stabilises the HER2:HER3 dimer. Mutation at the HER2:HER3 intracellular interface prevents HER2:HER3 dimerisation and negates the lapatinib effect. Resistance may be mediated by endocytosis of the HER2:HER3 dimer, recycling and rephosphorylation of HER3.

Fluorophore-conjugated antibodies have been optimised in cell lines, with the development of dual antibody assays to measure HER2:HER3 dimerisation in paraffin embedded tumour tissue. A prospective clinical trial is being set up in order to validate these assays alongside clinico-pathological and genetic biomarkers for prediction of response to HER2-targeted therapy.

Table of contents

Acknowledgements	3
Abstract	4
Table of contents	5
List of Figures	10
List of Tables	14
List of abbreviations	15
Chapter 1: Introduction	19
1.1 Breast cancer	20
1.1.1 Adjuvant therapy	21
1.1.1.1 Adjuvant hormone treatment.....	21
1.1.1.2 Adjuvant chemotherapy	22
1.1.1.3 Adjuvant and neoadjuvant targeted treatment	23
1.2 Estimation of Prognosis.....	25
1.2.1 Clinicopathological factors	25
1.2.2 Genomic biomarkers; prognostic and predictive	26
1.2.2.1 Difficulties in the validation of gene expression signatures	29
1.2.2.2 Prognostic gene expression signatures validated for clinical use	30
1.2.3 Proteomics	32
1.3 FRET-FLIM technology	34
1.4 HER receptor family	37
1.4.1 HER dimerisation	40
1.4.2 Endocytosis	42
1.4.3 Ubiquitination.....	45
1.5 Targeting the HER pathway in cancer	46
1.5.1 HER2:HER3 dimerisation and targeted monoclonal antibodies.....	46
1.5.2 Tyrosine Kinase inhibition	47

1.6 Summary	48
Chapter 2: Materials and Methods	51
2.1 Reagents	51
2.1.1 Mammalian Cell Lines	51
2.1.2 Reagents for Cell Culture	51
2.1.3 Transfection Reagents.....	51
2.1.4 Reagents for Molecular Biology.....	52
2.1.5 Cell stimulation	52
2.1.6 Cell Inhibitors	52
2.1.7 Reagents for Immunoprecipitation.....	53
2.1.8 Reagents for Western Blotting.....	53
2.1.9 Reagents for Cell Proliferation assay	55
2.1.10 Reagents for Immunohistochemical and Immunofluorescence Staining	55
2.1.11 Antibodies	55
2.1.11.1 Anti-HER2 antibodies.....	55
2.1.11.2 Anti-HER3 antibodies.....	56
2.1.11.3 Miscellaneous antibodies	56
2.1.11.4 Secondary antibodies.....	57
2.2 Methods	57
2.2.1 Plasmid Constructs	57
2.2.2 Plasmid Purification.....	58
2.2.3 Cell culture	58
2.2.4 Transient Cell Transfection	58
2.2.5 Cell Treatments.....	59
2.2.6 Western Blotting.....	60
2.2.7 Co-immunoprecipitation	60
2.2.8 Cell Proliferation Assay	61
2.2.9 Antibodies and direct conjugation to fluorophores	62
2.2.10 Conjugated antibodies	62

2.2.11 Preparation of Cells for Imaging.....	63
2.3 Formalin-fixed, paraffin-embedded & fresh frozen resources.....	63
2.3.1 Cell pellets.....	63
2.3.2 Breast Tissue & Data Bank	64
2.3.3 METABRIC cohort/dataset.....	65
2.3.4 Immunohistochemical staining of FFPE samples	65
2.2.4 Preparation of pellets and FFPE tissue for FLIM imaging.....	66
2.4 Structural modelling	66
2.5 Microscopy.....	67
2.5.1 Confocal microscopy.....	67
2.5.2 Multiphoton Fluorescence Lifetime Imaging.....	67
2.5.3 Single Photon Fluorescence Lifetime Imaging (Galileo)	67
2.6 Analytical Methods.....	68
2.6.1 FLIM/FRET Analysis	68
2.6.2 Survival analysis	68
Chapter 3: Molecular determinants of the lapatinib-induced HER2:HER3 dimer	69
3.1 Introduction.....	69
3.1.1 Structural conformation of the HER family.....	69
3.1.2 HER1 homodimerisation.....	71
3.1.2.1 Active vs inactive /asymmetric vs symmetric TKD dimer formation	71
3.1.2.2 Full-length HER1 dimerisation	73
3.1.3 HER2 homo- and heterodimerisation	73
3.1.3.1. HER2 homodimerisation	73
3.1.3.2 HER2 heterodimerisation	74
3.1.4 HER3 homodimerisation.....	75
3.1.5 Tyrosine kinase inhibitors	76
3.1.5.1 Type I vs II TKIs	77
3.1.5.2 Oncogenic mutations	78

3.2 Results	80
3.2.1 Optimisation of HER2-HER3 cell-based assay.....	80
3.2.2 Stabilisation of HER2:HER3 dimers on lapatinib treatment.....	81
3.2.3 Disruption of HER2:HER3 dimerisation by site-directed mutagenesis of the juxtamembrane domain of HER2 and the kinase domains of HER2 and HER3	83
3.2.4 HER3 ATP binding pocket competency is required for HER2:HER3 dimerisation	86
3.2.5 Proposed model of the lapatinib-bound HER2:HER3 dimer	89
3.2.6 I1714 (HER2) and K742G716G718 (HER3) are important determinants of HER2 and HER3 phosphorylation.....	93
3.3 Discussion	95
Chapter 4: Functional significance of the lapatinib induced HER2:HER3 dimer	100
4.1 Introduction.....	100
4.1.1 Molecular mechanisms of action of lapatinib	100
4.1.2 HER2 and HER3 receptor trafficking	101
4.1.3 HER3 rephosphorylation as a potential escape mechanism from TKI treatment	107
4.2 Results	109
4.2.1 Lapatinib treatment attenuates HER2 ubiquitination and allows HER2 accumulation.....	109
4.2.2 HER3 accumulates in SK-BR-3 cells, more so than HER2 on extended lapatinib treatment.....	109
4.2.3 Dimer formation is necessary for HER3 re-phosphorylation on extended lapatinib	112
4.2.4 Expression of the dimerisation mutant, HER2(I714Q)-GFP reduces cell proliferation	117
4.2.5 HER3 re-phosphorylation is dependent upon HER3 recycling to the plasma membrane.....	119
4.3 Discussion	127
Chapter 5: Development of a FRET/FLIM based biomarker – challenges and pitfalls.....	133
5.1 Introduction.....	133

5.1.1 Existing prognostic protein-based biomarkers for HER2-positive breast cancer	134
5.1.2 Clinical applications of FRET/FLIM.....	138
5.1.3 Tumour heterogeneity.....	140
5.1.3.1 Challenges in assessing tumour heterogeneity	141
5.1.3.2 Combining whole body imaging and microscopic imaging.....	141
Results	143
5.2.1 Distribution of HER2 and HER3 expression across METABRIC TMA of primary patient tumours	143
5.2.2 Validation of antibodies targeted to HER2 and HER3 in cell lines.....	147
5.2.3 FRET/FLIM measurement of HER2:HER3 dimerisation in cell lines	153
5.2.4 Validation of fluorophore-conjugated antibodies in formalin fixed, paraffin-embedded cell pellets	156
5.2.5 FRET/FLIM measurement of HER2:HER3 dimers in FFPE cell pellets	159
5.2.6 FRET/FLIM measurement of HER2:HER3 dimers in FFPE tumour tissue.....	161
5.2.7 Development of a method for measurement of protein:protein interactions in isolated tumour cells	163
5.3 Discussion	166
Chapter 6: Summary and Future Directions	171
6.1 Summary	171
6.2 Future directions.....	172
References.....	177
Appendix.....	192

List of Figures

Chapter 1

Figure 1. 1 Probe array and target preparation for spotted cDNA microarrays ⁶³	27
Figure 1. 2 Potential application of gene expression derived signatures ⁷²	29
Figure 1. 3 Jablonski inspired representation of Förster resonance energy transfer: FRET. 36	
Figure 1. 4 HER family dimerisation ¹³⁴	38
Figure 1. 5 Downstream signalling post HER2:HER3 dimerisation ¹³⁴	39
Figure 1. 6 Schematic representing HER trafficking and ubiquitination	44

Chapter 3

Figure 3. 1 Multiple sequence alignment of the kinase domains of the HER family	70
Figure 3. 2 Schematic diagram of the symmetric/inactive HER1 homodimer, vs the asymmetric/active homodimer ¹⁹⁵	72
Figure 3. 3 Schematic diagram showing HER3 homodimerisation and lattice formation ¹⁹⁷	76
Figure 3. 4 FRET/FLIM analysis reveals that erlotinib and gefitinib, but not lapatinib, induce dimerisation of HER1	79
Figure 3. 5 Optimisation of HER2:HER3 dimerisation cell based FRET assay	81
Figure 3. 6 Dimerisation of HER2 and HER3 induced by lapatinib, demonstrated by FRET/FLIM analysis.	82
Figure 3. 7 Lapatinib induced dimerisation of HER2 and HER3 may be disrupted by mutation at the internal dimerisation site of HER2 (HER2(I714Q)) or at the juxtamembrane domain (HER2(V697R))	84
Figure 3. 8 Effect of mutations at the C-lobe of HER3 TKD upon ligand-induced and lapatinib-induced HER2:HER3 dimerisation	86
Figure 3. 9 HER3 ATP pocket competency is required for HER2:HER3 dimerisation and may be partially overcome by constitutive activation of HER2 ATP pocket (HER2(YVMA))	87

Figure 3. 10 Proposed model of lapatinib-induced HER2:HER3 dimerisation (figure provided by Dr F Autore).....	88
Figure 3. 11 Validation of proposed lapatinib-induced HER2:HER3 dimer using site-directed mutations	92
Figure 3. 12 Phosphorylation of wild-type and site-directed HER2 and HER3 mutants on ligand and/or lapatinib treatment.....	94

Chapter 4

Figure 4. 1 HER family receptor internalisation and trafficking ²⁷⁵	104
Figure 4. 2 Proposed model of homo- or heterodimer-mediated recycling. ²⁸¹	105
Figure 4. 3 Ubiquitination and accumulation of HER2 on lapatinib treatment.....	110
Figure 4. 4 Accumulation of HER2 and HER3 on 24 hours lapatinib treatment	111
Figure 4. 5 Rephosphorylation of HER3 on 24 hours treatment with lapatinib	113
Figure 4. 6 Reduction of HER3 re-phosphorylation on transfection of the dimerisation mutant, HER2 (I714Q)-GFP.....	114
Figure 4. 7 Transfection of HER2-GFP or HER2(I714Q)-GFP leads to increased HER3 degradation	116
Figure 4. 8 Proliferation assays of MCF-7 cells transfected with HER2-GFP or dimerisation mutant (HER2(I714Q)-GFP), untreated or treated with lapatinib.	118
Figure 4. 9 Monensin treatment reduces HER3 re-phosphorylation	120
Figure 4. 10 Monensin increased ligand-induced HER3 degradation.....	121
Figure 4. 11 HER3-GFP co-localisation with Rab11-RFP on lapatinib treatment.....	123
Figure 4. 12 HER3-GFP does not co-localise with anti-mouse Cy3 IgG bound to mouse anti-EAA1 IgG upon long term lapatinib treatment	124
Figure 4. 13 HER2-GFP and HER2(I714Q)-GFP do not co-localise with Rab11-RFP on lapatinib treatment	125

Figure 4. 14 Monensin treatment reduces HER3-GFP and Rab11-RFP co-localisation at 24 hours of lapatinib treatment 126

Figure 4. 15 Schematic representing intracellular trafficking of HER receptors..... 128

Chapter 5

Figure 5. 1 Schematic diagram of proximity ligation assay for measurement of, e.g. HER2:HER3 oligomerisation³⁴⁶ 137

Figure 5. 2 Multiphoton FLIM measurements of the intermolecular FRET between HER1-GFP and ubiquitin-mRFP1³..... 139

Figure 5. 3 Immunohistochemistry stain for HER2 and HER3 in METABRIC tissue samples 144

Figure 5. 4 Kaplan-Meier curves demonstrating distant metastasis-free survival and overall survival according to HER2 or HER3 expression by IHC 146

Figure 5. 5 Validation of intracellular HER2 antibodies in cell lines 149

Figure 5. 6 Validation of extracellular HER2 antibodies in cell lines 150

Figure 5. 7 Validation of HER3 antibodies 152

Figure 5. 8 Measurement of HER2:HER3 dimerisation on treatment with lapatinib and NRG1 154

Figure 5. 9 Degree of HER2:HER3 dimerisation in SK-Br-3 cells measured by FRET/FLIM, using different antibodies 155

Figure 5. 10 Assessment of fluorophore-conjugated antibodies in PPFE cell pellets 157

Figure 5. 11 HER2 antibody and DARPIn staining of HER2 overexpressing tumour tissue 158

Figure 5. 12 HER2:HER3 dimerisation measured in cell pellets, as measured by FRET/FLIM 160

Figure 5. 13 HER2:HER3 dimerisation in tumour tissues expressing various levels of HER2 protein 162

Figure 5. 14 Extraction of tumour cells from endobronchial ultrasound guided lymph node aspiration 164

Chapter 6

Figure 6. 1 Neoadjuvant clinical trial schema 175

List of Tables

Chapter 1

Table 1. 1 Routes of endocytosis for transmembrane receptors	43
--	----

Chapter 2

Table 2. 1 Composition of various % gels used for Western blotting.....	54
---	----

Table 2. 2 Cell densities and amounts of transfection reagent used per well, for various sized dishes for transient cell transfection.....	59
--	----

Chapter 6

Table 6. 1 Clinical trial primary and secondary end-points	175
--	-----

List of abbreviations

AI	Aromatase inhibitor
ANOVA	Analysis of variance
AO	Adjuvant online (Adjuvant!)
ATP	Adenosine tri-phosphate
cDNA	complementary DNA
CMF	Cyclophosphamide, methotrexate, and 5-fluorouracil
CT	X-ray computed tomography
DARPin	Designed ankyrin repeat proteins
DMSO	Dimethyl sulfoxide
DNA	Deoxyribonucleic acid
EBUS	Endobronchial ultrasound
ECD	Extracellular domain
EDTA	Ethylenediaminetetraacetic acid
EE	Early endosome
EEA	Early endosome antigen
EGF	Epidermal growth factor
ER	Oestrogen receptor
ERC	Endocytic recycling compartment
ESCRT	Endosomal sorting complex required for transport
¹⁸ F-FDG	Fluorodeoxyglucose (18F)
FDA	Food and drug administration
FFPE	Formalin-fixed paraffin-embedded

FISH	Fluorescent in situ hybridisation
FLIM	Fluorescent lifetime imaging microscopy
FOXO	Forkhead box O
FRET	Förster resonance energy transfer
GA	Geldanamycin
GFP	Green fluorescent protein
Grb-2	Growth factor receptor-bound protein 2
HA	Haemagglutinin
Hb-EGF	Heparin-binding-EGF-like growth factor
HER	Human epidermal growth factor receptor
HR	Hazard ratio
HSP-90	Heat shock protein-90
IGF-1R	Insulin-like growth factor-1 receptor
IHC	Immunohistochemistry
JM	Juxtamembrane
LB	Lysogeny broth
LE	Late endosome
MAPK	Mitogen-activated protein kinase
METABRIC	Molecular Taxonomy of Breast Cancer International Consortium
mRNA	Messenger ribonucleic acid
MRI	Magnetic resonance imaging
MVB	Multi-vesicular body
NPI	Nottingham prognostic index
NRG1	Neuregulin/Heuregulin 1

NSCLCa	Non-small cell lung cancer
OD	Optical densitometry
PBS	Phosphate buffered saline
pCR	Pathological complete response
PCR	Polymerase chain reaction
PET	Positron emission tomography
PI3k	Phosphatidyl inositol 3'kinase
PLC	Phospholipase C
PR	Progesterone receptor
PTB	Phosphotyrosine binding domains
PTEN	Phosphatase and tensin
PTP	Protein tyrosine phosphatase
PVDF	Polyvinylidene fluoride
RFP	Red fluorescent protein
RNA	Ribonucleic acid
SH	Src-homology
Sos	Son-of-sevenless
TBNA	Transbronchial fine needle aspiration
TBS	Tris-buffered saline
TGF	Transforming growth factor
TGN	Trans-Golgi network
TKD	Tyrosine kinase domain
TKI	Tyrosine kinase inhibitor
TM	Transmembrane

TMA	Tissue microarray
TN	Triple negative
TNM	Tumour, nodes, metastasis

Chapter 1: Introduction

The aim of this thesis work is to interrogate the effects of tyrosine kinase inhibitors (TKIs) on the human epidermal growth factor receptor (HER) tyrosine kinase family, and establish novel prognostic and predictive biomarkers, with optical proteomics, in order to better profile tumours, predict outcome and sensitivity to treatment¹⁻³. This project is placed in clinical and biochemical context.

Breast cancer is the second most common cause of cancer death, after lung cancer, leading to death in 15% of all women⁴. Incremental benefits in patient survival have been achieved over recent decades through improved diagnostic, staging, and operative techniques as well as better chemotherapeutic agents. More recently the development of drugs designed to target processes that are dysregulated in the cancer cell promised to significantly improve outcomes with less toxicity, but these improvements have not yet been realised. For the next benefits in patient outcome, we must better profile both the tumour and the molecular effects of novel targeted drugs. Both prognostic tools, which help us to decide which patients are at a high risk of relapse, and predictive tools, which define the effects of a drug upon tumour biology, are required for the prescription of rationalised treatment schedules. We are entering the era of personalised medicine whereby cancer treatment may be individualised according to the molecular tumour profile. I outline the progress in biomarker development required to enable the evolution of tailored cancer therapy.

Protein-protein interactions and post-translational modifications form the functional expression of gene mutations, and thus, present a potential oncogenic mechanism and a target for treatment⁵⁻⁷. The effect of novel drugs designed against these targets often cannot be directly monitored, leading to potentially inefficient and inappropriate drug use. The ability to image these protein interactions and modifications may prove to be an invaluable decision aid in the prescription of targeted drugs. The technology used to image these post-translational modifications is described.

As protein-protein interactions within the HER family are thought to be tumourigenic^{8,9} inhibitors to these receptors have been designed to reduce mitogenic potential. However, their mechanisms of action are not fully understood. This work aims to interrogate this system in vitro with optical imaging and classical biochemical methods, in order to understand the behaviour of these receptors, both in the native state and in response to inhibitors. Novel biomarkers may become evident with this approach. These biomarkers will be validated on archived formalin fixed paraffin embedded tissue (FFPE). Clinical outcome is

recorded for each tumour and thus a link between the biomarker and tumour relapse may be established.

1.1 Breast cancer

The incidence of breast cancer has been steadily increasing over the past decade as have the number of drugs used for cure. Breast cancer is now the most common cause of cancer in women by far, with 48,788 new cases reported in the UK in 2009 alone⁴. 48% of breast cancers occur in the 50-70 age group. Women in this age group now undergo screening as part of the NHS Breast Screening Programme in England. Over the last decade, incidence rates have remained stable (approximately 120 cases per 100,000 women) but mortality rates have decreased (to approximately 25 cases per 100,000 in 2010)¹⁰, likely due to improved surgical techniques¹¹ and the use of adjuvant treatments such as hormones as outlined below. However, this improvement in patient survival is starting to reach a plateau.

Surgery remains the first option for cure in patients with localised disease. Adjuvant treatment is administered after surgery in order to reduce the risk of recurrence, and consists of hormones, chemotherapy or targeted treatments. However, it is difficult to predict which individuals would have survived without adjuvant treatment. If the risk of recurrence is greater than risk of serious treatment-related toxicity, adjuvant treatment is usually prescribed, which may expose many women to potentially toxic drugs without benefit. An absolute risk reduction of greater than 2-3% in mortality is generally considered an acceptable margin for the use of adjuvant chemotherapy. There is a critical need to identify those women at high risk of recurrence and choose the therapy to which they are likely to respond.

The development of targeted agents, such as the monoclonal antibody trastuzumab, has represented a significant advance in both the adjuvant setting and for metastatic disease. However, not all patients respond to this drug. The development of more accurate profiling of tumours and drug effects seems to be the next logical step in the rational introduction of targeted therapy. I first outline current adjuvant treatment regimens prior to examining the prognostic tools available to predict which patients benefit from such treatment.

1.1.1 Adjuvant therapy

Systemic adjuvant therapy is prescribed after definitive surgical treatment to those patients who are deemed to be at a high risk of recurrence, with the aim to reduce the risk of relapse and affect a cure. Adjuvant therapy can be divided into three groups of drugs: hormonal therapy (most commonly tamoxifen and aromatase inhibitors), cytotoxic chemotherapy (anthracyclines and taxanes) and targeted drugs (most notably trastuzumab). These treatments have been shown to reduce the risk of relapse and cancer related death but systemic drugs, chemotherapy in particular, have significant toxicity profiles. The benefits of adjuvant therapy must be carefully weighed against the toxicities as patients are often healthy, post surgery, and may potentially be cured. The absolute benefits of treatment are highest in those with the worst prognosis.

Patients receive adjuvant treatment, ideally, within eight weeks of surgical excision of the primary tumour, reducing the likelihood of establishment of micro-metastatic clusters. Neoadjuvant therapy (primary therapy) is prescribed prior to definitive surgical excision for the down-staging of locally advanced and inflammatory breast cancer. Neoadjuvant therapy enables *in vivo* study of tumour sensitivity to drugs, allowing the validation of novel predictive biomarkers.

1.1.1.1 Adjuvant hormone treatment

Breast tumours are classified according to the expression of steroid receptors on the cell surface, namely oestrogen (ER) and progesterone (PR) receptors. This classification system not only directs the prescription of endocrine therapy to target these receptors, an early example of targeted therapy, but also holds prognostic value. Oestrogen and progesterone positive disease confers good outcome versus tumours which do not express any of these receptors.

Tamoxifen binds to the oestrogen receptor and blocks gene transcription¹². It is a partial oestrogen agonist, exhibiting antagonistic action within breast cells but agonist effects on bone and endometrial tissue. It provides an absolute gain in mortality of 9.2%, and an 11.8% gain in prevention of recurrence¹³. Aromatase inhibitors (AI) prevent peripheral aromatisation of androgens to oestrogen but do not affect ovarian oestrogen production. Hence AIs are not suitable in pre-menopausal women as oestrogen production is mainly ovarian. Examples are anastrozole and letrozole, which are reversible non-steroidal inhibitors, and exemestane, an irreversible steroidal aromatase inhibitor. They are increasingly used in post-menopausal women and offer an improvement in disease free survival and lower recurrence rates compared to women on tamoxifen, but overall survival is

similar in both groups^{14,15}. However, extended AI therapy after five years of tamoxifen treatment demonstrates a survival benefit¹⁶.

Side effects of hormonal treatments are often mild but may have a profound effect on quality of life, considering the length of treatment required. For instance, side effects of tamoxifen treatment include hot flushes, vaginal dryness, atrophy and bleeding, menstrual irregularity, loss of libido, and thromboembolic events. AIs in particular, are associated with increased risk of osteoporosis and consequent fractures, which may in part be alleviated by sequential use of tamoxifen and letrozole over 5 years¹⁵. Despite the excellent clinical outcomes experienced by many patients on these treatments, approximately 30% relapse¹⁷, exhibiting broad endocrine resistance, or agent-specific resistance. In the latter case, appropriate drug selection may eradicate remaining disease. ER positivity describes a heterogeneous group of tumours¹⁸. Molecular description of these tumours with, for instance gene-expression derived signatures may help delineate high and low risk groups within the ER positive population¹⁹. The development of better prognostic and predictive markers may help to improve drug selection and minimise toxicity.

1.1.1.2 Adjuvant chemotherapy

In the 1970s, single agent chemotherapy provided early signs of improvement in patient outcome, but this was soon superseded by combination regimes. A recent meta-analysis by the Early Breast Cancer Trialists' Collaborative Group confirmed an improved five-year survival for cytotoxic combinations²⁰. Fifteen-year mortality rates demonstrate persistence of benefit from chemotherapy¹⁷. The recent addition of taxanes for patients with lymph node involvement improves five-year survival to 90%^{20,21}. The benefits of adjuvant chemotherapy are present in both ER positive and negative tumours, independent of hormone treatment²⁰.

A variety of combination treatments may be used, including CMF (cyclophosphamide, methotrexate, and 5-fluorouracil), anthracyclines or taxanes. Anthracyclines, such as epirubicin or doxorubicin, have been shown to be superior to traditional CMF regimes on meta-analysis²⁰. However, chemotherapy is not without toxicities. Alopecia, nausea, vomiting, fatigue and myelosuppression are common across many regimes. Long term toxicities include neurotoxicity, premature menopause and specifically, cardiac toxicity and myelodysplastic syndromes with anthracyclines²². Therefore the side effects of chemotherapy must be weighed carefully against the potential benefits when making the decision to treat. Attempts have been made to rationalise which patients would benefit most from specific drugs. For instance, a pooled analysis of eight breast cancer trials found that the added benefits of anthracycline chemotherapy are seen in women who have HER2 amplified tumours²³. This phenomenon may be due to the fact that amplification of the

topoisomerase II α (TOP2A) gene, a key enzyme in DNA replication and cell division, and a target for anthracyclines, is invariably associated with simultaneous HER2 amplification. Although the use of anthracyclines and trastuzumab, a monoclonal antibody targeted to HER2, may offer synergistic benefit in this group, the combination of these drugs causes additional toxicity²⁴. Additional biomarkers of chemosensitivity are required to rationalise drug regimens.

Taxanes stabilise microtubules, inhibiting the normal dynamic reorganisation of microtubules during cell division, thus causing cytotoxicity. A meta-analysis of 13 adjuvant studies demonstrated a 5% benefit in disease free survival and 3% benefit in overall survival of adding taxanes to standard CMF or anthracycline based chemotherapy regimens^{20,25}. The small absolute benefit in survival must be balanced against side effects from chemotherapy when deciding on whether to prescribe these drugs. In this case, better prognostic and predictive biomarkers would aid decision-making.

1.1.1.3 Adjuvant and neoadjuvant targeted treatment

In the 1980s Denis Slamon carried out the first 'bench to bedside' experiments by correlating overexpression of HER2 in breast cancer with poor prognosis and designing a clinical drug, trastuzumab (Herceptin), to specifically target this receptor²⁶. This was the first advance in targeted treatment since the use of tamoxifen for ER positive cancer, and led to a flood of research interest in designing new targeted therapies. The HER2 receptor is one of a family of epidermal growth factor receptors and plays a physiological role in cell proliferation, organ developments, and repair, exemplified in cardiac development²⁷. Overexpression of the receptor by gene amplification has been demonstrated in 18-25% of breast cancers and is associated with early relapse and shorter survival times^{26,28}. Receptor amplification leads to increased signalling, via the phosphatidylinositol-3-kinase (PI3k)-Akt pathway, driving oncogenic proliferation and cell survival.

Trastuzumab, a recombinant humanised monoclonal antibody to the extracellular domain (ECD) of HER2, has shown benefits in combination with chemotherapy in the treatment of patients with HER2 positive breast cancer in the metastatic and adjuvant setting²⁹⁻³⁵. Five large RCTs have assessed the benefit of trastuzumab in the adjuvant setting, demonstrating a 40-50% reduction in the risk of recurrence and a one third reduction in mortality²⁹⁻³³. Pooled results included 9,117 patients and showed significant reductions in recurrence (hazard ratio (HR) 0.53, $p = 0.00001$) and death (HR 0.052, $p < 0.00001$), but increased cardiotoxicity (4.5 versus 1.8%) in the trastuzumab arms. These five trials form the basis of current recommendations on the use of adjuvant trastuzumab with chemotherapy. The first four studies show robust improvements in disease-free survival, with some improvement in

overall survival, despite a variety of chemotherapy regimens used in combination with trastuzumab. Although the fifth study, FinHer, showed no significant difference in overall survival, there is a significant improvement in three year disease-free survival. The main aim of this study was to compare docetaxel to vinorelbine, and therefore the number of patients treated with trastuzumab is much smaller than the other four trials. Trastuzumab has been widely accepted as part of routine clinical practice in the adjuvant treatment of node-positive or node-negative high-risk tumours. However, questions remain regarding the best schedule (concurrent or sequential) and duration (six, 12 or 24 months) of treatment. These questions are currently being addressed in large, continuing phase III studies. Resistance may develop and only 40% of patients with HER2 positive metastatic disease respond to trastuzumab³⁶. Primary resistance is evident and eventually tumours become insensitive to the drug, exhibiting secondary resistance. The mechanisms of resistance are not entirely clear, but are discussed in **chapter 1.5.1**.

Small molecule TKIs such as lapatinib, have been developed in order to overcome these resistance mechanisms. Lapatinib, a competitive reversible TKI targeted against HER1 and HER2, is the most clinically advanced within this class of drugs, and has shown benefit in the metastatic setting by increasing progression free survival, in combination with capecitabine chemotherapy³⁷. Neo-adjuvant studies have demonstrated the benefit of trastuzumab use in combination with chemotherapy, prior to surgery, to the same extent as adjuvant trastuzumab³⁸⁻⁴¹. However, novel HER2 targeted drugs such as lapatinib, and pertuzumab, a monoclonal antibody to the HER2 dimerisation domain, have more recently been tested in this setting in an attempt to establish the best drug combination⁴²⁻⁴⁴. These studies demonstrated excellent pathological complete response (pCR) of approximately 29% and overall response rates of 70-80% in the arm containing taxane and trastuzumab alone. Data from the GeparQuinto study showed no benefit by the substitution of trastuzumab with lapatinib in this regimen, but worse side effects⁴⁴. On the other hand, the NeoALLTO study demonstrated an improvement of pCR to 51.3% on the addition of both lapatinib and pertuzumab to the standard taxane/trastuzumab combination⁴³. The NeoSphere study showed an improvement in pCR with the addition of pertuzumab, to trastuzumab and taxane, with a pCR of 45.8% thus highlighting the importance of quantification of HER2:HER3 dimerisation in tumour samples⁴².

These results demonstrate that although the nature of combination treatment has yet to be established, the addition of targeted therapy is likely to improve outcome measures. The results of biomarker studies from these trials are likely to prove invaluable in the determination of the precise regimen to be used in each individual patient. Further novel drugs targeting the HER family are under development, but it becomes increasingly difficult

to choose which drug a patient should receive. Knowledge of the behaviour of HER signalling, both in the native state and when interacting with inhibitors, is likely to be vital in selecting the correct inhibitor for the correct patient. We first review available prognostic biomarkers prior to addressing the HER family *in vitro*, including mechanisms of actions of targeted drugs.

1.2 Estimation of Prognosis

A prognostic marker is a clinical or biological tumour variable that is associated with a predictable risk of cancer recurrence or mortality in the absence of systemic therapy. A predictive marker is a variable that is associated with a response to treatment, and does not inform on the natural history of the disease. A biomarker is more generally defined as a substance that indicates a biological state. This may involve a pathogenic process, such as mitogenesis, or response to a treatment. Estimation of prognosis at diagnosis is crucial as the risk of recurrence influences the treatment offered by the oncologist. At diagnosis, patients are in turmoil and search for reassurance regarding the possibility of cure. Currently clinical, pathological and more recently, molecular methods of risk prognosis are combined in order to answer this question.

1.2.1 Clinicopathological factors

The tumour, nodes, metastases (TNM) staging system is the most basic prognostic tool. Patients in the adjuvant setting will not have tumour metastases. Nodal involvement remains the strongest prognostic factor⁴⁵. Tumour size becomes more relevant in node negative disease, as does lymphovascular invasion and histological grade^{46,47}. Hormone receptor status is prognostic and predictive. Oestrogen and progesterone positive tumours exhibit better outcomes than hormone-negative⁴⁸. HER2 status is an independent poor prognostic factor, but the worst outcomes are associated with triple negative (TN) disease whereby none of these receptors are expressed⁴⁹. In terms of clinical factors, age (<35years) at diagnosis is a poor prognostic factor⁵⁰.

The Nottingham Prognostic Index (NPI)⁵¹, Adjuvant! Online (AO)^{52,53} and the St. Gallen guidelines⁵⁴ are examples of integration of these prognostic factors to predict outcome. In general patients with poor prognostic features, classified according to age, tumour size, status of axillary lymph nodes, histology, grade and hormone-receptor status, benefit most from adjuvant therapy^{55,56}. The NPI (computed according to the following formula: $0.2 \times \text{size(cm)} + \text{grade} + \text{nodal status}$), classifies patients into low, moderate or high clinical risk

categories. St. Gallen guidelines classify patients into low risk if node negative with tumour size ≤ 2 cm, grade 1, absence of peritumoural vascular invasion, age ≥ 35 years and HER2 negative. High risk patients are deemed to be node positive, either with 1-3 nodes positive and HER2 positive, or with more than 4 positive lymph nodes. All other patients are of intermediate risk in this classifier. AO is a computer program, based upon information from the Surveillance, Epidemiology and End Results (SEER) registry, which provides estimated 10-year survival probabilities and risk of relapse on the basis of a model incorporating patient's age, comorbidity, tumour size, tumour grade, oestrogen-receptor status, and number of involved lymph nodes. It allows graphical presentation of average risks and benefits during consultations. Although these prognostic calculators are derived from large tumour registries, they can only classify women into one of several groups, e.g. high, low or intermediate risk. AO can provide estimations of risk reductions on the use of various treatments for individual patients, but it cannot be used to definitively categorise a patient as, for instance, cured from their disease. Recent development of molecular-based profiling tools, such as genomic classifiers, may help to identify more accurately, the individual patients at high risk of recurrence.

1.2.2 Genomic biomarkers; prognostic and predictive

Recent clinical evidence indicates that the traditional clinicopathological parameters (e.g. tumour size, lymph node status) used in prognostic models such as Adjuvant Online⁵² or the St Gallen's Consensus⁵⁵ may not correlate well with prognosis in some breast cancer subtypes^{57,58}. Prognostic models using multigene signatures such as MammaPrint⁵⁹ or Oncotype Dx⁶⁰ have been shown to outperform clinicopathological-based tools in predicting distant metastases⁶¹. The advent of gene expression profiling technology allowed quantification of the expression of multiple genes simultaneously in human tissue samples, as shown in **Figure 1.1** below. The use of complementary DNA (cDNA) microarrays for gene expression profiling in cancer aims to produce a better system for classifying tumors, a clarification of the origin of these diseases, more accurate prognostic tools and an improved ability to select appropriate therapy. Genome-analysis technologies are improving at a colossal rate with whole genome analysis representing the full diversity of breast cancer, as well as highlighting potential targets for therapy⁶². It is beyond the scope of this thesis to review the breadth and depth of various gene signatures in development. I focus on a few examples to illustrate the strengths and weaknesses of gene signatures as biomarkers.

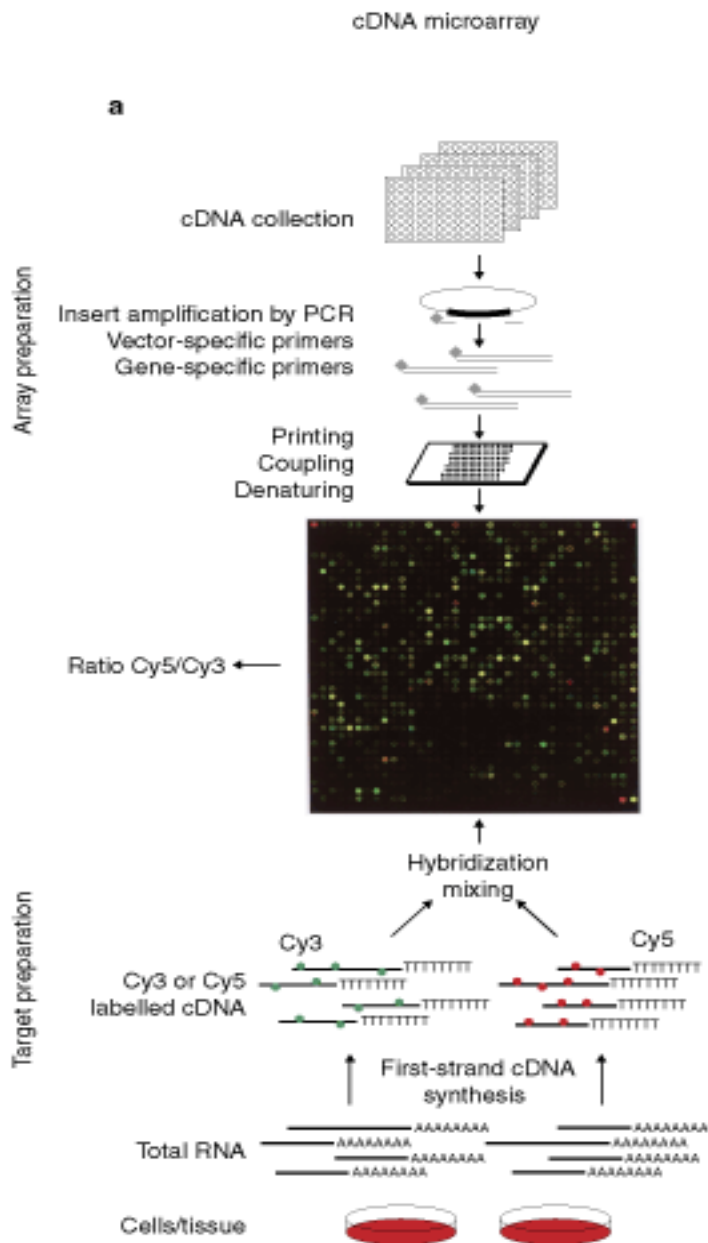


Figure 1. 1 Probe array and target preparation for spotted cDNA microarrays⁶³

Array preparation: inserts from cDNA collections are amplified using either vector-specific or gene-specific primers. PCR products are printed at specified sites on glass slides using high-precision arraying robots. Through the use of chemical linkers, selective covalent attachment of the coding strand to the glass surface can be achieved.

Target preparation: RNA from two different tissues or cell populations is used to synthesise single-stranded cDNA in the presence of nucleotides labelled with two different fluorescent dyes (for example, Cy3 and Cy5). Both samples are mixed in a small volume of hybridization buffer and hybridized to the array surface, usually by stationary hybridization under a cover-slip, resulting in competitive binding of differentially labelled cDNAs to the corresponding array elements. High-resolution confocal fluorescence scanning of the array with two different wavelengths corresponding to the dyes used provides relative signal intensities and ratios of mRNA abundance for the genes represented on the array.

The first step in improvement of tumour classification was the elucidation of different patterns of gene expression in oestrogen receptor-positive 'basal-like' versus 'luminal' type breast cancers⁶⁴, corresponding with a poor versus good prognosis, respectively¹⁸. This was followed by development of an abundance of prognostic gene expression based signatures but as of yet, few are clinically validated^{59,60}. In order to validate these signatures, they must be derived from a 'training set' of patients and show prognostic capacity on an alternate, independent 'validation set' of patients. Gene sets derived for different signatures are largely non-overlapping which raises questions about their biological significance and clinical uses. Venet *et al.* demonstrated that the majority of randomly generated gene expression signatures are associated with outcome as a large proportion of the transcriptome is associated with proliferation⁶⁵. Thus, correlation with outcome does not imply biological significance or causation. As signatures become validated, we will start to face the problem of how to choose which signatures to use, and how to best combine them, and whether a combination provides additional information above a single signature. For example, Haibe-Kains *et al.* demonstrated similar prognostic performance of three different gene expression signatures, derived by different methods⁶⁶. However, in an alternate patient dataset, using alternate gene signatures, Prat *et al.* demonstrated an increase in performance prediction on combination of signatures⁶⁷.

With the wealth of data contained within these signatures, it should become possible to define tumours according to their biology rather than the simple classification into good or poor prognosis group. For instance, the development of gene expression signatures such as the 'hypoxia-response' signature⁶⁸, derived from aggressive tumours which can withstand hypoxic conditions, or signatures which are based upon specific targeted pathways, such as the Ras/Raf pathway, may have the added benefit of directing the use of targeted therapy, as well as demonstrating prognostic benefit (**Figure 1. 2**).

Predictive gene signatures which can predict response to chemotherapy, as well as targeted agents may further help design drug combinations which best match the individual tumour⁶⁹. Consideration of tumour biology in combining gene signatures may improve outcome prediction. For instance, the invasiveness gene signature (IGS)⁷⁰ derived from CD44+CD24-/low stem-cell like tumour cells, better predicts survival in combination with a wound response signature⁷¹, which may reflect tumour microenvironment, whilst the IGS may reflect metastatic potential of the primary tumour. However, these signatures have not yet been cross-validated in independent patient data sets or approved for clinical use.

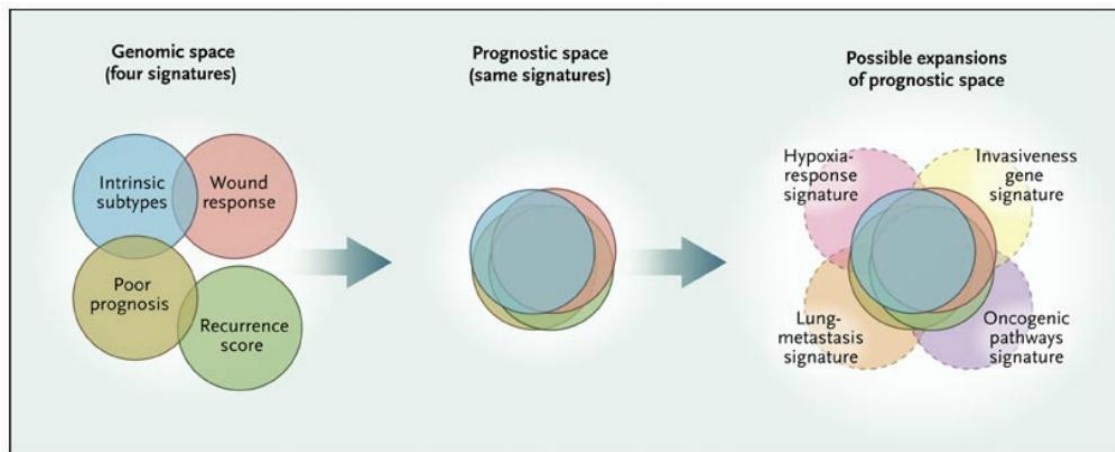


Figure 1. 2 Potential application of gene expression derived signatures⁷²

A potential method of application of a variety of gene signatures in a complementary method to help improve prognostic capacity of signatures beyond classification into ‘good’ and ‘poor’ prognosis groups. The gene signatures shown are composed of largely non-overlapping genes but show a high degree of overlap in the prediction of clinical outcome (prognostic space). With the advent of novel signatures which address specific aspects of tumour biology, these signatures may be used to refine clinical prognosis and direct the use of targeted therapies. [Prognostic space denotes the range of prognostic possibilities covered by a particular prognostic indicator, in this case an indicator characterized by the altered expression of a particular set of genes.]

Although a combination of gene signatures may improve prognostic capacity, margins of benefit may be too narrow or costs too high (2000 Euros per patient) to allow routine use in the clinic. The major question within the field of gene expression signatures still surrounds the contribution of individual genes to the oncogenic pathway. Although some genes are consistent across various signatures, hundreds of others are not and the clinical relevance of these genes is unknown. Therefore, biologically driven biomarkers which add to knowledge derived from clinicopathological variables and gene expression signatures, are required. We first discuss gene expression signatures validated for clinical use, prior to exploring other types of biomarkers.

1.2.2.1 Difficulties in the validation of gene expression signatures

Although a large number of gene expression signatures have been derived using both cancer cell lines and patient samples, both malignant and benign, the validation of these signatures prove to be the rate-limiting step in their implementation into clinical practice. The reasons for this are multi-factorial. Derived gene lists within one dataset may be highly variable and depend on the patients included in the training set⁷³. Several published gene classifiers did not classify patients better than by chance^{73,74} and different statistical methods may identify multiple prognostic assays from the same data set^{75,76}. Variation may occur within the patient groups assessed, processing and storage of tumour samples, hybridisation

protocols, scanning or statistical analysis⁷⁷. Within the arena of statistical analysis, inadequate control for multiple testing is a problematic issue as the number of patient samples are very small in relation to the expression of thousands of genes. One study suggested that thousands of samples were needed to generate a robust prognostic signature⁷⁸, and increasing the number of patients in a dataset to over 1000 does lead to improvements in signature stability⁷⁹. However, it is difficult to recruit such high patient numbers. The chance that a random gene signature may be prognostic within a dataset may range from 1 to 40%⁸⁰. However this may be corrected for by increasing the significance threshold, using a set of randomly chosen signatures alongside the signature of interest, and by increasing the number of validation data sets⁸⁰. Most importantly, thorough validation, preferably in multiple independent datasets, is essential in the development of gene signatures for translation to clinical use⁸⁰⁻⁸². Examination of these challenges may help us design novel prognostic biomarkers. For instance, the selection of a key protein:protein interaction as the basis of our biomarker encompasses both biological significance and greatly reduces the number of input parameters, compared to thousands of genes, thus allowing the use of smaller patient numbers for validation.

1.2.2.2 Prognostic gene expression signatures validated for clinical use

The Mammaprint gene expression signature is the commercialised version of the US food and drug administration (FDA) approved 70 gene signature, derived from expression profiles of 78 primary breast tumours from young (<55years of age), lymph-node negative patients⁵⁹. This signature was a strong independent predictor of metastases at 5 years with a hazard ratio (HR) of 5.1, for those patients classified in the poor versus good prognosis group. However, 3 poor prognosis patients (8%) were misclassified as good prognosis, and 12 good prognosis patients were misclassified (27%), according to the set sensitivity threshold. The retrospective nature of patient inclusion may bias outcome. Patients were allocated into two groups depending upon whether they developed recurrence within 5 years (poor prognosis) or remained disease free at 5 years (good prognosis). Another criticism was that the signature was derived from lymph node negative patients only, and thus may only be applicable in this sub group.

This signature has since been validated for patients with lymph node metastases, although patients with apical lymph node involvement were excluded⁸³. Furthermore, 61 patients from the original training set were included in the analysis as these patients had previously been selected due to early metastases. Although, exclusion would have introduced selection bias, this validation set is not strictly an independent set of patients. The signature has been validated as a strong independent prognostic factor compared to clinicopathological

variables in node-negative patients in further retrospective studies^{61,84-86}. However, the estimated hazard ratios for distant metastasis and death in the poor prognosis group were lower than those in the initial study (2.32, versus 5.1 from the first study, and 2.79 versus 8.6, respectively)⁶¹. Pertinent to the HER2-positive patient group, the MammaPrint signature does identify a group of low risk patients (approximately 20% of the total number)⁸⁷. How this result should alter prescription of adjuvant therapy is unknown.

Questions still remain regarding the integration of these signatures into clinical practice, specifically regarding which subgroup of patients would benefit from the addition of this signature to established prognostic tools. The MammaPrint gene signature has been shown to provide additional prognostic information, especially within a subgroup of ER-positive, lymph node-negative patients who have a low or discordant score on the basis of Adjuvant Online!, St Gallen and/or the NPI criteria^{88,89}. The gene signature predicted a discordant prognosis in approximately 1 in 4 patients in either the good or the poor prognosis group (7 and 13 patients respectively) as categorised by traditional prognostic tools⁸⁸. The patients with a poor prognostic signature in the good prognosis group had a lower rate of disease-free survival and overall survival at 10 years, 70% and 86% respectively, compared to those with a good prognostic signature in this group (DFS of 87%, OS of 100%). Hence the prognostic signature may be of benefit in this small subgroup. The NPI was comparable to the 70-gene signature, with discordance of 27%, and is significantly cheaper and quicker to carry out, but 25% of the patients highlighted as high risk are different. There is insufficient evidence to alter the decision to give adjuvant treatment to patients in the poor prognosis group by standard clinicopathological variables, with a good prognosis signature. We do not yet know which biomarker best predicts outcome for patients who have discordant results from standard biomarkers and gene expression signatures. A prospective clinical study, MINDACT, (Microarray in Node-negative and 1 to 3 positive lymph node Disease May Avoid Chemotherapy) has been ongoing since 2007 in order to answer this question and assess whether the MammaPrint signature safely selects fewer patients for adjuvant chemotherapy compared to traditional prognostic tools^{90,91}.

The Oncotype DX assay is a 21-gene expression signature, derived from node-negative ER-positive breast cancer patients, treated with tamoxifen, which has also been validated but not yet approved by the FDA for clinical use^{60,92-94}. This gene signature was shown to be a more robust prognostic assay in multivariate analyses, compared to histopathological grading, performed by 3 pathologists, due to interobserver variability⁶⁰. This is particularly important in intermediate, e.g. grade 2, cases where the interobserver variation is most distinct. This signature is also undergoing prospective validation in a large phase III trial, Tailor X, similar to the MINDACT trial.

Despite molecular estimation of high-risk disease in node-negative breast cancer patients by Oncotype Dx and Mammaprint, 69% and 44% of patients, respectively, experienced long-term disease-free survival. The lack of accuracy of the existing prognostic tools may relate to the effect of time-dependent changes in survival hazard ratios of the clinical variables. Using data from more than 10,000 cases from 12 studies, a recent study by Pharoah and colleagues demonstrate that the initial differences in survival between breast cancer subtypes are affected by the increasing survival times⁹⁵. In order to improve prognostic performance, it may be necessary to assess the function of the gene product, i.e., the protein, ideally at various time points within patient follow-up. Although the cause of a disease is frequently an aberration at the genetic level, the functional consequences are mediated via protein networks, with various components of the network undergoing different degrees of activation (usually as a consequence of specific post-translational modifications such as phosphorylation), driving oncogenesis. Following successes in cancer therapy derived from targeting the MDM2-p53 interaction^{96,97}, the importance of protein-protein interactions is increasingly recognized, both for understanding cell physiology and for developing novel treatments⁹⁸. Recently, the predictive performance of prognostic gene expression signatures was improved by incorporating protein interaction data^{99,100}. Aggregation of gene expression signatures upon the background of protein-interaction networks highlights key deregulated pathways, common to these signatures, e.g. involving the cell cycle, and improves understanding of the biological processes associated with the gene expression changes¹⁰¹. Despite the importance of the additional information supplied by the protein interactome configuration to improve the existing prognostic signatures for predicting patient outcome¹⁰⁰, this protein interaction information has rarely been incorporated in diagnostic/prognostic assays.

1.2.3 Proteomics

As I have described, gene profiling alone cannot provide information of events at the functional, or protein level. Therefore the study of protein-protein interactions in a tumour is vital to address the functional consequences of genetic aberrations. Two events are key in the regulation of the 23, 000 proteins encoded in the human genome: direct protein-protein interactions in interactomes, and post-translational modifications, such as protein phosphorylation, glycosylation, sulphation, acetylation and ubiquitination^{102,103}.

The biochemical genomic approach commonly used to understand these protein functional events involves protein extraction from cells, followed by one- or two-dimensional (2D) gel electrophoresis coupled with mass spectrometry (MS). The current method of matrix-

assisted desorption/ionization time-of-flight (MALDI-TOF) MS allows the analysis and identification of very small amounts of protein isolated from the gel¹⁰⁴. Shotgun methods provide useful alternatives to gels. Proteins are digested into more complex peptide mixtures that are then analysed directly by liquid chromatography coupled to MS. However, the hydrophobic nature of cell membrane proteins such as the HER receptors, which are important sensors for changes in the extracellular environment, makes them difficult to extract by digestion. Thus they are under-represented in proteomic analyses. Harsh treatments such as high pH and proteinase K (hpPK) have been used to disrupt sealed membrane compartments and cleavage of accessible protein domains on non-solubilised membrane sheets.

Such methods have been used, for example, to identify proteins secreted by cancer cell lines in response to the TKI gefitinib, in order to identify novel biomarkers of drug activity¹⁰⁵. However further work is required to validate markers such as these for clinical use. Unravelling the ways in which membrane proteins (such as the HER dimers; see section **1.4.1**) interact with each other appears to be crucial in achieving the goal of understanding the biological role of individual proteins in cellular pathways. Extraction methods for mass spectrometric analyses such as hpPK are unlikely to preserve protein complexes. Furthermore, complexed proteins identified by tandem affinity purification (TAP) procedure coupled to MALDI-TOF MS¹⁰⁶, are not necessarily involved in bimolecular physical interactions. Detection sensitivity is influenced by the affinity of interactions, abundance of protein partners as well as whether the association is direct or through intermediate binding partners. For the two-hybrid screens which do detect bimolecular physical interactions, several analyses of genomic two-hybrid results suggest that only about 50% are correct¹⁰⁷. For patient-derived cancer tissues, the quantification of these protein modifications or complexes is further hampered by the heterogeneity of tumour and non-neoplastic components within the clinical samples.

Immunohistochemical methods have been applied to breast tumour tissue in order to examine protein expression compared to established prognostic factors. Seemingly similar patients classified by traditional prognostic factors, in fact display heterogeneous protein expression patterns¹⁰⁸. No doubt proteomics offers a further method of profiling tumours. The actualisation of personalised medicine will require integration of clinical, pathological, genomic and proteomic data, in synergy, to improve prognostication, target the development of new therapies and tailor the delivery of chemotherapeutics.

1.3 FRET-FLIM technology

The use of an imaging-based *in situ* approach to monitor protein modifications and protein complexes will provide significant advantages over incumbent technologies:

- [i] The post-translational protein modifications or protein complexes are better preserved and directly observed *in situ*;
- [ii] An increase in sensitivity of detecting membrane events that is associated with the employment of near-field optics and, therefore, reduced contribution of out-of-focus signal;
- [iii] The possibility of monitoring the kinetics of various protein events, their timing and their cellular localisation, physiologically *in situ*;

This project uses fluorescence lifetime imaging microscopy (FLIM) technology, together with traditional biochemical methods, to examine protein-protein interactions in cancer cell lines and tissue.

A fluorophore is a molecule containing a fluorescent group. The fluorescent group absorbs energy at a specific wavelength, is excited, and then emits energy at a longer, specific wavelength as it reverts to ground state. This emission of light is fluorescence and the fluorescent lifetime, τ , is the average lifetime that a fluorophore remains in the excited state. Fluorescence is defined as the radiative deactivation of the first electronically excited singlet state¹⁰⁹. Fluorophores are attached to the proteins of interest by direct conjugation of antibodies, for use in tissue, or by the creation of DNA constructs expressing the protein of interest with a fluorophore tag, for use in cancer cell lines. The fluorescent lifetime varies according to the fluorophore and its environment, but is consistent for a specific fluorophore in a specific setting.

Förster resonance energy transfer (FRET) is the process of non-radiative energy transfer from one fluorophore (donor) to another (acceptor) whilst in close proximity¹⁰⁹(**Figure 1. 3**). The spectrally overlapping fluorophores must be within nanometre proximity for FRET to occur. The FRET efficiency is relative to the inverse sixth power of the distance, R , between the two molecules:

$$\text{FRET}_{\text{eff}} = 1 / [1 + (R/R_0)^6]$$

Where the Förster radius R_0 (typically 1-10nm) is the distance at which FRET_{eff} is half its maximal value and depends on the spectral characteristics of the fluorophore. In order for FRET_{eff} to be significant, the distance between the fluorophores must be within nanometres.

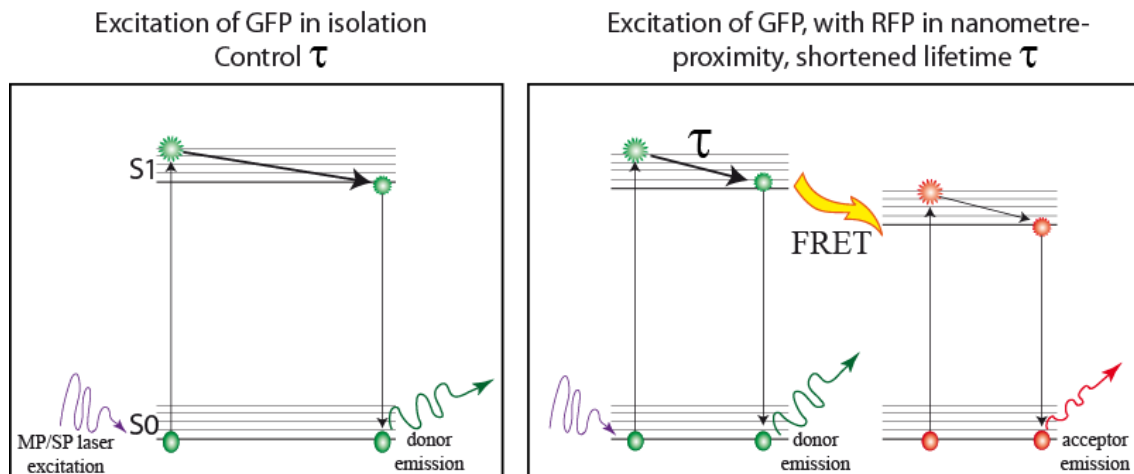
Thus, within experimental conditions, FRET is only likely to occur when two fluorophores, and their attached proteins are directly interacting.

FRET occurs only when the absorption spectrum of the acceptor overlaps the emission spectrum of the donor, and the dipole orientations of the fluorophores are parallel. For example, the absorption peak of red fluorescent protein (RFP) is 587 nm, the emission peak of green fluorescent protein (GFP) is 509 nm, and the excitation (absorption) peak of GFP is at 488nm. Therefore GFP-RFP form an appropriate FRET pair and are used in this project to quantify protein-protein interactions. GFP is excited by a short pulse of light at 488nm (laser source) and the intensity of the fluorescence signal is measured as a function of time. The fluorescence lifetime may then be calculated by fitting an exponential model to the decay of signal.

FLIM/FRET technology has contributed significantly to our understanding of the molecular pathways involved in the transduction of extracellular signals through the cell signalling machinery. These assays quantify post-translational modifications such as protein phosphorylation, ubiquitination, sumoylation as well as protein-protein interactions between signalling receptors such as the receptor tyrosine kinase family¹¹⁰⁻¹¹⁵. Time-domain FLIM, as used in my work, differs from frequency domain FLIM but such differences are largely beyond the scope of this thesis¹¹⁶⁻¹¹⁸. The main advantage of using donor FLIM over other FRET assays that are based on intensity measurements of sensitized acceptor emission is that it does not require corrections for donor emission crosstalk in the acceptor channel, direct acceptor excitation at the donor excitation wavelength, or knowledge of detection-correction (which involves quantum yields, donor and acceptor detector efficiencies and varies with conditions such as pH, optical alignment, etc)^{117,119,120}.

Measuring FRET on tissue microarrays (TMAs) allows *in situ* quantification of post translation modifications in tumour tissue. For instance, a two-antibody FRET approach has been applied to human cancer tissues to detect the nano-proximity between a donor fluorophore-conjugated anti-protein kinase C (PKC) or anti-HER1 antibody, and an acceptor fluorophore-labelled phosphor-specific antibody, providing highly specific quantification of PKC or HER1 phosphorylation^{121,122}.

FRET/FLIM is an *in situ* technique, which avoids protein extraction and disruption involved in classical biochemical assays used to study protein interactions. In the context of this project, there is a paucity of studies imaging interactions in the HER family, in the presence of inhibitors^{123,124} and none of these examine the HER2 receptor and the effect of tyrosine kinase inhibitors such as lapatinib, with FLIM/FRET technology.



tau (τ), the fluorescent lifetime, is typically between 10^{15} and 10^9 seconds

Figure 1. 3 Jablonski inspired representation of Förster resonance energy transfer: FRET

Figure adapted from Principles of Fluorescence Spectroscopy, Lakowicz, J.R.

As a fluorophore absorbs light, it is excited from the ground state (S_0) to a higher vibrational level (S_1 = first electronic state). At each energy level it exists in a number of vibrational energy levels (horizontal lines). When a molecule returns to S_0 from the lowest energy vibrational state of S_1 , fluorescence occurs. The donor fluorophore (GFP) is excited by a light source at a specific wavelength (left). This fluorescence lifetime decay produces the control lifetime, tau. When GFP is in close proximity to the acceptor, RFP (right), energy from the excited GFP is transferred to RFP, and FRET occurs (yellow arrow), thus reducing the control lifetime.

1.4 HER receptor family

The HER receptors are a family of cell surface, receptor tyrosine kinases which are integral to cell signalling and proliferation^{125,126}. They are referred to as the human epidermal growth factor receptor, HER, or the ErbB receptors, due to homology to an erythroblastoma viral gene product, v-erbB. The constituent members are epidermal growth factor receptor (EGFR, or HER1), and three homologs HER2, HER3 and HER4. HER1 and HER2 are the most researched and are clinically relevant in oncology.

These helical transmembrane receptors possess an N terminal extracellular ligand-binding domain (ECD), a transmembrane domain and a C-terminal intracellular tail which restrains the catalytic function of the tyrosine kinase (TK) domain¹²⁷ (**Figure 1.4**). Within the extracellular portion of the receptor, there are 4 ecto-domains: two homologous domains I and III, and two cysteine rich domains, II and IV. The tyrosine kinase region consists of a flexible juxtamembrane (JM) region, the N and C lobes, containing the ATP binding site between these lobes, and a C terminal tail¹²⁸. In the inactive, tethered state, domains II and IV interact in HER1, maintaining autoinhibition. HER2 is thought to be tethered in the inactive state by similar interactions between domains I and III¹²⁹. Activation leads to extension of the ECD and allows interaction between domain II of one receptor with its dimer partner¹³⁰⁻¹³².

There are over 20 known ligands for HER1, HER3 and HER4. HER1 binds epidermal growth factor (EGF), transforming growth factor alpha (TGF α) and amphiregulin with high affinity¹³³. HER1 and HER4 both bind heparin-binding-EGF-like growth factor (Hb-EGF), betacellulin and epiregulin. HER3 and 4 bind neuregulin proteins 1 and 2 (nrg1 and nrg2) and HER4 binds NRG 3 and 4²⁷. These ligand-receptor combinations represent only a small fraction of all those possible within this complex interconnecting system. HER2 has no known ligand and heterodimerisation of this receptor to another of the HER family is required for activation and signalling. HER3 possesses an inactive intracellular kinase domain, and therefore may only form the permissive partner of a heterodimer, activating another HER member. Both HER1 and HER4 may signal autonomously via homodimerisation and transactivation of their tyrosine kinases¹²⁸.

Ligand induced activation of HER1 frees the ECD from a 'tethered' inactive state to an open 'active' state. The active state binds freely with alternate members of the HER family. Ligand binding allows a change in structural conformation of the kinase domains and activation of one tyrosine kinase by the dimer partner. This TK kinase domain catalyses the phosphorylation of tyrosines in the C-terminal tail of the activating partner, leading to

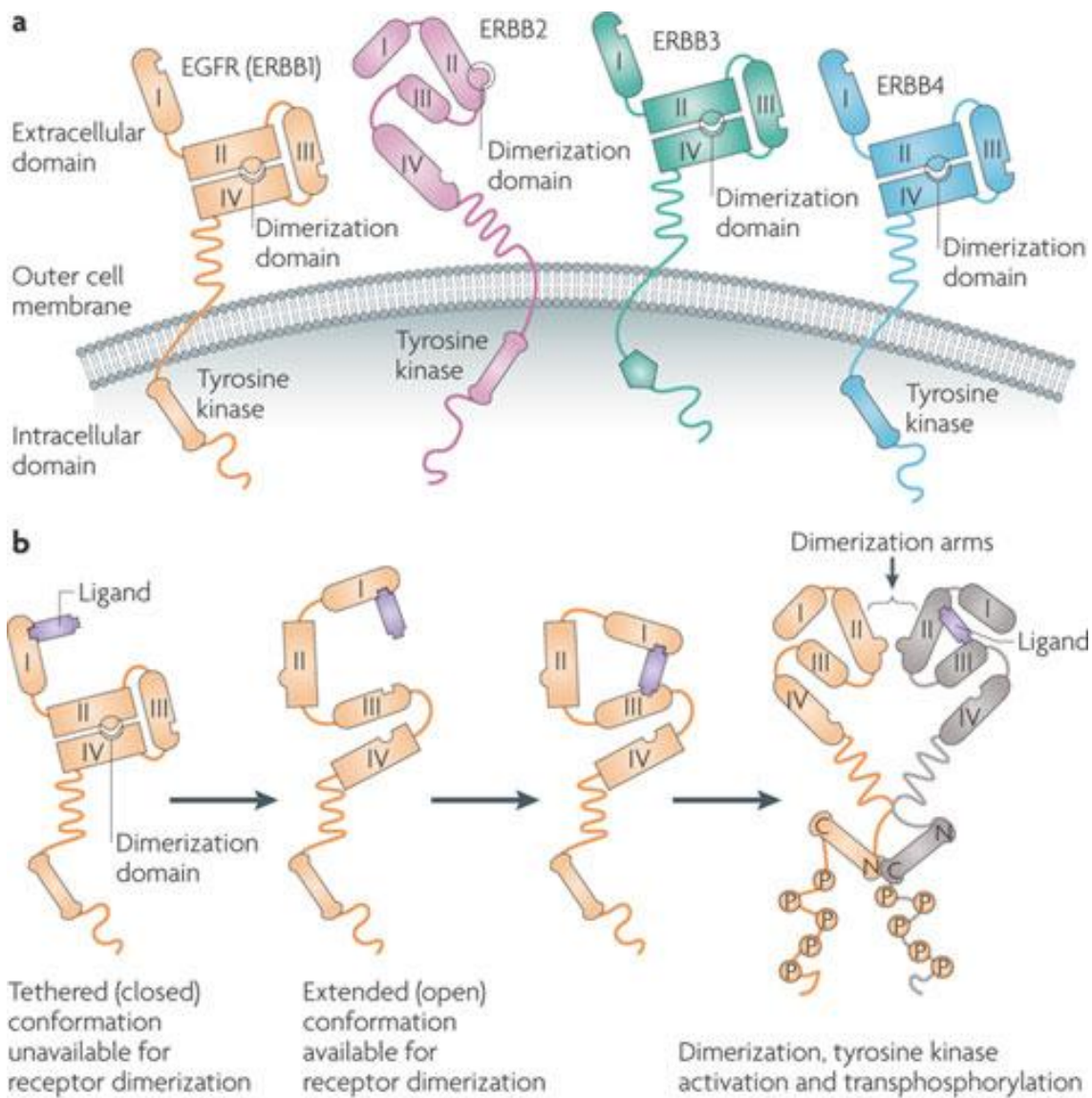


Figure 1. 4 HER family dimerisation ¹³⁴

A. The HER receptor family consists of 4 receptors. HER1 (ErbB1/EGFR), HER3/ErbB3 and HER4/ErbB4 have been crystallised as a closed, ‘tethered’ structure in the inactive state, by crosslinkage between different domains, as illustrated. HER2/ErbB2 has no known ligand and may exist in an open or extended state. However, an alternate theory is that it may be held in a closed state by domains I and III. It is unclear which of these two forms is the dominant.

B. Ligand binding induces a conformational change, in which the receptor adopts the open structure. This exposes domain II for dimerisation with HER3, as well as bringing the intracellular tyrosine kinase domains into close proximity, for transphosphorylation and activation. The kinase domain binding is asymmetric with the amino-terminal (N-terminal) lobe of one TK interacting with the carboxyl-terminal (c-terminal) lobe of the other.

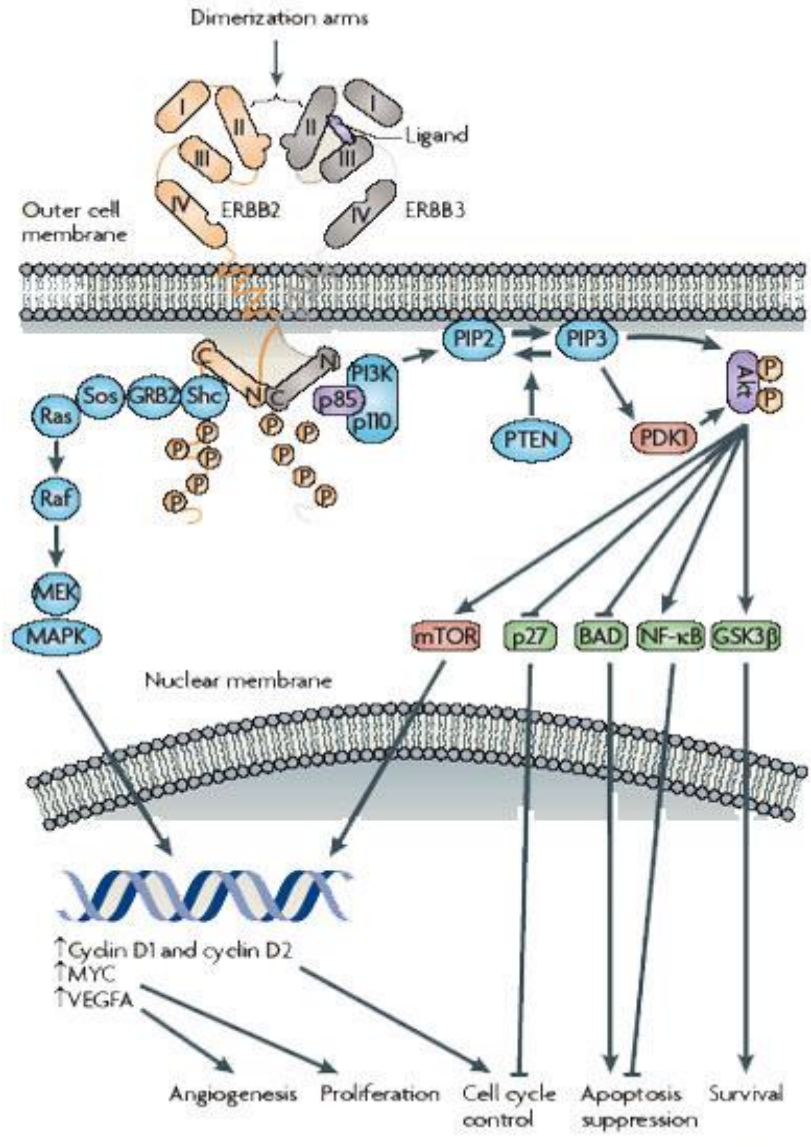


Figure 1. 5 Downstream signalling post HER2:HER3 dimerisation ¹³⁴

Ligand binding induces dimerisation and signalling through a variety of intracellular pathways. The two key binding partners are PI3-K/Akt pathway, which promotes cell survival, and the MAPK pathway, which stimulates proliferation. This is a highly simplified diagram and many other pathways are involved in HER/ErbB signalling. These two pathways are shown for simplicity. HER3/ErbB3 possesses over 6 different binding sites for PI3K, and is a potent activator of this pathway. The p85 subunit shown here, is vital for transduction of the signal from the HER2:HER3 dimer. PI3K consists of a p85 regulatory subunit, dimerised with a p110 catalytic subunit. Activation of the Akt pathway, initiates a cascade of cellular processes, including proliferation, survival and inhibition to normal cell cycle control mechanisms. An alternative signalling pathway is initiated with the binding of adaptor proteins, such as Grb2-Sos-Ras complex, which influences similar cellular processes.

recruitment of proteins containing Src-homology(SH)2 or phosphotyrosine binding domains(PTB)^{126,135}. Thus downstream signalling pathways are activated involving phosphatidylinositol 3'kinase (PI3k) or adaptor proteins such as Grb2^{27,136}(**Figure 1. 5**).

The downstream pathways associated with HER signalling are many and varied, but primarily involve the Ras/MAPK (mitogen-activated protein kinase) or the PI3K-Akt pathway. HER1 dimers recruit the Ras/MAPK pathway via Grb-2 and Sos (son-of-sevenless), whereas HER2:HER3 dimers seem to recruit PI3K but not Grb-2. In fact HER3, once within in a dimer, is a potent activator of PI3K, which has been recruited by its partner. It possesses 6 different sites binding sites for PI3k¹³⁷. These signaling pathways are involved in the regulation of a host of cellular functions, including proliferation, migration and apoptosis.

Attenuation of signal transduction is an important negative regulatory feedback mechanism, and is mediated, in part, by ubiquitin ligases, e.g. cCbl, adaptor proteins, e.g. Grb2, and other signaling proteins such as the small GTPase Cdc42, all of which are involved in the control of endocytosis and degradation of HER1. Spatio-temporal regulation of these receptors has been thoroughly investigated for HER1, in part by FRET-based probes^{123,138} but HER2 kinetics remain poorly characterised.

HER2 amplification and overexpression has been reported in a number of solid tumours, most frequently in 18-25% of breast cancers²⁶. Overexpression is also found in a subset of patients with gastric, ovarian and salivary gland tumours¹³⁹⁻¹⁴¹. Activating mutations may be present in HER2, similar to HER1 (described below and section **1.5.2**), in approximately 5% of non-small cell lung cancers¹⁴². HER1 is commonly overexpressed in lung, colorectal, squamous and head and neck carcinomas¹⁴³. HER2 and HER1 are potent targets for treatment in these subsets of patients and novel drugs have been designed to specifically target these receptors.

1.4.1 HER dimerisation

Although HER1 and HER4 may signal autonomously, via homodimerisation, the majority of HER complexes are heterodimers. The structural biology of HER receptors is integral to dimerisation, as subtle conformational changes regulate binding to partners. Once again, the molecular dynamics of HER1 are best characterised and serve as a model for HER2:HER3 interaction. At baseline HER1 is in the inactive state, whereby the ECD adopts a 'closed conformation', with a buried tyrosine kinase domain. Crystal structure studies have shown that ligand binding induces a structural change in the ECD which is transmitted to the TK domain and allows it unfurl to become catalytically active^{131,132}(**Figure 1. 4**).

HER1 may be activated by two mechanisms: dimerisation with HER1 or other members of the HER family, or by the release of autoinhibition by, e.g. a mutation at leucine 834 (L834R). HER1 undergoes autoinhibition by interaction of the kinase domain with neighbouring α -helices, e.g. an activation loop, which forms a hydrophobic patch, preventing substrate binding at rest. Receptor dimerisation buries the hydrophobic patch in the dimer interface, thus allowing activation and phosphorylation¹⁴⁴. Leucine 834 and 837 are found within the activation loop and are frequently mutated to arginine and glutamine, respectively, (L834R, L837Q) in non-small cell lung cancer (NSCLCa) patients. These mutations, especially L834R, destabilise activation loop binding, allowing constitutive signalling of HER1, and are implicated in malignant cell transformation¹⁴⁵.

HER2 shows homology to the HER1 activation loop and thus, may possess similar inhibitory/activating mechanisms. Proteomic studies have confirmed the correlation of activation loop phosphorylation, at Tyr887, with HER2 activation¹⁴⁶⁻¹⁴⁸. EGF induced heterodimerisation of HER1 and HER2 is correlated with an increase in Tyr887 phosphorylation, and treatment with HER2 kinase inhibitors results in reduced Tyr887 phosphorylation in cell lines. The activation loop may play a similar role in constitutive HER2 signalling.

HER1 dimers exist in 2 predominant forms: asymmetric and symmetric. The asymmetric dimer has been shown to be functionally dominant and is formed from the C-lobe of one kinase monomer (the activator or donor) and the N-lobe of the other monomer (the kinase domain that is being activated; the receiver or acceptor)¹⁴⁴. Mutation analyses of specific residues within the asymmetric dimer interface confirm its critical role in HER1 activation. For example, Val924 is at the dimer interface but sterically far from the kinase domain. However, mutation to arginine (V924R), reduces ligand induced phosphorylation of HER1¹⁴⁹. The HER2:HER3 heterodimer functions as an oncogenic unit in solid tumours but the structural conformation of this dimer is not entirely solved. As HER3 shows sequence homology to the dimer interface on HER1 in the C-lobe kinase but not in the N-lobe, it may only act as an activator but not a receiver. Therefore it is likely that in the formation of the HER2:HER3 dimer, HER3 is the activator and HER2, the catalytically active receiver, as depicted in **Figure 1. 5**. As HER3 is kinase-dead, it does need to be activated. Within this project, mutation analyses of tyrosine residues in the JM region of HER2 and 3, homologous to those described above for EGFR, are being used in order to interrogate this system and model the response to inhibitors.

1.4.2 Endocytosis

Ligand-induced activation of the HER receptor leads to endocytosis, intracellular trafficking and eventual degradation of a proportion of the receptor pool, thus attenuating the signal. The process is a complex one, and receptor trafficking is fundamental to regulation of signalling processes within the cell. The best characterised member of the family is HER1, due to the early discovery of the EGF ligand, the presence of a fully functioning receptor including a ligand and tyrosine binding domain, and a wealth of experimental tools including anti-HER1 antibodies. Information about HER2 trafficking, and to a lesser extent, HER3, has been gleaned via protein homology with HER1. Although this project focuses on the HER2:HER3 receptor pair, it is important to review the available information on HER1 endocytosis, trafficking and ubiquitination as well as studies of HER2:HER3 interactions. Hypotheses around HER2 intracellular trafficking may be derived from data pertaining to HER1.

Binding of EGF to HER1 causes endocytosis of the activated receptor, followed by efficient lysosomal degradation. This process is known as EGF-induced downregulation and is a negative feedback mechanism to receptor signalling¹⁵⁰. The basal turnover rate of HER1 has a $t_{1/2}$ life of 6-10 hours whereas, if the receptor is overexpressed, as in A431s (a human epidermoid cancer cell line), the $t_{1/2}$ life is prolonged dramatically up to 24 hours¹⁵¹⁻¹⁵³. Reduced turnover of the receptor leads to accumulation at the cell surface membrane and prolonged signalling. Internalisation rates are thought to be saturable and at steady state cell growth, the majority of the HER1 receptors are localised at the cell membrane due to a higher rate of recycling compared to internalisation^{154,155}. The basal turnover rate of HER2 has a $t_{1/2}$ life of 6-10 hours and the receptor also reported to be predominantly localised at the cell surface¹⁵⁶. The trafficking of HER2 and HER3 will be further discussed in **Chapter 4.1.2**.

The rate of internalisation is affected by the method of endocytosis, concentration of ligand, and expression of the receptor itself, amongst many other factors, which in turn affects the duration of receptor signalling. Endocytosis of a membrane bound receptor may occur by a variety of methods as described in Table 1¹⁵⁷. Binding of EGF to the receptor induces clathrin mediated endocytosis, and clathrin independent internalisation of HER1 (CME and CI). At low to physiological concentrations of EGF, CME is the major pathway of HER1 internalisation and is the fastest and most highly regulated^{158,159}. Ligand binding stimulates phosphorylation, ubiquitination, clustering in clathrin coated pits, binding to endosomal sorting complex required for transport (ESCRT) proteins, membrane invagination and release of vesicles known as endosomes¹⁶⁰(**Figure 1.6**). HER1 remains associated with

EGF in the acidic environment of the early endosome, where it may retain the capacity to continue signalling, and is then recycled to the cell surface. Early endosomes merge and mature to form multivesicular bodies (MVB) and late endosomes (LE). HER1 complexes in these cell compartments may be recycled, or accumulate in the intraluminal membrane, whereby they cannot be recycled and are destined for lysosomal degradation. This process of internalisation is highly regulated by ubiquitination, in this case the E3 ubiquitin ligase cCbl, ESCRT proteins and the binding of adaptor proteins such as Grb2¹⁵⁰. Importantly, HER dimerisation affects internalisation and degradation, with for instance, dimerisation of HER1 with HER2, conferring resistance to degradation and continued signalling to HER1¹⁶¹.

Type of endocytosis	Proteins involved	Endosomal process	Final destination
Clathrin mediated	Clathrins, Dynamins, Epsins, ubiquitin	Early, Late endosomes, MVB	Lysosome
Clathrin and Dynamin indepdt	Cdc42, tyrosine kinase, PKC	Endosome	Lysosome
Clathrin indepdt, dynamin depdt	Dynamins, epsins	endosome	lysosome
Caveolae	Caveolin, dynamin, PKC	Caveosome	Endosome, Golgi ER
Macropinocytosis	Cdc42, ruffles, nexins	Macro-pinosome, sorting endosome	Lysosome, Trans-Golgi network

Table 1. 1 Routes of endocytosis for transmembrane receptors

The morphological and functional attributes of the major pathways of endocytosis of transmembrane proteins are listed above, alongside their final destination, if degraded. Alternatively the protein may be recycled to the cell surface. PKC- protein kinase C, MVB- multivesicular bodies.

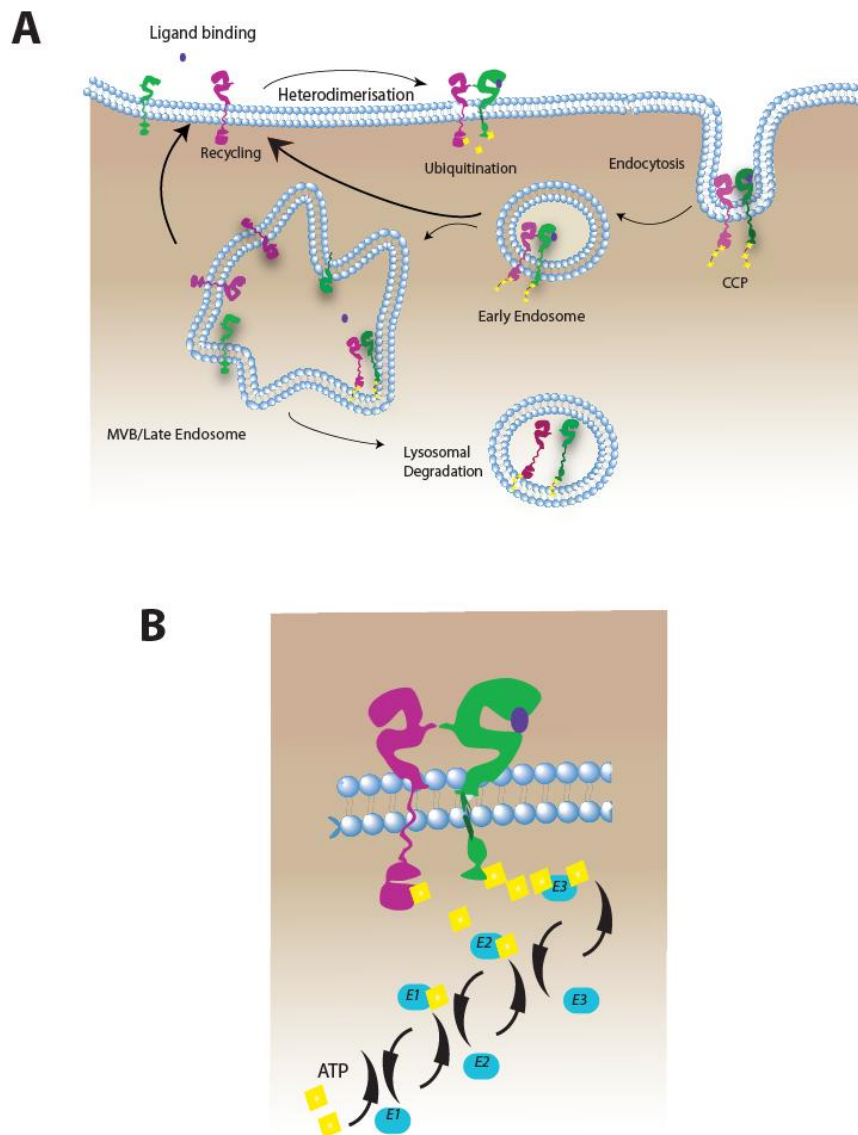


Figure 1. 6 Schematic representing HER trafficking and ubiquitination

(A) Ligand binding induces heterodimerisation, activation, ubiquitination and internalisation by clathrin coated pits (CCP) or by clathrin independent mechanisms. Within the early endosome (EE), the receptors are sorted for recycling to the cell surface or lysosomal degradation. This process is highly regulated by ESCRT proteins and ubiquitin binding proteins. The acidic pH within the EE allows the ligand-dimer complex to remain intact. It is postulated that this complex may continue to signal intracellularly. EE endosomes mature to MVB and LE, whereby the ligand dissociates and further receptor sorting occurs. (B) Ubiquitination of the ErbB receptors requires a chain of covalent reactions which is highly regulated by the ubiquitin enzymes involved. This is initiated by E1, an ubiquitin-activating enzyme, forming an E1-Ub thioester. The activated ubiquitin is transferred to an ubiquitin conjugating enzyme (E2), which then allows binding of this ubiquitin to the receptor via a specific ubiquitin-protein ligase. It may be further conjugated to form a polyubiquitin chain, and the receptor is targeted for degradation by the 26s proteasome. E3 ligases are specific and vary according the receptor: cCbl binds to HER1 and HER2, with less affinity, CHIP binds ErbB2, NRDP1 binds ErbB3, and AIP4/Itch binds ErbB4. Escape from E3-liagse mediated degradation occurs in tumours expressing mutant forms of the tyrosine kinase of the E3-ligase.

1.4.3 Ubiquitination

Ubiquitin, a small polypeptide, is intrinsic to a variety of cell processes including cell division, growth, signalling, and apoptosis¹⁶². Ubiquitination is a protein modification whereby ubiquitin is attached to a protein, thus marking it for degradation (**Figure 1.6B**). Ubiquitin is activated by an ubiquitin-activating enzyme, E1, in an ATP dependent fashion, forming an E1-Ub thioester. Activated ubiquitin is then transferred to a member of the ubiquitin-conjugating enzyme (E2) family. In the presence of a specific ubiquitin-protein ligase (E3), it is conjugated to the target protein, where it may be further conjugated with activated ubiquitin to form a mono- or polyubiquitin chain. Distinct functions have been assigned to different types of ubiquitin modification, e.g. k48 polyubiquitination leads to proteasomal degradation whereas k63 polyubiquitination may lead to DNA repair, endocytosis or the activation a variety of cell signalling enzymes¹⁶³. Ubiquitination may be reversed by deubiquitination enzymes (DUBs) and is highly regulated by E2s and E3s; there are over 80 different DUBs, over 40 different E2s and over 500 different E3s¹⁶⁴.

Ubiquitination plays an integral part in the attenuation of HER1 signalling as binding of EGF induces ubiquitination by the E3 ubiquitin ligase, Cbl¹⁶⁵. This occurs via phosphorylation of Tyr1045 as well as binding to Grb2. Similar degradation mechanisms exist for the other members of the HER family. CHIP or cCbl is the E3 ligase for HER2, Nrpd1 for HER3 and Atrophia-1-interacting protein 4 (AIP4) for HER4¹⁶⁶⁻¹⁶⁸.

Prolonged signalling due to defective internalisation and inefficient ubiquitination and degradation in lysosomes, allows recycling back to the cell surface and may promote oncogenesis^{161,169}. Chimeric ubiquitin ligases, which are designed to exhibit enhanced binding to HER2, induce ubiquitination and degradation of the receptor, more so than the wild type¹⁷⁰. This observation is supported by evidence that monoclonal antibodies targeted to the HER2 receptor, e.g. trastuzumab, may induce degradation via Cbl-mediated polyubiquitination at tyrosine 1112¹⁷¹. However, the role of c-Cbl is unclear as HER2 exhibits resistance to c-Cbl induced degradation in the absence of these antibodies¹⁷². The chaperone-binding ubiquitin ligase CHIP has been shown to produce efficient ubiquitination of HER2, and may be amenable to pharmacologic manipulation¹⁶⁶.

Protein kinase C alpha (PKC α) is implicated in aberrant HER2 signaling in patients with tumours overexpressing HER2, but without gene amplification¹⁷³. PKC α has been shown to divert HER1 from a degradative fate to recycling to the cell membrane¹⁷⁴. This study showed a similar fate for HER2, and treatment with lapatinib reduced PKC α phosphorylation, indicating crosstalk between PKC α and HER2. Heat shock protein-90 (HSP-90) is a

chaperone protein, also implicated in the retention of HER2 at the plasma membrane, acts by blocking the binding site of the E3 ubiquitin ligase, CHIP. Treatment with HSP-90 inhibitors, such as geldanamycin, triggers HER2 polyubiquitination and accelerates degradation in a proteasome-dependent manner¹⁵⁶. HSP90 inhibitors are currently being tested in clinical trials in breast cancer.

Receptor dimerisation and subsequent events are key to HER signalling and down-regulation. It is likely that aberrations in both these processes are relevant to the oncogenic capacities of the HER family. Hence receptor dimerisation and intracellular trafficking are discussed further in **Chapter 4, Chapter 5** and examined in this section, in relation to HER2, in the hope of better understanding mechanisms that may be relevant to HER2 inhibitors.

1.5 Targeting the HER pathway in cancer

The prominence of HER signalling in a variety of tumour types, has led to the development of inhibitors to the process, as described above. However 70-80% of patients will exhibit resistance to these drugs and interrogation of the HER pathway may provide insights into novel mechanisms of action as well as the development of resistance.

1.5.1 HER2:HER3 dimerisation and targeted monoclonal antibodies

The HER2:HER3 heterodimer is an oncogenic unit and has been shown to drive tumour cell proliferation¹⁷⁵. Overexpression of HER2 alone does not promote cell division as effectively as HER2 coupled to HER3, via the PI3K pathway. HER3 is the preferred dimerisation partner for HER2 and this heterodimer is believed to be the most active dimer, thus forming a key target for inhibition^{175,176}. This increased oncogenic potential may be attributed to HER3 facilitated binding to the PI3K-Akt pathway, as HER3 possesses a direct binding site for the p85 subunit of PI3K, unlike HER2¹⁷⁷.

The HER2 receptor has been targeted clinically by the monoclonal antibody trastuzumab. It is postulated that trastuzumab may exert its anti-tumour effects by inhibition of the HER2:HER1 dimer or degradation of the HER2 receptor by ubiquitination, or inhibition of the PI3K-Akt pathway, or via antibody-dependent cell-mediated cytotoxicity (ADCC)^{171,178-180}. Theories on mechanisms of resistance involve the expression of a constitutively active mutated receptor, p95HER2, present in about 20% of cases, activation of other tyrosine kinases e.g. insulin-like growth factor receptor (IGF-R)-17, or inactivation of tumour suppressor genes, e.g. phosphatase and tensin (PTEN)¹⁸¹⁻¹⁸³. Trastuzumab binds to domain IV on the ECD which does not interfere with dimerisation, and therefore, is not hypothesised

to interfere with HER2:HER3 dimerisation. Prevention of HER2:HER3 dimerisation with pertuzumab, a monoclonal antibody which binds to dimerisation domain II of HER2, has been shown to induce tumour regression, thus highlighting the need for both partners of the heterodimer in mitogenesis¹⁸⁴. This inhibitor shows clinical promise, and is synergistic to trastuzumab¹⁸⁵. Although antibodies raised against HER3 have shown *in vitro* activity by, for instance, inhibiting both neuregulin-induced and unstimulated cell growth¹⁸⁶⁻¹⁸⁸, the translation to clinical use has not yet been realised.

Patients exhibiting trastuzumab-resistance due to expression of p95HER2, may be sensitive to lapatinib, as the latter drug targets the intracellular domain of the receptor, which is not mutated¹⁸¹. Trastuzumab is ineffectual in these patients as the truncated receptor sheds the extracellular domain, but remains kinase active and is constitutively switched on. Widespread testing for the p95HER2 expression in patient tumours is not readily available, but could tailor anti-HER2 therapy in the clinic.

1.5.2 Tyrosine Kinase inhibition

Small molecule kinase inhibitors, such as erlotinib and lapatinib are specifically targeted to the tyrosine kinase domain (TKD) of HER1 and HER2, in order to disrupt downstream pathways of the HER family. These drugs bind to the ATP binding site within the TKD, inhibiting signal transduction via the Ras-RAF1, MAPK, and PI3K-Akt pathways, leading to apoptosis. Erlotinib (Tarceva) and gefitinib (Iressa) bind reversibly to the ATP binding site of the active form of HER1, whereas lapatinib (Tykerb) preferentially binds to the inactive HER1 and HER2 kinase^{189,190}. The use of lapatinib in the metastatic setting, with the cytotoxic capecitabine, is clinically effective³⁷ and ongoing studies are examining its role in the neoadjuvant setting, as described previously. However, its molecular effects are not entirely resolved and are explored in this thesis in a structural context.

Structural integrity is vital to TKI binding and thus efficacy, as demonstrated by HER1. Key mutations in HER1 in lung cancer have been established to confer sensitivity to treatment with TKIs. For example, L834R and L837Q in the activation loop reduce autoinhibition and increase HER1 activation, as previously described. This supports sensitivity to gefitinib, which binds to the active receptor¹⁹¹. Conversely, a T766M mutation, in exon 20, at the ATP binding site of HER1 confers resistance to gefitinib as it results in steric hindrance to the drug binding in this pocket. The structural interactions of TKIs with the HER family are described in detail in **Chapter 3.1.5**, in order to derive a model for the lapatinib-bound HER2:HER3 dimer, knowledge of which may improve understanding of lapatinib resistance or sensitivity.

Erlotinib and gefitinib produce transient inhibition in the wild type receptor. HER1 re-activation after inhibition has been shown to be associated with upregulation of HER3 *in vivo* and *in vitro*¹⁹². Autocrine ligand production is also postulated to confer resistance to TKIs. HER1 signalling which has been blocked by erlotinib or gefitinib is replaced by HER2 and/or HER3 recruitment by autocrine production of neuregulin and betacellulin¹²⁴. Therefore crosstalk between the members of the HER family is highly implicated in resistance to treatment. HER3 is also likely to play an important part in resistance to HER2-targeted therapies and is investigated. TKIs targeted against HER2, such as lapatinib, should form an effective block to signaling by disruption of HER3-dependent signaling through the PI3K-Akt pathway. However, this inhibition is transient and mechanisms of overcoming the TKI are unclear, but explored further in **Chapter 4**. Combination treatments including an antibody preventing dimerisation, alongside a TKI, may be necessary for prolonged attenuation of the HER2 signal.

1.6 Summary

Over recent decades we have made significant progress in the treatment of breast cancer due to advances in surgery, radiotherapy, and the use of non-specific cytotoxic agents. The definition of a HER2 positive tumour sub-group and the development of a specific therapy targeting this receptor, has revolutionised treatment for patients with this poor prognosis tumour. However, the rapid rate of improvement in patient survival we saw a decade ago is now starting to plateau. In order to further improve patient outcomes, it is imperative that we return to the molecular biology of breast cancer and the host of novel targeted agents which are being developed to treat this disease.

Although adjuvant treatment has been shown to benefit a great proportion of breast cancer patients, it may not benefit all those patients for whom it is prescribed. Clinical outcome after therapy cannot be accurately predicted for an individual patient, which may lead to over-treatment and increased patient morbidity. Breast cancer is a heterogeneous disease and current methods of sub-classification are not sufficient for accurate prognostication. For instance, ER positive tumours generally have a good prognosis, but up to 30% may relapse¹⁷. Patients with these tumours are at higher risk of recurrence, but not differentiated by ER as a biomarker. The development of gene expression arrays has started to improve tumour classification by more accurately profiling the tumour¹⁹. However, correlation of a gene expression signature read-out with clinical outcome does not imply biological significance or causation. Furthermore, validation is problematic, as illustrated by the fact

that of the many gene signatures available only one has been FDA-approved for use in breast cancer.

Biologically driven biomarkers are required in addition to the available prognostic tools described. The functional assessment of the gene product, i.e. protein-protein interactions and post-translational modifications, may improve prognostic and predictive performance, and could be used in combination with gene expression signatures^{99,100}. Targeting specific events such as the MDM-p53 interaction^{96,97} illustrates the importance of protein-protein interactions in understanding cell physiology and highlighting targets for treatment. FRET/FLIM technology is a highly specific method of assessing *in situ* protein interactions or modifications and has been applied to tumour tissue^{121,122}. This technology offers additional information over simple intensity-based quantification of protein expression.

Members of the HER family are overexpressed in a variety of cancers and treatments targeted to these receptors have been very successful. For example, gefitinib, erlotinib and lapatinib are a group of TKIs which inhibit HER phosphorylation thus attenuating downstream signalling. I propose to use FRET/FLIM to investigate further the molecular effects of lapatinib, a drug which is likely to play an important role in the future treatment of HER2 positive breast cancer. I will interrogate the effects of lapatinib, amongst other TKIs upon the HER signalling network. While the studies were performed using a specific TKI, results are likely to be relevant for other emerging compounds in the therapeutic pipeline¹⁹³.

Despite the promise of fewer toxicities and better response rates of targeted therapies, primary and secondary resistance is evident. Structural conformation and site-directed mutagenesis studies have demonstrated mechanisms of resistance and sensitivity, which now direct treatment decisions for drugs targeting HER1 in lung cancer. However, the effect of lapatinib upon HER2 dimerisation, especially in a structural context, and receptor trafficking is not fully understood. We have used a multi-disciplinary approach, consisting of chemical biology methods, FRET/FLIM technology and computational modelling in order to characterise lapatinib-induced events relating to the HER family. There is potential to uncover, not only mechanisms of action of TKIs but also mechanisms of resistance *in vitro*, which may be translated for clinical benefit.

Although HER2 overexpression is both prognostic of poor outcome and predictive of a response to trastuzumab and lapatinib, resistance eventually develops. In the metastatic setting, only 40% of patients respond to trastuzumab. In the neoadjuvant setting, novel HER2 targeting agents improve pathological response rates but the optimum schedule and combination regimen has not yet been established. The assessment of HER2:HER3 dimerisation, an oncogenic unit in HER2 positive breast cancer, may delineate a separate

group of patients which may benefit from drugs specifically targeting the dimer, such as pertuzumab. Such an assay could also be used to monitor drug efficacy in order to define optimal treatment regimens and duration. I aim to translate the FRET/FLIM technology used to interrogate the HER family *in vitro* to an assay which may be applied to tumour tissue as a predictive or prognostic biomarker.

The work described within this thesis encompasses translation of relevant biomolecular processes *in vitro* at the cellular level to the design and development of molecular diagnostics which could bring about health benefits to the cancer patient. The questions I hope to answer are:

1. How does lapatinib affect the oncogenic HER2:HER3 dimer, both in terms of structure and function?
2. What are the long term consequences of lapatinib binding to HER2, and can they help to explain drug resistance?
3. Can we translate this *in vitro* assay to a clinically useful biomarker which can be used in tumour tissue?

The benefits of chemotherapy and targeted therapies in breast cancer are clear. However, In order to further improve upon current mortality and morbidity rates, it is imperative we fully investigate the molecular effects of novel agents and devise new prognostic and predictive biomarkers in order to select the right treatment for the right patient at the right time.

Chapter 2: Materials and Methods

This project received the approval of the local ethics committees. The Guy's & St Thomas' Breast Tissue & Data Bank Access Committee approved use of tissue from the Tissue Bank.

2.1 Reagents

2.1.1 *Mammalian Cell Lines*

MCF-7 human breast cancer cells were obtained from the Cancer Research UK (CR-UK) Cell production facilities.

SKBR-3 human breast cancer cells and were a kind gift from the Breakthrough Breast Cancer Unit (Guys Hospital)

2.1.2 *Reagents for Cell Culture*

High glucose Dulbecco's modified Eagle's media - DMEM (Sigma-Aldrich, Gillingham, UK)

McCoy's media (Sigma-aldrich)

Full medias contain 10% Penicillin/Streptomycin (10,000 IU Penicillin and 10,000 µg/ml Streptomycin) (Life Technologies Ltd, UK), 2mM L-Glutamine (Life Technologies Ltd, UK), and 10% heat-inactivated Foetal Bovine Serum (Sera Laboratories International Ltd)

Trypsin/EDTA (0.25% trypsin, 0.02% EDTA) (PAA)

2.1.3 *Transfection Reagents*

Opti-MEM-1 (Gibco)

FuGene 6 (Roche Diagnostics)

FuGene HD (Roche Diagnostics)

2.1.4 Reagents for Molecular Biology

DH5 α TM bacterial cells (Invitrogen)

LB agar and broth (Sigma)

Ampicillin (Sigma) used at 100 μ g/ml

Kanamycin (Sigma) used at 50 μ g/ml

Qiaprep^R Spin Endofree Maxiprep kit (Qiagen)

2.1.5 Cell stimulation

NRG1: Neuregulin/ recombinant human heregulin $-\beta$ 1, 50ng/ml (PeproTech, USA)

EGF: recombinant human epidermal growth factor, 50ng/ml (PeproTech, USA)

2.1.6 Cell Inhibitors

Geldanamycin (InvivoGen, USA): Heat Shock Protein (Hsp)-90 inhibitor; used at 3 μ M in DMSO

Trastuzumab (Herceptin, Genentech) was a kind gift from Dr Paul Ellis; used at 1 μ M in PBS

Lapatinib (LC labs, USA) and a kind gift from Professor György Kéri (Vichem Chemie Research Ltd Hungary): anti-HER1 and HER2 TKI; used at 1-10 μ M in DMSO

AG 1478 (erlotinib), gefitinib and canertinib was a kind gift from Professor György Kéri: anti-HER1 and pan-HER TKIs; used at 10 μ M-40 μ M in DMSO

Cycloheximide (Sigma-Aldrich): inhibitor of protein synthesis via translational elongation; used at 25-50 μ g/ml in DMSO

Monensin A (Sigma-Aldrich): inhibitor of intracellular protein transport and recycling via inhibition of Na-H exchange; used at 1-10 μ M in ethanol

Bafilomycin A (Sigma-Aldrich): specific inhibitor of vacuolar-type H⁺ATPase; used at 0.25 μ M in ethanol

2.1.7 Reagents for Immunoprecipitation

Lysis Buffer:

50mM Tris/HCl pH7.4, 150mM NaCl, 2.5mM EDTA (ethylenediaminetetraacetic acid), 2.67mM EGTA (ethylene glycol tetraacetic acid), 10% Glycerol, 1% Triton X-100 (polyethylene glycol p-(1,1,3,3-tetramethylbutyl)-phenyl ether)

Freshly added: 1mM iodoacetamide (IAA) or 10mM N-Ethylmaleimide (NEM), 0.2mM sodium orthovanadate, 0.01 μ M Calyculin (in EtOH), 1:100 P8340 Protease inhibitor cocktail (Calbiochem USA) (aprotinin 0.8 μ M, leupeptin 20 μ M, AEBSF 1040 μ M, E-64 protease inhibitor 14 μ M, pepstatin-A 15 μ M, bestatin 40 μ M)

HNTG Buffer:

20mM HEPES pH7.5, 150mM NaCl, 0.1% Triton, 10% Glycerol, 10mM IAA or 10mM NEM

TBS: Tris-buffered saline (25mM Tris, 100mM NaCl, pH 7.5)

Protein A+G-Agarose beads for IP (Alpha diagnostic international)

2.1.8 Reagents for Western Blotting

Sample Buffer: (5x)

312.5 mM Tris-HCl (pH6.8), 10% w/v SDS, 50% Glycerol, 250mM DTT, 0.03% w/v bromophenol blue

Gels: 30% Acrylamide/Bis solution 37.5:1 (BioRad), ammonium persulphate (Sigma)

Precision Plus protein dual colour standard (BioRad)

SDS-PAGE Running Buffer (Invitrogen)

Transfer buffer: 7.2g glycine, 1.7g Tris base, 200mls methanol, made up to a final volume of 1L distilled H₂O

PVDF transfer membrane (Immobilon)

4% BSA (Bovine Serum Albumin from BioSera) made up in TBS with 0.1% Tween

Re-blot Plus (Millipore, USA)

Pierce ECL Western Blotting substrate (ThermoScientific)

Coomassie stain: 0.25% w/v Coomassie brilliant blue R-250, 7% acetic acid, 40% methanol, made up to 1L distilled water

Destain solution (7% acetic acid, 10% methanol, made up to 1L distilled water)

Resolution Gels

Stock solutions	Concentration used in gel	10%	7%	5%
Distilled water		19.81ml	24.82ml	28.15ml
1500mM Tris/Hcl pH8.8	375mM	12.5ml	12.5ml	12.5ml
30% Acrylamide/Bis	see columns	16.667ml	11.667ml	8.339ml
10% SDS	0.1%	0.5ml	0.5ml	0.5ml
10% (NH ₄) ₂ S ₂ O ₈	0.1%	0.5ml	0.5ml	0.5ml
TEMED,(100%) (N,N,N,N-Tetramethylethylenediamine)	0.0004 v/v	0.02ml	0.02ml	0.02ml

Stacking gel

Stock solutions	Concentration used in gel	5%	4%
Distilled water		8.03ml	8.45ml
1000mM Tris/Hcl pH6.8	170mM	2.125ml	2.125ml
30% Acrylamide/Bis	see columns	2.09ml	1.667ml
10% SDS	0.1%	0.125ml	0.125ml
10% (NH ₄) ₂ S ₂ O ₈	0.1%	0.125ml	0.125ml
TEMED,(100%) (N,N,N,N-Tetramethylethylenediamine)	0.001 v/v	0.012ml	0.012ml

Table 2. 1 Composition of various % gels used for Western blotting

Volumes represent required amount for 8 1.0mm gels.

2.1.9 Reagents for Cell Proliferation assay

Cell Proliferation Reagent WST-1 (Roche)

2.1.10 Reagents for Immunohistochemical and Immunofluorescence Staining

Target Retrieval Solution pH6.0 (Dako Ltd, UK S2369)

DakoHercep Target Epitope retrieval solution

DakoHercep Wash Buffer 10x

TBS: Tris-buffered saline (25mM Tris, 100mM NaCl, pH 7.5)

Dulbecco's Phosphate buffered saline (1x without Ca and Mg) (PAA, Austria)

Sodium borohydride (Sigma-Aldrich)

4% (w/v) paraformaldehyde (PFA; Sigma-Aldrich) in PBS

4% Neutral Buffered Formalin

Moviol:10% (w/v) Mowiol 4-88, 25% glycerol, 100mM Tris-HCl pH 8.5 (Calbiochem)

DABCO: 2.5%(w/v) 1,4-diazabicyclo[2.2.2]octane (Sigma-Aldrich)

Immersion oil 510 (Zeiss)

2.1.11 Antibodies

2.1.11.1 Anti-HER2 antibodies

Customised rabbit monoclonal antibody raised against HER2, (epitope CTAENPEYLGGLDV-CONH₂) (engineered by glbiochem)

Anti-HER2 clone Ab17 mouse monoclonal antibody (Labvision)

Anti-HER2 clone L26, mouse monoclonal antibody was a kind gift from Prof Yarden's lab, Rehovot, Israel

Anti-HER2 clone N24 mouse monoclonal antibody (Labvision)

Anti-HER2 Designed ankyrin repeat protein (DARPin) was a kind gift from Prof Kerry Chester, UCL, London

The antibodies listed above were conjugated with fluorescent dyes and used for immunofluorescence and FRET/FLIM. They are further described below (Conjugated antibodies).

29D8 Cell signalling rabbit monoclonal antibody; 1:1000 for immunoblotting; 1:50 for immunoprecipitation

Oracle™ clone CB11, affinity purified mouse monoclonal IgG antibody, supplied ready to use for HER2 immunohistochemistry in the Leica Microsystems Bond-max fully automated staining system

Anti-phosphoHER2(Tyr1248) rabbit monoclonal antibody; 1:1000 for immunoblotting (Millipore, USA)

2.1.11.2 Anti-HER3 antibodies

Anti-HER3 Clone H3.90.6 (YY) mouse monoclonal antibody, was a kind gift from Prof Yarden's lab

Anti-HER3 M01, clone 2E9 mouse monoclonal antibody (Abnova)

Anti-HER3 MAB 3483 mouse monoclonal antibody (R&D)

Anti-HER3 RTJ2 mouse monoclonal antibody (Millipore)

The antibodies listed above were conjugated with fluorescent dyes and used for immunofluorescence and FRET/FLIM. They are further described below (Conjugated antibodies).

1B2E Cell signalling rabbit monoclonal antibody; 1:1000 for immunoblotting

Anti-phosphoHER3 rabbit monoclonal antibody; 1:1000 (21D3, Cell signalling)

2.1.11.3 Miscellaneous antibodies

Anti-ubiquitin antibody; 1:1000 for immunoblotting (P4D1, Cell signalling)

UBI anti-ubiquitin antibody; 1:100 for immunofluorescence (CRUK)

Anti-GFP mouse antibody; 1:300 for immunoprecipitation, 1:10000 for immunoblotting (3E1, Invitrogen)

Anti-HA antibody; 1:40 for immunofluorescence (SantaCruz)

2.1.11.4 Secondary antibodies

Secondary antibodies for immunoblotting: polyclonal goat anti-rabbit/mouse HRP, 1:2000/1:3000 respectively (DAKO)

Goat anti-rabbit/anti-mouse IgG-Cy3: 1:200 (Jackson-Stratech)

Goat anti-mouse IgG-Cy2 1:200 (Jackson-Stratech)

Goat anti-rabbit IgG-Cy5 1:250 (Jackson-Stratech)

Donkey anti-rabbit IgG-Cy 2 1:200 (Jackson-Stratech)

Donkey anti-mouse IgG-Cy3 1:250 (Jackson-Stratech)

2.2 Methods

2.2.1 Plasmid Constructs

The HER2-mGFP construct was made by excision of HER2 from HER2-YFP (a kind gift from Selene Roberts, Daresbury laboratory) with XhoI and HindIII, and ligation into pEGFP-N1 (Clontech) containing an A206K mutation in the EGFP, enabling the EGFP to fold in a monomeric way. HER3-mRFP was made by PCR of the C-terminal half of HER3, to include the BamHI site contained in the gene and adding a NotI site at the C-terminus. (HER3-EGFP was used as the template for this, also a kind gift from Selene Roberts). The PCR fragment was ligated into the BamHI and NotI sites of pCDNA3.1-mRFP. The N-terminal half of HER3 was then excised from HER3-GFP by digestion with BamHI, and this was ligated into the BamHI site of the previous construct and checked by restriction digestion and agarose gel electrophoresis for correct orientation. A prior member of the supervisor's laboratory, Soren Prag, made the mRFP1-Ubiquitin. Further site-directed mutagenesis in the HER2-eGFP vector described above, were carried out by colleagues Dr Tai Kiuchi, Dr Melanie Keppler, and Dr Elena Ortiz-Zapater, as shown below:

HER2-eGFP: I714Q (acceptor impaired), V697R (JM mutation, acceptor impaired), V956R (donor impaired), K753M (mutation at ATP binding site rendering the receptor kinase dead), N764RK765F, I748RV750R (both mutations to validate HER2-HER3 dimer model).

HER2-HA and HER3-HA were a kind donation from Prof Yarden and HER3(K723MG697DG699D)-HA were a kind donation from Dr Angus Cameron and Dr

Jereon Claus, Cancer Research UK labs, Lincolns Inn Fields, in collaboration with our group for publication.

2.2.2 Plasmid Purification

50µl chemically competent DH5α bacterial cells were transformed with 1µl of the appropriate plasmid by incubating together on ice for 30 minutes followed by heat shock at 42°C for 30-45 seconds. The cells were then chilled on ice and 200µl LB broth was added before the cells were allowed to recover at 37°C with shaking for 45-60 minutes. The cells were then spread on agar plates containing appropriate selection antibiotics (100µg/ml ampicillin or 50 µg/ml kanamycin), and incubated at 37°C overnight. For amplification a colony was picked and grown in 5 ml LB broth with antibiotics for 4-6 hours with shaking at 37°C. This was then grown up in 250ml LB broth overnight to an optical density (at 600 nm) of 4-5 units. Plasmids were purified using the Qiaprep^R Spin Endofree Maxiprep kit, according to Qiagen's instructions (cells were harvested by centrifugation; pellets were resuspended in RNase containing buffer; cells were lysed; precipitation buffer was added to the lysates; precipitated lysates were allowed to flow through an equilibrated maxi column; the column was washed through with buffer and the flow-through was discarded; DNA was eluted into a centrifuge tube using elution buffer; isopropanol was added to precipitate DNA prior to centrifugation; the pellet was washed in 70% ethanol prior to further centrifugation; the pellet was air dried before resuspension in water). The DNA concentration was determined using a nanodrop ND-1000 Spectrophotometer.

2.2.3 Cell culture

MCF-7 human breast cancer cells were grown in DMEM full media. Cells were maintained at 37°C in a water saturated incubator with an atmosphere containing 5% CO₂. Adherent cells were grown in culture until 60-75% confluent, typically in a 75cm² tissue culture flask. The growth medium was aspirated, cells were washed with 10mls PBS and then incubated with 2mls trypsin/EDTA at 37°C for 3 minutes. 10mls of full media was then added to the cells to inactivate the trypsin/EDTA. The cells were split in a 1:3 or 1:4 dilution three times every 2-3 weeks.

SK-BR-3 cells were grown in a similar fashion but in McCoys full media, and were split in a 1:2 dilution every 2-3 days.

2.2.4 Transient Cell Transfection

Cells were transfected with plasmid DNA using FuGene6, according to the manufacturer's protocol (Roche). Briefly, cells were plated and allowed to grow for 24hours. Table X

describes the cell densities used for transfection of various size wells, and the DNA-Opti-MEM-Fugene quantities used for each type of well. For FLIM experiments cells were seeded in a 24-well plate containing 13mm coverslips for 24hours. A DNA-Opti-MEM complex was made with FuGene6 as shown in Table X, and incubated at room temperature for 30 minutes. For biochemistry experiments, cells were seeded in 6cm plates, or 6 well plates, and for the formation of cell pellets (see below), cells were plated in 15cm dishes.

The cell media was replaced with Opti-MEM containing 5% FBS and the DNA/FuGene complex was added to the cells. Incubation and protein expression was allowed for 24-36 hours. In cases of co-transfection, such as HER2GFP-HER3HA, cells were transfected using a donor:acceptor plasmid ratio of 1:3, but maintaining the total DNA content per well, i.e. 0.1µg HER2-GFP DNA, 0.3µg HER3-HA DNA per well for a 24 well plate, maintaining a total of 0.4µg DNA per well.

	Cell Density	Optimum (µl)	DNA (µg)	Fugene (µl)
24 well plate	6x10 ⁴	50	0.4	1.2
6 well plate	5x10 ⁵	250	2	6
60mm dish	1x10 ⁶		4	12
150mm dish	1x10 ⁷	2500	32	96

Table 2. 2 Cell densities and amounts of transfection reagent used per well, for various sized dishes for transient cell transfection.

These values were used for transfection of both MCF-7 and SKBR3 cells with transfection efficiencies of around 50-75% depending on the cell type and plasmid vector used.

2.2.5 Cell Treatments

Cell stimulation was performed with Heregulin-B2 (or NRG1) (50ng/ml) for HER2 and HER3 experiments between 5-60 minutes, as determined by optimization experiments. Inhibition was performed using the humanised monoclonal antibody trastuzumab (Herceptin) at 1mg/ml, or Lapatinib (10µM), or geldanamycin (3µM). Inhibition was performed prior to stimulation for time periods ranging from 60 minutes to 6 hours at 37 °C. Experiments always included non-stimulated and non-inhibited controls. In the case of degradation experiments, cells were pre-incubated with cycloheximide, 25-50µg/ml for 1 hour, followed by inhibition or stimulation for upto 24hours, in the presence of cycloheximide.

2.2.6 Western Blotting

Cells were cultured until 80% confluent in 6 well or 12 well tissue culture dishes. Cells were stimulated or inhibited as described above from 5 minutes to 6 hours. For those experiments requiring incubation with a reagent for more than 60 minutes, cycloheximide (20 μ M) was used one hour prior to treatment.

Cells were then washed twice in cold TBS and lysed on ice by scraping into 100-350 μ l of 1.5 fold sample buffer, heated to 75°C. The lysates were centrifuged at 4°C at 16,000g for 5 minutes to clear debris. The total protein content of the samples was determined using the BCA assay (Pierce).

Aliquots were loaded onto 7.5% Tris-glycine SDS- polyacrylamide gels. Gels were run on an Invitrogen X-Cell mini-gel system. The gels were subjected to constant voltage electrophoresis at 30-40mAmp per gel, until the protein marker for 50kDA reached the bottom of the gel. After separation on the 7.5% Tris-glycine gel, proteins were electrophoretically transferred onto PVDF membranes using the Invitrogen XCell II™ transfer apparatus (arrangement: sponge, two filter papers, gel, membrane, two filter papers, sponge).

The membranes were then blocked in 4% BSA/TBS-Tween for 45minutes at room temperature with shaking, then incubated with primary antibodies diluted in the blocking buffer overnight at 4°C. Blots were rinsed once and washed two times with TBS-Tween for 5 minutes each on a roller, prior to incubation with horse radish peroxidase-conjugated secondary antibodies in blocking buffer for one hour at room temperature. They were then washed a further two times as before. The membranes were placed in an X-ray cassette, covered in enhanced chemiluminescent (ECL) substrate for one minute as per manufacturer instructions. The blots were then exposed on Hyperfilm and developed using Imaging Systems Xograph compact X4 developer.

For reprobing with a second primary antibody, blots were treated with Re-blot plus diluted to 1:10 with TBS-Tween for 15 minutes at 37°C with agitation and then incubated overnight with primary antibodies as above.

2.2.7 Co-immunoprecipitation

Cells were cultured in 60mm dishes for 24 hours, until they were 70-80% confluent. If necessary, transient transfection was carried out as described above, and cells were allowed to grow in antibiotic free media for 24-36 hours. Cell treatment was carried out as above, and cycloheximide (20 μ M) was used in experiments with an incubation time of greater than one hour.

At the point of lysis, 350µl of ice-cold lysis buffer was used to lyse cells, which were scraped and incubated for 30 minutes on ice with occasional mixing. The lysates were centrifuged as above to clear cell debris and protein concentration determination carried out.

Lysates were rotated with 20µl washed Protein A/G beads for 30 minutes at 4°C in order to pre-clear the lysate, which was then spun down to remove the beads. The immunoprecipitation antibody was added to 300µl of lysate, containing identical amounts of protein (approximately 250-350µg of protein), and incubated overnight at 4°C with gentle shaking. Washed protein A/G beads were added for one hour, after which the supernatant containing unbound protein was aspirated off and stored at -20°C. Beads were washed with 500ul ice-cold HNTG buffer 3-4 times, and heated with 1.5x sample buffer at 95°C for 15 minutes, with bromophenol blue dye.

Equivalent volumes of lysates, both whole cell lysate and the immunoprecipitate sample, were loaded onto 5-7.5% Tris-glycine SDS- polyacrylamide gels and run as described above through to development.

2.2.8 Cell Proliferation Assay

Cell proliferation was assessed using Cell Proliferation Reagent WST-1 (Roche) as per the manufacturer's protocol. In order to test the effect of overexpression of various HER2 mutants, reverse transient transfection was carried out prior to assessment of proliferation. A DNA-Opti-MEM complex was made with Fugene 6 as described above, and was left to incubate for 30 minutes. Cells were trypsinised, and resuspended in Opti-MEM containing 5%FBS, at the appropriate concentration, as shown in Table X. The transfection mix was then added to the cell suspension, and cells were seeded at the densities described above. Proteins were allowed to express for 24 hours prior to commencement of the proliferation assay. A transient transfection efficiency of approximately 70% was achieved using this method.

Cells were cultured in 96-well plates, in a final volume of 100µl/well, at 37°C. 5 plates were set up; one each to be assessed at 0, 24, 48, 72 and 96 hours. Once cells had been transfected for 24 hours, media was changed to McCoy's full media, using a multi-channel pipettor. One 96-well plate was immediately removed for assessment of cell density using the WST-1 reagent at this point (0 hours), and inhibitors or ligand were then added. Media containing inhibitor or ligand was refreshed every 24 hours and a 96-well plate was assessed every 24 hours for the duration of the experiment. In order to assess a plate, 10µl of Cell Proliferation Reagent WST-1 was added to each well and the plate was returned to incubate at 37°C for 4 hours. The plate was then removed, shaken thoroughly on a shaker

for 1 minute and the absorbance of the samples measured on a microplate reader at 450nm. A control blank was included on all plates.

2.2.9 Antibodies and direct conjugation to fluorophores

Cells and tissues sections were stained with immunoglobulins (IgGs), labelled directly or indirectly with fluorophores. Antibodies were kindly conjugated to Cy-dyes or Alexa-dyes according to protocol (Fluorolink™) at pH 8.5 by Dr Gilbert Fruhwirth, as described previously. Briefly, un-conjugated dye was separated from the labelled antibody on a gel filtration column. A 10µl aliquot of the labelled antibody was diluted and absorption measured at 280nm and 489nm for Cy2, 280nm and 552 nm for Cy3, 280nm and 650 nm for Cy5 and 280nm and 558nm for Alexa 546. Antibodies conjugated are listed below.

The dye:protein final ratio was estimated by the following equations:

$$(\text{Cy2 D/P})_{\text{final}} = [1.13 (A_{489})] / [A_{280} - (0.15 \times A_{489})]$$

$$(\text{Cy3 D/P})_{\text{final}} = [1.13 (A_{552})] / [A_{280} - (0.08 \times A_{552})]$$

$$(\text{Cy5 D/P})_{\text{final}} = [0.68 (A_{650})] / [A_{280} - (0.05 \times A_{650})]$$

$$(\text{Alexa 546 D/P})_{\text{final}} = [1.64 (A_{558})] / [A_{280} - (0.12 \times A_{558})]$$

where Ax is the absorbance at wavelength x. The final ratio of protein:dye was aimed for 1:3 for acceptor fluorophore (Cy3 or Cy5)-labelled protein, and the amount of dye (Cy2 or Cy3) used for labelling the donor protein was reduced accordingly to achieve a ratio of protein:dye of 1:1. Final dye/protein ratios are listed with the relevant antibodies below.

2.2.10 Conjugated antibodies

Customised rabbit monoclonal antibody raised against HER2, (epitope CTAENPEYLGLDV-CONH2)(Gibcochem) conjugated to Cy3 (D:P =1.5:1, used at 40µg/ml)

Anti-HER2 clone Ab17 mouse monoclonal antibody (Labvision) conjugated to Cy5 (D:P=3.5:1, used at 20µg/ml)

Anti-HER2 clone L26, mouse monoclonal antibody was a kind gift from Prof Yarden's lab, Rehovot, Israel, conjugated to Cy5 (D:P ratio=4:1, used at 10µg/ml)

Anti-HER2 clone N24 mouse monoclonal antibody (Labvision) conjugated to Cy5 (D:P ratio=3.8:1, used at 10 µg/ml)

Anti-HER2 Designed ankyrin repeat protein (DARPin) was a kind gift from Prof Kerry Chester, UCL, London, conjugated to Cy5 (D:P ratio=3:1 , used at 8µg/ml)

Anti-HER3 Clone H3.90.6 (YY) mouse monoclonal antibody, was a kind gift from Prof Yarden's lab, conjugated to Cy3 (D:P ratio=1.27:1, used at 1.36µg/ml)

Anti-HER3 M01, clone 2E9 mouse monoclonal antibody (Abnova), conjugated to Alexa-546 (D:P ratio=0.71:1, used at 10µg/ml)

Anti-HER3 MAB 3483 mouse monoclonal antibody (R&D), conjugated to Alexa-546 (D:P ratio=0.69:1, used at 10µg/ml)

Anti-HER3 RTJ2 mouse monoclonal antibody (Millipore), conjugated to Cy5 (D:P ratio=1.1:1, used at 10µg/ml)

Anti-HA mouse antibody, conjugated to Cy3 or Alexa-546 (D:P ratio=2.1:1, and 1.8:1 respectively used at 15µg/ml)

2.2.11 Preparation of Cells for Imaging

Cells were washed in PBS, and fixed with 4% PFA for 20 minutes, washed 3 times in PBS, treated with fresh 0.1% sodium borohydride/PBS (1mg/ml) for 3 minutes to reduce background autofluorescence, washed 3 times in PBS, followed by distilled water, and mounted onto standard glass microscope slides using 8ul of Mowiol/DABCO (antifade) mounting medium. Sections were allowed to solidify overnight at room temperature and then sorted at -20°C.

Samples for immunofluorescence were treated as above, but with the addition of 0.1% Triton-X for 10 minutes, after fixation with PFA, blocking with 1% BSA solution for 30 minutes followed by incubation with the conjugated antibody, diluted in blocking buffer, for 4 hours in the dark, or with the unconjugated antibody for an hour, and the secondary antibody for 45 minutes.

2.3 Formalin-fixed, paraffin-embedded & fresh frozen resources

2.3.1 Cell pellets

In order to translate the dual-antibody based HER2-HER3 assay from application in vitro, on mammalian cell lines, to human tissues, either fresh frozen or formalin-fixed paraffin embedded (FFPE), a block of cell pellets were made in order to test the fluorophore-conjugated antibodies prior to application in human tissue. SK-BR-3 cells, which

endogenously express high levels of HER2 protein, were used to make cell pellets. These cells were also transiently transfected with HER3-HA in a subset of pellets (SK-BR-3-HER3HA) in 15cm dishes as described above.

Two 15cm dishes were seeded per pellet, for 24-36 hours, until fully confluent. Cells were serum starved overnight, and neuregulin treatment was applied for 15 minutes prior to fixation. At fixation, media was aspirated off, and cells washed with 20mls of PBS, twice. Sterile cell scrapers were used to scrape off the cells. 10mls of PBS was added to each dish and mixed in the dish to form a cell suspension, which was transferred to a 50ml centrifuge tube. Cells were spun down for 5 minutes at 200g to form a pellet. Supernatant was then aspirated off, and the cell pellet was resuspended in 15mls of neutral buffered formalin. The cells were left to rotate with formalin for one hour at room temperature.

The fixed cells were then taken to the Breast Tissue & Data Bank for further processing. The cells were spun down once again at 200g for 5minutes to re-form a pellet, and the supernatant was decanted. The bottom of the Falcon tube was cut off using a scalpel, just above the cell pellet. The pellet was then carefully removed from the Falcon and placed in speciwrap containing a few drops of formalin. The speciwrap was folded to fit inside a biopsy cage, and then placed in a cassette with lid. It was processed overnight, as standard, dehydrated in a series of alcohols and xylene, followed by embedding in molten paraffin wax, and held at no more than 60°C until the next morning.

2.3.2 Breast Tissue & Data Bank

The Guy's and St Thomas'/King's College London Breast Tissue and Data Bank (GSTT/KCL BTDB) is a Human Tissue Authority licensed tissue bank which has been banking breast tissue and clinical data on patients over the last 30 years. The Tissue Bank maintains over 7200 FFPE primary tumours, 2500 fresh frozen tumours and 900 matched tumour and blood DNA samples, all of which are associated with prospectively acquired pathological and clinical data. This invaluable resource is ideal for the validation of potential biomarkers. The production of tissue microarrays (TMAs) has allowed organisation of breast tumour tissue cores from hundreds of patients, into several blocks, upon which biomarkers may be tested in a high-throughput fashion, whilst avoiding significant depletion of tissue resources. Typically each TMA will contain a reference core of renal tissue, with all other tumour cores, numerically coded and linked to clinical outcome data. A typical core is 10mm in diameter; approximately 80 cores are embedded in one TMA block. Sections from TMA blocks were cut at a thickness of 3-5µm for the purposes of imaging within this project, and mounted on charged glass slides. FFPE tissue requires dewaxing and antigen retrieval prior to

processing for standard immunohistochemistry or fluorescence lifetime imaging. The FFPE cell pellets described above were processed in an identical manner prior to imaging.

2.3.3 METABRIC cohort/dataset

The METABRIC (Molecular Taxonomy of Breast Cancer International Consortium) project represents a cohort of patients who were recruited from 1989 and 2002 from 5 cancer centres across Canada and the UK, including Guy's & St Thomas' NHS Trust Hospitals, Cambridge Breast Unit, Addenbrooke's Hospital, Nottingham University City Hospital in the UK and the Tumour Bank of British Columbia, Vancouver and the Manitoba Tumour Bank in Canada¹⁹⁴. The cohort selection criteria entailed female patients with primary breast cancer, who had not had neoadjuvant treatment and had been followed-up for more than 5 years. METABRIC has been approved by the 'NHS National Research Ethics Service, Cambridgeshire 4 Research Ethics Committee' with reference number: 07/MRE05/35.

The aim of this project was to collect clinical and genomic data on breast tumour in order to create a robust taxonomy based upon molecular signatures as well as clinical parameters, thus allowing optimisation of adjuvant treatment. Patients were recruited chronologically but into 3 groups: lymph node negative (no chemotherapy), lymph node positive and ER positive (hormone +/- chemotherapy) and lymph node positive but ER negative (chemotherapy alone).

Clinical parameters such as metastasis to lymph nodes and presence of hormone receptors have been used to decide on adjuvant treatment regimes, i.e. whether chemotherapy or hormone therapy, respectively, is required after surgery, as described in Chapter 1. This project aimed to analyse 2000 tumours by using a combination of high resolution array-CGH, expression profiling, sequencing and tissue microarray analysis, and correlate the molecular profiles obtained with the clinical outcome of the tumours. The clinical data collected included survival data, date and cause of death, treatment information and hormone receptor status, e.g. ER, PR and HER2 status. The data used in **Chapter 5** relates to the subset of patients which were recruited at Guy's and St. Thomas' Hospital, for whom tumour samples were stored in the GSTT/KCL BTDB. This sample set consisted of approximately 200 patients. Prof Sarah Pinder and Mr John Brown kindly marked original FFPE donor tissue blocks and used them to make TMAs, respectively, for high throughput analysis.

2.3.4 Immunohistochemical staining of FFPE samples

FFPE samples were baked at 56°C overnight, followed by normalisation room temperature. Dewaxing was then carried out by immersing slides in xylene for 7.5 minutes twice, followed by absolute ethanol twice for 5 minutes each, 70% ethanol for 5 minutes and washing in

distilled water for 3-5 minutes. Distinct methods of antigen retrieval were used within this project, depending upon the antibody used.

In the case of HER2 or HER3 antibody use, heat mediated antigen retrieval was used. This entailed heating within Coplin jars in a waterbath at 95-98°C for 40 minutes(+/-1minute) or in the Leica Bond Antigen retrieval system on a hot plate to 110°C for 25 minutes, with DAKO Hercep Epitope retrieval solution in both cases. Epitope Retrieval Solution 2 contains an EDTA based buffer and surfactant. Slides were immediately cooled for 20 minutes, transferred to wash buffer for a minimum of 10 minutes and then processed for IHC.

For IHC the following steps were taken, either manually or automated within the Leica Microsystems' Bond-max™ fully automated staining system:

Slides were incubated with the primary antibody of interest, diluted in Bond Primary Antibody Diluent, which contains Tris-buffered saline, surfactant, protein stabilizer and 0.35% ProClin 950 (active ingredient is the biocide, 2-methyl-4-isothiazolin-3-one), for 30-40 minutes. This was followed by incubation with Envision peroxidise-blocking reagent for 5 minutes, Envision horseradish peroxidise (HRP) for 30 minutes, DAB/Peroxide label for 5 minutes, and DAB enhancer for 5 minutes. A light Haematoxylin counterstain was applied and sections dehydrated, cleared and mounted using Eukitt mounting medium.

2.2.4 Preparation of pellets and FFPE tissue for FLIM imaging

FFPE tissue or cell pellets underwent dewaxing and antigen retrieval as described for IHC. Sample borders were demarcated with a wax pen, and samples were washed 3 times with TBS, followed by incubation with 0.1% sodium borohydride in TBS, to quench autofluorescence, followed by a further 3 washes with TBS. Slides were blocked with filtered 1%BSA in TBS, followed by incubation with the fluorophore-conjugated antibody of interest, diluted in filtered 1%BSA in TBS, overnight at 4°C. Slides were then washed 3 times with TBS, for 5 minutes each time, followed by distilled water. Coverslips were applied with Mowiol medium containing DABCO and left for at least 6 hours at room temperature prior to transfer to -20°C for storage.

2.4 Structural modelling

I collaborated with Prof Franca Fraternali and Dr Flavia Autore who carried out the structural modeling and created the model of the lapatinib-bound HER2:HER3 dimer. Briefly, they modeled the HER2:HER3 dimer by comparative homology modelling using a multiple templates approach. To build the HER1-like dimer they used the crystal structure of the

HER1 homodimer (PDB 3GT8)¹⁹⁵, the crystal structure of HER1 complexed with imatinib (PDB 1XXK)¹⁹⁶ and only one chain of the crystal structure of the HER3 homodimer (3KEX)¹⁹⁷. To build the HER3-like dimer they used the HER3 homodimer structure (3KEX), the crystal structure of HER1 imatinib bound (PDB 1XXK) and the crystal structure of the inactive HER1 AMP-PNP bound (2GS7)¹⁹⁵. The sequence alignment used to build the model has been created by using PRALINE with the homology-extended alignment strategy¹⁹⁸. They generated three-dimensional models using the MODELLER package¹⁹⁹. The selected model was chosen on the basis of the MODELLER objective function's discrete optimized protein energy (DOPE) score.

2.5 Microscopy

2.5.1 Confocal microscopy

Images were acquired on a confocal laser scanning microscope (model LSM 510 meta, Carl Zeiss Inc.) using a 63X/1.4Plan-APROCHROMAT oil immersion objective. Each image represents a single section in the Z-series, taken across the depth of the cell in 0.5µm intervals.

2.5.2 Multiphoton Fluorescence Lifetime Imaging

Time-domain FLIM was performed with an in-house developed multiphoton microscopy system. The FLIM instrument was based around an inverted epi-fluorescence microscope (Nikon TE2000 including 100W mercury lamp). The light source was a solid-state-pumped (8-W Verdi, Coherent), femtosecond self-modelocked Titanium-Sapphire (Mira, Coherent) laser system. Fluorescence lifetime imaging capability was incorporated with addition of time-correlated single photon counting (TCSPC) electronics (Becker & Hickl, SPC 700).

Imaging data was collected with typical data comprising 256x256 pixel resolution and 256 time channels, in 117 frames over 300 seconds. This arrangement facilitates analysis using multi-exponential decay models. A 40x oil immersion objective (Nikon) was used throughout multiphoton imaging. Epifluorescence images of GFP, RFP, Cy3, Alexa-546 or Cy5 in the same image field, were acquired prior to FLIM.

2.5.3 Single Photon Fluorescence Lifetime Imaging (Galileo)

The single photon imaging platform used was built in-house and based on a TE2000 fluorescence microscope with a Nikon 20x air objective (Nikon, Kingston upon Thames, UK) and a CCD camera for detection of fluorescence. Fluorescence excitation is provided by a 553nm emitting laser diode (BDL-473_SMC, Becker and Hickl) which generates optical

pulses with a duration of 40ps at a repetition rate of 80MHz. Fluorescence lifetime imaging capability was incorporated with addition of a PMT detector (PMH-100, Becker and Hickl) and time-correlated single photon counting (TCSPC) electronics (SPC830, Becker & Hickl). Single photon, time-resolved fluorescence is detected at $593\pm 10\text{nm}$ using a photomultiplier tube (PMH-100, Becker and Hickl) with a 200ps time resolution and 20x (NA0.5) objective. Automated operation is achieved by incorporating a motorized microscope stage (Märzhauser GmbH, Wetzlar, Germany), a closed-loop objective lens mount with a $500\mu\text{m}$ range of travel (Piezosystem Jena GmbH, Jena, Germany) and a motorized filter cube selector.

2.6 Analytical Methods

2.6.1 FLIM/FRET Analysis

The FLIM images obtained with our lifetime microscope were batch analysed by a PC workstation running in-house exponential fitting software (TRI2) written in CVI by Dr Paul Barber, based on the Levenburg-Marquardt algorithm with instrumental response iterative reconvolution capabilities²⁰⁰. This program outputs files where all the fitting parameters are recorded for each images pixel into Excel format. These files are then analysed to produce a distribution of lifetime, and an average lifetime, from which FRET efficiency can be calculated using the following equation:

$\text{FRET}_{eff} = 1 - \tau(da)/\tau(d)$, where $\tau(da)$ is the fluorescent lifetime of the donor fluorophore, in the presence of the acceptore, and $\tau(d)$ is the fluorescent lifetime of the donor fluorophore alone.

All data was fitted with a single exponential decay analysis.

2.6.2 Survival analysis

Cox proportional hazard models were fitted using the 'survival' package²⁰¹ in R²⁰². Kaplan-Meier curves and logrank tests were also performed using the 'survival' package. All survival analysis was carried out in collaboration with Dr Katherine Lawler, bio-informatician, and created in R.

Chapter 3: Molecular determinants of the lapatinib-induced HER2:HER3 dimer

3.1 Introduction

3.1.1 Structural conformation of the HER family

The members of the HER family (HER1/EGFR, HER2, HER3 and HER4) are structurally composed of an extracellular ligand binding domain, a transmembrane (TM) region connecting the cytoplasmic juxtamembrane (JM) domain, a tyrosine kinase domain (TKD) and C-terminal tail with phosphorylation sites as described in **Chapter 1.4**. Here we review the structural details of the HER family members and their interactions with TKIs. Downstream signaling is reliant upon receptor dimerisation (ligand-dependent or -independent), allosteric activation and autophosphorylation (in *trans*)¹³⁴. Not only is the activation of the HER family dependent upon interaction with other partners and ligand control, but the structure of the receptor itself, imposes further constraints. An intramolecular tether between domains II and IV hold HER1, 3 and 4 in an auto-inhibited conformation^{203,204} whereby the C terminal tail of the receptor cannot be activated by the kinase in *cis*, unless the tether is removed, e.g. by conformational changes elicited on ligand binding. Although it has been proposed that HER2 exists in an activated form, Alvarado *et al* show that inhibitory interactions between domains I and III in HER2 may hold this receptor in a stronger auto-inhibitory state that HER1, with failure to form homo- or heterodimers in vitro¹²⁹.

Multiple crystal structures of the ECDs of HER1-HER4 have already been solved^{203,205} but our knowledge of the intracellular structures, especially for HER2 and HER3, is more limited. There is high sequence conservation, approximately 75% between HER2 and HER1 and 60% between the HER3 and HER1 TKDs¹⁹⁷ (**Figure 3.1**). The TKDs all adopt a typical bi-lobed folding. The N-lobe is mostly made up of β -strands with one α -helix whereas the C-lobe is mostly made up of α -helices. The lobes are separated by a deep cleft, which is the ATP binding domain. Access to this cleft may be manipulated by changes in orientations of the N- and C-lobes of the TKD, depending on the activation state²⁰⁶ or oncogenic mutations and can control access to TKIs as discussed further below. In order to understand the differential effects of anti-proliferative drugs upon the HER family, we must understand the

intricacies of receptor activation, including various methods of receptor dimerisation and the subtle conformational changes involved. HER1 dimerisation kinetics have been thoroughly investigated compared to HER2 or HER3. We first review the data on HER1 dimerisation as an aid to find tools to elucidate the HER2:HER3 heterodimer.



Figure 3. 1 Multiple sequence alignment of the kinase domains of the HER family

Residues conserved in all four members are highlighted in blue. The mutated residue I714 (HER2) that is part of the receiver interface is highlighted in yellow while the mutated residue V945R (HER3) at the activator interface is highlighted in green. The mutated residues inspired by the model assembly (I748, V750, N764 and K765 (HER2)) are marked in orange while the residues mutated at the ATP binding pocket (K742, G716 and G718 (HER3)) are marked in magenta. [JM-B = distal part of the juxtamembrane region (region B), P-loop = phosphorylation loop]

3.1.2 HER1 homodimerisation

Ligand-induced HER1 homodimerisation and allosteric activation have been well-established^{126,207}. The extracellular domain (ECD) of HER1 has been highly characterized using crystallographic studies^{131,208,209}, and the mechanism of ECD interaction during HER1 homodimerisation has been elucidated¹³¹. The EGF bound ECDs were found to be arranged in a back-to-back C shape with EGF binding between domain I and III. A hairpin from domain II of each receptor interacts with the other¹³¹.

3.1.2.1 Active vs inactive /asymmetric vs symmetric TKD dimer formation

Besides the ECD, the intracellular TKD is also important to HER1 dimerisation and TKD activity is further controlled by the JM domain^{195,210}. Studies of the TKD of HER1 have demonstrated the activation of HER1 by the formation of asymmetric dimers whereby the N-lobe of one kinase domain (donor or activator) stabilizes the C-lobe of the other (acceptor or receiver), as described in **Chapter 1.4.1**, and shown in **Figure 3. 2**¹⁴⁹. Within this asymmetric interaction, the receptor is in the 'active' conformation, with an α -C helix positioned so as to stabilize the dimer interface by creating a salt bridge between Lys721 and Glu738 (**Figure 3. 2**). The 'inactive' conformation consists of the α -C helix in the 'out' position and resembles the inactive Src/CDK2-like kinase¹⁸⁹. Symmetric or 'inactive' dimer formation is mediated by the N-lobes of both tyrosine kinase domains and both C-terminal tails are embedded in the interacting interface as shown in the N-lobe mediated HER1 inactive homodimer.

These conformations have also been established for HER3 and are likely conserved throughout the family of HER receptors¹⁹⁷. Dimers likely exist in the native state of the cell, as a mixture of the two types described. The balance between the numbers of active versus inactive dimers will dictate receptor activation, and is likely influenced by the type and structure of receptor, i.e. HER2 is the receptor most likely to engage with other active receptors, as well as the presence of ligands or inhibitors.

A third conformation of the HER1 TKD has been discovered recently, which is intrinsically disordered and resistant to dimerisation, thus regulating HER1 signaling²¹¹. Lapatinib binding kinetics are slower than expected as, according to this study, the predominant population of HER1 is in the disordered state rather than the inactive state. On examination of the HER2 kinase, the same level of intrinsic disorder was not found; this receptor has a more ordered, stable TKD dimer interface compared to HER1, and likely exists in the inactive form. This phenomenon may help to explain why HER2 is more readily recruited to the active dimer as it does not need to overcome the disordered state, as opposed to HER1.

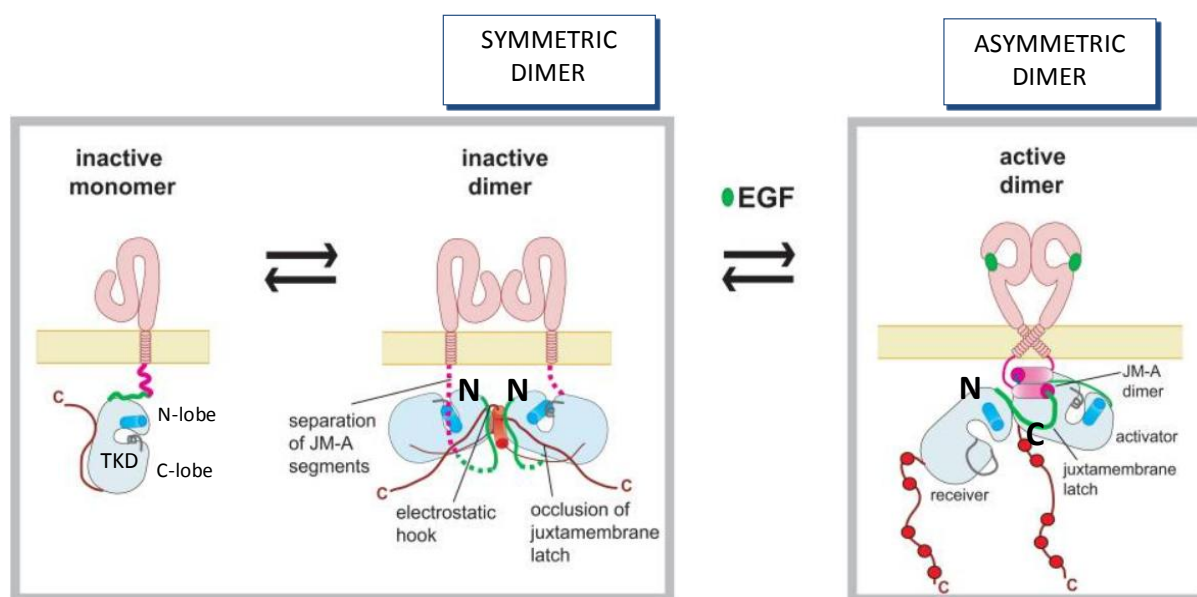


Figure 3. 2 Schematic diagram of the symmetric/inactive HER1 homodimer, vs the asymmetric/active homodimer¹⁹⁵

The TKD is shown interacting in an N:N lobe-mediated fashion for the inactive dimer and N:C lobe-mediated fashion for the active dimer. JM regions are demonstrated in pink (JM-A) and green (JM-B) and the α -C helix, as a blue cylinder. The C terminal tail is depicted in purple (C). Red dots on the asymmetric dimer depict phosphorylation of sites on the active dimer but are not present on the inactive dimer.

Zhang *et al* found that the core of the intracellular dimerisation site of two HER1 TKD monomers was dominated by hydrophobic interactions including I706 on one monomer (N-lobe of the kinase domain) and V948 from the other monomer (C-lobe of the kinase domain)¹⁴⁹. These residues are also known as I682 and V924, whereby the 24-residue membrane-targeting signal sequence is not included as it is deleted in the mature protein. The former annotation is used for all residues within this report. Mutations at either site led to dimer disruption. These sequences are highly conserved between HER1, HER2 and HER3, as shown in **Figure 3.1**. The C-terminal part of the JM domain, or the JM-B region (residues 697-709) is also involved in the asymmetric dimer interface¹⁴⁹. Oncogenic mutation within the highly-charged N-terminal region of the JM (JM-A) domain highlighted an alternative site within HER1 (V665) which was essential to stabilization of the homodimer^{195,212,213}. This mutation has been observed in lung tumours which display constitutive HER1 activation. V655N promotes the capacity of HER1 to act as an acceptor, releasing it from the auto-inhibited state, thus promoting cellular transformation²¹⁴. The capacity of single residue mutations to affect receptor behaviour demonstrates the importance of subtle conformational changes to receptor function, in part, by stabilising or disrupting receptor dimerisation.

We carried out site-directed mutagenesis at the N-lobe of HER2 TKD (HER2(I714Q)), equivalent to HER1(I706Q) and at the JM-B site (HER2(V697R)), equivalent to the HER1(V689R) to create two impaired 'acceptor' mutants in HER2. Due to the lack of critical N-lobe residues in HER3, this receptor may only act as a 'donor'. Hence site-directed mutagenesis was carried out at the C-lobe of HER3 TKD (HER3(V945R)) to create a 'donor' impaired mutant. These mutants were used as tools to unravel the integral mechanics of the intracellular HER2:HER3 dimer.

3.1.2.2 Full-length HER1 dimerisation

The majority of studies have shown allosteric HER1 activation by cell-based assays and isolated kinase domain measurements. The tools for studying full length receptor kinetics have only recently been developed, lending insight to the relevance of extracellular events to intracellular dimerisation and propagation of signaling, and vice versa. For instance, Wang *et al.* purified a near full length mutant HER1, which contains the L858R mutation that leads to disruption of the autoinhibited conformation²¹⁵. Additional mutations at the dimer interface were introduced (I706Q and V948R in the N- and C-lobes respectively), which demonstrated the critical contribution of this asymmetric dimer interface to HER1 kinase activity within the near full length receptor²¹⁵.

Furthermore, live imaging of full-length HER receptors allows the examination of dimerisation events and the ensuing kinetics. Quantum dot tracking has been used to visualize live homodimerisation events for HER1²¹⁶. Unoccupied receptors form transient homodimers, but ligand bound receptors form more stable, less mobile dimers which are spatially confined in microdomains, which may be regulated by the cell's actin cytoskeleton. Treatment with a HER1 kinase inhibitor enhanced receptor mobility compared to ligand-bound phosphorylated receptors, suggesting a role for activation in regulating mobility and further receptor interactions.

3.1.3 HER2 homo- and heterodimerisation

3.1.3.1. HER2 homodimerisation

Initial studies on HER2 homodimerisation focused on the TM region. HER2 homodimers formed of the TM domain may exist in one of 2 forms, determined by dimer formation between the N-terminal or the C-terminal²¹⁷. The C-terminal dimerisation motif is more stable and likely to represent the inactive state. However receptors may easily shift between the two conformations, thus regulating receptor dimerisation, activation and downstream

signalling. Fleishman *et al* propose that in cells overexpressing HER2, active dimers are more predominant because of a shift in the equilibrium with the inactive receptor dimer, partly mediated by interactions at the N-terminal of TM domain favouring the active dimer²¹⁷. An oncogenic mutation, V664E, found within the TM domain, favours this hypothesis^{218,219}. The polar, negatively charged glutamic acid (E) is likely to be exposed during C-terminal mediated dimerisation, thus destabilising these dimers and shifting the balance to active, N-terminus mediated dimers. Conversely, substitution of valine for a larger isoleucine at position 655 (V655I) may destabilise the dimer leading to a reduction in activation; a property which may explain the protective effects of the mutation against breast cancer²²⁰.

With regard to the intracellular dimerisation interface, Aertgeets *et al* first published the crystal structure of the HER2 TKD bound to a type I TKI, SYR127063²⁰⁶. The HER2 kinase domain is solved in an active conformation, which undergoes allosteric activation by homodimerisation, with the TKD forming an asymmetric, active dimer. This dimer is similar to that seen in HER1 homodimerisation (**Figure 3. 2**). They hypothesise that the increased flexibility in the α -C helix of HER2 compared to the rest of the HER family allows easier activation of partners, thus explaining why it is the preferred partner for heterodimerisation.

3.1.3.2 HER2 heterodimerisation

The HER2:HER3 hetero-dimer is believed to be the most active, efficiently driving downstream signaling pathways and cellular proliferation via the PI3K/AKT and MAPK pathways^{197,206}. Considering HER3-mediated PI3-kinase (PI3K) signaling has been shown to be vital to cell motility, invasion and metastasis²²¹, it is crucial to unravel the molecular factors relevant for this signaling pathway including dimerisation events. While the structural details for the HER1 homo-dimer are becoming increasingly refined^{215,216,222}, similar molecular information for the hetero-dimers is not yet available. Structural studies have demonstrated allosteric activation of HER2 either by homo-dimerisation or by heterodimerisation with HER1²⁰⁶ but the structural basis for the HER2:HER3 heterodimer has not yet been solved. The relative contribution of distinct dimer interfaces, e.g. TM vs TKD mediated, to the formation of heterodimers between HER2 and HER3 is also unknown. As previously described, HER3 can serve only as the donor or activator within this heterodimer^{149,197}. For example, dimerisation between TKD of HER1 and HER3 is in the asymmetric conformation, much the same as that described for HER1 homodimerisation¹⁹⁷. Mutation at the C-lobe TKD of HER3 (V945R) was shown to disrupt this 'asymmetric' dimer interface, and is used in our experiments to elucidate the structure of the lapatinib bound HER2:HER3 dimer.

Although HER3 is generally thought of as kinase-dead, Shi et al demonstrate a low level of HER3 kinase-mediated trans-autophosphorylation²²³. Sequence conservation and structural analyses demonstrate an intact ATP binding pocket is retained. A number of studies have recently highlighted the importance of nucleotide pocket occupation for regulating kinase domain conformation independent of kinase activity²²⁴⁻²²⁶. In the analogous case of STRAD, which like HER3 is a pseudokinase, an intact and occupied ATP binding pocket is critical for STRAD to activate the associated kinase LKB1 through a conformational mechanism^{227,228}. To investigate the importance of the HER3 TKD on heterodimer formation, a series of mutations were introduced to disrupt the HER3 nucleotide pocket on kinase domain conformation and HER2:HER3 pocket and nucleotide binding (K742MG716DG718D, or KGG). K742 is a highly conserved ATP coordinating residue throughout the HER family (**Figure 3. 1**) and this residue is most commonly targeted to generate kinase inactive mutants of active kinases. The introduction of positively charged residues into the conserved glycine rich loop (G716D and G718D) is additionally designed to repel the negatively charged phosphates of ATP and thus preclude binding.

3.1.4 HER3 homodimerisation

In the case of HER3 homodimerisation, Jura *et al* published the seminal paper solving the HER3 kinase domain structure as locked in the inactive conformation much like HER1 and HER4¹⁹⁷. Furthermore, HER3 forms an N-lobe mediated 'inactive' dimer within the crystal, which may be an auto-inhibitory mechanism whilst the receptor is not ligand bound (**Figure 3. 3A**). Within this conformation, the C-terminal tail may link dimers, forming a crystal lattice of concatamers, much like those seen with HER4 homodimers, which bury the dimerisation interface for HER3. One N-lobe dimer is connected to 2 other dimers via the C-terminal tail and the TKD C-lobes of the adjacent kinase domains (**Figure 3. 3B**). As the C-lobe of HER3 is always ready to engage in dimerisation with other members of the HER family, this method of oligomerisation may form an alternative regulatory mechanism to preserve HER3 in an inactive conformation in the native context.

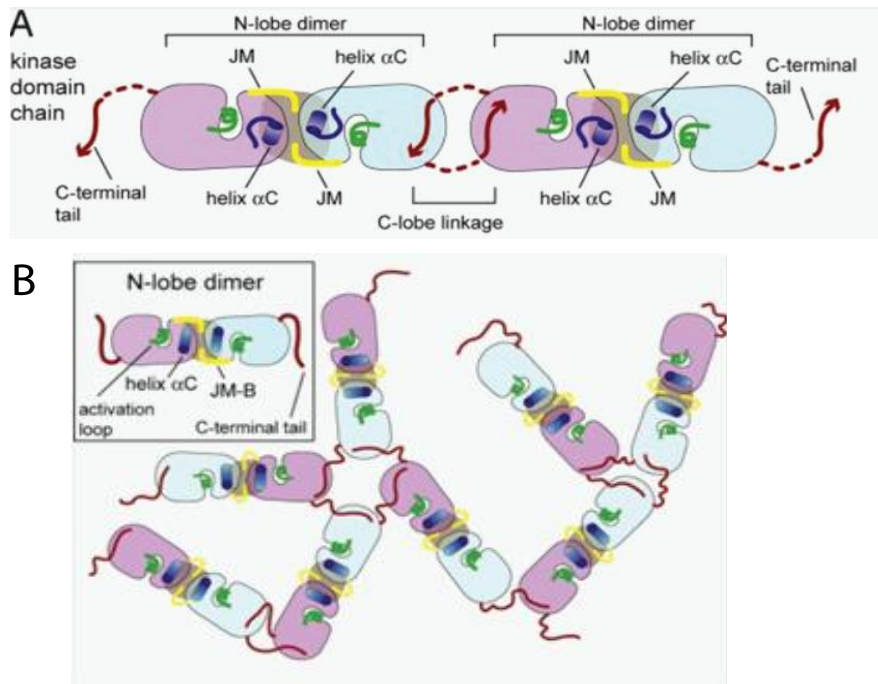


Figure 3.3 Schematic diagram showing HER3 homodimerisation and lattice formation¹⁹⁷

(A) Symmetrical inactive HER3 homodimerisation mediated by the N lobes of both tyrosine kinase domains.
 (B) Possible mechanism of HER3 oligomerisation mediated by the C-terminal tails and TKD C-lobe.

3.1.5 Tyrosine kinase inhibitors

The clinical use of TKIs has been outlined previously (**chapter 1.5.2**). We now focus on the structural interactions of these drugs with HER1, 2 and 4. **Table 1** illustrates the inhibition constants or IC_{50} for those TKIs mainly in current clinical use, alongside their crystal structures. Lapatinib is the most potent inhibitor of HER2 compared to any of others listed. This effect may be related due to the binding mode of lapatinib (see below, **3.1.5.1 Type I vs II TKIs**) and the likely existence of HER2 in the native inactive conformation²²⁹. Although clinical doses of erlotinib and gefitinib classically do not inhibit HER2, the inhibition constants demonstrate that these drugs may be effective at higher doses²³⁰. A high dose of erlotinib (40 μ M) is used in our experiments, alongside canertinib, in order to compare the effects of type I and type II TKIs as described below. Considering HER3 is a catalytically inactive pseudokinase, no information is available on whether HER3 binds TKIs and it is presumed for our purposes that lapatinib does not bind to HER3.

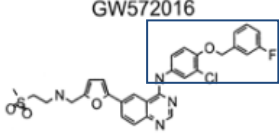
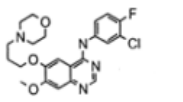
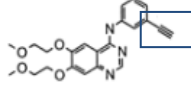
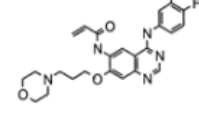
	HER1	HER2	HER4	
 GW572016 ZD 1839	Lapatinib	3nM	13nM	347nM
 OSI-774	Gefitinib	0.4nM	870nM	1.1μM
 CI-1033	Erlotinib	0.7nM	1.0μM	1.5μM
	Canertinib*	30nM	127nM	388nM

Table 1 Inhibition constants (K_i) for type I (gefitinib, erlotinib, canertinib) and type II (lapatinib)¹⁸⁹

*Canertinib is a covalent modifier, so K_i values are not appropriate measures of potency. For this compound the IC₅₀ values are given. Blue boxes highlight a bulky 3-fluorobenzyl-oxy group in lapatinib and an acetylene group in erlotinib which bind differentially to TKIs and lead to the preference for erlotinib for the active formation of HER1 compared to lapatinib which binds the inactive receptor.

3.1.5.1 Type I vs II TKIs

Tyrosine kinase inhibitors (TKIs) of the HER family may bind to the receptor in an active-like (type I) or inactive-like (type II) conformation, as defined by the arrangement of the α -C helix activation loop^{149,189,190,231-233}. Type II inhibitors bind to the ATP cleft and an adjacent hydrophobic pocket created by the activation loop (containing the conserved DFG motif) in a 'DFG-out' conformation. For instance, the aromatic rings of erlotinib position the drug so that the acetylene group (highlighted with a blue box in Table 1) is directed into the ATP binding pocket when the receptor is in the active conformation¹⁹⁰. In the case of lapatinib, a bulky 3-fluorobenzyl-oxy group (highlighted with blue box in Table 1) requires accommodation within an extra hydrophobic pocket, which is only created when the α -C helix is in an outward position, in the inactive conformation¹⁸⁹. When the kinase domain is in the active conformation, steric clashes occur between the α -C helix and the fluorobenzyl-oxy group, causing lapatinib to bind preferentially to the inactive conformation. Crystallization studies have demonstrated binding of all type II inhibitors to a non-phosphorylated kinase, with the activation loop in the afore-mentioned position, whereas type I TKIs are insensitive to the phosphorylation state of the kinase.

Lapatinib is a potent reversible type II TKI of HER1 and HER2, with a prolonged drug off rate compared to type I TKIs such as gefitinib or erlotinib¹⁸⁹. We have shown the effect of Type I TKIs on HER family dimerisation by inducing HER1 homo-dimerisation (**Figure 3.4**)²³⁴. Although, lapatinib was not shown to stabilize HER1 homo-dimers in this study, it is likely that, as type I and type II TKIs recognise different native kinase conformations, this confers differential effects on the distinct HER family receptors^{189,232,233}. Lapatinib may affect HER2:HER3 dimer stability by exerting allosteric effects on the intracellular dimerisation sites of the inactive receptors. Whether this reflects the effect of phosphorylation upon dimer assembly is not clear. Although separate crystal structures for the HER2 and the HER3 kinase domains are available, a structure for the (lapatinib-bound) hetero-dimer does not exist^{235,236}.

3.1.5.2 Oncogenic mutations

The HER2 TKD has been shown to be held in an inactive conformation, partly by bonds between the α -C helix and a β 4-sheet within the TKD²²⁹. Oncogenic mutation of Gly residues within this critical region (e.g. 776 and 778) have been discovered, most frequently in patients with lung cancer and lead to receptor activation and decreased sensitivity to lapatinib. A small number of breast tumours also contain HER2 TKD mutations but their relevance to treatment is unknown²³⁷. Furthermore, the HER2 G776 YVMA insertion (herein referred to as HER2(YVMA)), one of the commonest found in lung cancer, was demonstrated to lead to higher levels of HER2 phosphorylation, transactivation of kinase-dead HER1, and resistance to TKIs targeting HER1²³⁸⁻²⁴¹. This insertion is at the C-terminal end of the α -C helix in the TKD. It is proposed that the conformational change induced by this insertion narrows the ATP binding cleft and increases kinase activity²⁴². We have generated this mutant in order to determine its effect on HER2 dimerisation and to test whether it can compensate for an incompetent partner ATP pocket in HER3.

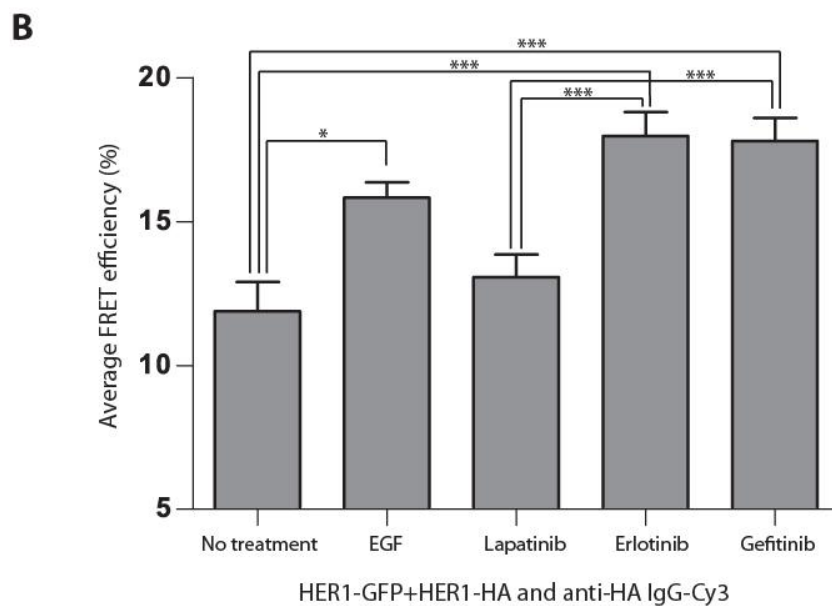
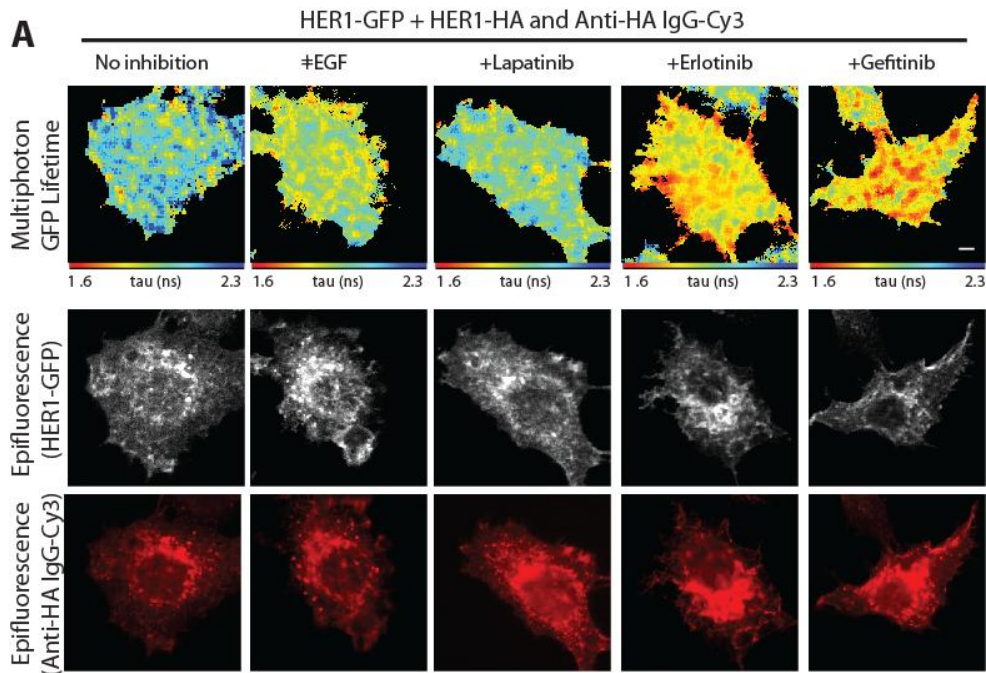


Figure 3. 4 FRET/FLIM analysis reveals that erlotinib and gefitinib, but not lapatinib, induce dimerisation of HER1

A) MCF-7 cells were transfected with vectors encoding HER1-mGFP and EGFR-HA. Cells were incubated for 24 h, serum starved for 1 h, and stimulated with EGF (50 ng/ml) for 1 h. Alternatively, cells were treated with lapatinib, gefitinib, or erlotinib as indicated (10 μ M) for 1 h, prior to fixation and staining with an anti-HA antibody conjugated to Cy-3. Scale bars = 5 μ m. B) Cumulative histogram of FRET efficiency between HER1-mGFP and HA-Cy3 (bound to HER1-HA) calculated with the following equation in each pixel and averaged per cell: FRET efficiency = 1 tau (da)/tau (control), where tau (da) is the lifetime displayed by cells co-expressing both HER1-mGFP and HER1-HA stained with an anti-HA IgG-Cy3, whereas tau (control) is the mean HER1-mGFP lifetime measurement in the absence of the Cy3 acceptor. Data were obtained from 4–11 cells/treatment group and are representative of 2 independent experiments. Values of p are <0.001 (***) and <0.05 (*) according to analysis of variance with post hoc testing with Tukey-Kramer's multiple comparison test.

3.2 Results

3.2.1 Optimisation of HER2-HER3 cell-based assay

Initially a FRET-FLIM cell based assay for the quantification of HER2:HER3 dimerisation was established and optimised. Although a direct protein interaction (nanometer (nm) proximity) between HER2 and HER3 can be inferred by co-precipitation experiments²⁴³, it has not formally been demonstrated by, e.g. FRET/FLIM. To investigate the spatial distribution of the HER2: HER3 complex in situ, we monitored Förster Resonance Energy Transfer (FRET) between HER2-EGFP and HER3-HA (stained with anti-HA IgG conjugated to Cy3), or HER3-RFP using fluorescence lifetime imaging microscopy (FLIM) which is a gold standard technique for measuring protein proximity within the typically <10nm range.

As the fluorophores themselves may cause steric hindrance, disrupting protein-protein interactions, optimisation involved the testing of two different types of FRET/FLIM assay:

Use of two fluorophore-fusion proteins measuring FRET between HER2-EGFP and HER3-mRFP or

Use of one fluorophore-fusion protein and one fluorescently conjugated antibody measuring FRET between HER2-EGFP and anti-HA igG-Cy3, bound to HER3-HA.

EGFP and RFP have a molecular weight of 26kDa and 30kDa respectively. Thus steric hindrance may occur between these fluorophores. However, the molecular weight of haemagglutinin (HA) is less than 10kDa, which may allow better stoichiometry for antibody binding and for FRET to occur between Cy3 and GFP. **Figure 3. 5** demonstrates a small but significant improvement in mean FRET efficiency detected between HER2-GFP and HER3-HA (detected with anti-HA IgG-Cy3) from 4% to 6.22%. Therefore, where available, HER3-HA tagged constructs were used for assessment of HER2:HER3 dimer formation.

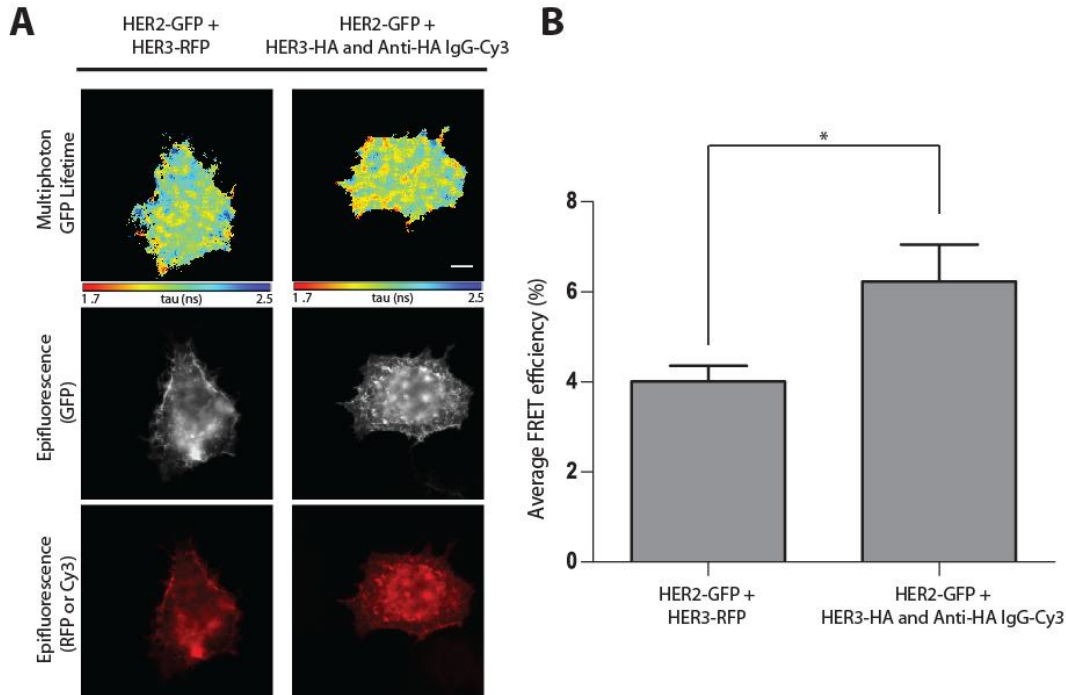


Figure 3.5 Optimisation of HER2:HER3 dimerisation cell based FRET assay

(A) MCF-7 cells were transfected with HER2-EGFP and HER3-mRFP or HER3-HA for 24 hours prior to fixation and staining with anti-HA IgG-Cy3. Scale bars = 5 μ M. (B) Cumulative histogram of FRET efficiency, calculated as described above. Data were obtained from 8-9 cells per condition, p value = 0.033 using the unpaired student's T-test.

3.2.2 Stabilisation of HER2:HER3 dimers on lapatinib treatment

We measured direct receptor-receptor interactions by FRET¹ to determine heterodimerisation of HER2-GFP and HER3-HA in the presence of lapatinib, high-dose erlotinib, canertinib, or the ligand, neuregulin (NRG1) (**Figure 3. 6**). Ligand treatment resulted in a two-fold increase of FRET efficiency between HER2 and HER3. This effect is consistent with published data demonstrating neuregulin-dependent regulation of HER2 oncogenic signalling^{184,244-246}. Lapatinib treatment induced stabilisation of the HER2:HER3 heterodimer to a higher extent than NRG1; a further 1.5-fold increase compared to the NRG1 effect (**Figure 3. 6B**). Treatment with the type I TKIs, erlotinib and canertinib, however, induced a much lower level of dimerisation compared to the type II TKI, lapatinib. This effect was comparable to the NRG1 effect alone. Within the type I TKI group, there was no significant difference between HER2:HER3 dimerisation induced by erlotinib or canertinib. A small but significant increase in dimerisation was noted on comparison of untreated cells, and those treated with type I TKIs (p<0.05 according to one-way ANOVA). These results indicate that HER2:HER3 dimers are stabilised by lapatinib inhibition, to a greater effect than ligand treatment or treatment with type I TKIs.

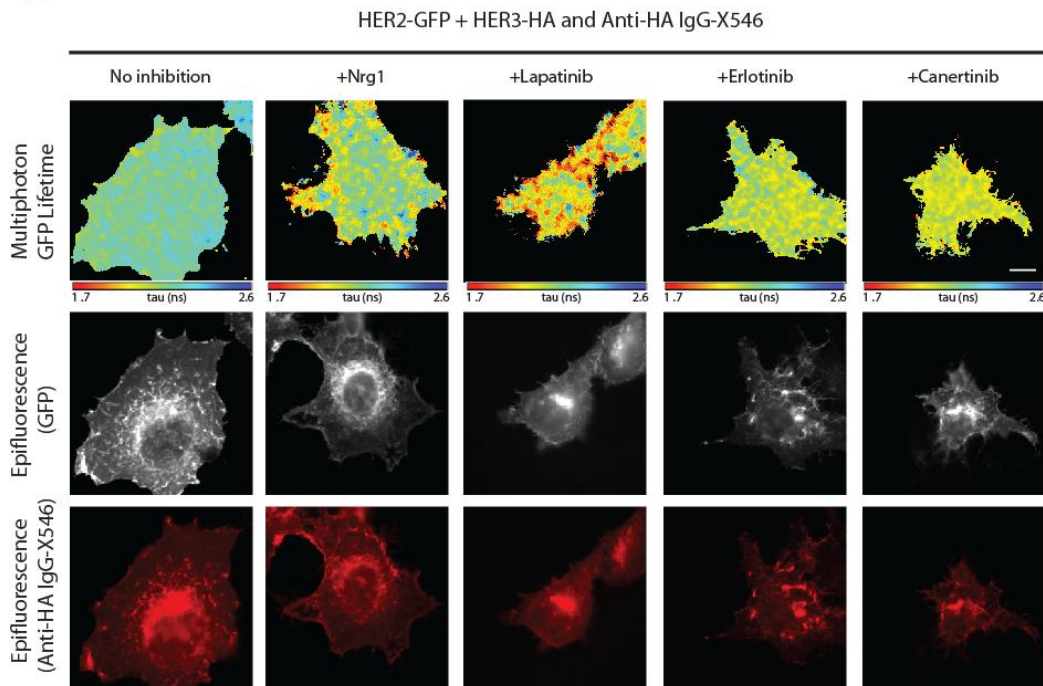
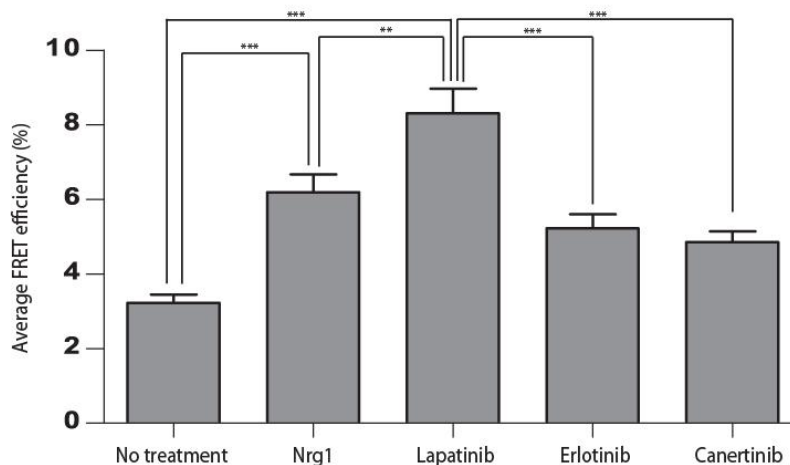
A**B**

Figure 3. 6 Dimerisation of HER2 and HER3 induced by lapatinib, demonstrated by FRET/FLIM analysis.

(A) MCF-7 cells were transfected with vectors encoding HER2-GFP and HER3-HA. Cells were incubated for 24 hours, serum starved for 1hour, and stimulated with NRG1 (50ng/ml) for 15 minutes, or inhibited with lapatinib (10 μ M), erlotinib (40 μ M), or canertinib (10 μ M) for 1 hour, prior to fixation and staining with anti-HA antibody conjugated to Alexa-546 (X546). A high dose of erlotinib was used in order to circumvent the lower IC50 of erlotinib for HER2 compared to lapatinib. Scale bars represent 5 μ m. (B) Cumulative histogram of FRET efficiency between HER2-GFP and HA-Alexa546 (bound to HER3-HA) calculated with the following equation in each pixel and averaged per cell: $FRET\ eff = 1 - \tau(DA) / \tau(control)$ where $\tau(DA)$ is the lifetime displayed by cells co-expressing HER2-GFP and HER3-HA stained with anti-HA IgG-Alexa546, whereas $\tau(control)$ is the mean HER2-GFP lifetime, measured in the absence of the Alexa-546 acceptor. Cumulative histogram of average FRET efficiency from 3 independent experiments. Results have been merged ($n > 40$ cells/condition) with error bars representing standard error of the mean (SEM). Values of p are < 0.001 (***) and < 0.01 (**) according to analysis of variance (ANOVA) with post hoc testing with Tukey-Kramer's multiple comparison test.

3.2.3 Disruption of HER2:HER3 dimerisation by site-directed mutagenesis of the juxtamembrane domain of HER2 and the kinase domains of HER2 and HER3

In order to examine the importance of the internal dimerisation site on HER2:HER3 dimerisation, we over-expressed the 'acceptor' impaired mutants, HER2(I714Q)-GFP (N-lobe kinase domain), and HER2(V697R)-GFP (JM region) and the 'donor' impaired mutant HER3(V945R)-RFP in MCF-7 cells with the wild-type partner. FRET analysis showed a reduction in lapatinib-induced dimerisation between HER2 and HER3, with the HER2 'acceptor' impaired mutants, HER2(I714Q) and HER2(V697R) (**Figure 3. 7**). Although there was a trend to a reduction in FRET efficiency in baseline dimer formation between HER2(I714Q)-GFP or HER2(V697R)-GFP versus wild-type HER2-GFP and HER3-HA (coupled to anti-HA IgG-Cy3) for untreated cells, this was not significant when analysed by ANOVA (for multiple comparisons across the groups). However analysis by student's T-Test demonstrated a significant decrease in dimer formation in untreated cells transfected with HER2(I714Q)-GFP ($p=0.0436$) or HER2(V697R) ($p=0.0171$), compared to dimer formation with the wild-type receptors.

These results suggest that within the lapatinib-induced HER2:HER3 dimer, the N-lobe of the HER2 kinase domain and the HER2 JM domain may play a central role in dimer formation. Mutations at these sites may also impair dimer formation in untreated cells, but to a much lower extent.

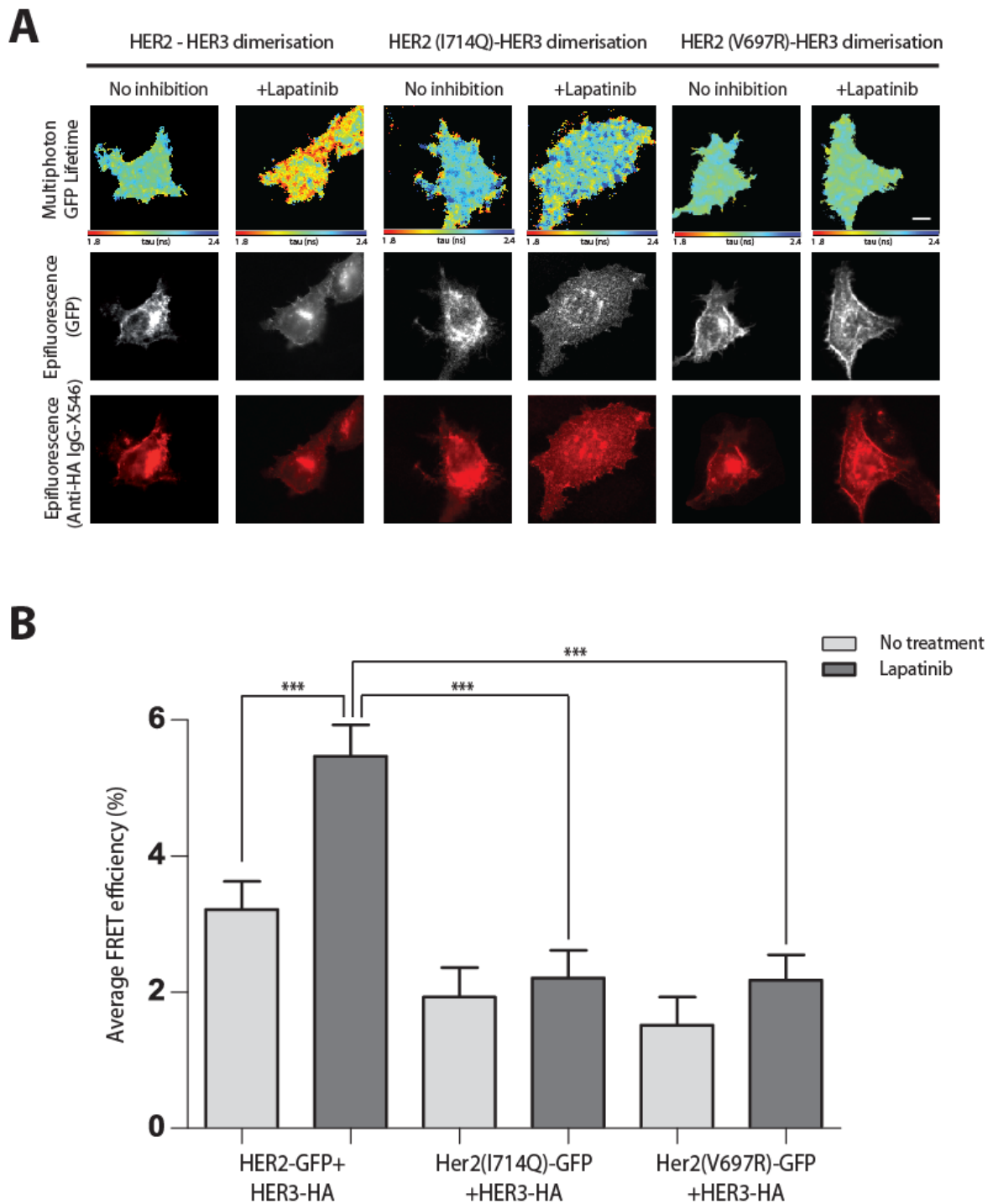


Figure 3. 7 Lapatinib induced dimerisation of HER2 and HER3 may be disrupted by mutation at the internal dimerisation site of HER2 (HER2(I714Q)) or at the juxtamembrane domain (HER2(V697R))

(A) MCF-7 cells were transfected with vectors encoding HER2-GFP (either wild type, or the N-terminus TKD mutant HER2(I714Q), or the JM mutant HER2(V697R)) and HER3-HA. Cells were incubated for 24 hours, and inhibited with lapatinib (10 μ M) for 1 hour, prior to fixation and staining with anti-HA antibody conjugated to Alexa-546. Scale bars represent 5 μ m. (B) The cumulative histogram of FRET efficiency between HER2-GFP and HA-Alexa546, bound to HER3-HA, calculated as described above, from 3 independent experiments, is shown (n>40cells/condition). Values for p are <0.001(***) according to one-way ANOVA with Tukey's post-hoc test.

This hypothesis was further tested by mutation of the C-lobe TKD residue in HER3(V945R), a 'donor' impaired mutant (**Figure 3. 8**). These cells were treated with NRG1 as well as lapatinib, in order to determine the effect of C-lobe mutation upon dimerisation within a ligand-activated asymmetric dimer (**Figure 3. 2**) as opposed to the lapatinib-induced dimer. Mutation at the HER3 C-lobe TKD (HER3(V945R)-RFP) did not attenuate the lapatinib effect, demonstrating a significant near-two fold increase in HER2:HER3 dimerisation with the TKI. However, NRG1-mediated HER2:HER3 dimerisation was significantly reduced on transfection of the 'donor' impaired HER3(V945R)-RFP mutant, when compared to wild-type (**Figure 3. 8**). The extent of heterodimerisation was reduced to the same level as that seen with untreated cells, transfected with HER3(V945R)-RFP.

This finding supports the model of a ligand-induced, asymmetric HER2:HER3 dimer, mediated by interaction between the N and C lobes of the kinase domain of HER2 and HER3, respectively (**Figure 3. 2**), which is disrupted by mutation of the C-lobe of HER3 TKD(HER3(V945R)). This seems to be in contrast to the lapatinib (type II TKI) induced dimer which is disrupted by mutation at the N-lobe of HER2 and HER3 TKD but not at the C-lobe of HER3 TKD. As lapatinib binds to HER2 in the inactive form, it is likely to induce formation of the inactive dimer, potentially mediated by interactions between the N-lobes of the HER2 and HER3 TKDs, resembling the symmetric dimer in **Figure 3. 2**.

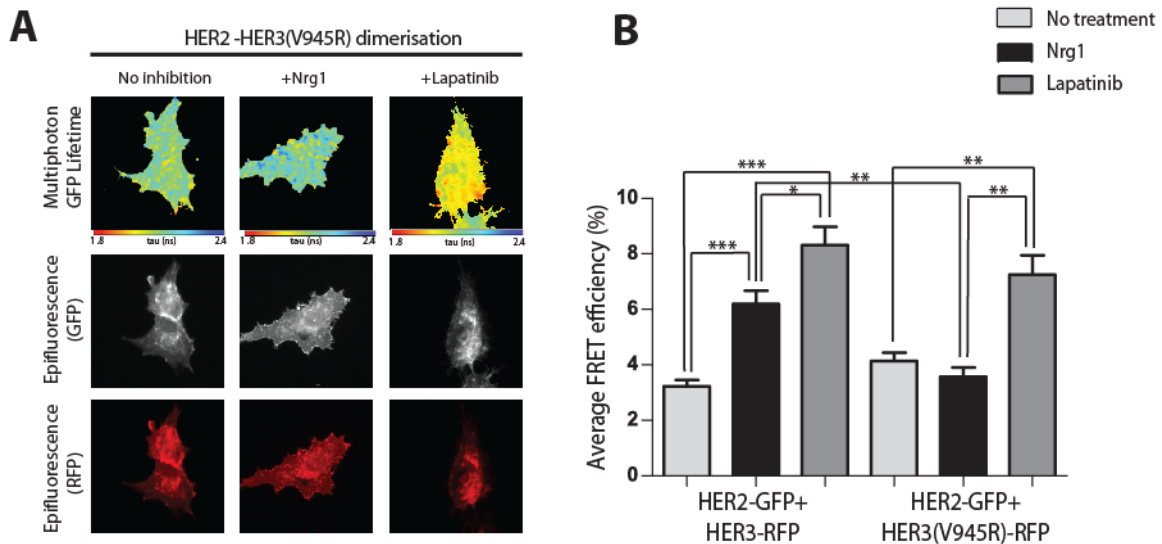


Figure 3. 8 Effect of mutations at the C-lobe of HER3 TKD upon ligand-induced and lapatinib-induced HER2:HER3 dimerisation

(A) MCF-7 cells were transfected with vectors encoding HER2-GFP and HER3-RFP, either wild type or C-lobe TKD mutation; HER3(V945R). Cells were incubated as described above, and treated with vehicle, lapatinib or NRG1 prior to fixation. Scale bars represent 5 μ m. (B) Cumulative histogram of FRET efficiency between HER2-GFP and wild-type or mutant HER3-RFP, from 3 independent experiments (n=18-47 cells/condition). Values for p are <0.001(***), <0.01(**) and <0.05(*).

3.2.4 HER3 ATP binding pocket competency is required for HER2:HER3 dimerisation

Mutation at the ATP binding site of HER3 completely abolished FRET between HER2-GFP and anti-HA IgG-Alexa 546 bound to HER3-HA (**Figure 3. 9**) implying a critical role for the HER3 ATP pocket in HER2:HER3 dimerisation. Lapatinib did induce very low levels of dimerisation with wild-type HER2 in this case (14% of that shown by wild-type HER3). These data imply that the conformation and/or occupation of the HER3 nucleotide pocket is critical for stable dimerisation with HER2. An analogous ATP promoted interaction occurs with the pseudokinase STRAD where occupation of the inactive ATP binding pocket plays an essential role in the activation of the associated kinase LKB1²²⁷. However, active HER2 ATP pocket conformation, as conferred by the HER2(G776YVMA)insertion^{238,247}, compensates for the inactive HER3 ATP pocket, increasing HER2:HER3 FRET three-fold compared to that seen between HER2(YVMA)-GFP and wild-type HER3-HA, and overcomes the lack of heterodimerisation noted with HER2-GFP and HER3(KGG)-HA. Lapatinib treatment does not significantly increase dimerisation, between HER2(YVMA)-GFP and HER3-HA or HER3(KGG)-HA, compared to the control non-treated cells. This effect is in line with published data demonstrating attenuated response to lapatinib in cell lines expressing this mutation²³⁸.

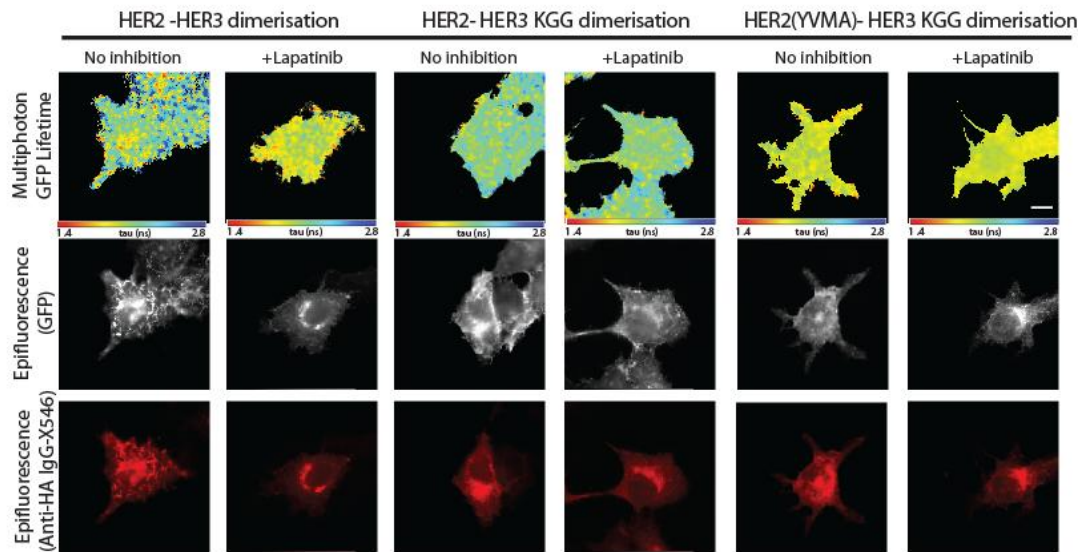
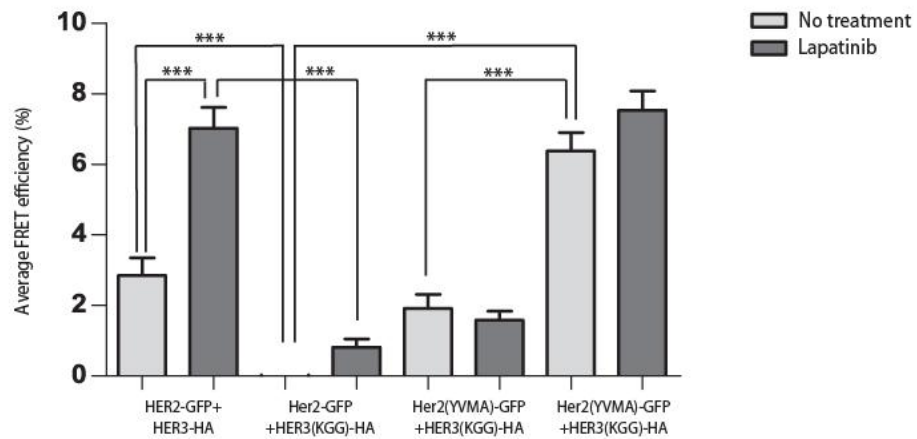
A**B**

Figure 3. 9 HER3 ATP pocket competency is required for HER2:HER3 dimerisation and may be partially overcome by constitutive activation of HER2 ATP pocket (HER2(YVMA))

(A) MCF-7 cells were transfected with vectors encoding HER2-GFP or HER2(G776YVMAins)-GFP (HER2(YVMA)-GFP) and HER3-HA, either wild type or the HER3K742MG716DG718D (HER3(KGG)-HA) site directed mutation. Cells were incubated for 24 hours, and inhibited with lapatinib (10 μ M) for 1 hour, prior to fixation and staining with anti-HA antibody conjugated to Alexa-546. Scale bars represent 5 μ m. (B) The cumulative histogram of FRET efficiency calculated as described above, from 2-3 independent experiments, is shown (n=8-28 cells/condition), with error bars representing SEM. Values for p are <0.001(***) according to one-way ANOVA with Tukey's post hoc test.

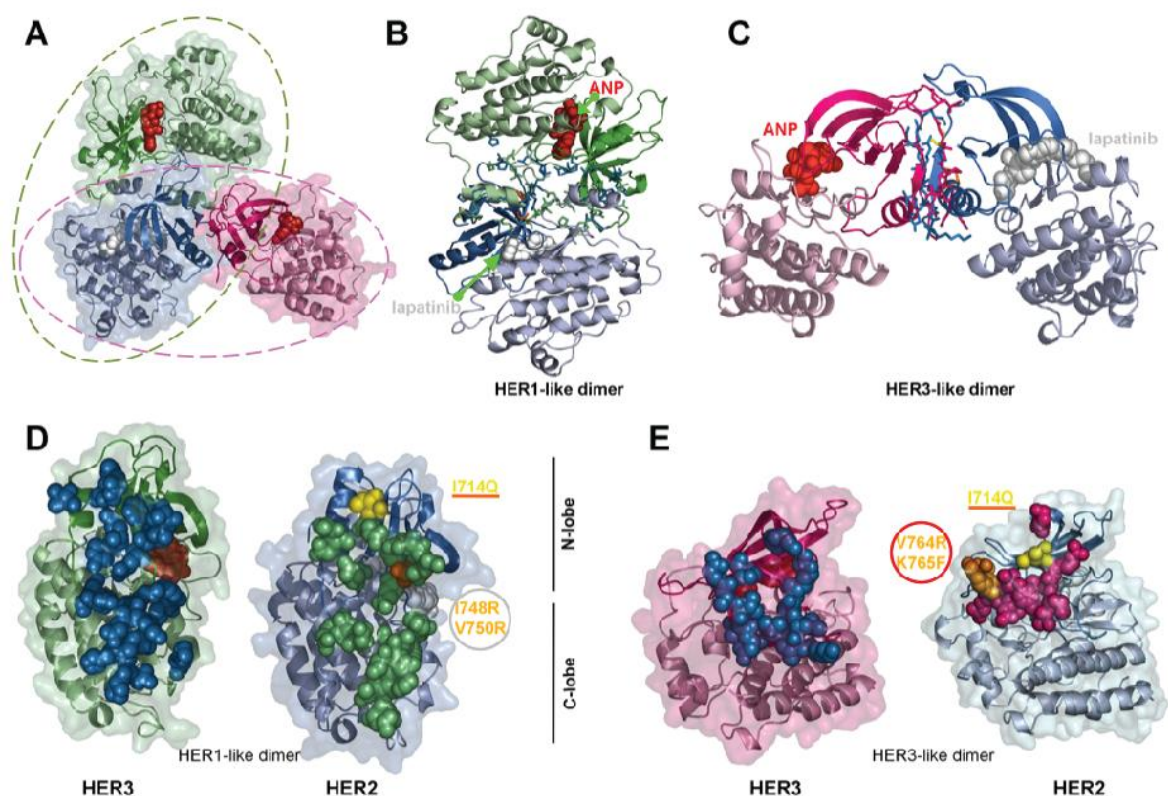


Figure 3.10 Proposed model of lapatinib-induced HER2:HER3 dimerisation (figure provided by Dr F Autore)

(A) Proposed models for HER2:HER3 dimerisation. We propose two association modes, one called HER1-like dimer (green dashed circle) and one HER3-like dimer (magenta dashed circle). The HER2 (blue) kinase domain has been superposed in the models, the HER3 of the HER1-like dimer is shown in green and the HER3 of the HER3-like dimer in magenta. Lapatinib is represented with white spheres and ANP (phosphoaminophosphonic acid adenylate ester) with red spheres. (B-C) HER1-like dimer and HER3-like dimer models are shown, respectively. The residues at the interface are drawn in liquorice representation. (D) Interfaces of interaction of the HER2:HER3 model in the HER1-like dimer assembly. The residues buried upon dimer formation are highlighted in green and blue for HER2 and HER3, respectively. The residue I714(HER2) is shown in yellow while in brown are highlighted the mutated residues, HER2(I748R/V750R). (E) Interfaces of interaction of the HER2:HER3 model in the HER3-like dimer assembly. The residues buried upon dimer formation are highlighted in magenta and blue for HER2 and HER3 respectively. The residue I714(HER2) is shown in yellow, while the mutated residues, HER2(N764R/K765F) are highlighted in brown. The mutants highlighted with the red line and the red circle affect lapatinib induced HER2:HER3 dimerisation, while those highlighted with the grey circle did not affect the lapatinib induced HER2:HER3 dimerisation.

3.2.5 Proposed model of the lapatinib-bound HER2:HER3 dimer

Thus far we have demonstrated the stabilisation of the HER2:HER3 dimer on lapatinib treatment. Homology modeling was used by our collaborators, Dr Franca Fraternali and Dr Flavia Autore (Structural chemistry group) to predict a structural model for this dimer. The high percentage of sequence identity in the HER family TKD and the recently published crystal structures of the inactive dimers, for both HER1¹⁹⁵ and HER3 homo-dimers^{197,223}, have allowed prediction of models for the inactive HER2:HER3 dimer. Specifically, two models for HER2:HER3 dimerisation have been proposed: the HER1-like dimer and the HER3-like dimer (**Figure 3. 10**), based respectively on the crystal structures of HER1 and HER3 homo-dimers^{195,197}. The dimer interfaces differ mainly in the role played by the C-tail, which is intrinsic within the HER1:HER1 dimer interface, but is not present at the HER3:HER3 interface.

In order to differentiate between these two HER2:HER3 dimer associations, residues buried upon dimer formation have been identified using POSPcomp²⁴⁸. **Table 2** lists all the residues from HER2 and HER3 involved in the dimerisation sites for both models. The residue I714(HER2) is buried deep within the interface for the HER3-like dimer but is not so critical for the HER1-like dimer association. Replacement of a non-polar hydrophobic isoleucine with a polar hydrophilic glutamine should lead to repulsion at the dimer interface demonstrated in the HER3-like dimer but not in the HER1-like dimer. Disruption of the lapatinib-induced HER2:HER3 dimer upon mutation of either of these sites is demonstrated in **Figure 3. 7** and **Figure 3. 8**. The predicted structures have been used to guide the design of further HER2 mutants targeting the interfaces specific to each of the proposed association models. In particular two double mutants have been designed to disrupt the dimerisation interfaces: the HER2(I748RV750R) addressing the HER1-like dimer interface and the HER2(N764RK765F) targeting the HER3-like dimer interface, highlighted in brown in **Figure 3. 10D** and **E** respectively). The N764 and K765 residues are not at the interface in the HER1-like dimer, whereas in the HER3-like dimer they are buried deep within the dimer interface (**Figure 3. 10E**). The substitution of an arginine with a bulky phenylalanine hydrophobic residue should generate clashes at the HER2:HER3 interface. Furthermore, the substitution of an asparagine with a positively charged arginine should lead to repulsion from another positively charged HER3 residue (R702) within 4Å radius, disrupting the HER3-like dimer interface.

Alternatively, to test the HER1-like dimer, we substituted two hydrophobic residues on HER2 with two positively charged residues (I748R, V750R), which should lead to repulsion from the positively charged residues, K315 and K316, on the opposite interface of HER3.

Figure 3. 11A and B demonstrate disruption of the lapatinib induced HER2:HER3 dimer on transfection of the HER2 (N764RK765F) mutation, buried at the interface of the HER3-like dimer, with a greater than four-fold reduction in HER2:HER3 dimerisation compared to wild-type. Furthermore, transfection of the HER2 (I748RV750R) mutation, buried at the interface of the HER1-like dimer, did not significantly alter the lapatinib induced effect, leading to a near 3-fold increase in heterodimerisation compared to the untreated control. The magnitude of the effect was not significantly different to that seen with wild-type HER2 and HER3. Although no significant difference in dimerisation was seen between the untreated control arms for all conditions, there was a trend to reduction in dimer formation with the HER2 (N764RK765F) mutation compared to wild type or HER2(I748RV750R). On further analysis using a student's T-Test, a significant reduction in the extent of HER2(N764RK765F):HER3 dimer formation in untreated cells was noted compared to wild-type ($p < 0.001$). This result suggests the presence of HER2:HER3 dimers at baseline in a HER3-like dimer conformation as described by our model, and may explain the preference of lapatinib to bind and stabilize this particular configuration. Overall these results provide evidence supporting the HER3-like dimerisation model over the HER1-like model.

Model A**HER2 Residue Delta SASA**

ALA	710	31.17
GLN	711	17
ARG	713	75.89
TRP	739	36.43
GLU	744	46.14
ASN	745	37.53
VAL	746	33.63
ILE	748	30.45
ARG	784	32.5
GLN	799	45.74
PRO	802	18.25
TYR	803	26.66
LEU	1000	83.02
ASP	1001	12.64
THR	1003	16.79
PHE	1004	79.53
TYR	1005	47.72
SER	1007	31.11
LEU	1008	38.47
LEU	1009	27.61
ASP	1011	70.87
ASP	1012	32.34
ASP	1013	16.07

HER3 Residue

VAL	699	18.82
ARG	702	47.15
TRP	728	22.44
SER	734	19.13
ILE	735	67.66
ILE	737	40.44
ARG	773	21.31
LEU	775	30.08
GLN	788	15.04
PRO	791	9.65
LEU	792	13.1
HIS	802	16.34
PRO	845	32.5
PRO	990	46.43
GLU	991	57.78
HIS	993	29.78
GLY	994	12.11
ASN	997	40.54
LYS	998	166.65
LYS	999	43.3
GLU	1001	82.11
GLU	1002	11.43

Model B**HER2 Residue Delta SASA**

ALA	710	32.66
GLN	711	25.48
MET	712	21.7
ARG	713	35.5
ILE	714	65.31
LYS	716	15.32
ASN	764	12.18
LYS	765	76.98
GLU	766	37
LEU	768	18.82
ASP	769	45.02
TYR	772	25.05

HER3 Residue

LYS	698	96.61
VAL	699	26.84
LEU	700	46.74
ALA	701	28.21
ARG	702	28.24
ILE	703	20.82
LYS	705	21.17
GLN	754	37.27
ALA	755	56.77
VAL	756	51.53
THR	757	13.32
ASP	758	18.79
LEU	761	17.45
PRO	779	14.29

Table 2. Residues involved in the HER2:HER3 internal dimer interface for the two possible dimer interfaces depicted in Figure 3. 10 (Table provided by Dr F Autore)

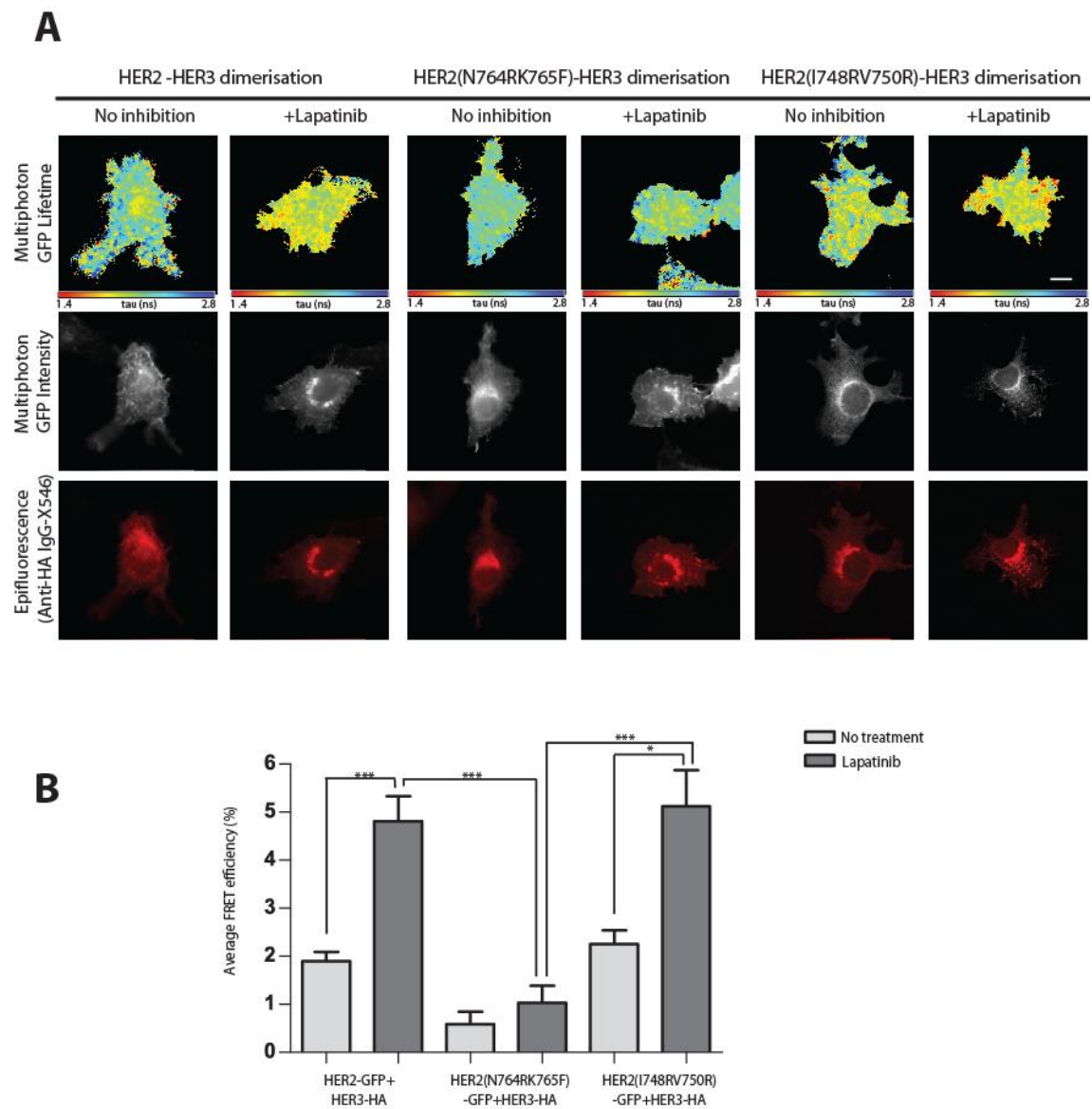


Figure 3. 11 Validation of proposed lapatinib-induced HER2:HER3 dimer using site-directed mutations

(A) MCF-7 cells were transfected with vectors encoding HER2-GFP (either wild type, or the validation site directed mutations, HER2(N764RK765F) or HER2(I748RV750R)) and HER3-HA. Cells were incubated for 24 hours, and inhibited with lapatinib (10uM) for 1 hour, prior to fixation and staining with anti-HA antibody conjugated to Alexa-546. Scale bars represent 5µm. (B) The cumulative histogram of FRET efficiency between HER2-GFP and HA-Alexa546, bound to HER3-HA, calculated as described above, from 3 independent experiments (n=15-38 cells/condition). Error bars representing SEM, values for p are <0.001(***) and <0.05(*). There was no significant difference between cells treated with lapatinib, or untreated cells for cells transfected with HER2(N764RK765F)-GFP.

3.2.6 I1714 (HER2) and K742G716G718 (HER3) are important determinants of HER2 and HER3 phosphorylation

In order to examine how disruption in dimer formation, as measured by FRET/FLIM, affected receptor function, we tested the effect of mutants disrupting HER2:HER3 heterodimerisation, HER2(I714Q)-GFP and HER3(KGG)-HA, on HER2 and HER3 phosphorylation. As expected, lapatinib treatment abolished wild-type HER2 phosphorylation (**Figure 3.12A**). Neuregulin (NRG1) treatment increased HER2 and HER3 phosphorylation, implying allosteric activation of HER2, by HER3. However, over-expression of the HER2 (I714Q, N-lobe kinase domain mutant) resulted in minimal levels of HER2 phosphorylation compared to the untreated, wild-type receptor. Activation of this mutant could not be rescued on NRG1 stimulation. Significant HER3 phosphorylation was only seen on exposure to the ligand, NRG1. Phosphorylation of HER3, in the presence of HER2 (I714Q), was reduced to 60% of that seen with wild-type HER2 (**Figure 3. 12A, upper panel**). These observations are in line with a reduction of HER2:HER3 dimerisation following over-expression of the N-lobe kinase domain HER2 mutant, resulting in reduced phosphorylation and activation of dimers (**Figure 3. 7**).

Although, expression of the JM HER2(V697R) mutant did lead to a trend to reduction of HER2 phosphorylation, either for untreated or ligand treated cells compared to wild-type control, this difference was not significant. Phosphorylation of HER3 in the presence of HER2(V697R)-GFP was significantly reduced compared to wild-type. However, this effect was of a much smaller margin compared to the effect seen in the presence of HER2(I714Q)-GFP. Within the context of the HER2:HER3 dimer, it is seen that the N-lobe of the HER2 kinase domain is essential to HER2 phosphorylation, but the JM region plays a less critical role (**Figure 3.12A**).

Over-expression of the ATP nucleotide pocket mutant HER3 (KGG) abolished HER3 phosphorylation at baseline, and reduced NRG1-induced phosphorylation to less than 10% of that seen with wild-type HER3 (**Figure 3.12B**). This result is as expected as site-directed mutagenesis in the ATP binding pocket within the TKD inhibits activation of the kinase, thus attenuating phosphorylation of tyrosine residues in the C-terminal tail, e.g. tyrosine 1289. Despite transfection of HER2-GFP alongside HER3, phosphorylation of HER2 was not reliably seen and therefore is not presented here. The biochemistry data presented in **Figure 3.12C** was kindly carried out by Mr Jeroen Claus in collaboration for publication.

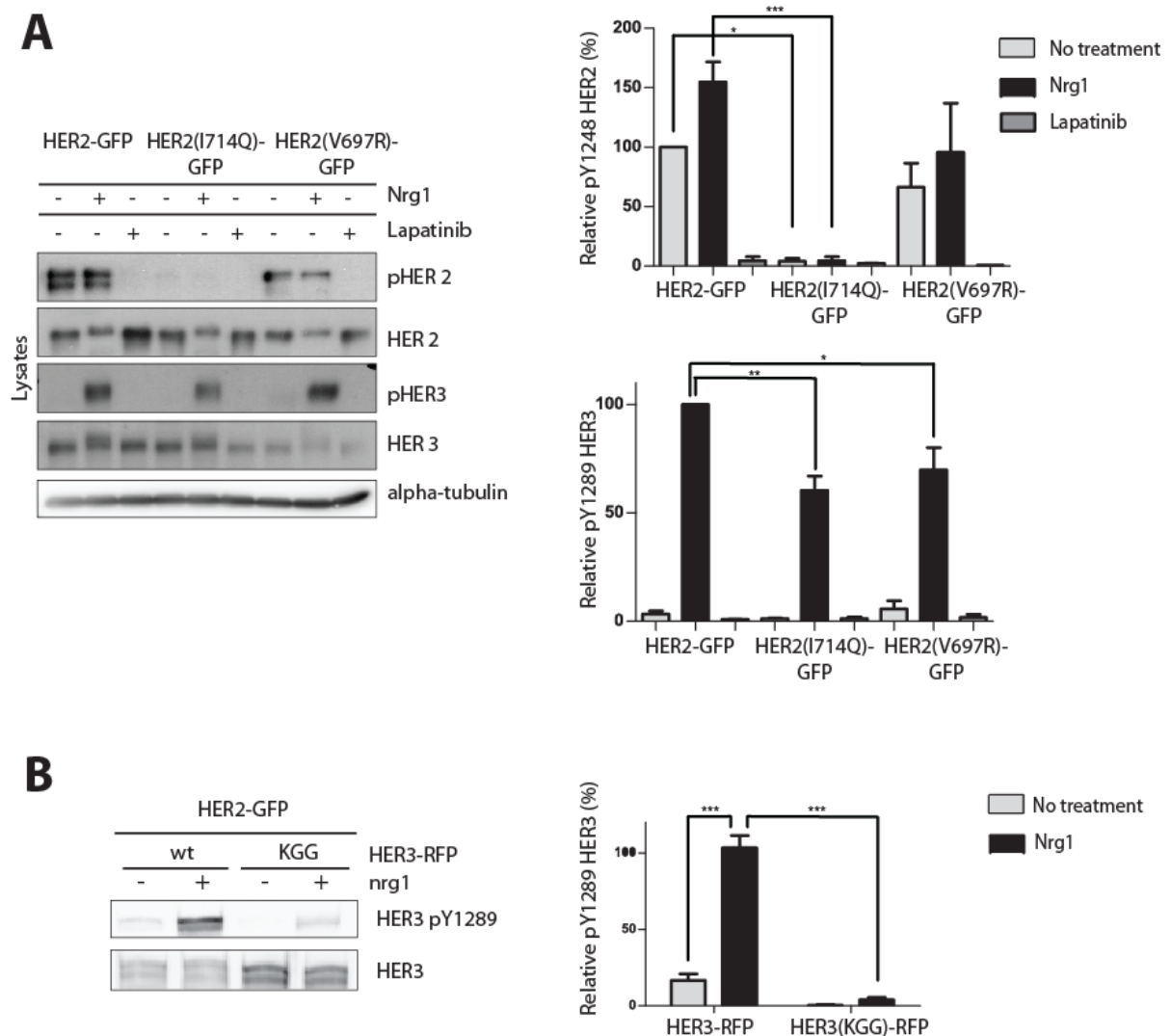


Figure 3. 12 Phosphorylation of wild-type and site-directed HER2 and HER3 mutants on ligand and/or lapatinib treatment

(A) MCF-7 cells were transfected with wild type HER2-GFP or the N-lobe TKD mutant, HER2(I714Q)-GFP, or the juxtamembrane domain mutant HER2(V697R)-GFP for 24 hours in 5% Optimem. Cells were serum starved in 0% FBS DMEM for 1 hour and then treated with neuregulin (NRG1, 50ng/ml) for 15 minutes or lapatinib (Lap, 10 μ M) for 1 hour, prior to lysis. The histograms (lower panels) depict densitometry of phosphorylated HER2 levels, normalized to total HER2 levels (upper histogram), and phosphorylated HER3 levels, normalized to total HER3 (lower histogram). Error bars represent the standard error of the mean (SEM) from 3 independent experiments, p values are <0.001(***), or <0.01(**) or <0.05(*) using one way ANOVA. (B) MCF-7 cells were similarly co-transfected with HER2-GFP and mRFP-HER3, wild type, KGG mutant or empty vector, for 24 hours, serum starved and then treated with neuregulin for 15 minutes. The histogram represents densitometry of phosphorylated HER3 levels, normalized to total HER3 levels. Error bars represent SEM from 3 independent experiments, p values are <0.001(***)

3.3 Discussion

The propagation of an external signal to the interior of the cell requires protein-protein interactions, in this case, between HER family members¹²⁶. Although ligand-induced HER2:HER3 dimerisation efficiently drives downstream signaling, conformational restraints ensure secondary levels of control to prevent inappropriate receptor activation. The structure of an inactive receptor, either as monomer or dimer, is integral to regulation of activation, as shown by the effects of oncogenic mutations in HER1. In this case, the extent of conformational change induced by a single point mutation, e.g. L858R, is sufficient to drive the formation of active asymmetric dimers, and resistance to drugs such as lapatinib, targeting the inactive conformation²¹⁵. Although lapatinib is one of the key HER2-targeted drugs in clinical use, little is known about its effect upon HER2 conformation and ensuing molecular dynamics.

Without a quantifiable tool for the measurement of HER2:HER3 dimerisation, we cannot easily unpick the differential effects of type I vs type II TKIs upon heterodimer formation. Therefore, we established the first FRET/FLIM assay quantifying lapatinib-induced HER2:HER3 dimerisation in cells, providing a structural model for this dimer, which is further interrogated by site-directed mutagenesis. During the optimization of this assay, we confirm findings from Hoffman *et al* regarding the steric hindrance produced by fluorescent proteins²⁴⁹. In their study, CFP was fused to the C-terminus and the FIAsh binding motif was inserted in the third intracellular loop of an A2A adenosine receptor. Treatment with an agonist evoked conformational changes to the receptor that led to a greater separation of the two fluorophores. A comparison of a tetracysteine tag with YFP demonstrated that the insertion of the two fluorescent proteins can lead to steric hindrance within the receptor. This effect is likely to be greater for intra-molecular FRET compared to inter-molecular FRET. We have shown that FRET/FLIM quantification of HER2:HER3 dimerisation may be improved by substitution of one fluorophore with a HA tag, against which a fluorophore-tagged antibody may be used.

This FRET/FLIM assay has been used to demonstrate heterodimerisation of HER2 and HER3 upon lapatinib treatment. Lapatinib has been shown to inhibit HER2 phosphorylation and lead to stabilization and accumulation of inactive HER2 homo- and hetero-dimers (HER2:HER3 or HER2:HER1) by immunoprecipitation and computational modeling techniques²⁴⁴. Scaltriti *et al* demonstrated a qualitative increase in dimer formation using immunoprecipitation, only quantifying the increase in total HER2 and reduction in phospho-HER2 on lapatinib treatment. However, using the FRET/FLIM assay, we are better able to quantify the extent of in-situ heterodimerisation, compared to ligand-induced and type I TKI-

induced dimer formation, and start to infer the nature of the conformational changes brought about by these agents.

Treatment with type I TKIs which bind to the active form of the monomer, such as canertinib and erlotinib, did not induce hetero-dimerisation of HER2:HER3 to the same extent as lapatinib. However, both NRG1 and the type I TKIs induced comparable levels of dimerisation, which may be due to the formation of active, asymmetrical dimers. Although the lapatinib effect upon HER2:HER3 dimerisation is in agreement with the co-immunoprecipitation data from Scaltriti *et al*, Sanchez-Martin have shown a decrease in HER2:HER3 dimers upon lapatinib treatment²⁵⁰. However, this group used different cell culture conditions to our group, with 2 hours of treatment, compared to 1 hour in our experiments, and using lapatinib at a lower dose (5 μ M compared to 10 μ M). These conditions may decrease the sensitivity of the assay. For instance both our group and Sanchez-Martin *et al* show phosphorylation of HER2 and HER3 in untreated SK-BR-3 cells. However, the immunoprecipitation assay does not demonstrate any dimer formation at baseline, questioning how the receptors may be activated and phosphorylated. Furthermore, no quantification of dimer effect or statistical analysis of TKI effect is demonstrated in this data. The degree of dimer formation after 2 hours of TKI treatment may not be identical to that seen at 1 hour by ourselves and Scaltriti *et al*, due to, for instance ongoing processes such as receptor internalisation. On the other hand, we have demonstrated a degree of baseline dimer formation between HER2 and HER3, likely explaining HER3 and HER2 phosphorylation at baseline, and we have used the more sensitive FRET/FLIM assay to quantify interactions. Although Sanchez-Martin *et al* use intensity based measurements of fluorophore-tagged secondary antibodies bound to HER2 and HER3 with acceptor photo-bleaching to attempt to assess FRET, this method is much less sensitive compared to FRET/FLIM, leading to very wide confidence intervals as shown in their data. Within the context of the differences in experimental conditions and techniques, I feel that our data, in line with Scaltriti *et al*, is likely to depict the early effects of lapatinib upon HER2:HER3 dimerisation.

Site-directed mutagenesis at the HER3 C-lobe TKD lobe disrupted NRG1-induced dimerisation, presumably mediated by an asymmetric N-C TKD lobe dimerisation model as validated for HER1¹⁴⁹ homo-dimerisation and HER1:HER3 heterodimers¹⁹⁷. This mutation did not disrupt the lapatinib-induced symmetric dimer. These results lend evidence to our predicted models for the lapatinib-induced HER2:HER3 dimer. These models consist of catalytically inactive monomers of HER2 and HER3, bound in an N-lobe kinase domain mediated, symmetrical form. This model contrasts with the asymmetric lapatinib bound HER2:HER3 dimer presented by Scaltriti²⁴⁴ *et al*; the only other model for the lapatinib

bound heterodimer found in the literature. Their model is based upon the energy gain of HER2 dimers associated with lapatinib compared to those associated with ATP, and demonstrates the increased stability of HER2 non-phosphorylated dimers, but their heterodimer molecular model is not validated. On the other hand our symmetric model is in line with more recent data for HER1, demonstrating lapatinib induced stabilisation of the HER1 receptor kinase in an inactive conformation and the presence of a symmetric kinase homo-dimer using negative-stain electron microscopy²⁵¹. Both Mi *et al*²⁵¹ and Bublil *et al*²³⁴ demonstrate differential activity of type I and type II TKIs upon formation of HER1 TKD homodimers. Bublil *et al* show an increase in HER1 homodimerisation with type I TKIs but not with lapatinib. This may be due to the native conformation of the HER2 receptor as opposed to the HER1. It is likely that in the native conformation, HER2 may be present as an inactive monomer, whereas HER1 may be in a more disordered state²¹¹. Mi *et al* illustrate how the equilibrium between asymmetric and symmetric HER1 homodimers may be influenced by the type of TKI present. Our data suggests a similar mechanism for the stabilisation of inactive symmetric HER2:HER3 dimers on lapatinib treatment. However the extent of heterodimer stabilisation with lapatinib is much greater than that seen with either type I TKI. Phosphorylation status of the receptor and differential dimerisation states of the TKD, may also influence dimer mobility, co-confinement and internalisation²¹⁶. This result may have implications upon downstream effects leading to accumulation of inactive lapatinib-bound heterodimers^{216,244}.

We validated our HER2:HER3 model using mutations within the hypothesised dimer interfaces. For instance, the lapatinib effect is disrupted by mutation at a single residue in the N-lobe of the HER2 tyrosine kinase domain (I714Q), suggesting the HER3-like model over the HER1-like as a proposed model of lapatinib induced interaction. Although site-directed mutation of the JM domain caused a similar disruption in HER2:HER3 dimerisation, there was no significant decrease in HER2 phosphorylation, as opposed to the TKD mutant. This result suggests that, although the JM domain may play a role in stabilizing the heterodimer, it is not as critical as that seen in HER1 homodimers^{174,195,212,252}, and activation of the receptor can still occur, leading to downstream phosphorylation. However, it seems the TKD mutant disrupts the heterodimer to the extent that HER2 activation and phosphorylation is almost entirely abolished. The HER2 TKD mutant demonstrates the importance of the intracellular dimerisation interface in the lapatinib-induced dimer, further supporting literature in the HER1 field, that the intracellular domain is likely to be at least as instrumental as the extracellular domain in maintaining dimer stability^{216,222,252}. Although this mutation has not yet been sequenced within breast tumours, such mutations, which disrupt HER2:HER3

dimerisation, may confer a favourable outcome. Whether preformed heterodimers confer resistance or sensitivity to lapatinib is a further question, tackled in Chapter 5.

One area of uncertainty is regarding the phosphorylation of HER2 at baseline, without NRG1 treatment. We have demonstrated with Western blot analysis, the phosphorylation of both HER2 and HER3 on NRG1 treatment above baseline. This result is in line with HER2:HER3 heterodimer formation as seen by FRET/FLIM, allosteric trans-activation of the TKD and phosphorylation of the C-terminal tail. However, a significant level of HER2 phosphorylation is seen in untreated MCF-7 cells with little corresponding HER3 phosphorylation. Homodimer formation due to overexpression of HER2-GFP may cause this effect, and would explain the lack of phosphorylation of HER2(I714Q)-GFP at baseline. Alternatively, dimer formation between the overexpressed HER2 and HER4, a receptor which is expressed in high levels in MCF-7 cell lines, may also explain baseline HER2 phosphorylation. The determination of HER2 homodimer formation by FRET/FLIM was unsuccessful due to the toxicity and lack of physiological response demonstrated on transfection of HER2-GFP and HER2-HA into MCF cells.

Intriguingly we also found that dimerisation of HER2 with HER3 critically depends on the conformation of the catalytically inactive HER3 kinase domain. Mutations designed to disrupt the HER3 nucleotide binding pocket entirely abolished FRET between HER2 and HER3. Our data indicate that HER3 ATP binding pocket occupation is important for HER3 function through conferring conformational stability, independently of catalytic activity. These findings are in line with a growing body of work on conformational roles of nucleotide binding pocket occupation that are independent from catalytic activity^{224-228,253}. The fact that HER2:HER3 dimerisation can be modulated by the state of the HER3 ATP binding pocket, is an entirely novel finding and indicates that the ATP binding pocket of HER3 might represent a significant drug target. ATP pocket directed inhibitors which hinder HER3 binding to partner kinase domains might be powerful agents in preventing HER3 dependent resistance. Conversely, presence of the HER2(YVMA) mutation, conferring constitutive ATP pocket activation²³⁸, can compensate for HER3 ATP pocket incompetency. Wang et al have shown transphosphorylation of kinase-dead HER3 and HER1 by HER2(YVMA). Our results suggest that increased heterodimerisation of HER2(YVMA) with the kinase-dead HER3 receptor could lead to its transphosphorylation. The structural basis behind this phenomenon is not entirely clear. This HER2 mutation is one commonly found in non-small cell lung cancer patients^{239,241} and an equivalent TKD mutation has been identified in a sub-group of breast cancer patients²⁴⁰, highlighting a group of tumours which may be susceptible to drugs targeting the intracellular dimerisation interface.

Within this chapter, we have discovered some of the conformational consequences of lapatinib binding with HER2. Paradoxically, we have found that this drug drives HER2 into the non-phosphorylated symmetric HER2:HER3 dimer. What is the functional significance of this effect? Treatment with BRAF inhibitors has been shown to drive dimer formation of wild-type RAF inhibitors^{224,225}. In a similar fashion, TKI treatment may lead to dimer stabilisation and the development of resistance to treatment. In the next chapter, we explore the longer term effects of lapatinib treatment in order to understand how mechanisms of resistance to lapatinib may develop, and if the accumulation of the heterodimer may eventually contribute to this effect.

Chapter 4: Functional significance of the lapatinib induced HER2:HER3 dimer

4.1 Introduction

Thus far, we have established that lapatinib induces the formation of a symmetric HER2:HER3 dimer which is not phosphorylated, over a short time period of an hour. We now look to define the functional consequences of dimer formation. It is well known that interaction between active HER2 and HER3 in the asymmetric dimer forms one of the most proliferative HER dimers via coupling with Akt signaling. Furthermore there is interdependence of these two receptors as, in HER2 overexpressing cells, the loss of HER3 attenuates cell proliferation^{175,184}. However, it is not known whether the formation of the inactive dimer affects downstream signalling, receptor levels or trafficking in order to escape lapatinib-mediated inhibition. Therefore, we first review known mechanisms of action of lapatinib, HER dimer mediated endocytosis and recycling, and HER3 as a potential player in the development of resistance to lapatinib treatment.

4.1.1 Molecular mechanisms of action of lapatinib

Macroscopically, HER2-overexpressing cell lines such as BT474 have been used to demonstrate the anti-proliferative effect of lapatinib²⁵⁴. At the molecular level, it is well known that lapatinib effectively suppresses HER1 and HER2 phosphorylation in cell lines, animal models and human tumour samples^{189,254-256}. The off-rate for lapatinib is much longer than the type I TKIs, leading to a more sustained mechanism of action¹⁸⁹. The structure of lapatinib bound to HER1 is different to gefitinib or erlotinib as described previously (**Chapter 3.1.5**), which may contribute to the slow inhibitor dissociation rate. As erlotinib binds to the active form of the receptor, it may be able to bind and dissociate much more rapidly compared to lapatinib which binds to the inactive form and may require a conformational change. Alternatively the structural differences in between the two drugs may lead to different binding affinities, which may be higher for the inactive receptor. Whichever the case, receptor phosphorylation recovers to only 15% at 72 hours after lapatinib washout, compared to 60% for erlotinib at the same time point¹⁸⁹.

Downstream signaling via AKT and Erk1/2 MAP kinases is inhibited, which correlates with cell apoptosis, as opposed to treatment with trastuzumab which affects neither HER2 phosphorylation nor cell proliferation^{257,258}. It is unclear whether the lack of HER2 phosphorylation alone is sufficient to activate downstream apoptotic pathways or whether off target TKI effects are involved. For instance, lapatinib has been shown to promote up-regulation of pro-apoptotic TRAIL death receptors, DR4 and DR5 via the c-Jun amino-terminal kinase (JNK)/c-Jun signaling axis²⁵⁹, and the pro-apoptotic protein Bcl-2 interacting mediator of cell death (BIM) via lapatinib-induced inhibition of the MEK-ERK pathway²⁶⁰. Data pertaining to the role HER2 phosphorylation or dimerisation in the down-regulation of cell proliferation is lacking.

How lapatinib-induced HER2:HER3 dimer formation affects individual receptor trafficking, and degradation is to be investigated. A few studies have examined the effects of lapatinib on total HER2 levels. Scaltriti *et al* have demonstrated accumulation of HER2 at the cell surface over 24-48hours of lapatinib treatment, secondary to attenuation of HER2 ubiquitination, thus increasing susceptibility to antibody-dependent cell-cytotoxicity (ADCC) conferred by trastuzumab²⁴⁴. These receptors were in the form of HER2 homodimers and HER2:HER3 heterodimers. Sanchez-Martin *et al*, however, showed a decrease in total HER2 levels after 24 hours of lapatinib treatment²⁵⁰. However, these cells were also exposed to the HER3 ligand, NRG1, which is known to lead to active HER2:HER3 heterodimer formation and ensuing receptor degradation. Neither study has examined changes in HER3 levels or receptor distribution on extended lapatinib treatment.

The relevance of HER2:HER3 dimer formation to lapatinib efficacy or the development of resistance is not well delineated. Cook *et al* examined the role of HER3 within a PI3K-driven mouse model treated with lapatinib²⁶¹. They showed that the driving oncogenic unit within this tumour was a complex of HER2, HER3 and PI3K. Lapatinib treatment attenuated HER3 phosphorylation in line with the literature^{192,262,263}, and thus, PI3k activation leading to reduced tumour growth. This model reflects coupling between HER3 and HER2 as a likely oncogenic driver in HER2-overexpressing cancers, and highlights the importance of ablation of HER3 in attenuating downstream signaling and tumour growth. Intracellular trafficking and recycling of this heterodimer is likely to play a key role in the maintenance of oncogenic signaling and is further reviewed below.

4.1.2 HER2 and HER3 receptor trafficking

Having reviewed the well known characteristics of HER1 internalisation, trafficking and degradation (**Chapter 1**), we now focus on HER2, HER3 and the effect of dimer formation

upon these processes. The rates of receptor turnover vary across the different members of the HER family and depend on the dimerisation status of the receptor. The HER2 receptor has a half life ($t_{1/2}$) of 6-10 hours^{156,264,265}, whereas the half life of HER3 is approximately 2-3 hours^{167,266}. HER3 shows similar kinetics to HER2 with reduced internalisation, down regulation and degradation in comparison to HER1²⁶⁷. HER3 is endocytosed in a clathrin-dependent manner, in the absence of ligand, independently of its tyrosine phosphorylation²⁶⁸. The effect of ligand binding upon HER3 endocytosis is more controversial. Baulida *et al* report a very low rate of ligand-induced receptor internalisation²⁶⁹ in contrast to Waterman *et al.* who demonstrate efficient HER3 and neuregulin internalisation over 20 minutes²⁶⁶, followed by entry to the recycling pathway. A chimeric receptor consisting of a HER1-derived TKD and the HER3 C-terminal tail, was used to demonstrate that ligand binding or TKD activation via an alternate receptor, e.g. HER2, initiates effective signalling followed by shunting to the HER3-characteristic recycling pathway²⁷⁰. Therefore it is felt that the C-terminal tail of HER3 and co-receptor activation may be important factors in deciding the trafficking fate of the HER3 receptor. Post-translation modifications regulate ligand-bound HER3 degradation via the E3 ligase Nrdp1 and the Nrdp1 regulator, USP8¹⁶⁷, which is in turn regulated by Akt. This pathway may link HER3 expression with Akt downregulation, as discussed in section 4.1.3.

As HER2 has no known ligand, a more rapid turnover is not inducible by this means. In cells which overexpress HER2, accumulation at the plasma membrane is reported^{136,271,272}. The mechanism behind this phenomenon is not entirely clear. Chimeric receptor studies demonstrate that the carboxyl tail of HER2 (fused to the ECD of HER1) internalises three to four times more slowly than the full length HER1 receptor, leading to reduced receptor degradation²⁶⁵. Impairment of HER2 internalisation may be due to actin associated proteins in the plasma membrane domain causing retention in the membrane, or by infrequent recruitment to clathrin coated pits at the carboxyl-terminus of HER2 due to inability to interact with the clathrin adaptor protein complex-2 (AP-2)^{267,271,273,274}. An alternate school of thought is that HER2 is recycled to the cell surface rather than targeting for lysosomal degradation²⁶⁶.

Figure 4.1 shows a detailed view of HER1 receptor trafficking to recycling or degradation²⁷⁵, which is thought to be representative of HER family trafficking. What is commonly referred to as the 'early endosome' has been more recently distinguished into 2 different compartments²⁷⁶: the sorting endosome and the endocytic recycling compartment (ERC). The sorting endosome is defined as the first discernible organelle to which internalised transferrin receptors are delivered, after a brief time period (1-2minutes). They are tubulovesicular structures which have a low luminal pH (6.0), and usually mature to late

endosomes over 5-10 minutes. The low pH will often lead to the dissociation of ligands, and a change in intracellular fate for the receptor. For instance, TGF α disassociates from HER1 dimers in the acidic sorting endosome, allowing HER1 recycling as opposed to EGF which remains within the HER1 dimer complex and targets the receptor for degradation²⁶⁶.

The transport of receptors for recycling occurs within tubules which branch off the sorting endosome, to deliver their cargo to the ERC. Rab 5, a small GTPase regulatory protein, and early endosome antigen 1 (EAA1), a phosphoinositide binding protein, regulate fusion between primary endocytic vesicles and sorting endosomes^{277,278}. Receptors may recycle from the sorting endosome directly back to the plasma membrane in a rapid manner (2-6 minutes), or via a long-lived organelle, the ERC. The ERC has many complex functions which include recycling of the majority of proteins to the surface membrane, but also transport of cargo to late endosomes via the trans-Golgi network (TGN). Late endosomes are endocytic organelles which do not receive a direct input of vesicles that have originated from the plasma membrane and are not on the recycling route. Early endosomes or sorting endosomes mature to form late endosomes by acidification, mediated by vacuolar-ATPases, which are blocked by bafilomycin, and by fusion into large vesicles, which are also known as multi-vesicular bodies (MVB). The main function of late endosomes/MVBs is lysosomal degradation of proteins.

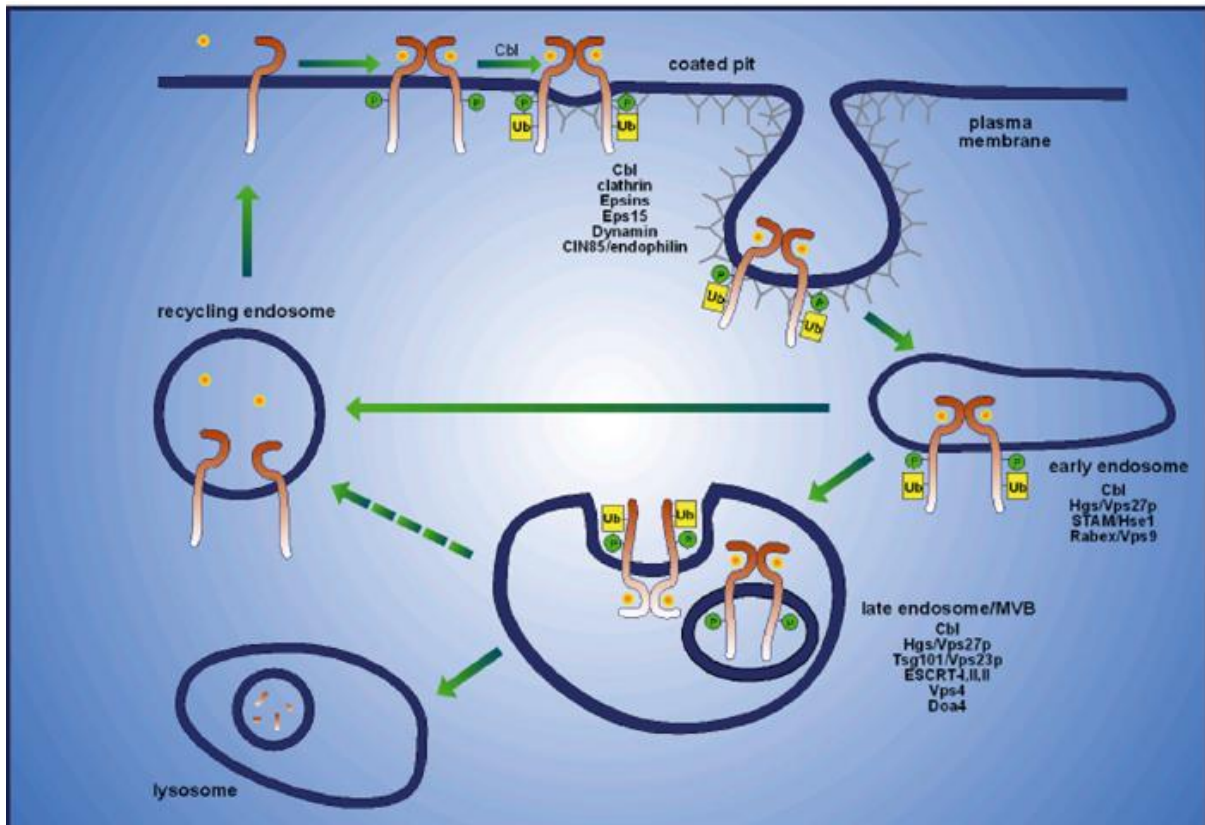


Figure 4. 1 HER family receptor internalisation and trafficking²⁷⁵

Ligand binding induced phosphorylation of HER1 and recruitment of the E3-ligase cCbl, which targets HER1 for ubiquitination. Receptors are internalised via clathrin-coated pits by a multiprotein complex that includes coat adaptors such as Epsin and Eps15. Fission of clathrin-coated vesicles is mediated by a GTPase, dynamin. HER family receptors may also endocytose via non-clathrin-dependent pathways, and then merge with the pathways depicted above. Endocytic vesicles shed clathrin and mature to early endosomes, or the sorting endosome, which has a low pH (6.0). HER1 trafficking from early to late endosomes/MVB is dependent on its continued association with Cbl and its sustained ubiquitination. MVB sorting is regulated through recognition of ubiquitinated cargo by Hgs/Vps27p, Tsg101/Vps23p and other components of ESCRT complexes. Fusion of the MVB with the lysosome results in degradation of the contents of the internal vesicles. Recycling of receptors back to the plasma membrane can occur throughout the endocytic pathway, either rapidly from the early endosome/sorting endosome, or more slowly through the recycling endosome/endocytic recycling compartment.

EGF-induced homodimerisation of HER1 induces efficient internalisation and degradation of the receptor, as described in **Chapter 1**. However HER1 signalling is prolonged when it forms a dimer with HER2 or HER3^{161,279} as shown in **Figure 4. 2**. Whether attenuated endocytosis is responsible is not entirely clear. HER1 dimer formation with HER2 reduced internalisation rates more so than with HER3, but both heterodimers endocytosed slower than the HER1 homodimer. However, Worthylake *et al* demonstrated no change in internalisation of the heterodimer versus homodimer. It is generally agreed that, once internalised, the HER1:HER2 heterodimer is not efficiently sorted to lysosomes but mostly recycled to the cell surface^{156,161,279}. This effect is blocked by monensin, a drug known to inhibit recycling of transmembrane receptors²⁸⁰. Degradation of HER1 within the HER1:HER3 heterodimer is more pronounced compared to the HER1:HER2 dimer²⁶⁸. It is unclear why this is the case but reduced HER1 recycling may be due to a lower propensity of HER1:HER3 dimers to form and lower dimer stability compared to the HER1:HER2 dimer. There is no evidence pertaining to the fate of the HER1 partner within this system. It is assumed that the dimer disassociates in the acidic condition of the early endosome but it is not known if the partner is degraded or also recycled back to the cell surface. In regard to HER2:HER3 dimer trafficking, there is a real paucity of data describing dimer kinetics.

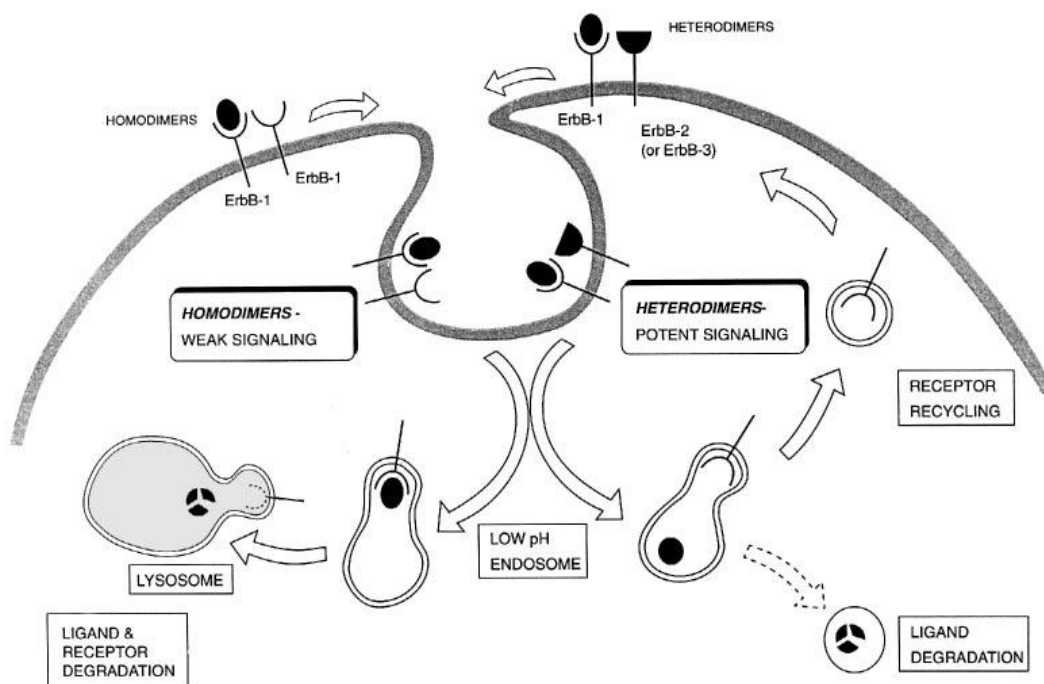


Figure 4. 2 Proposed model of homo- or heterodimer-mediated recycling.²⁸¹

HER1 homodimers mediated by EGF binding internalise to sorting endosomes and are targeted for efficient lysosomal degradation and termination of signalling. However, HER1:HER2 heterodimers evade down-regulation, potentially by releasing EGF in the low pH of the sorting endosome, thus allowing receptor recycling back to the cell surface, augmenting EGF signalling.

Importantly, signaling from HER family receptors is not confined to the plasma membrane, but was shown to continue after the receptor had been internalised²⁸²⁻²⁸⁴. Immunoelectron microscopy of overexpressed HER1 receptors in A431 cells demonstrated the cytosolic orientation of the tyrosine-phosphorylated tail and the presence of an active receptor in endosomes, which suggests receptor signaling after internalisation²⁸⁴. Expression of a dominant negative dynamin (K44A) mutant blocks HER1 internalisation and leads to increased cell proliferation and activation of pathways involving phospholipase C(PLC) γ and Shc, with a reduction in MAPK activity and HER1 phosphorylation²⁸⁵. It is assumed that this effect is due to a loss of signaling from internalised HER1, which is unlikely to be able to access the PLC γ pathway en route to the late endosome. Recent analysis of detergent-resistance membrane fractions has demonstrated the presence of endocytic lipid rafts, which allow internalised HER1 to efficiently associate with effector substrates such as Grb-2 or Shc, thus propagating the HER1 mediated signal²⁸². Teis *et al* demonstrated that disruption of an endosomal complex of an adaptor and scaffold protein (p14-MP1) by gene disruption of p14, led to attenuation of signaling via ERK and HER1, and loss of cell proliferation²⁸⁶. HER1 signaling to ERK at the endosomal surface was vital for regulation of proliferation. Introduction of a mutant p14, which could localize to the plasma membrane but not the endosome, failed to rescue this growth defect. Therefore, endocytosis alone does not terminate signaling, and the latter examples demonstrate the different signaling pathways which can be harnessed by internalised receptors versus those on the plasma membrane, depending upon the local availability of substrates. Although there is no evidence pertaining to signaling from internalised HER2 and HER3, cytosolic HER2 has been shown to associate with PLC γ ²⁸⁷.

Lack of TKD phosphorylation may also affect receptor endocytosis and recycling. Tyrosine kinase activity has been demonstrated to be essential for normal HER2 trafficking once the receptor has been internalized²⁸⁸. Abolition of tyrosine kinase activity by site-directed mutagenesis leads to normal receptor internalisation, but increased recycling of the inactive receptor to the cell surface compared to degradation of the wild-type active receptor. Waterman *et al* demonstrate a slow ligand-induced endocytosis of HER3 followed by a rapid recycling to the cell surface, which they attribute to the lack of kinase activity of HER3²⁸⁶. The recycling of this receptor is very similar to a kinase-defective non-small cell lung cancer-associated HER1 mutant which demonstrates altered trafficking through endocytic recycling compartments²⁸⁹. This phenomenon suggests a mechanism by which the HER1 mutants evade degradation and continue oncogenic signaling. However, drug treatment may influence this process. For instance, treatment with the Hsp90 inhibitor, geldanamycin, has been shown to improve endosomal sorting of HER2 to the lysosome, leading to enhanced

degradation²⁹⁰. The effect of TKI treatment upon turnover rate is unknown but endocytosis and cellular trafficking of the HER family are important mechanisms for termination of HER-mediated signaling and require further investigation in the case of HER2 and lapatinib.

4.1.3 HER3 rephosphorylation as a potential escape mechanism from TKI treatment

Emerging studies on lapatinib resistance suggest a vital role for HER3 signaling both *in vitro* and in animal models^{192,261-263}. These studies demonstrate an initial reduction of HER2 and HER3 phosphorylation, followed by recovery of HER3 phosphorylation after approximately 12 hours, up to 24 to 96 hours, both in cell lines and from animal models¹⁹². Increased HER3 phosphorylation is attributed, in part, to increased HER3 expression with a rise in HER3 mRNA^{262,291} potentially mediated by the Akt/FOXO3 and MAPK pathways^{262,263}. Although these downstream signaling pathways may lead to compensatory HER3 activation, they are not an easy target for therapy. For example, inhibition of PI3K does not result in abolition of signaling due to the activation of complex downstream pathways involving induction of MAPK/ERK activity²⁶². Furthermore, the PI3K inhibitor induces HER3 phosphorylation without an increase in HER3 expression, thus questioning current models which explain HER3 reactivation by an increase in transcription. This link is reciprocal, with MAPK inhibitor treatment leading to upregulation of Akt signaling²⁶².

Elucidation of a crucial, 'targetable' mechanism of HER3 re-activation is difficult. Sergina *et al* and Amin *et al* have postulated that tyrosine kinase inhibition of HER2 by lapatinib is incomplete, and that a feedback mechanism via reduction of PI3K/AKT signaling leads to re-phosphorylation of HER3^{192,262}. Sergina *et al* found that suppression of HER2 levels with siRNA transfection led to a reduction in TKI-refractory HER3 phosphorylation^{192,263}. They suggest that a forward shift in the HER3 phosphorylation-dephosphorylation equilibrium leads to a higher steady state level of HER3 phosphorylation. A higher dose of the TKI can abolish HER3 phosphorylation but this dose is not clinically viable²⁶².

Cellular localization of HER3 may be a driving factor in the development of resistance. SK-BR-3 cells exposed to 5 μ M gefitinib for 48 hours, demonstrate relocalisation of HER3 to the cell surface membrane, which can be suppressed using monensin treatment to inhibit vesicular trafficking¹⁹². On inhibition of receptor recycling, the dephosphorylation of HER3 from cells pre-treated with gefitinib, is also attenuated. The effects of lapatinib on HER3 trafficking have not yet been studied and may lead to the identification of novel targets for therapy in lapatinib-resistant tumours. Treatment with anti-HER3 siRNA or anti-HER3 antibodies leads to apoptotic cell death¹⁹² and re-sensitises both drug-refractory cells and

tumour xenografts to lapatinib²⁶³. These studies demonstrate a dual approach to HER2 and HER3 targeted-treatment, highlighting a strategy to overcome HER3 mediated resistance to HER family TKIs. However, this hypothesis has not yet been tested in the clinic.

We have attempted to further describe the effects of the formation of the lapatinib-induced HER2:HER3 heterodimer in breast cancer cells, with an aim to highlight the importance of dimer formation upon the ensuing HER3 re-activation.

4.2 Results

4.2.1 Lapatinib treatment attenuates HER2 ubiquitination and allows HER2 accumulation

As ligand binding to HER3 normally leads to HER2:HER3 dimerisation, receptor ubiquitination and degradation^{167,266,281}, we examined whether lapatinib binding to HER2, leading to inactive HER2:HER3 dimerisation, led to the same post-translational modifications of HER2. As a positive control, we used the heat shock protein-90 (Hsp-90) inhibitor, geldanamycin (GA), which blocks ATP binding to Hsp-90, favouring poly-ubiquitination and proteasomal degradation of the protein²⁹²⁻²⁹⁴. The E3 ligases CHIP and Cul5 have both been implicated in this interaction^{166,295}. **Figure 4. 3A and B** demonstrate a greater than ten-fold level of HER2 ubiquitination, on immune-precipitation, with geldanamycin treatment as opposed to treatment with lapatinib. HER2 ubiquitination levels are undetectable for untreated and lapatinib treated cells at baseline, in line with the literature²⁴⁴. It is likely that reduced HER2 phosphorylation, due to lapatinib treatment, results in reduced binding of an E3 ubiquitin ligase to HER2, allowing evasion from ubiquitination and degradation. Consequently, we demonstrate the degradation of HER2 at 4 hours of GA treatment, as opposed to HER2 accumulation on lapatinib treatment over the same period (**Figure 4. 3C and D**). The histogram demonstrates a two-fold increase in HER2 over 4 hours of lapatinib treatment, which is representative of the steady-state level seen at 24 hours (**Figure 4. 4**).

4.2.2 HER3 accumulates in SK-BR-3 cells, more so than HER2 on extended lapatinib treatment

Long term effects of lapatinib treatment upon HER2 levels have been shown to be similar at 12, 24, and 48 hours²⁴⁴. We chose the 24 hour time-point to examine the effects of extended lapatinib exposure upon endogenously overexpressed HER2 in SK-BR-3 cells. A clinically achievable dose of 1 μ M²⁹⁶ was used as higher doses of 10 μ M led to excessive cell toxicity and cell death over the extended time period. In **Figure 4. 4** we demonstrate an approximately two-fold increase in total HER2 levels on 24 hours of treatment with lapatinib. However, there is a greater, approximately three-fold increase of total HER3 within these cells. This result seems to indicate that the HER2:HER3 dimer, stabilised upon 1 hour of lapatinib treatment, may differentially affect HER2 and HER3 recycling leading to receptor accumulation at different rates.

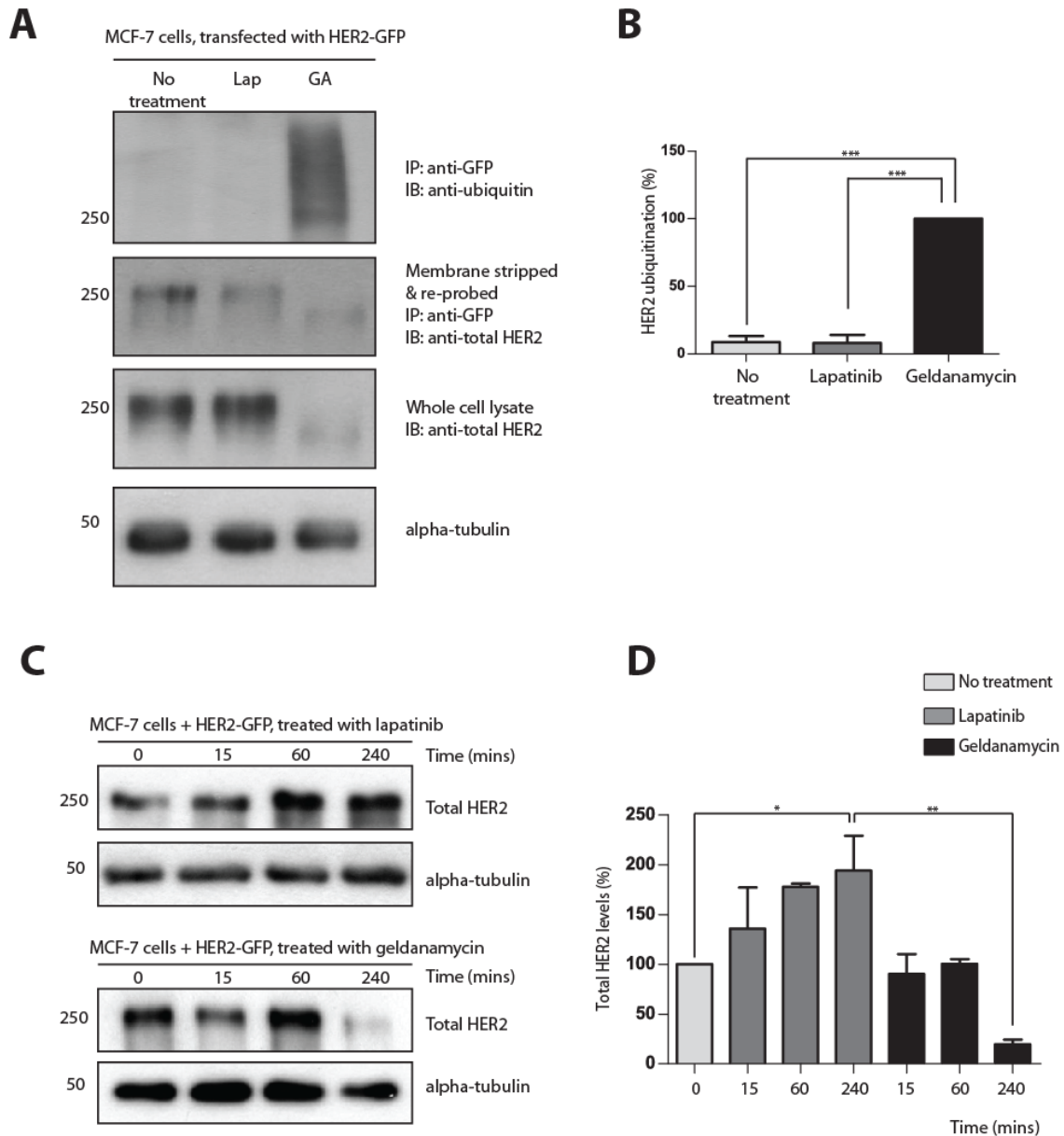


Figure 4. 3 Ubiquitination and accumulation of HER2 on lapatinib treatment

(A) MCF-7 cells were seeded in 60mm plates and transfected with HER2-GFP and treated with lapatinib (10 μ M), geldanamycin (GA, 3 μ M) or vehicle at the time-points indicated, for upto 4 hours, prior to lysis. Whole cell lysates were subject to immune-precipitation with an anti-GFP antibody, as described in *Materials and Methods*. Immunoblot was carried out using the antibodies indicated above. (B) Histogram represents densitometry of mean levels of ubiquitination, normalised to total HER2-GPF expression. Total HER2 levels were normalised by α -tubulin expression. (C) MCF-7 cells were transfected with HER2-GFP for 24hours prior to treatment as described above. (D) Histogram represents densitometry of mean total HER2 levels, normalised to the loading control (α -tubulin). Error bars are representative of the SEM from 3 independent experiments, p-values are <0.001(***), <0.01(**) or <0.05 (*) using one way ANOVA and students T-Test.

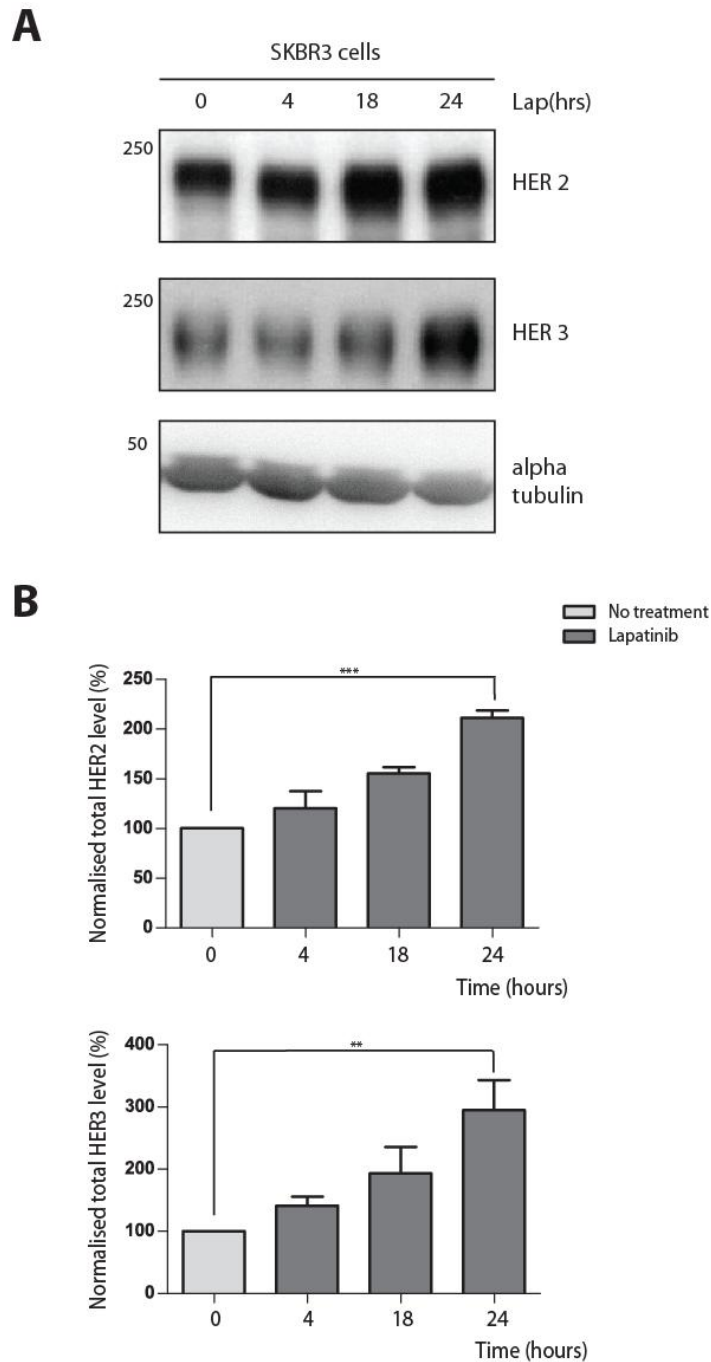


Figure 4. 4 Accumulation of HER2 and HER3 on 24 hours lapatinib treatment

(A) SK-BR-3 cells were seeded in 6 well plates for 23 hours prior to 1 hour pre-incubation with cycloheximide (CH, 50 μ g/ml). Cells were then treated with lapatinib (1 μ M), or vehicle for the time-points indicated, in the presence of CH, prior to lysis. The lysates were run to produce the Western blot shown, as per description in *Materials and Methods*. (B) The histograms depict densitometry of total HER2 levels (upper panel), normalised to α -tubulin levels and total HER3 levels and normalised to α -tubulin levels (lower panel). Error bars represent SEM from 3 independent experiments, p values are 0.0001(***) or 0.0071(**) using students T-test.

4.2.3 Dimer formation is necessary for HER3 re-phosphorylation on extended lapatinib

Treatment of SK-BR-3 cells with lapatinib for 24 hours (**Figure 4.5**) leads to HER3 re-phosphorylation, to a mean of 60% of the baseline level of untreated cells. This is in line with previous data, showing HER3 re-phosphorylation after extended lapatinib treatment in SK-BR-3 and T47D cells, providing a hypothesis for the emergence of resistance to TKI treatment^{192,262,263}. Re-phosphorylation of HER3 is not due to loss of lapatinib activity as phospho-HER2 levels remain undetectable from 1 to 24 hours of lapatinib treatment (**Figure 4.5A**). HER1 is not rephosphorylated and total HER1 levels are reduced at 24 hours. Hence, HER1 is unlikely to be the activating partner for HER3. The level of HER4 expression within this cell line was undetectable, in line with the literature²⁹⁷, and therefore, is also unlikely to be the co-receptor. The question of which receptor does indeed rephosphorylate HER3 is still largely unanswered, both within our group, and in the literature.

Over-expression of the HER2 mutant (I714Q), which attenuates lapatinib-induced dimerisation of HER2 and HER3, allows us to examine the effects of dimerisation on this system (**Figure 4. 6**). We observed a four-fold reduction in HER3 re-phosphorylation at 24 hours treatment with HER2(I714Q) as compared to wild-type, while phospho-HER2 levels remained low after 24 hours of treatment. We hypothesized that this phenomenon could be due to changes in receptor trafficking. Ligand-induced hetero-dimerisation of HER2:HER3 leads to receptor internalization, and sorting either to be degraded or recycled to the membrane for further signaling^{266,270,281,298,299}. This is a key mechanism by which the duration and intensity of HER3 signaling is controlled, and is further investigated in the context of lapatinib treatment.

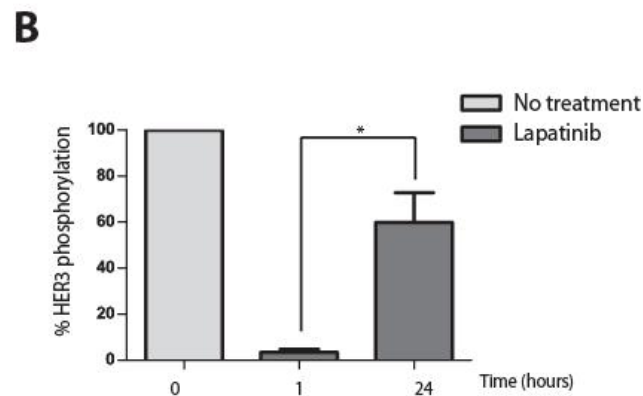
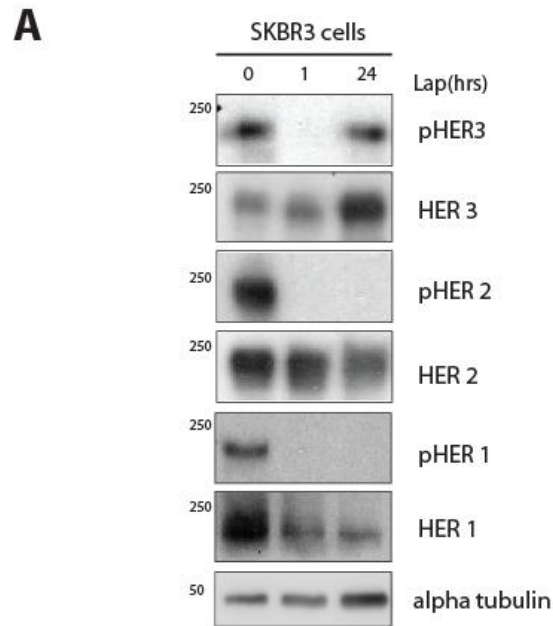


Figure 4. 5 Rephosphorylation of HER3 on 24 hours treatment with lapatinib

(A) SK-BR-3 cells were seeded for 24 hours prior to treatment with 1 μ M lapatinib (or vehicle) for the indicated time points, prior to cell lysis. (B) The histogram depicts phosphor-HER2 levels, normalised to total HER2 levels, which were normalised by the loading control (α -tubulin). The immunoblots and histogram is representative of 3 independent experiments. Error bars are representative of SEM, and the p value=0.011(*) using the unpaired students T-Test.

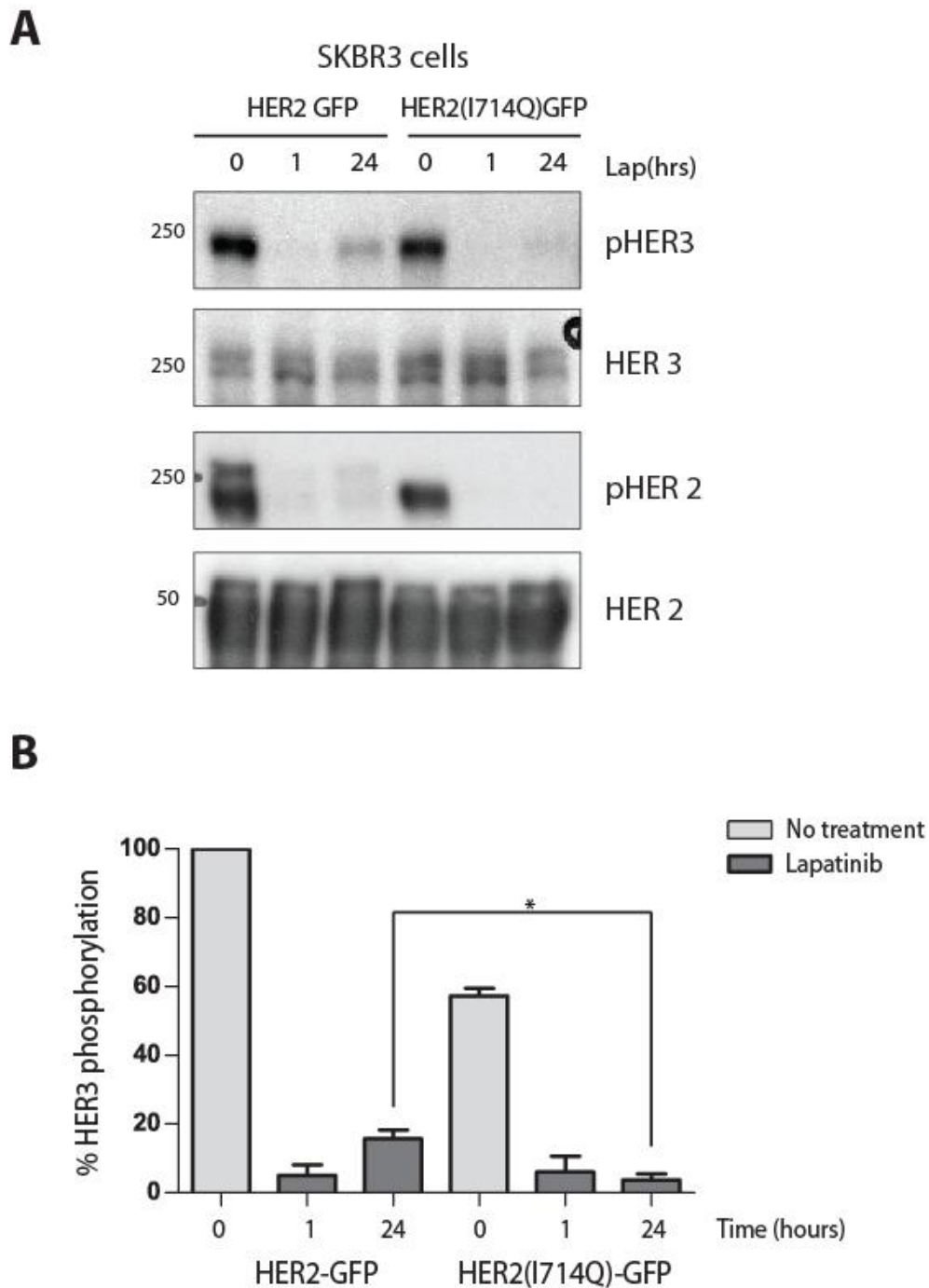


Figure 4. 6 Reduction of HER3 re-phosphorylation on transfection of the dimerisation mutant, HER2 (I714Q)-GFP

(A) SK-BR-3 cells were transfected with HER2-GFP, or the dimerisation mutant (HER2(I714Q)-GFP) for 24 hours prior to treatment with lapatinib 1 μ M, or vehicle, for the times indicated (hours), prior to cell lysis. (B) The histogram depicts densitometry of phosphor-HER3, normalised to total HER3, which is itself normalised by loading control (α -tubulin). Data is representative of 3 independent experiments. Error bars are representative of SEM, and the p value=0.0199 (*) as measured by unpaired students T-test.

Of note, levels of HER3 rephosphorylation are approximately one third lower in cells transfected with the HER2 construct (**Figure 4. 6B**) as opposed to those seen with the endogenous protein (**Figure 4.5B**). The immunoblots in **Figure 4. 7** demonstrate a large decrease in total HER3 levels on transfection of HER2-GFP. The reduction in total HER3 is sufficient to explain the reduction in levels of HER3 rephosphorylation seen in **Figure 4. 6B**. Furthermore, within the transfected groups in **Figure 4. 7** no accumulation of HER3 is seen, either with wild-type HER2 or HER2(I714Q)-GFP, which may also reduce the level of HER3 rephosphorylation on lapatinib treatment of transfected cells. The blots in **Figure 4. 7** have been overexposed in parts, in an attempt to demonstrate both endogenous and transfected levels of the proteins on the same image. Although quantification has been carried out, it is unreliable due to overexposure in some lanes, hence leading to wide standard error bars. However, the immunoblots clearly demonstrate reduced total HER3 levels in SK-BR-3 cells transfected with HER2-GFP. This phenomenon may be due to an increase in degradation of total HER3, a reduction in HER3 transcription or an increase in expression of microRNA (miRNA) targeting HER3. The overexpression of HER2 within these cells may alter downstream signaling pathways affecting HER3 receptor expression. For instance, FoxO1A from the transcription factor family of forkhead box O (FoxO) has been shown to be a target for HER2 in HER2-overexpressing cells, leading to reduced FoxO1A levels³⁰⁰. Garrett *et al* have previously shown that activation of a different member of the FoxO family, FoxO3, is involved in HER3 up-regulation via nuclear translocation²⁶³. Hence it is feasible that overexpression of HER2 within our experiments led to a change in activation or localization of downstream transcription factors, such as the FoxO family, leading to reduced transcription and expression of HER3.

However, the lapatinib-induced effect on HER3 rephosphorylation seen in non-transfected cells is still seen in cells transfected with wild-type HER2-GFP, albeit at a lower level. Hence, I have presumed that lapatinib is still able to induce the formation of symmetric inactive dimers as a pre-requisite to HER3 rephosphorylation, which can be attenuated on dimer disruption using the HER2(I714Q) mutant (**Figure 4. 6**). As no naturally occurring cell line expressing such a mutant has been isolated, this hypothesis is difficult to test further.

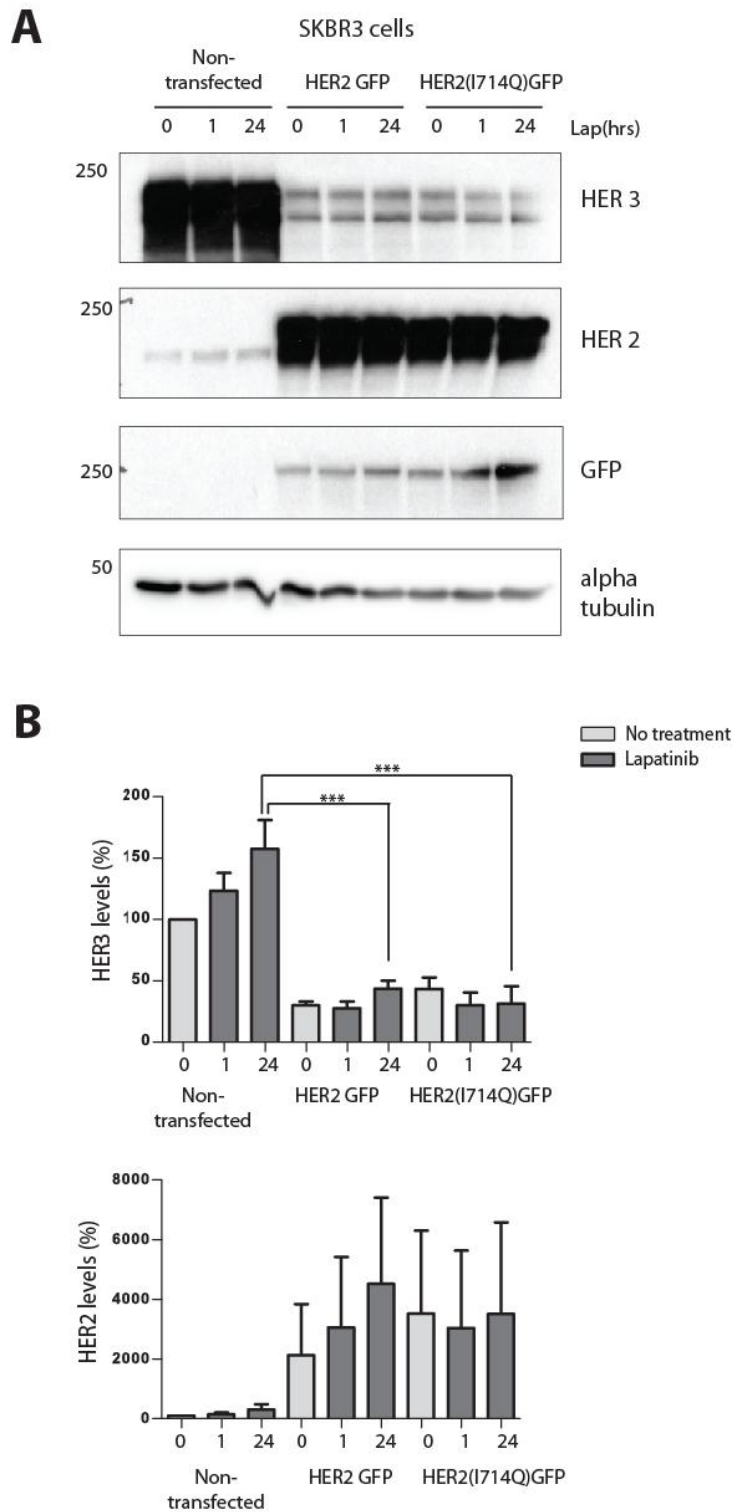


Figure 4. 7 Transfection of HER2-GFP or HER2(I714Q)-GFP leads to increased HER3 degradation

(A) SK-BR-3 cells were transfected with HER2-GFP or the dimerisation mutant (HER2(I714Q)-GFP), or left untransfected, for 24 hours prior to treatment with lapatinib (1 μ M) for the time-points indicated, prior to lysis. (B) Histograms depict average densitometry for total HER3 (upper panel) or total HER2 (lower panel), normalised by the loading control (α -tubulin). Error bars are representative of the SEM from 2 experiments, and p values are <0.001(***) using one way ANOVA.

4.2.4 Expression of the dimerisation mutant, HER2(I714Q)-GFP reduces cell proliferation

I next investigated the functional significance of lapatinib treatment and of transfection of the dimerisation mutant, HER2(I714Q)-GFP upon cell proliferation. MCF-7 cells were used as this breast cancer cell line does not intrinsically overexpress HER2. However, it does express high levels of the co-receptor, HER3²⁹⁷. Therefore, I utilised this system to transfect in wild-type HER2-GFP or the dimerisation mutant, HER2(I714Q)-GFP, in order to examine effects of dimer formation and lapatinib treatment upon cell proliferation.

As expected, treatment with lapatinib, a HER1 and HER2 inhibitor, does not significantly alter non-transfected MCF-7 proliferation rate, compared to untreated cells, as shown in **Figure 4.8A** (red and orange lines). HER1 and HER2 levels in MCF-7 cells are low to undetectable²⁹⁷. Optical densitometry (OD) values are normalised to the time-point 0 value for each condition, i.e. the OD for cells transfected with HER2-GFP at 0, 24 and 48 hours are normalised by the average value noted for HER2-GFP at time-point 0. Cells transfected with the dimerisation mutant, HER2(I714Q)-GFP (dark blue line) exhibited significantly lower cell density compared to cells transfected with the wild-type (pale green), as shown in **Figure 4.8A** and **B**. As this mutant abolishes HER2 phosphorylation in absence of lapatinib, this result provides evidence of a link between receptor phosphorylation and cell proliferation.

Figure 4.8B demonstrates the difference in cell density at 48 hours. This time-point was chosen, rather than 72 hours, as at the later time point, a variable loss of transient transfection of the constructs was observed. However, transfection at 48 hours was observed to more robust. Furthermore, increased cell proliferation of non-transfected cells, whether lapatinib treated or not, led to such high cell densities after 48 hours that OD values started to dip, presumably due to cell over-confluence. Thus the 48 hour time-point was used to represent end-point cell density rather than 72 hours.

Transfection of HER2-GFP, either wild-type or mutant, induced significant lapatinib-sensitivity, as opposed to non-transfected cells treated with lapatinib, which did not differ significantly from untreated non-transfected cells. Although transfection of the dimerisation mutant reduced cell proliferation, lapatinib treatment conferred equivalent cytotoxicity to cells transfected with either wild-type or mutant HER2.

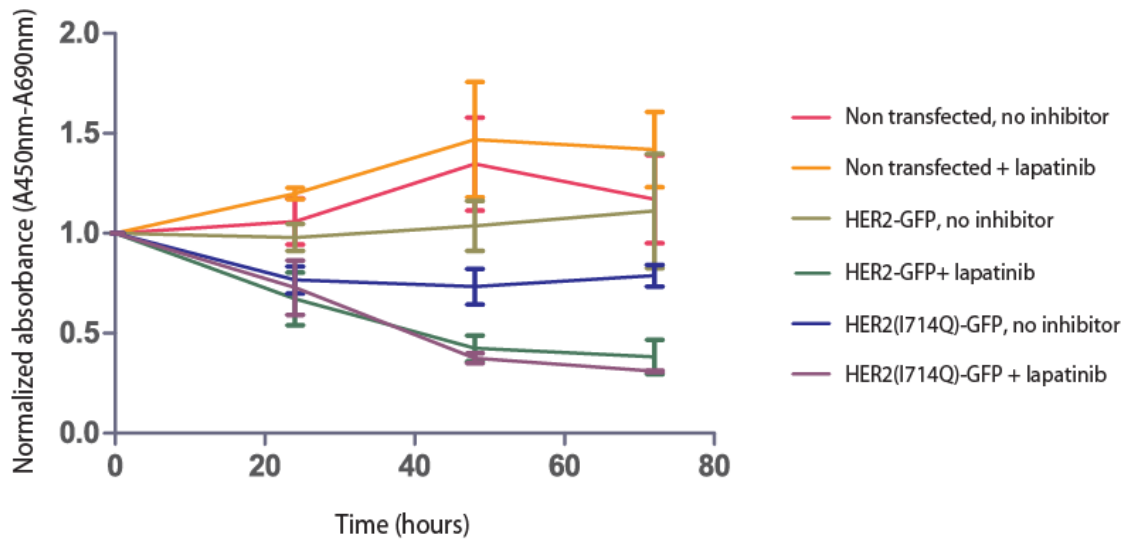
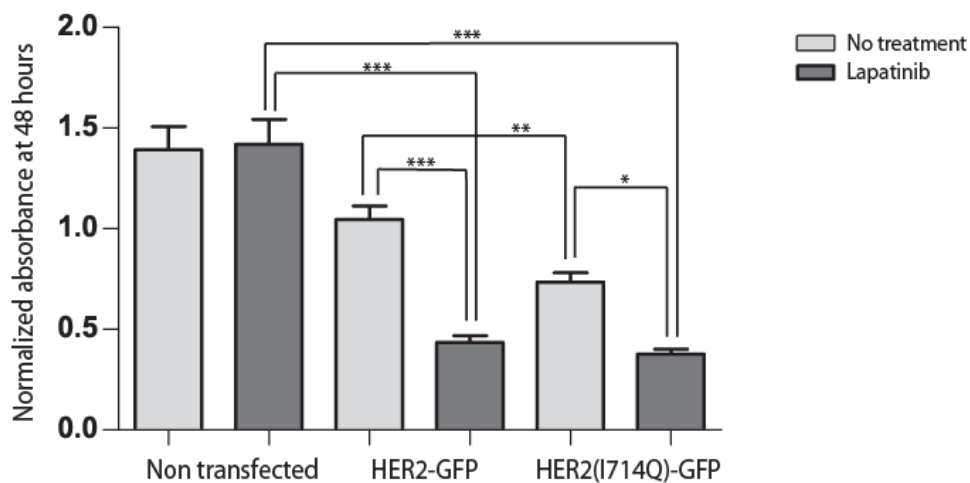
A**B**

Figure 4. 8 Proliferation assays of MCF-7 cells transfected with HER2-GFP or dimerisation mutant (HER2(I714Q)-GFP), untreated or treated with lapatinib.

(A) MCF-7 cells were reverse-transfected in 96 well plates, with HER2-GFP, HER2(I714Q)-GFP, or with vehicle, for 24 hours, prior to treatment with lapatinib (10 μ M) or vehicle. Proliferation assays were carried out over the next 72 hours as described in *Materials and Methods*. Proliferation was determined using WST-1 according to manufacturer's instructions via ELISA reader every 24 hours. The proliferation chart demonstrates the ELISA readout, corrected using a reference wavelength (690nm), normalised according to untreated cells at time-point 0 for each condition. The ELISA readout is assumed to be proportional to cell density. Hence average fold change in cell density is represented. Each time point was carried out in triplicate per condition. The chart is representative of 3 independent experiments, with bars representing SEM. (B) Histogram representing average fold change in cell density at 72 hours, representative of 3 independent experiments. Error bars represent SEM and p-values are <0.001(***), <0.01(**) or <0.05(*) using one way ANOVA.

4.2.5 HER3 re-phosphorylation is dependent upon HER3 recycling to the plasma membrane

We studied the various contributions of HER3 recycling and degradation by adopting an imaging approach as well as an inhibitory strategy to interfere with either of the two processes governing this equilibrium. First we determined the extent of endogenous HER3 degradation in SK-BR-3 cells and found that over a 24 hour period of NRG1 treatment approximately 35% of HER3 is degraded (**Figure 4. 10**). We used two small molecule inhibitors, monensin and bafilomycin to distinguish receptor recycling from receptor degradation.

Monensin is a Na⁺/H⁺ antiporter which inhibits intracellular protein transport including recycling¹⁹². Bafilomycin A1 is a vacuolar H⁺-ATPase inhibitor, which inhibits acidification of sorting endosomes and thereby slowing maturation to late endosomes and subsequent lysosomal degradation³⁰¹⁻³⁰³. The importance of HER2:HER3 dimer recycling in HER3 re-phosphorylation was tested by inhibiting recycling vesicle trafficking using monensin. We observed a three-fold reduction of HER3 re-phosphorylation, from 60% to 10% on monensin treatment (**Figure 4. 9**, furthest right 3 rows). In contrast, treatment with bafilomycin did not significantly affect the HER3 re-phosphorylation level. Furthermore, monensin treatment, in the presence of NRG1, led to an increase in HER3 degradation, from 35% with NRG1 alone, to 60% degraded with the addition of monensin (**Figure 4. 10**). The latter effect may be explained by monensin-induced inhibition of HER3 recycling leading to enhanced degradation as one of the remaining fates of endocytosed HER3.

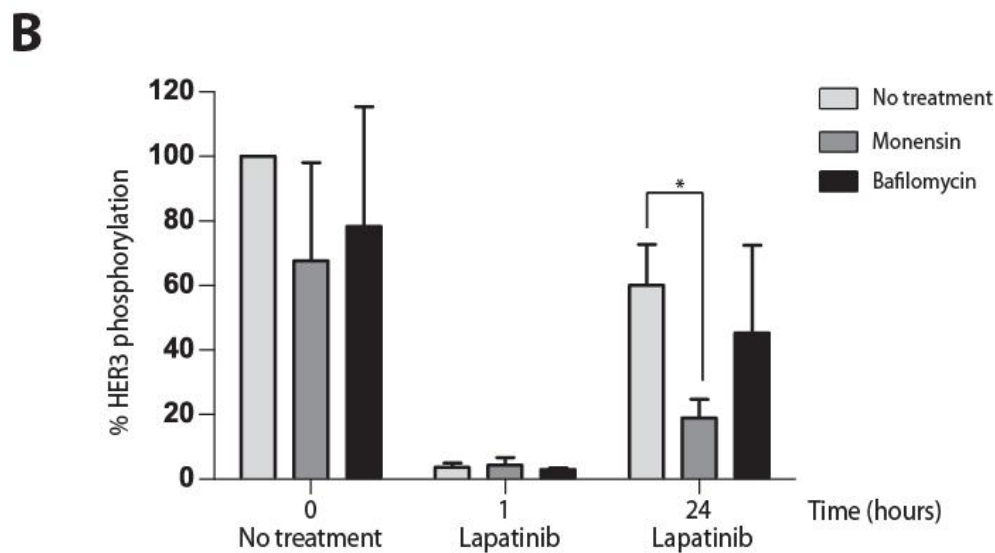
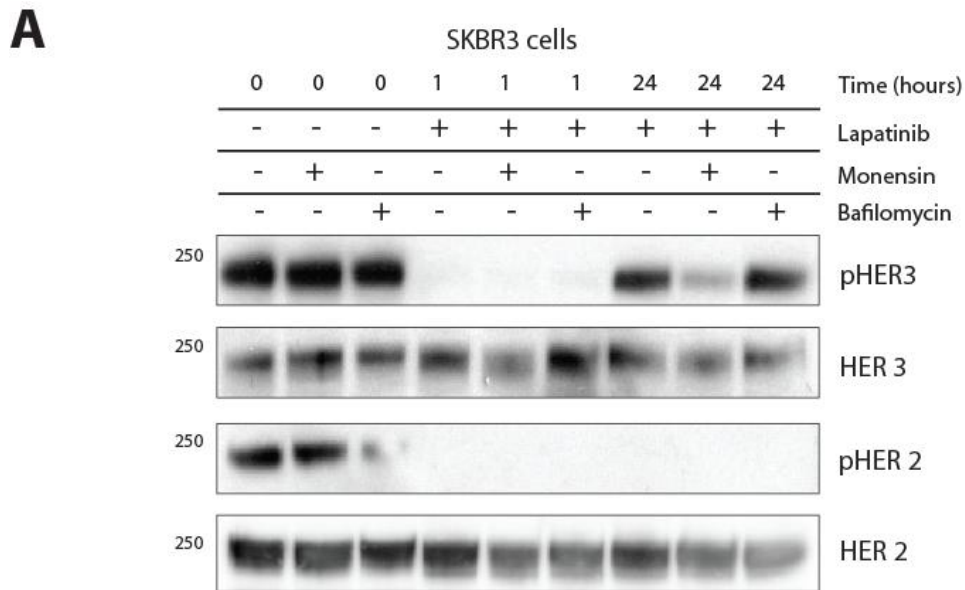


Figure 4. 9 Monensin treatment reduces HER3 re-phosphorylation

(A) SK-BR-3 cells were seeded for 24hours prior to treatment with lapatinib (1 μ M) or bafilomycin (100nM) for the times indicated, prior to lysis. In the case of monensin, treatment consisted of 3 hours incubation with 10 μ M monensin prior to fixation where indicated. (B) The histogram depicts densitometry of phosphor-HER3 levels, normalised to total HER3 levels, normalised by loading control (α -tubulin). Data is representative of 3 independent experiments; error bars are representative of SEM, p value =0.0367 (*) using the unpaired Student's T-Test.

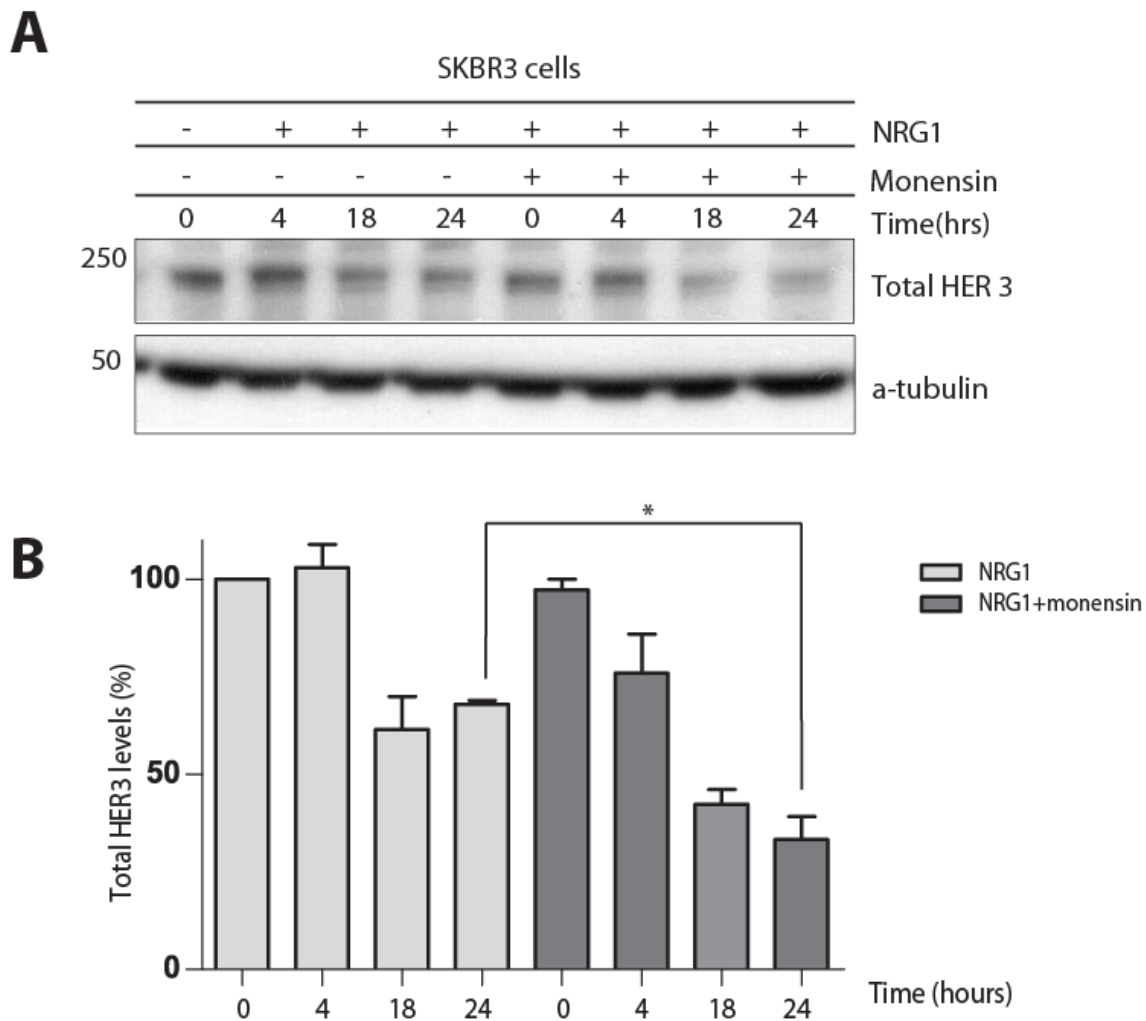


Figure 4. 10 Monensin increased ligand-induced HER3 degradation

(A) Western blot of SKBR3 cells, seeded for 23 hours, prior to incubation with cycloheximide (20 μ g/ml) for 1 hour, in order to arrest protein synthesis. Cells were then treated with neuregulin (50ng/ml) or neuregulin and monensin (1 μ M) for the times indicated, prior to lysis, in the presence of cycloheximide. (B) Histogram depicting densitometry of total HER3 at the time points indicated compared to baseline as time-point 0. Total HER3 levels were normalized for α -tubulin levels (loading control shown in Western blot panel). Data are representative of 3 independent experiments; error bars represents SEM, p value = 0.0196(*) using the unpaired Student's T-Test.

I used confocal microscopy to investigate the location of HER3 with respect to the small Rab GTPase Rab11, which was previously used as a marker for 'slow' receptor recycling via the ERC³⁰⁴, compared to the Rab4, a marker for 'rapid/fast' recycling endosomes. **Figure 4. 11** shows co-localization of HER3-GFP with the endosomal marker Rab11 (white arrows), but not EEA1 (a marker of early endosomes) (**Figure 4. 12**), showing that HER3 is primarily being recycled via the 'slow' Rab11 route after 24 hours of lapatinib treatment. There is no co-localisation between HER3-GFP and Rab11-RFP in non-treated cells, or in cells treated with lapatinib for 1 hour. Not only is there an increase in the amount of intracellular HER3 co-localising with Rab11 after 24 hours of lapatinib treatment, but the nature of the Rab11-labelled vesicle appears more to be tubulo-vacuolar rather than vesicular. There seems to be no significant change in the co-localisation of HER3-GFP with EEA1 IgG (bound to anti-mouse Cy3 IgG) on lapatinib treatment.

On examination of the distribution of HER2-GFP or the dimerisation mutant, HER2(I714Q)-GFP, there seems to be an increase in the levels of intracellular, peri-nuclear HER2 over the 24 hour time period of lapatinib treatment (**Figure 4. 13**). This is the case for both the wild-type or mutant receptor. However, no co-localisation between either type of receptor and Rab11-RFP is noted.

Treatment with monensin produced some interesting results. As in the case of the cells used for immunoblot, monensin (10 μ M) was added to the cell media for the last 3 hours of incubation, prior to fixation for immunofluorescence (**Figure 4. 14**). Non-treated cells contain a pool of intracellular HER3-GFP, a large part of which co-localises with Rab11-RFP on monensin treatment (upper panel). This suggests that HER3 normally undergoes recycling via the ERC, which can be attenuated, leading to accumulation of a proportion of the receptor within the ERC. On treatment with lapatinib for 1 hour (middle panel), in the presence of monensin, a larger fraction of intracellular HER3 appears to localize with Rab11, in enlarged vesicles (white arrow), consistent with the monensin-induced block of exit from endocytic recycling compartments. However, on extended lapatinib treatment (24 hours, lower panel) in the presence of monensin, HER3-GFP is observed in punctuate perinuclear structures which do not co-localise with Rab11-RFP (white arrows). This finding is discussed below. Together, these confocal studies support the inference that the monensin effect demonstrated on lapatinib-induced HER3 re-phosphorylation (**Figure 4. 9**) is due to inhibition of HER3 recycling, possibly via the ERC.

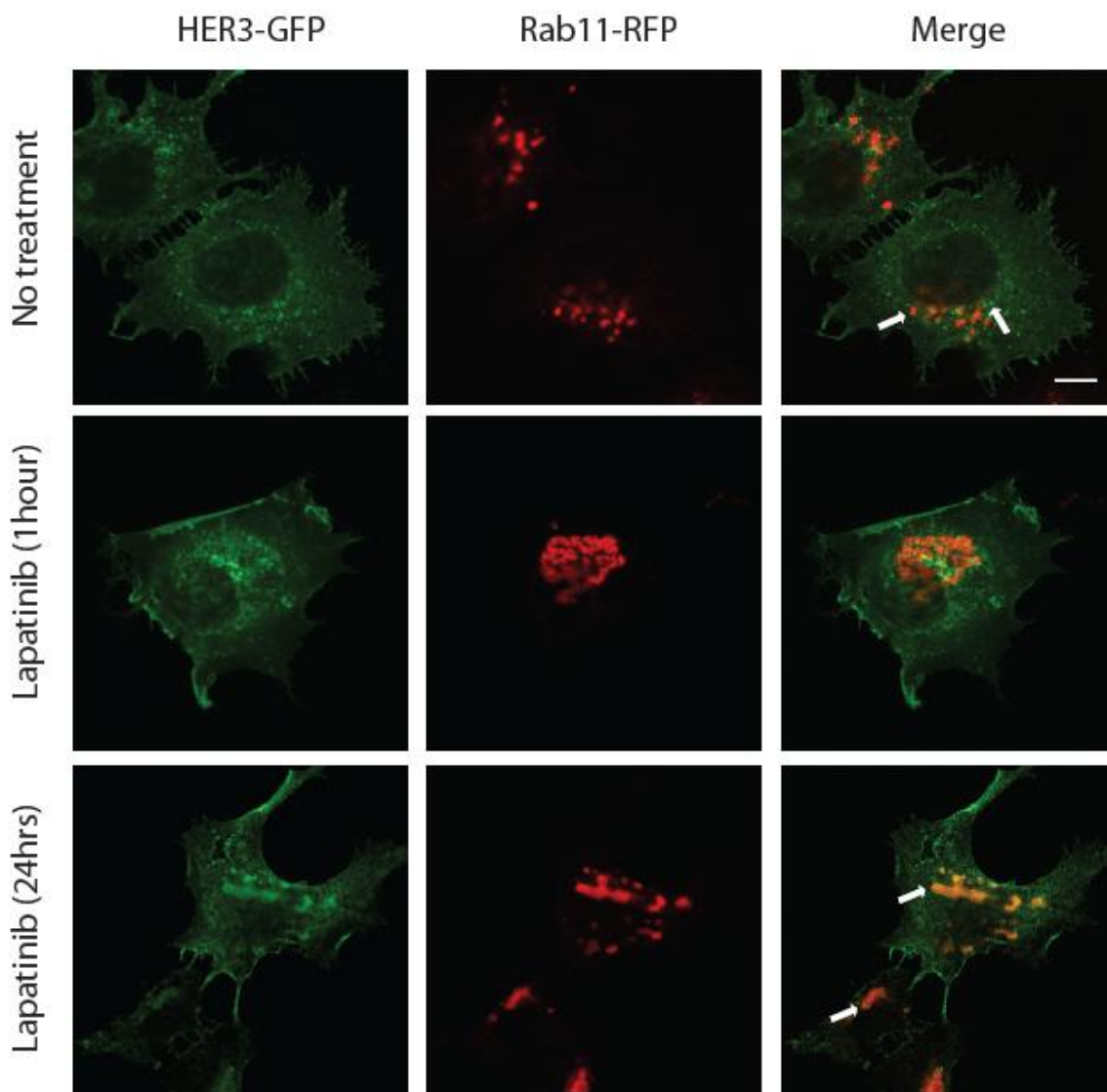


Figure 4. 11 HER3-GFP co-localisation with Rab11-RFP on lapatinib treatment

SK-BR-3 cells were seeded in 24 well plates and transfected with HER3-GFP and Rab11-RFP for 24hours in 5% Optimem. Cells were then treated with lapatinib for 24 hours, 1 hour or incubated with vehicle in 5% Optimem, prior to fixation with PFA and preparation for immunofluorescence as described in *Materials and Methods*. Images are representative of cells seen; at least 10 fields of view were examined per condition. Areas of co-localisation are highlighted with white arrows. The white scale bar represents 5 μ m.

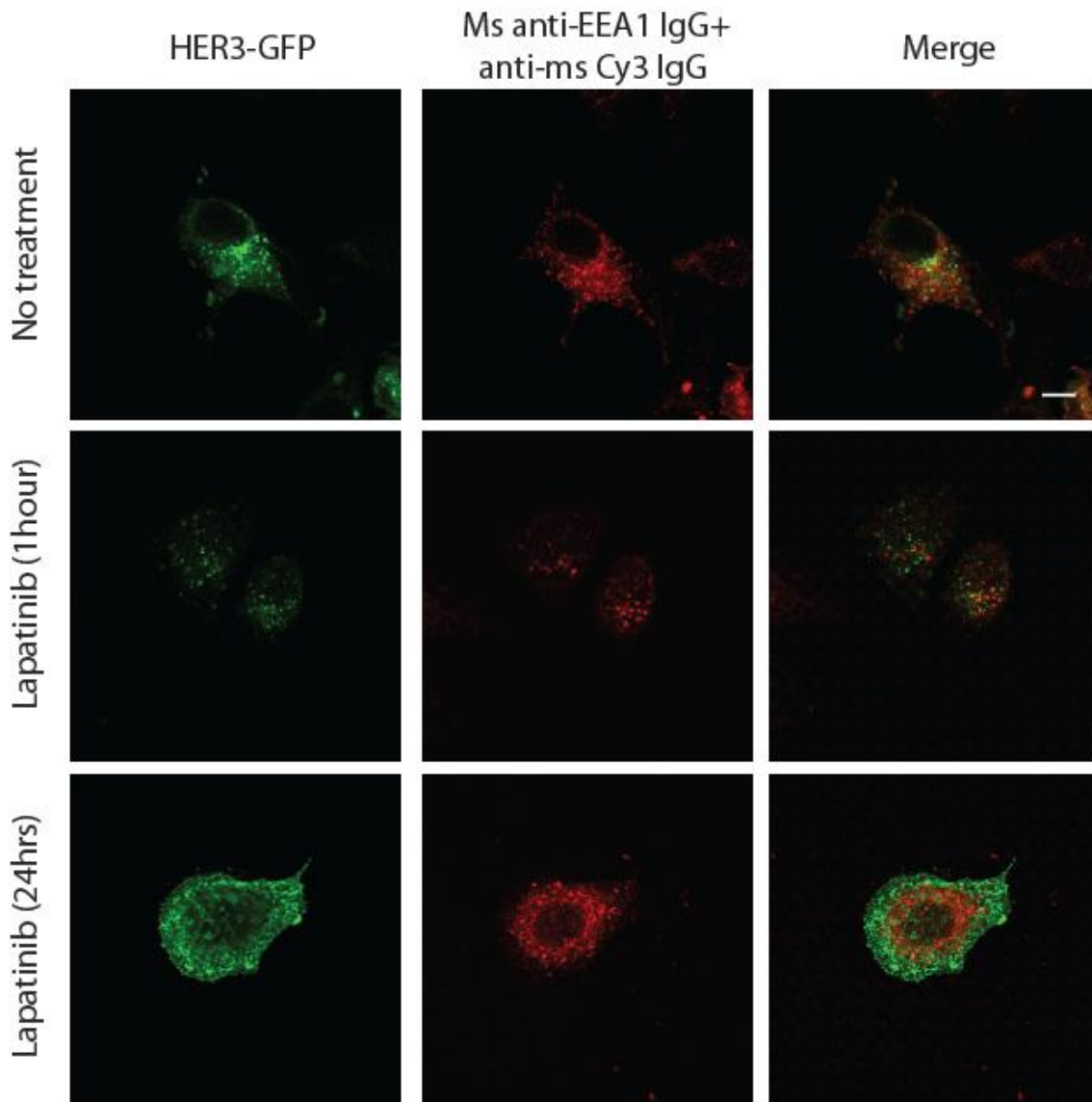


Figure 4. 12 HER3-GFP does not co-localise with anti-mouse Cy3 IgG bound to mouse anti-EEA1 IgG upon long term lapatinib treatment

SK-BR-3 cells were transfected with HER3-GFP and treated as described in **Figure 4. 11**, prior to fixation for immunofluorescence. Cells were stained with mouse anti-early endosomal antigen-IgG (EEA-1) followed by α -mouse-Cy3 IgG. Images are representative of cell seen; at least 10 fields of view were examined per condition. Co-localisation between HER3-GFP and Cy3 IgG was not observed. The white scale bar represents 5 μ m.

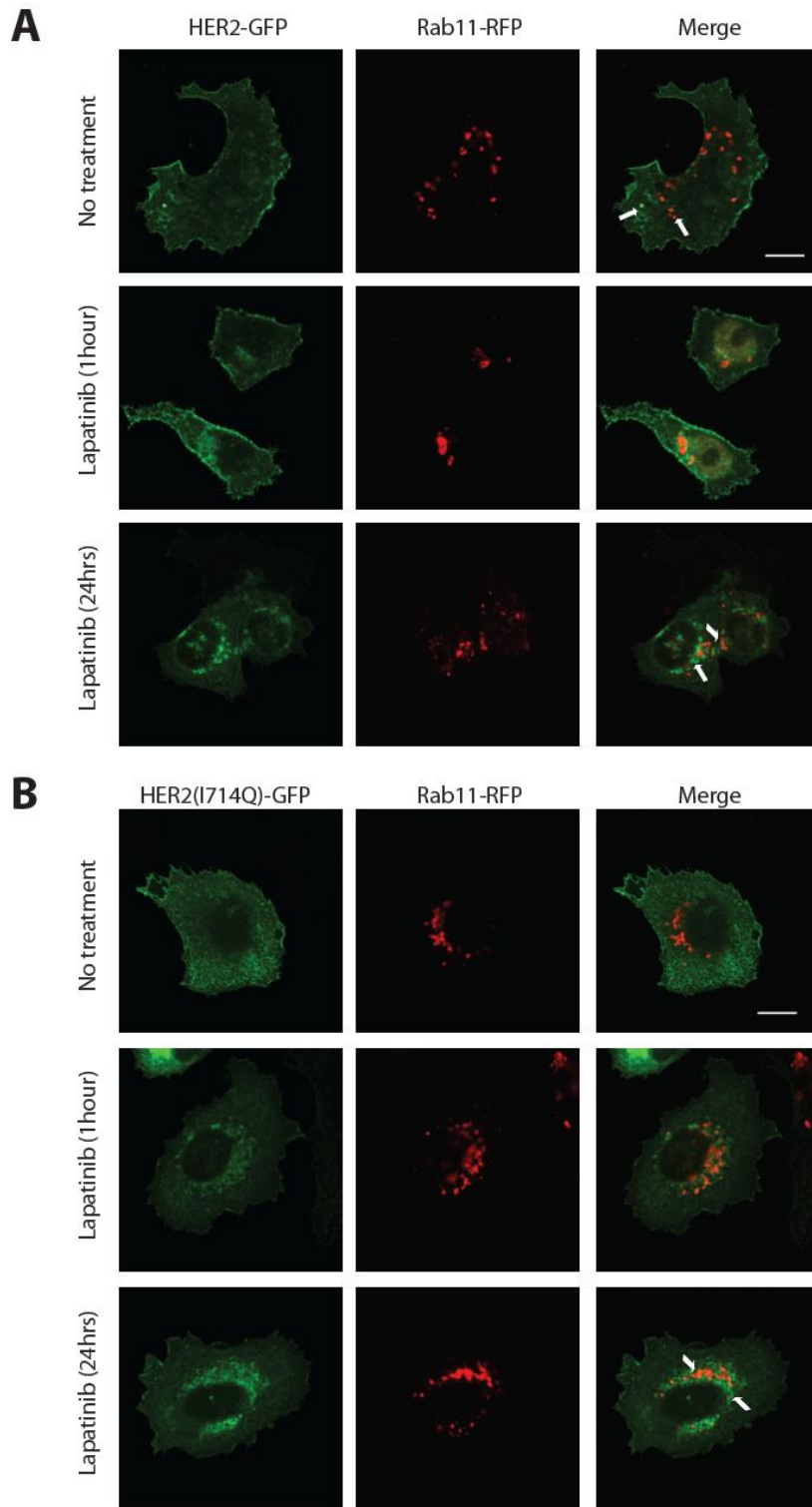


Figure 4. 13 HER2-GFP and HER2(I714Q)-GFP do not co-localise with Rab11-RFP on lapatinib treatment

SK-BR-3 cells were transfected with HER2-GFP or HER2(I714Q)-GFP, and Rab11-RFP and treated as described in **Figure 4. 11**, prior to fixation for immunofluorescence. Images are representative of cell seen; at least 10 fields of view were examined per condition. Co-localisation between HER2-GFP and Rab11-RFP was not observed as demonstrated with white arrows. The white scale bar represents 5 μ m.

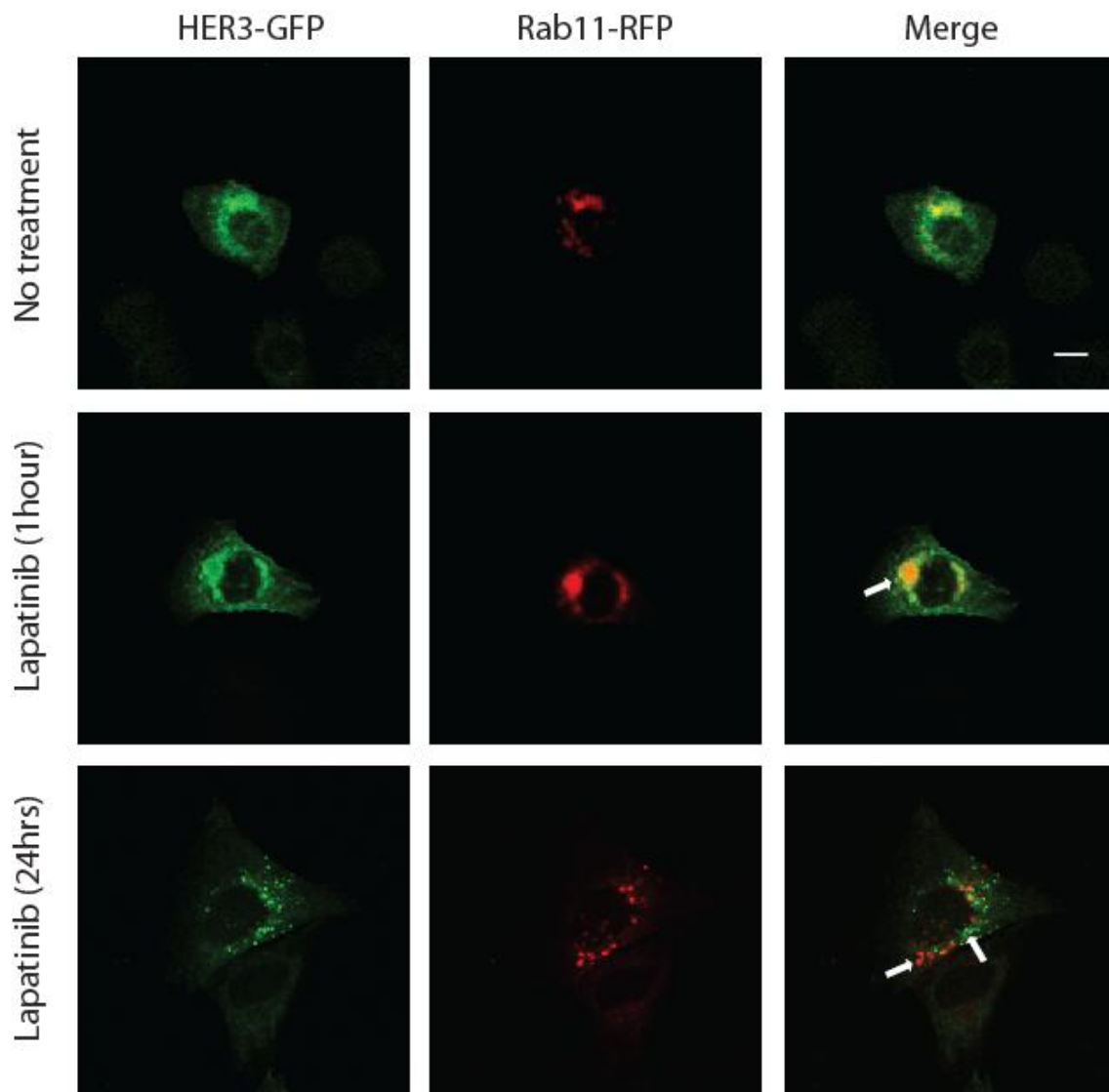


Figure 4. 14 Monensin treatment reduces HER3-GFP and Rab11-RFP co-localisation at 24 hours of lapatinib treatment

SK-BR-3 cells were transfected with HER3-GFP and Rab11-RFP and treated as described in **Figure 4. 11**, prior to fixation for immunofluorescence. In this case, all cells were treated with monensin (10 μ M) for 3 hours just prior to cell fixation. Images are representative of cell seen; at least 10 fields of view were examined per condition. Co-localisation between HER3-GFP and Rab11-RFP was observed at 1hour of lapatinib treatment but not at 24 hours as demonstrated by the white arrows. The white scale bar represents 5 μ m.

4.3 Discussion

Production of a mutant in HER2 which attenuates lapatinib-induced dimerisation (I714Q), has provided a novel method for examination of the role of dimerisation in prolonged lapatinib treatment. We have shown, in line with published data^{192,262,263}, that rephosphorylation of HER3 occurs after 24 hours of lapatinib treatment despite phospho-HER2 levels remaining suppressed (**Figure 4.5**). HER3 rephosphorylation is a potential escape mechanism from TKIs and it may be mediated by a variety of mechanisms. These include up-regulation of HER3 via PI3K/Akt-induced de-phosphorylation of the transcription factor FoxO3a, leading to nuclear translocation and HER3 transcription^{192,263}. However, these pathways are not easy to target and use of an inhibitor to PI3K or MAPK did not abolish downstream signaling²⁶². Accumulation of both HER2 and HER3 over the 24 hour period of lapatinib treatment (**Figure 4. 4**) may lead, in part, to the increased levels of HER3 phosphorylation seen at 24 hours. Protein accumulation is likely to be due to lack of receptor ubiquitination, as this post-translational modification is a key event to the targeting of receptors to lysosomal degradation. This effect is in line with data from Garrett and Sergina *et al* who demonstrated a reduction in HER3 re-phosphorylation on the reduction of total active receptor levels by siRNA and antibody treatment targeting either HER2 or HER3^{192,263}. Although higher doses of lapatinib also reduced HER3 re-phosphorylation, neither of these treatment strategies are clinically viable.

Transfection of HER2 (I714Q) into this system attenuated HER3 re-phosphorylation, thus highlighting a novel, potentially vital step in the development of HER3-mediated resistance to lapatinib. We propose HER2:HER3 dimerisation as a critical prior event to HER3 re-phosphorylation on prolonged lapatinib treatment. The dimerisation mutant demonstrates functional significance of the, non-lapatinib bound HER2:HER3 dimer, as cellular proliferation of cells transfected with this mutant is significantly lower than that seen with wild-type HER2-GFP (**Figure 4. 8**). However transfection of the mutant was not protective of lapatinib-induced cytotoxicity. This cytotoxic effect may be induced by off-target lapatinib effects such as the upregulation of pro-apoptotic death TRAIL death receptors²⁵⁹ and the pro-apoptotic protein Bcl-2 interacting mediator of cell death (BIM)²⁶⁰.

Although our results have improved understanding of the mechanism by which HER3 recycles within the lapatinib-induced dimer, it is not entirely resolved. My proposed model of HER2 and HER3 intracellular trafficking on lapatinib treatment is shown as a schematic in **Figure 4.15**. Both HER2 and HER3 are phosphorylated in non-treated cells (time-point 0, **Figure 4.5**).

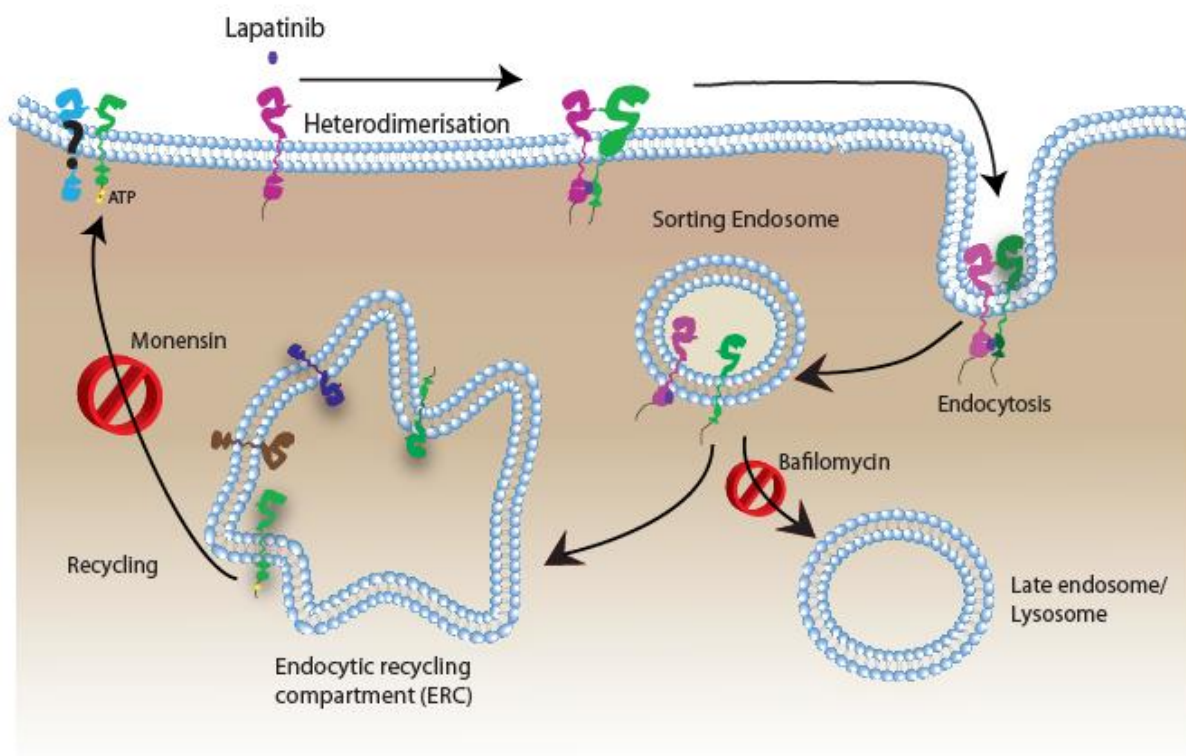


Figure 4. 15 Schematic representing intracellular trafficking of HER receptors

The model represents intracellular events pertaining to HER3 (green receptor on plasma membrane) after lapatinib binding to HER2 (pink receptor). The unphosphorylated HER2:HER3-lapatinib complex is stabilised and internalises to the sorting endosome. HER2 and HER3 may dissociate in this vesicle with HER3 trafficking to the endocytic recycling compartment (ERC). It is then sorted for recycling and may associate with substrates such as Src or PLC γ (represented by purple and brown receptors within the ERC). HER3 may re-phosphorylate in the ERC or at the plasma membrane (yellow stars represent ATP). The receptor(s) with which HER3 interacts for rephosphorylation are unknown and represented by the question mark over the blue receptor at the plasma membrane. Monensin inhibits receptor recycling to the cell surface whereas bafilomycin inhibits maturation of sorting endosomes to the late endosome.

This phenomenon may be due to increased levels of HER2 in this cell-line pushing the HER dimerisation equilibrium towards the formation of HER2 homodimers and HER2:HER3 heterodimers. Alternatively, autocrine production of ligand, e.g. NRG1³⁰⁵, may lead to HER2:HER3 dimer formation. Whichever the case, treatment with lapatinib (1 hour) abolishes phosphorylation of both receptors but, as we know from **Chapter 3**, stabilises the HER2:HER3 complex. This kinase inactive, receptor complex may be slowly internalised at a similar rate to the constitutive internalisation of kinase-dead HER3²⁶⁶, which is more rapid than HER2 internalisation. This reaction is unlikely to occur in clathrin-coated pits as ligand activation is required for the trafficking of e.g. HER1 receptors in this rapid, saturable mechanism of endocytosis²⁶⁷. Once within the sorting endosome, HER3 may disassociate from HER2 within the acidic environment of this cellular compartment, leading to dimer disruption, as supported by the confocal images of different patterns of co-localisation of HER3 and HER2 with Rab11 after extended lapatinib treatment (**Figure 4. 11** and **Figure 4. 13**).

The structures within which internalized HER3 and Rab-11 co-localise after 24 hours of lapatinib treatment (demonstrated in **Figure 4. 11**, white arrows) resemble fused vacuolar structures in which receptors are sorted for recycling. Treatment with bafilomycin³⁰¹⁻³⁰³, which slows maturation from the sorting endosome to late endosome, does not affect HER3 rephosphorylation (**Figure 4. 9**). Therefore it is likely that HER3, after dissociation from the dimer, is trafficked from the sorting endosome to the endocytic recycling compartment (ERC), which is comprised of fused tubulo-vacuolar structures. This observation is in line with the confocal images demonstrating co-localisation between HER3 and Rab-11, a membrane marker present primarily in the ERC²⁷⁶. HER3 rephosphorylation to 60% of baseline (**Figure 4.5**) may occur at the cell surface or at any point along the recycling pathway from the ERC. However, this phenomenon is unlikely to occur in endosomal membranes to which protein tyrosine phosphatases (PTP) are tightly anchored³⁰⁶. For instance, recently, PTP1B which is a phosphatase for HER1 has been shown to be on the cytoplasmic face of the endoplasmic reticulum, a specific location in the cell where it can interact with endocytosed HER1, via direct membrane contacts sites between the endoplasmic reticulum and endosomes³⁰⁷. This is another example whereby HER phosphorylation state can be directly influenced by receptor traffic and is specifically regulated at different intracellular organelles, by virtue of location-specific receptor-phosphatase interactions.

HER3 may associate with a variety of substrates within the endosome, as discussed below, and traffic in a complex to the cell surface whereby HER3 becomes phosphorylated either by these substrates or alternate membrane-bound receptors. The biochemical data that

demonstrate attenuation of HER3 re-phosphorylation by monensin, a drug which inhibits the function of cellular recycling pathways, corroborate this model. Monensin reduces recycling from the ERC to the cell surface, thus allowing intracellular accumulation of HER3 and increased dephosphorylation by phosphotyrosine phosphatases. Confocal images from short-term lapatinib treatment support this conclusion by demonstrating enlarged recycling vesicles in which HER3-GFP and Rab11-RFP co-localise (**Figure 4. 14**, middle panel). However, monensin treatment of cells exposed to lapatinib for 24 hours leads to the accumulation of HER3 within punctuate perinuclear structures which do not co-localise with Rab11, and do not appear to represent the ERC. A possible explanation is that extended lapatinib treatment increases the level of HER3 recycling, and hence the load processed through the ERC, which is likely the rate-limiting factor within this recycling pathway. Blockage of ERC function, as effected by the pH-neutralising capacity of monensin, could lead to accumulation of HER3 in the short term (1 hour lapatinib) but shunting to alternate endocytic vesicles in the long term (24 hours lapatinib) as the receptor load outweighs ERC processing capacity. HER3 may accumulate in these vesicles or traffic to late endosomes for degradation. As monensin is a sodium ionophore which collapses sodium-hydrogen gradients³⁰⁸, it may disrupt the pH in late endosomes or lysosomes in the short term, which would attenuate receptor degradation and allow HER3 accumulation within these vesicles. In summary, although it has not been possible to elucidate every step in the HER3 recycling pathway, the evidence shown supports HER3 rephosphorylation on extended lapatinib treatment, due to a higher rate of recycling via the ERC.

A key question within this field concerns which receptor is in fact responsible for HER3 rephosphorylation. HER2 tyrosine kinase activity has been suggested as a potential mechanism of reactivation of HER3²⁶³ but a consistent absence of HER2 phosphorylation is seen at the time-point of HER3 rephosphorylation on our immunoblots, in line with the literature^{192,262}. Hence any contribution of residual HER2 kinase activity is likely to be minimal. An alternative receptor kinase may be implicated. A variety of candidates have been tested, by other groups and us, including IGF-1R, C-MET, HER1, and HER4³⁰⁹, MUC4 with no positive results²⁶³. Activation of MET via HER3 has been shown to lead to resistance to gefitinib treatment in lung cancer cell lines and in 22% of lung tumours which were resistant to gefitinib³¹⁰. Similarly in gastric cancer cell lines, MET receptor activation has been shown to rescue cells from lapatinib-induced cytotoxicity and represents a mechanism of resistance to lapatinib³¹¹. An alternate membrane-bound receptor tyrosine kinase, bearing a kinase domain similar to MET, AXL, has also been implicated in the development of resistance to lapatinib³¹². IGF-1R has been implicated in mediation of resistance to trastuzumab via HER1³¹³. Another suggestion is that the residual kinase activity of HER3 is

sufficient to auto-phosphorylate the up-regulated receptor. However this activity is 1000 fold less than that shown by HER1 and Shi *et al* hypothesise that it would only be sufficient to activate a competent TKD in trans rather than autophosphorylation of HER3²²³. The cellular location of HER3 may also play a role in the activation of a HER3-dependent resistance mechanism. For instance, HER3 may associate with substrates which are only present in the endosomes, such as PLC γ . Such an association has been demonstrated between cytosolic HER2 and PLC γ ²⁸⁷, and HER1 and Src in endocytic recycling compartments²⁸⁹. The identity of the partner for HER3 re-phosphorylation is still elusive.

We have demonstrated, amongst others^{192,262,263}, the vital role of HER3 in mediating resistance to HER targeted TKIs. However, in targeting this receptor for treatment, we face several challenges. Firstly, disruption of the HER2:HER3 dimer at the extracellular components may not be sufficient to affect intracellular binding. For example, pertuzumab, an antibody to the HER2:HER3 extracellular dimerisation interface, is very effective at inhibiting ligand-induced heterodimerisation^{184,245}, but is much less effective at disrupting ligand-independent HER2:HER3 dimerisation^{314,315}. This is likely to be due to the different structural characteristics of the HER3 ECD in the liganded versus unliganded conformation. Secondly, the function of HER3 is not mediated through its tyrosine kinase catalytic activity. Within the last two chapters we have highlighted two key areas which may be useful targets for novel therapies: the kinase domain ATP binding site and its dimerisation domain. As mutation of the ATP pocket in HER3 abolished HER2:HER3 dimerisation, this pocket could be targeted by the ATP analogue class of TKIs which target noncatalytic functions. Lapatinib-induced TKD-mediated HER2:HER3 dimerisation seems to be a key event leading to altered HER3 trafficking and re-phosphorylation. Therefore, allosteric drugs targeting this site or pre-existing somatic mutations equivalent to HER2(I714Q) could also attenuate the development of HER3-mediated resistance. Such strategies disrupting the kinase domain-mediated dimer could prove powerful, paired with existing HER2 targeted drugs which disrupt the extracellular dimerisation site, such as pertuzumab. Furthermore, if receptor recycling is critical to the development of resistance, the recycling pathway may be a key novel target in circumventing TKI mediated resistance.

Several studies have demonstrated utility of lapatinib in early HER2-positive breast cancer^{43,44}. However not all tumours which overexpress the HER2 receptor are sensitive to lapatinib³¹⁶, and resistance eventually develops. Lapatinib induced hetero-dimers may persist within these tumours and highlight patients at risk of early recurrence, who may benefit from increased surveillance. Furthermore, tumours which do not classically overexpress HER2 (by FISH or immunohistochemistry), may yet respond to HER2-targeted drugs, such as lapatinib^{317,318}. With the advent of new HER2 targeted drugs, combination

regimes need to be designed rationally with appropriate biomarkers. For example, as pertuzumab is less effective at disrupting ligand independent HER2:HER3 dimerisation^{314,315} combination treatment with lapatinib may lead to a failure of efficacy in the clinic due to the stabilisation of the lapatinib-induced HER2:HER3 dimer. These examples require a validated biomarker assessing the effect of the HER2 targeted drug upon HER2:HER3 dimerisation and the degree of persisting hetero-dimers. I have attempted to translate this FRET/FLIM HER2:HER3 dimer assay to a dual antibody-mediated assay to measure HER2 and HER3 interactions in patient tumour samples, as described in the next chapter.

Chapter 5: Development of a FRET/FLIM based biomarker – challenges and pitfalls

5.1 Introduction

As discussed in **Chapter 1**, a number of prognostic tools, based upon clinical data, anatomical staging and histopathological features, predicting the risk of metastatic relapse are used by oncologists to more accurately guide clinical decision-making^{52,54,59}. The appeal of these instruments lies in their simplified and averaged format, but this is also their major flaw as they cannot predict outcome on an individual level.

It is hoped that translational genomic and proteomic research will discriminate more accurately than is possible at present between patients with a good prognosis and those who carry a high risk of recurrence. Rational treatments, targeted to the specific molecular pathways of an individual's high-risk tumour, are at the core of tailored therapy. Recent experience with molecule-targeted therapeutics suggests that the efficacy of such therapies would be improved if we could selectively treat patients on the basis of aberrations in protein function/activity within specific biochemical pathways, rather than simply the level of target antigen expression³¹⁹. FRET-FLIM imaging of protein function and protein complex formation could potentially improve patient selection for targeted therapy, by specifically identifying for each patient whether the targeted pathway is active in a particular tumour sample, thus truly tailoring medicine to the individual.

Since the widespread adoption of the HER2-targeted inhibitor, trastuzumab (a monoclonal antibody to the extracellular domain of HER2) for HER2 over-expressing breast cancer, there has been a surge in the development of targeted, potential anti-cancer drugs. During drug development, only one in 10,000 compounds screened at the target localisation stage will succeed to approval for clinical use. This process may take more than 10 years³²⁰. Furthermore, once the drug is within the clinical sphere, clinical outcomes rarely meet initial expectations. For instance, although the tyrosine kinase inhibitors (TKIs), erlotinib and gefitinib, are targeted to HER1, and approved for use in non-small cell lung cancer³²¹, response rates are less than 10% in unselected populations and overexpression of HER1 does not correlate with response to treatment^{322,323}. There is a real need for validated predictive biomarkers for drug activity, both for drug development and to rationalise clinical drug use. We propose that quantification of associations between signaling proteins by

FRET/FLIM may allow delineation of the specific molecular pathway alterations within the cancer patient at a subcellular level.

The cancer genome or proteome is relatively plastic and can be reprogrammed, at different stages of tumour development, to carry out various cellular processes such as proliferation, invasion and metastasis, or reversion to dormancy³²⁴. This plasticity gives rise to spatial heterogeneity of cancer within the body and makes it challenging to fully assess treatment response. Molecular imaging provides a solution by mapping the spatial response of the tumour to treatment within the individual and thereby, to monitor progress throughout the patient journey. Hence, a further challenge in mapping response to treatment is tumour heterogeneity, which is only just beginning to be described in terms of gene expression³²⁵. We have reviewed recent advances in prognostic and predictive tools, in terms of gene expression signatures in **Chapter 1.2.2**. We now describe the potentially complementary tools of assessment of protein expression and interaction in the development of novel prognostic and predictive biomarkers.

5.1.1 Existing prognostic protein-based biomarkers for HER2-positive breast cancer

Evaluation of HER2 overexpression by immunohistochemistry (IHC) or gene amplification using fluorescent in situ hybridisation (FISH), is not only the strongest prognostic factor in patients with HER2-positive disease, irrespective of lymph node status³²⁶, but also remains the sole criteria by which we choose to prescribe HER2-targeted therapy^{327,328}. However, of these HER2-positive patients only 50% respond to, for instance, trastuzumab in the metastatic setting^{35,329}. As HER2 gene amplification or protein overexpression alone does not appear to be the only key to drug response, we have sought to quantify HER2 interaction with HER3, in order to create a new prognostic or predictive biomarker.

The gold standard of measurement of HER2 overexpression is IHC, initially, which is scored according to the HercepTest™ guidelines:

0= no staining or membranous staining in <10% of invasive tumour cells

1= faint or barely perceptible membranous staining in >10% of invasive tumour cells

2= moderate complete membranous staining in >10% of invasive tumour cells

3= strong complete membranous staining in >10% of invasive tumour cells.

A negative score is 0 or 1, and a positive score, 3. An equivocal score, of 2, is followed by FISH analysis for determination of gene amplification. Patients with HER2-positive tumours by either method are eligible for treatment with HER2-targeted therapy. HER2 overexpression is an indicator of earlier disease recurrence and shorter overall survival. For instance, patients with HER2 negative tumours have a much lower risk of death; 63% of that for patients who are HER2 positive³²⁶. However, better predictive biomarkers are required in order to define which patients may benefit from HER2-targeted drugs.

Dimerisation of HER2 with other members of the HER family is important for activation, but in particular, dimerisation with HER3 has been shown, in vitro, to be a potent oncogenic unit¹⁷⁵. HER2:HER3 heterodimers are the most stable and form the most actively signalling pair of receptors within the HER family³³⁰. Quantification of this interaction may prove to be a better prognostic and/or predictive biomarker for the use of HER2-targeted treatment in breast cancer. Studies have sought to assess the level of expression of all 4 members of the HER family by IHC as prognostic or predictive biomarkers³³¹⁻³³⁵, with HER3 expression emerging as prognostic for poor clinical outcome, alongside HER1 and HER2, but HER4 expression as potentially associated with a good prognosis. Overexpression of both HER2 and HER3 is observed in a small number of cases (3-11%^{335,336}) and is associated with reduced overall survival and disease-free survival³³⁶. Assessment of expression of downstream effectors of HER2 and HER3, e.g. activated Akt and Erk, did not appear to add prognostic information and was not associated with survival³³¹.

HER3 protein overexpression is present in upto 75-85% of breast tumours^{332,335}, but may be also be seen in normal adult tissue³³⁷. Strong IHC staining, mainly found in tumours, is variably expressed, as assessed with different antibodies (3-50%^{335,338,339}) and seems to be predictive of poor survival compared to moderate or weakly stained tumours³³⁵. HER3 expression is associated with clinical markers of poor prognosis, such as tumour size>2cm and tumour type, and a dichotomous classification of protein expression (as positive or negative only) demonstrated an association between positive/strong HER3 staining and early local recurrence³³⁹. Splice variants of HER3 have previously been detected, the most common of which is a 1.4kB ectodomain transcript³⁴⁰⁻³⁴². This transcript is expressed in normal human tissues, implying a physiological role, in a variety of cancer cell lines and tumours including ovarian and squamous cell carcinomas. Although the lack of a transmembrane and intracellular domain has led to the assumption that this variant is mainly secreted, intracellular expression has also been demonstrated³⁴¹. This transcript exists as a dimer but does not bind ligand and its function is unknown. The prognostic implication of various splice variants is not yet clear.

Overamplification of the HER3 gene has been shown, by FISH to be prognostic of poor disease-free survival (hazard ratio 2.35, CI=1.08 to 5.11) but HER3 protein expression was not prognostic in this study³³². However, HER2 protein overexpression did not predict for early recurrence (HR 1.42 but CI-0.0-2.24 and p=0.129) either, which may suggest a selection bias within this patient group. Furthermore, HER3 staining was scored according to criteria developed for HER1, which may not be applicable for this protein as HER1 protein distribution is mainly membranous, whereas HER3 distribution has been shown to be more cytoplasmic³³⁶. The authors themselves comment on the inconsistency of the immunohistochemical studies due to the lack of availability of highly specific antibodies, especially for HER3, for which only one of numerous antibodies could be validated. Hence, assessment of HER3 protein overexpression by IHC alone seems fraught with difficulty and does not seem to be a robust biomarker.

Assessment of the activation state of both HER2 and HER3 is possible by IHC-based staining of phosphorylation at C-terminal tyrosine residues, and has been evaluated as a biomarker. Expression of both phosphorylated HER2 and phosphorylated HER3 has been shown to be prognostic of early relapse, and shorter time to death, in the case of phosphorylated HER2³³¹. However, co-expression of proteins does not necessarily indicate interaction. Proximity ligation assays use a fluorescence-based dual antibody technology, summarised in **Figure 5.1**, in order to measure protein proximity of the less than 40nm length scale^{343,344}. This method has been used to demonstrate correlation between detection of HER2:HER2 homo-oligomers or HER2:HER3 hetero-oligomers and early tumour recurrence, with a hazard ratio of 1.72 or 2.18 respectively or death, with a hazard ratio of 1.69 or 2.21 respectively³⁴⁵. However, technological issues mean that this assay may only measure protein oligomerisation but not direct interactions which by definition should be of the <10nm length scale, as considered further in the Discussion. FRET/FLIM technology may better quantify protein dimerisation and is further explored.

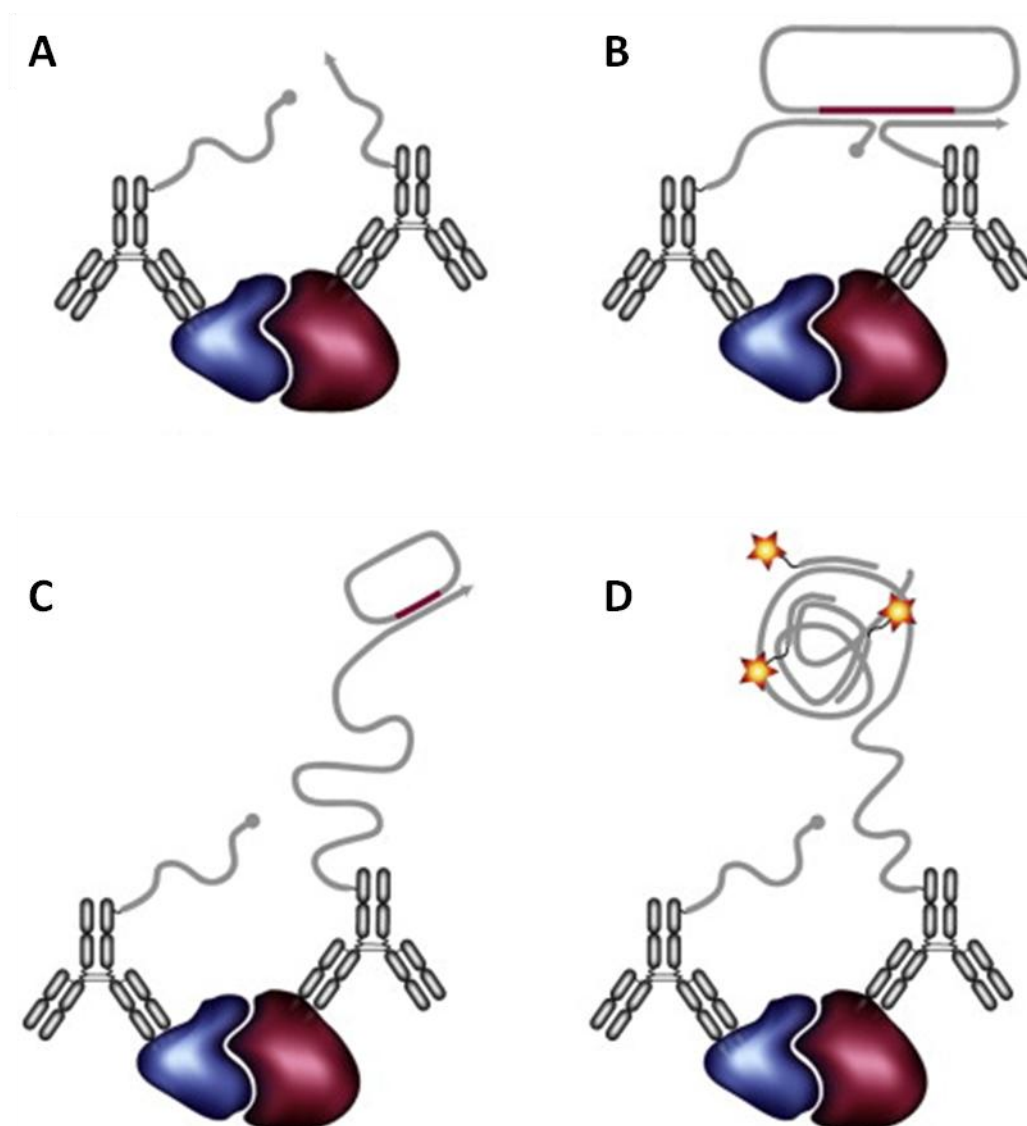


Figure 5. 1 Schematic diagram of proximity ligation assay for measurement of, e.g. HER2:HER3 oligomerisation³⁴⁶

(A) Proximity probes (antibodies with DNA strands attached) bind to target proteins, e.g. HER2 and HER3. (B) Circular DNA strands are added to the sample, and act as a template for hybridisation with the probes if they are within proximity. The purple area in the circular DNA strand represents a part of the template which corresponds in part to one proximity probe, and the other part, to the other probe, leading to assay specificity. Both probes must be within 40nm proximity in order to allow hybridisation with the template³⁴⁷. (C) Rolling-circle amplification of the circular DNA molecule is primed by one of the proximity probes, creating a product which remains attached to the probe. (D) A long single-stranded DNA molecule is generated, rolled up in a ball, which can be visualised by hybridisation of fluorescence labelled probes complementary to the amplification product.

5.1.2 Clinical applications of FRET/FLIM

Several methods have been used to quantify protein-protein interactions *in vitro*, but translation for use in clinical tumour samples has not yet been achieved for most, except FRET/FLIM based assays. For instance, protein-fragment complementation assays allow the study of protein-protein interactions *in vitro* or animal models, but rely on the introduction of the proteins of interest fused to an inactive fragment of a reporter protein, which regains activity once the proteins of interest interact³⁴⁸. However, these fusion proteins cannot be used in human tissue samples. Förster resonance energy transfer (FRET) imaging by fluorescence lifetime imaging (FLIM) has been used to quantify protein-protein interactions at the nanometre scale, *in vitro* and in live cells and animal models^{2,115,116,123,309,349-355}. One example of using FRET imaging to monitor, in the preclinical setting, the pharmacodynamic response to therapy *in situ* is the application of the probe SCAT3 to monitor caspase-3 activity during tumour cell apoptosis subsequent to cisplatin or photodynamic (PDT) treatment³⁵⁶. This technique was repeated at varying time-points in order to observe drug effects on the tumour. Such an assessment of 'on-target' drug effects could greatly improve response assessment.

A two antibody FRET/FLIM approach has been applied, by ourselves and others, to human cancer tissues to detect the nano-proximity between a donor fluorophore-conjugated anti-protein kinase C (PKC) or anti-HER1 antibody, and an acceptor fluorophore-labeled phospho-specific antibody, providing a highly specific quantification of phosphorylation^{121,122}. More recently, the first FRET/FLIM assay to quantify HER1 and HER2 homo- and heterodimerisation in tumour tissue has been established³⁵⁷. We have previously shown the translation of an *in vitro* protein-protein interaction assay, measuring HER1 ubiquitination, in cell lines, to a dual antibody-based assay for quantification of HER1 ubiquitination in tissue, using FRET/FLIM technology (**Figure 5. 2**)³. These images demonstrate *in vitro* assessment of functional HER1 modifications, i.e. ubiquitination, which is associated with downregulation and degradation of this receptor^{157,358,359}. Cell lines with varying susceptibility to HER1 degradation (panel B), mimic varying tumour phenotypes. Thus, translation of these assays for use in patient tumour tissue may delineate a group of patients who are more likely to respond to drugs manipulating this pathway. Development of instruments combining endoscopic cellular resolution imaging with technology to quantify fluorescent lifetime and FRET, is underway and will increase potential clinical applications³⁶⁰.

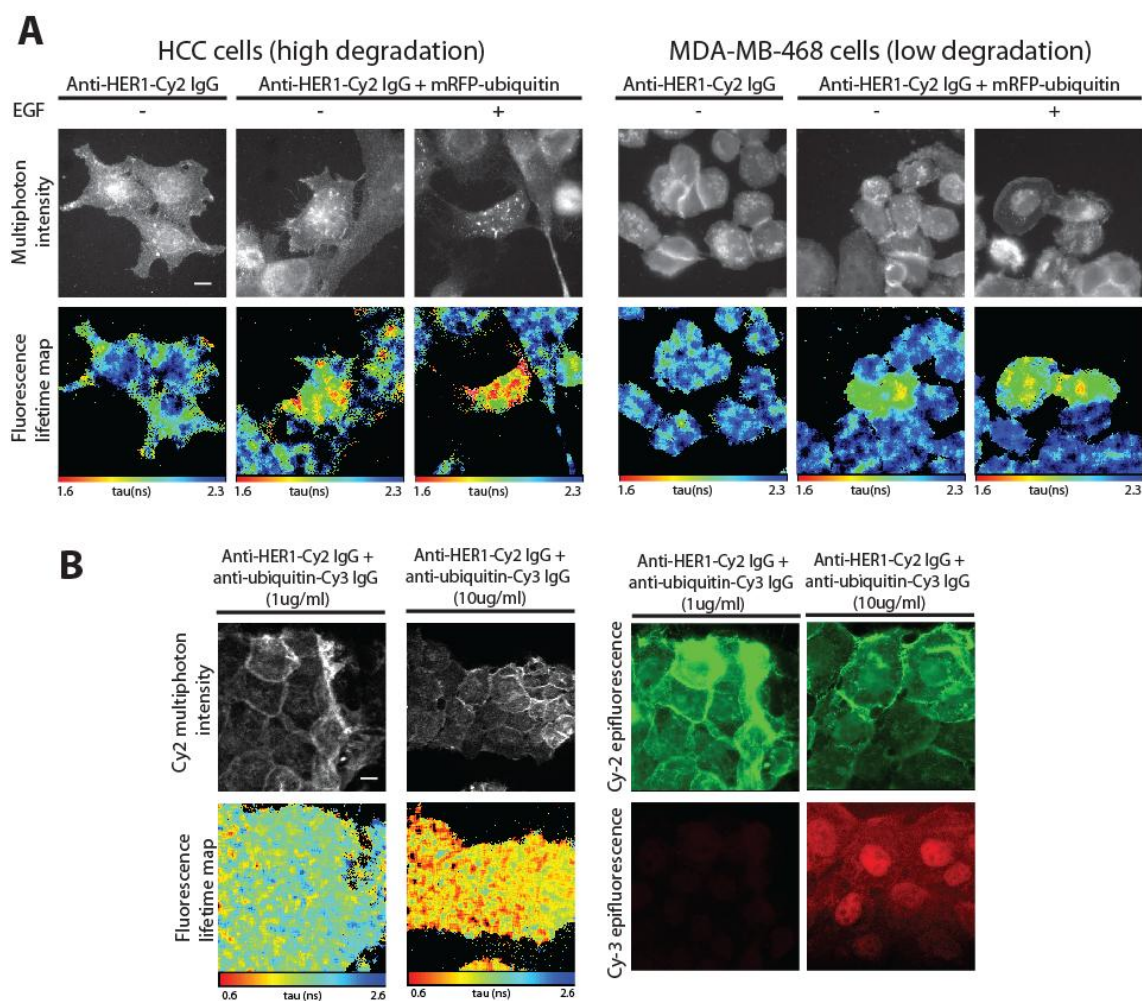


Figure 5. 2 Multiphoton FLIM measurements of the intermolecular FRET between HER1-GFP and ubiquitin-mRFP1³

A) Endogenous HER1 ubiquitination is assessed in the breast cancer cell lines, HCC and MDA-MB-468. HER1 ubiquitination is increased in cells which highly degrade HER1 on EGF treatment (HCC) as opposed to those which degrade HER1 less readily (MDA-MB-468). This is shown by the pseudocolour fluorescence lifetime maps. Here, FRET was measured between Cy2 and m-RFP.

B) Translation of the above FRET-by-FLIM assays to dual fluorophore-labelled antibody assays for application to endogenous protein interactions in tumour tissue. These figures show the initial assessment of FRET efficiency between anti-HER1-Cy2 and anti-ubiquitin-Cy3 in A431 cancer cells (with the established methodologies being applied to patient-derived cancer tissues). Anti-ubiquitin-Cy3 IgG concentration is at control level at 1ug/ml, whereby no ubiquitin staining is seen (epifluorescence Cy3 image), versus optimal concentration (10ug/ml), whereby a reduction in fluorescence lifetime of Cy-2 is seen on the pseudocolour lifetime images.

5.1.3 Tumour heterogeneity

In addition to the heterogeneity observed between individual cancer patients, cancer genome plasticity and the inhomogeneous tumour microenvironment, can give rise to intratumoural heterogeneity among cancer cells within the same tumour. This has been demonstrated by using next-generation sequencing in combination with physical dissection of the tumour specimen³⁶¹, or ultradeep sequencing to reveal the clonal frequency of individual mutations in order to reconstruct the evolutionary tree of the individual cancer clones^{362,363}. This phenomenon poses a new challenge in the attempt to image tumour biological response at a microscopic scale as discussed below. Detailed analysis and subclassification of entire ductal carcinoma in situ lesions, by immunohistochemistry and microarray analysis, showed intratumoural biological diversity in 46% of all samples^{364,365}. It is likely that histopathological analysis leads to an underestimation of total intratumour heterogeneity as only a small percentage of the tissue is examined. Disseminated tumour cells may exhibit a very different phenotype to that of the primary tumour. They may consist of stem cells, which are resistant to treatment or may express antigens which allow escape from immune surveillance in order to seed at a distant site and establish metastases. For example, comparison of the HER2 status of primary and metastatic lesions by IHC reveals significant discordance: 127 out of 342 patients, 90 having a HER2 positive primary tumour but HER2 negative metastases, and 37 having a HER2 negative primary tumour but HER2 positive metastases³⁶⁶. A similar series has observed heterogeneity for HER2 amplification within the primary tumour site³⁶⁷. This discordance between primary and metastatic tumour site could alter management of metastatic disease but is often not uncovered due to the difficulty in obtaining repeated, invasive biopsies on patients with metastatic disease.

Imaging techniques, such as FRET/FLIM have a limited depth of penetration and do not inform on whole body distribution. There is scope to link whole body imaging (e.g. PET/CT) to imaging of pathological mechanisms within the tumour cells at a nanometer scale. The enabling technologies linking these two imaging scales will include image-guidance by the co-registration of different images (e.g. PET and ultrasound (US)), to improve the current accuracy of sampling tumour-infiltrated lymph nodes, for instance. Image-guided biopsy may complement whole body imaging by improving the accuracy of assessment of response and recurrence, but is invasive. Tumour sites exhibiting poor response to therapy may be biopsied to define whether these cells exhibit a clonal change or a change in receptor expression. For instance, the difference or discordance in protein expression (e.g. HER2 status³⁶⁸) on cancer cells between the primary tumour and distant metastatic sites may correlate with a differential sensitivity to treatment.

5.1.3.1 Challenges in assessing tumour heterogeneity

Although molecular imaging may help delineate intra- and inter-tumour heterogeneity, these findings may create challenging clinical implications. For example, the smallest volume of the tumour expressing the imaged target which may warrant a change of treatment, and the implications of determining the molecular profile of the biopsied material from e.g. the secondary site, are issues which will have to be tackled in this context. The presence of an established targeted therapy such as trastuzumab indicates that HER2 detection either in a primary or metastatic site warrants treatment with the targeted drug. However, the proportion of HER2 receptors detected within the tumour may be difficult to standardise and quantify *in vivo*, due to the limits of resolution with PET imaging. Current histopathological recommendations define HER2 positivity as greater than 10% of cells exhibiting the strong membranous staining for the receptor on immunohistochemistry³⁶⁹. However, until these guidelines were published, controversies existed in this established field regarding standardised operating procedures, and proficiency testing within the laboratory. The direct translation of this definition to a 3-dimensional *in vivo* sample is fraught with further difficulties. Large scale observational clinical studies are required to assess the prognostic significance of varying levels of HER2 receptor detection within a tumour sample on imaging, prior to establishment of guidelines regarding treatment decisions.

5.1.3.2 Combining whole body imaging and microscopic imaging

Whole body imaging of tumour pathophysiological processes such as hypoxia, angiogenesis, apoptosis and proliferation visualises disease processes with millimeter resolution. In order to link these processes to molecular mechanisms which are mostly based on subcellular protein modifications, events such as HER dimerisation and phosphorylation must be visualised. One approach is to utilise whole body imaging modalities such as CT, PET, MRI or US to delineate disease at a whole body level and guide biopsy to specific sites of interest, where subcellular processes may be assessed by, e.g. FRET/FLIM. This strategy represents complementary information that completes the description of the cancer molecular phenotype.

Image-guided percutaneous biopsy is a well-established method in cancer diagnosis. For example, over the last 20 years, routine methods for the diagnosis and staging of breast cancer have relied on percutaneous biopsy under ultrasound or stereotactic mammographic guidance³⁷⁰. Breast cancer screening leads to a much higher detection rate of breast anomalies or microcalcifications. Most of these anomalies are not palpable and require image guidance to obtain diagnostic material. Image-guided biopsy has increased the accuracy of non-operative diagnosis and differentiation between malignant and benign

disease from 63% to 95%. In the meantime patient morbidity has decreased due to a reduction in the rates of open surgical biopsy. Immunohistochemical information from the tissue obtained by image-guided biopsy may also be used to guide treatment decisions for chemotherapy and targeted therapy. For example, percutaneous ^{18}F -FDG-PET-CT guided bone biopsies have been shown to change the diagnostic staging, and thus alter planned treatment in over half of the cancer patients studied³⁷¹. This group used repeated ^{18}F -FDG - PET/CT scans to position a needle in order to biopsy metabolically active bone lesions which were deemed equivocal on routine staging with CT, MRI or ^{18}F -FDG-PET. Intended treatment was altered in 56% of patients (n=20), with a variety of tumour types. This study illustrates the benefits of the combination of two imaging modalities in order to correctly biopsy equivocal sites, which may impact on treatment decisions.

The use of image-guided endoscopic biopsy can produce tumour cells or tissues for nanoscopic analysis in a relatively patient-compliant manner, thereby linking clinical imaging to a more precise assessment of molecular mechanisms. This multimodality imaging approach (in combination with genetics/genomic information) could be used to bridge the gap between our knowledge of mechanisms underlying the processes of metastasis and tumour dormancy and routine clinical practice. Treatment regimes could therefore be individually tailored both at diagnosis and throughout treatment, through monitoring of drug pharmacodynamics providing early readout of response or resistance. Delineation of the variety of phenotypes exhibited by tumour cells throughout the body, by examination of the malignant proteome, is necessary prior to answering the question of the clinical significance of tumour heterogeneity.

In the following section, I will describe in detail the work that has been undertaken to translate our pre-clinical FRET/FLIM assay for HER2:HER3 dimerisation, to measure endogenous protein-protein interactions in archived pathological material. We hypothesised that prognostic tools based on unraveling the molecular networks within the proteome that drive cancer proliferation, such as HER2:HER3 dimerisation, may help improve disease outcome predictions. Furthermore, this assay may improve upon current predictive biomarkers as there is a dearth of tools in this arena for HER2-targeted drugs. Resistance to treatment could be understood better by imaging the recruited signaling pathways in response to drug combinations. Translating such assays into clinical benefit will guide the rational use of expensive drugs.

Results

5.2.1 Distribution of HER2 and HER3 expression across METABRIC TMA of primary patient tumours

In order to describe the distribution of both HER2 and HER3 across our set of TMAs, a HER3 (RTJ2) antibody, a clone of which was previously used for IHC in tumour tissue³³⁹, and a HER2 antibody from the FDA approved DakoHercept test (Dako), were successfully applied to the METABRIC TMAs of formalin-fixed paraffin embedded (FFPE) primary tumour tissues.

Figure 5.3 demonstrates two different tumour cores, one of which is negative for HER2 and HER3 (upper panel) and one of which is strongly positive for both proteins (lower panel). The distribution of HER2 in the positive sample is predominantly membranous (black arrows) but an intracellular component is also detected (red arrow). In contrast, the predominant distribution of HER3 is intracellular (black arrows), with some membranous staining (red arrow) in line with published evidence³³⁶. These assays were applied across the whole patient cohort of 220 patients. Samples were scored independently by the supervisor, Dr Cheryl Gillett, who is experienced in breast histopathology interpretation and by the primary PhD researcher (Gargi Patel).

Although guidelines for HER2 scoring in IHC are well established (e.g. HercepTest™), no such guidelines exist for HER3. HER1 staining in IHC is scored according to the HER1 pharmDX™ guidelines which some groups have used to score the immunohistochemical staining patterns of other members of the HER family³³². These guidelines score as positive, any membranous staining by IHC, above background, whether it is complete or incomplete circumferential staining. The intensity of the staining may then be scored from 1-3+. However, this system is not applicable in our cohort as HER3 demonstrates a different cellular distribution both within our samples (**Figure 5. 3**) and in the literature³³⁶. On review of IHC staining of HER3 across the cohort, it became clear that patterns of HER3 staining were predominantly intracellular at various intensities, but the range of intensity was not high. Therefore, we scored tumour cores for HER3 as either negative or positive, if any staining above background was present, in more than 10% of tumour cells.

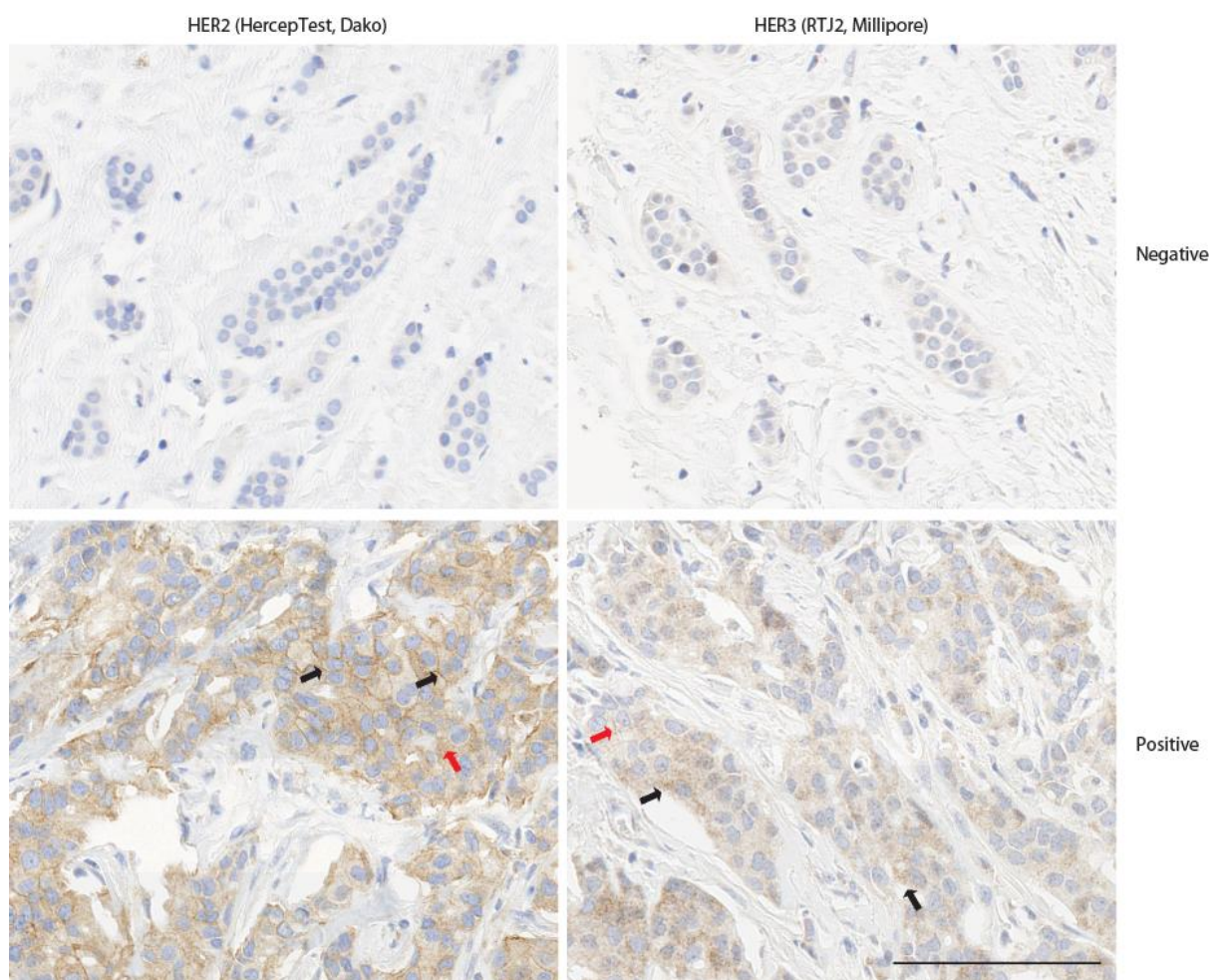


Figure 5. 3 Immunohistochemistry stain for HER2 and HER3 in METABRIC tissue samples

Tissue microarray sections were stained for IHC for HER2 or HER3 as described in Materials and Methods. Both the antibodies used, namely RTJ2 (Millipore) and the antibody from HercepTest (Dako), have been validated for use in FFPE tissue for IHC. The top panel shows an example of a tumour core which did not stain for either protein. The lower panel shows a tumour core which was positive for HER2 and HER3. The image on the left shows complete staining of cell membranes for HER2 in >10% of cells (black arrows). Although there is an increased intensity of HER2 on the membrane, cytoplasmic staining, of lower intensity, is also present (red arrow). The lower right image demonstrates a different distribution of staining for HER3. Although some low intensity membranous staining is present (red arrow), the majority of staining is cytoplasmic (black arrows) of a heterogeneous nature. Scale bar represents 100µm.

	TMA number	Total number of cores	Missing	No tumour	Not assessable	
HER2						
	81A	88	17	7	0	
	82A	44	18	3	0	
	83A	88	43	2	6	Total in analysis
Totals		220	78	12	6	124
HER3						
	81A	88	30	3	0	
	82A	44	23	0	0	
	83A	88	33	2	0	Total in analysis
Totals		220	86	5	0	129

Table 5. 1 Characteristics of cores assessed from METABRIC TMA

TMA's were composed of 44 or 88 cores per slide, with a further 7 or 11 normal tissue cores respectively, for orientation and had been made in triplicate. Only one of these triplicates was used within this initial step of assessing HER2 and HER3 expression within the METABRIC cohort (denoted as 'A' in the numeration above). Review of the data resulted in the omission of many cores due to the core being missing or unassessable on imaging, as shown in the table above. A total of 96 patients from the TMA's assessed for HER2 expression and 91 patients from the TMA's assessed for HER3 expression were lost from analysis due to these errors. Of the assessable tumour cores, a further 14 and 4 patients from the TMA's assessed for HER2 and HER3 respectively were lost to analysis due to a lack of follow up or outcome data.

In order to establish whether this cohort of patients was representative of the population, we assessed the prognostic significance of a variety of clinic-pathological factors which are known to be strongly predictive of outcome. For instance, lymph node positivity demonstrated a hazard ratio (HR) of 3.8 (confidence intervals, CI, 2.3-6.5), with a p value of 4.4×10^{-7} for DMFS and 3.7 (CI, 2.1-6.4) with a p value of 4.30×10^{-6} OS at 10 years on univariate analysis using Cox's proportional hazard models. Similarly, oestrogen positivity demonstrates a positive effect with a HR of 0.46 (CI, 0.26-0.81, $p=0.0073$) for DMFS and a HR of 0.39 (CI, 0.22-0.69, $p=1.43 \times 10^{-3}$) in line with the literature. Unfortunately neither HER2 nor HER3 emerged as a statistically significant independent prognostic predictor for outcome, either DMFS or OS. However, Kaplan-Meier curves demonstrating distant-metastasis free survival (DMFS) and overall survival (OS) at 10 years (**Figure 5.4**) demonstrate separation of the survival curves for patients who are HER2 positive (poorer outcome) versus those that are negative for both DMFS and OS. The survival curves for HER3 however demonstrate less separation and more overlap. The lack of statistical significance is likely to be due to the small numbers of events in each group.

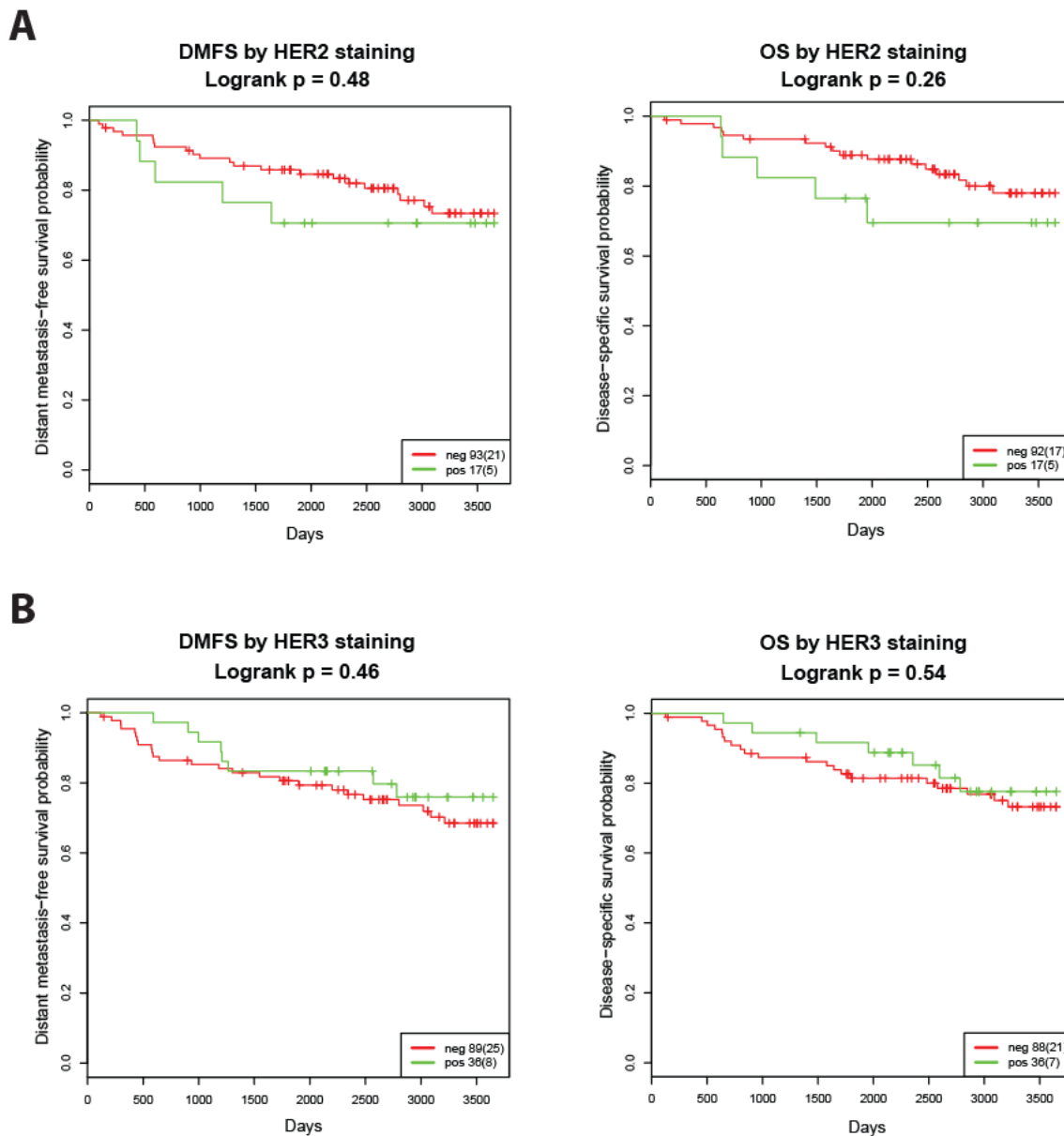


Figure 5. 4 Kaplan-Meier curves demonstrating distant metastasis-free survival and overall survival according to HER2 or HER3 expression by IHC

Distant metastasis-free survival (DMFS) and overall survival (OS) probabilities according to HER2 (A) and HER3 (B) overexpression. DMFS is reported as distant metastasis or disease-specific death and OS is reported as disease-specific death. Inset figure legend indicates number of patients within each group, and in brackets, the number of events for this group. Cox proportional hazard models were fitted using the 'survival' package²⁰¹ in R²⁰². Kaplan-Meier curves and logrank tests were also performed using the 'survival' package. This figure was created in collaboration with Dr Katherine Lawler, bio-informatician.

5.2.2 Validation of antibodies targeted to HER2 and HER3 in cell lines

In order to translate the pre-clinical FRET/FLIM assay for use in tumour tissue, several conditions must be fulfilled. The FRET/FLIM assay described in **Chapter 3** is based upon FRET interaction between GFP and RFP or Cy3 bound to an anti-HA antibody. However, antibodies, directly conjugated to a fluorophore are required if this assay is applied in FFPE tissue. Therefore, we first validated the antigen specificity of a variety of antibodies in cell lines transfected with the fluorescently tagged protein of interest. Those successfully validated were kindly conjugated with fluorophores by Dr Gilbert Fruhwirth. Monoclonal antibodies were selected as they are more specific than polyclonal antibodies which are raised against multiple epitopes on any given antigen. Furthermore, conjugation of monoclonal antibodies with fluorophores is more reliable compared to serum from polyclonal antibodies, which contains a heterogeneous complex mixture of antibodies, which may be conjugated with different dye: protein ratios.

Once conjugated, the antigen specificity was re-tested as the process of antibody conjugation (described in **Materials and Methods**) could lead to a loss of specificity. Furthermore, both antibodies must bind to the protein of interest in a configuration which sterically positions the fluorophores within an appropriate proximity for FRET to occur. Therefore, we first screened a variety of antibodies against HER2 and HER3 in order to provide a panel of antibodies which could then be applied in various combinations to select those which provide the highest level of interaction by FRET/FLIM.

Figures 5.5 and **5.6** demonstrate the validation of antibodies targeted against HER2. Initially the primary antibodies were tested in cells overexpressing the fluorescently tagged protein of interest, by indirect fluorescent labelling with a secondary antibody raised against the species in which the primary antibody was raised, as shown in **Figure 5. 5**. The upper panel shows co-localisation of overexpressed HER2-GFP and anti-rabbit IgG-Cy3, bound to a customised rabbit anti-HER2 primary antibody (raised against an immunizing peptide sequence around tyrosine 1248 of the human ErbB2 protein (CTAENPEYLGLDV-CONH2), referred to as 'in house antibody' herein) in MCF-7 cells, which do not express endogenous HER2 protein. **Figure 5. 5A** also shows a negative control, whereby a secondary antibody is applied alone without a primary antibody. The Cy3 epifluorescence image shows the lack of staining with a secondary antibody alone. The lower panel however demonstrates that once this monoclonal antibody is conjugated to a Cy3 fluorophore, the antigen specificity is lost, with non-specific staining in the Cy3 epifluorescence image. The causes for this loss of specificity are explored in the discussion below.

Similarly, **Figure 5. 5B**, upper panel, shows localisation of overexpressed HER2-GFP and anti-mouse IgG-Cy3 bound to the primary ant-HER2 antibody (Labvision, Ab-17). In this case, conjugation of this antibody with Cy5 does not affect antibody specificity as shown in the lower panel, top row. A non-specific antibody conjugated to Cy5 does not co-localise with HER2-GFP as shown by the images in the middle row. The antibody was also tested in SK-BR-3 cells in which HER2-GFP was expressed, as demonstrated in the lower panel. Endogenously expressed protein is detected (highlighted with yellow arrows) at a lower intensity compared to transfected protein (white arrows), as expected.

This method of validation was followed for all antibodies described below. The pertinent images for the relevant antibodies are shown. For example, if the antibody works equally well when used indirectly or when conjugated with a fluorophore, only the images of the directly conjugated antibody are shown. **Figure 5.6** shows co-localisation of HER2-GFP with two directly conjugated antibodies, clone L26 and N24, (donated by Prof. Yosef Yarden, Weizmann Institute of Science) and designed ankyrin repeat proteins (DARPin) conjugated to Cy5. As the DARPin has been genetically engineered to mimic naturally occurring ankyrin proteins, which are highly specific, high-affinity and mediate protein:protein interactions, this molecule was harnessed by collaborators for potential use in the development of FRET/FLIM assays. Ankyrin proteins usually consist of four or five repeat motifs and have a molecular mass of 14-18kDa. The small nature of these proteins can also make them ideal for use in FRET/FLIM assays, as they are more likely to achieve higher FRET efficiencies compared to larger bulkier antibodies², which typically have a molecular mass of 150kDa (IgG).

The proteins examined in **Figure 5. 6** are all raised to extracellular epitopes on HER2, and hence cells do not require permeabilisation during preparation. **Figure 5.6B** demonstrates that signal localisation is not affected whether this step is carried out. It was important to differentiate between antibodies which bind to extracellular epitopes of the protein versus the intracellular epitopes as localisation of both fluorophores on the same side of the plasma membrane is a pre-requisite in order for FRET to occur, as described above.

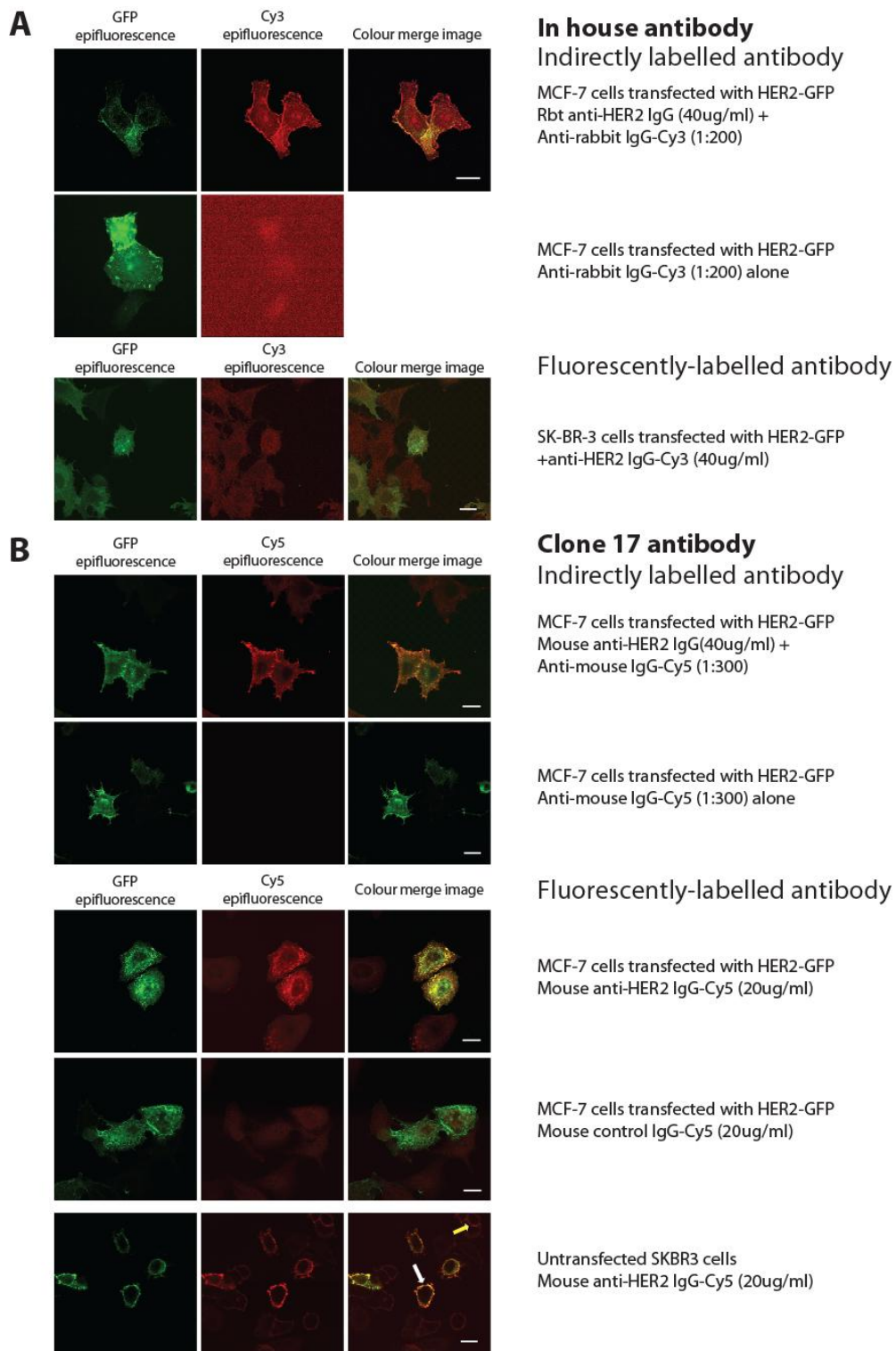
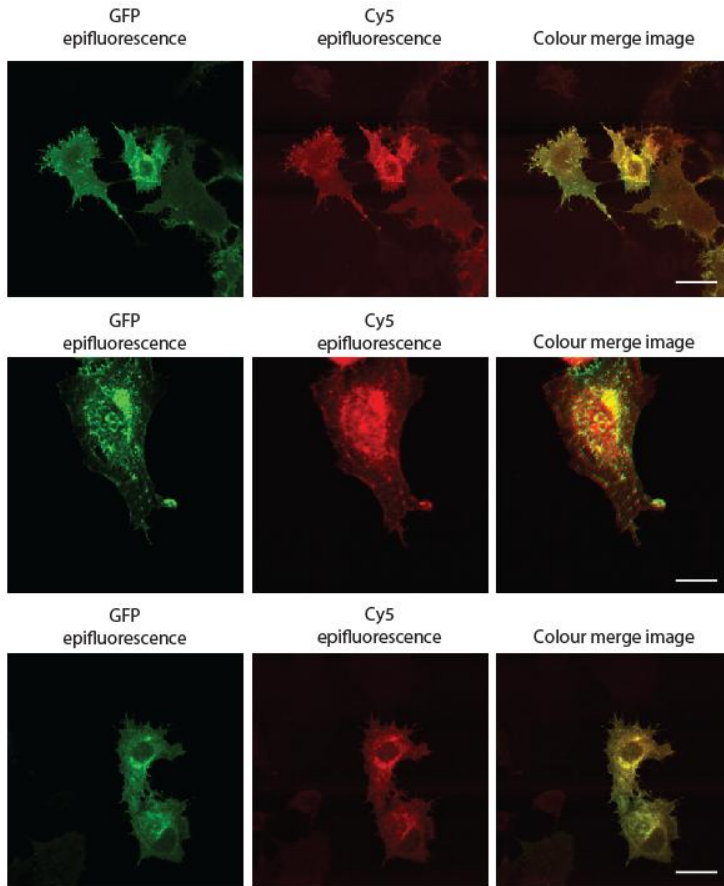


Figure 5. 5 Validation of intracellular HER2 antibodies in cell lines

(A)The top panel demonstrates validation of the in-house HER2 antibody, which shows colocalisation with HER2-GFP prior to conjugation with a fluorophore (in yellow/orange in the merged image). However after fluorescent labelling, the antibody seems to lose specificity. (B) Similar images for HER2, clone 17 are shown. This antibody not only shows specific staining of HER2 before and after being labelled but also identifies endogenously expressed HER2 (yellow arrow), as well as transfected HER2 GFP (white arrow), as shown in the bottom panel. Scale bars represent 5µm.

A**YY antibody**

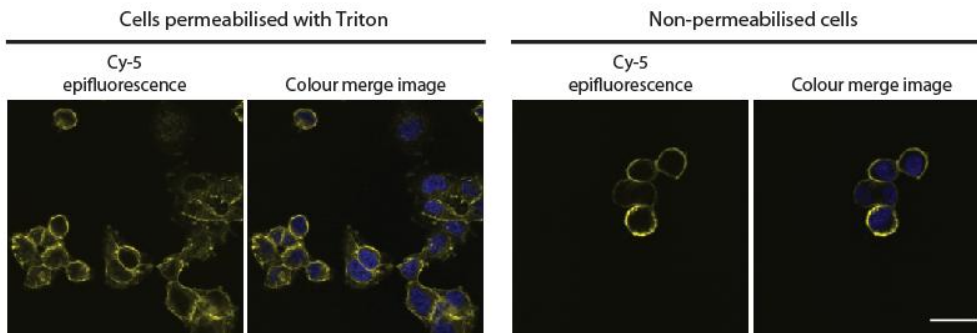
MCF-7 cells transfected with
HER2-GFP +
anti-HER2 IgG-Cy5 (10ug/ml)

DARPin

MCF-7 cells transfected with
HER2-GFP +
anti-HER2(DARPin)-Cy5 (8ug/ml)

N24 antibody

MCF-7 cells transfected with
HER2-GFP +
anti-HER2 IgG-Cy5 (10ug/ml)

B**Figure 5. 6 Validation of extracellular HER2 antibodies in cell lines**

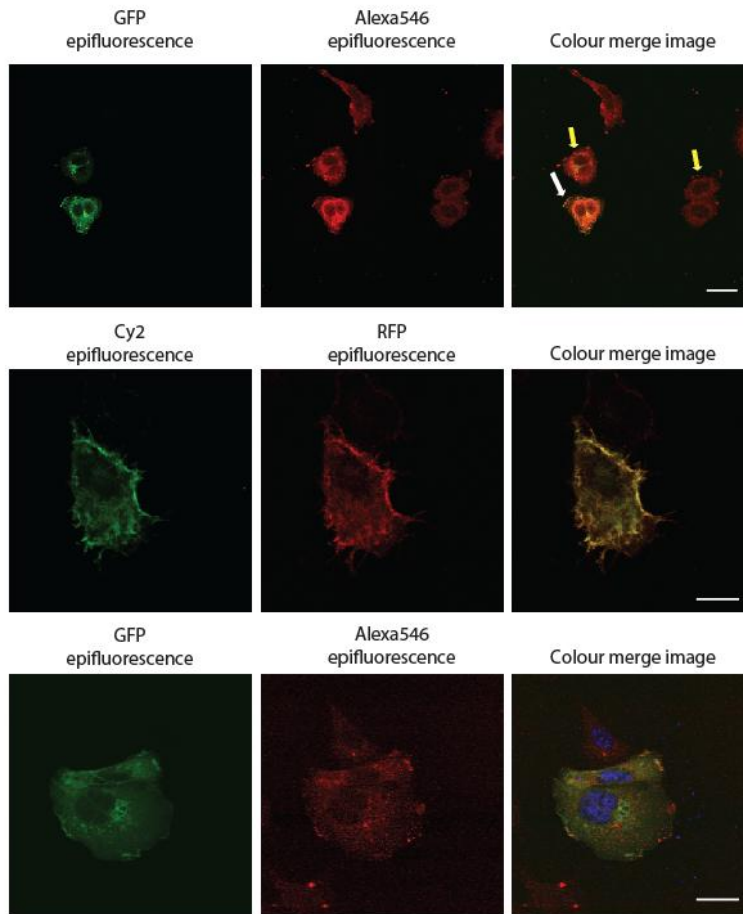
(A) Confocal images demonstrate colocalisation of a variety of HER2 antibodies targeted to extracellular epitopes of HER2. MCF-7 cells were seeded for 24 hours and transfected with HER2-GFP, prior to processing for immunofluorescence and staining with the indicated antibodies. Colour merge images demonstrate colocalisation of HER2-GFP and HER2 antibodies in all three cases (yellow/orange in colour). (B) As cells processed for antibodies targeted to extracellular epitopes do not require permeabilisation, the effect of Triton (permeabilisation) upon HER2 antibody staining with HER2(YY) antibody is shown here. Hoechst nuclear stain is shown in purple. Scale bars represent 5µm.

In the case of HER3, fewer antibodies targeting this protein are available, especially for use in immunohistochemistry and immunofluorescence.

Figure 5. 7 demonstrates colocalisation of four selected HER3 antibodies (donated by Prof. Yosef Yarden (herein referred to as YY), or purchased from R&D, Abnova (M01, clone 2E9, referred to as M01) or Millipore(RTJ2)) with HER3-RFP or HER3-GFP in MCF-7 cells, which overexpress HER3 endogenously in addition to the transfected, fluorescently tagged protein. The upper panel in **Figure 5. 7A** shows the use of a mouse HER3-targeted antibody (M01) to identify endogenously expressed HER3 alongside transfected HER3-GFP. The colour merge image highlights co-localisation of HER3-GFP and the conjugated antibody (white arrow) as well as membranous staining of endogenous HER3 protein (yellow arrows). Although the antibody donated by Prof Yarden (YY) shows strong specific staining of HER3, the R&D antibody was poor in comparison, with low intensity staining even at high antibody concentration. Neither of these antibodies recognised endogenous HER3 protein.

Although the intracellular HER3 antibody (RTJ2) did demonstrate good staining of HER3 on indirect labeling with a secondary Cy3 antibody (data not shown), this was no longer the case after conjugation with Cy5 fluorophores. **Figure 5. 7B** demonstrates non-specific staining of all cells of varying intensity, but not corresponding to regions of HER3-GFP expression (colour merge image). Therefore, this antibody was used for HER3 immunohistochemistry in formalin-fixed, paraffin-embedded tissue, with DAB staining, as opposed to optimization of a FRET/FLIM assay for HER2:HER3 interaction.

Having completed this initial screen of antibodies to HER2 and HER3, we selected candidates which could be suitable for demonstrating HER2:HER3 dimerisation by FRET/FLIM, initially in cells prior to translation for use in tissue. As only extracellular HER3 antibodies retained specificity after conjugation with a fluorophore, extracellular HER2 antibodies were required to maintain fluorophore proximity. In the case of HER3, the antibody donated by Prof Yarden (YY) and MO1 (Abnova) were selected, and in the case of HER2, the antibody donated by Prof Yarden (YY), N24, and the HER2 DARPin.

A**Extracellular HER3 antibodies****M01 antibody**

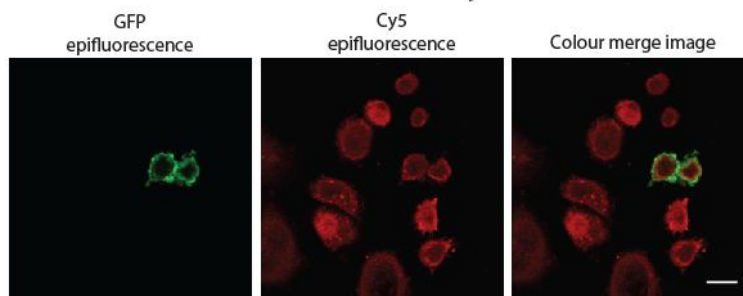
SK-Br-3 cells transfected with
HER3-GFP +
anti-HER3-Alexa546 (10ug/ml)

YY antibody

MCF-7 cells transfected with
HER3-RFP +
anti-HER3 IgG-Cy2 (1.36ug/ml)

R&D antibody

MCF-7 cells transfected with
HER3-GFP +
anti-HER3-Alex546 (10ug/ml)

B**Intracellular HER3 antibody****RTJ2 antibody**

SK-Br-3 cells transfected with
HER3-GFP +
anti-HER3-Cy5 (10ug/ml)

Figure 5. 7 Validation of HER3 antibodies

A variety of antibodies targeted to extracellular (A) or intracellular (B) epitopes were tested by immunofluorescence. Both MCF-7 and SK-BR-3 cell lines were used as they overexpress HER3 endogenously, and were also transfected with HER3-GFP or RFP as indicated. The colour merge images show areas of colocalisation in orange/yellow. In the uppermost panel, yellow arrows show endogenous HER3 protein, which is identified by the HER3 (M01) antibody, as well as the transfected HER2-GFP protein (white arrow). Scale bars represent 5µm.

5.2.3 FRET/FLIM measurement of HER2:HER3 dimerisation in cell lines

In **Figure 5. 8**, both anti-HER2 IgG-Cy5 and anti-HER3 IgG-Alexa546 (both antibodies donated by Prof Yarden, YY) were applied to stain untransfected SK-BR-3 cells, untreated or treated with ligand, NRG1 or lapatinib. The donor fluorophore (Alexa546) exhibits a reduction in fluorescence lifetime, in the presence of the Cy5 acceptor. The FRET efficiency derived as described in **Materials and Methods**, is therefore used to quantify the endogenous HER2:HER3 dimer population. At baseline, there is an innate level of dimerisation between HER2 and HER3, which increases approximately two-fold on treatment with either ligand or inhibitor. As there was no significant difference between ligand and inhibitor treatment, NRG1 was used in the screening of the remaining antibodies for the pair which demonstrated the highest level of FRET interaction between HER2 and HER3.

Four pairs of conjugated antibodies/DARPin demonstrated a positive FRET efficiency when both donor and acceptor were present, indicating a favourable configuration for fluorophore interaction as shown in **Figure 5. 8** and **Figure 5. 9**. Three pairs of antibodies demonstrated a baseline FRET efficiency of 5-10% (the pair of antibodies donated by Prof Yarden, (**Figure 5. 8**), the Abnova antibody (M01) and DARPin, and M01 and the HER2 antibody donated by Prof Yarden (**Figure 5. 9**)). Those pairs in which IgG HER3(M01)-Cy5 was used, demonstrated a significantly larger increase in FRET efficiency to 25% on ligand treatment as opposed to the HER3 antibody donated by Prof Yarden, except in the presence of IgG HER2(N24)-Cy5. In this case both baseline FRET efficiency and that detected on ligand treatment was significantly lower than the other pairs. These antibodies were then applied to FFPE material to assess antibody specificity in this medium.

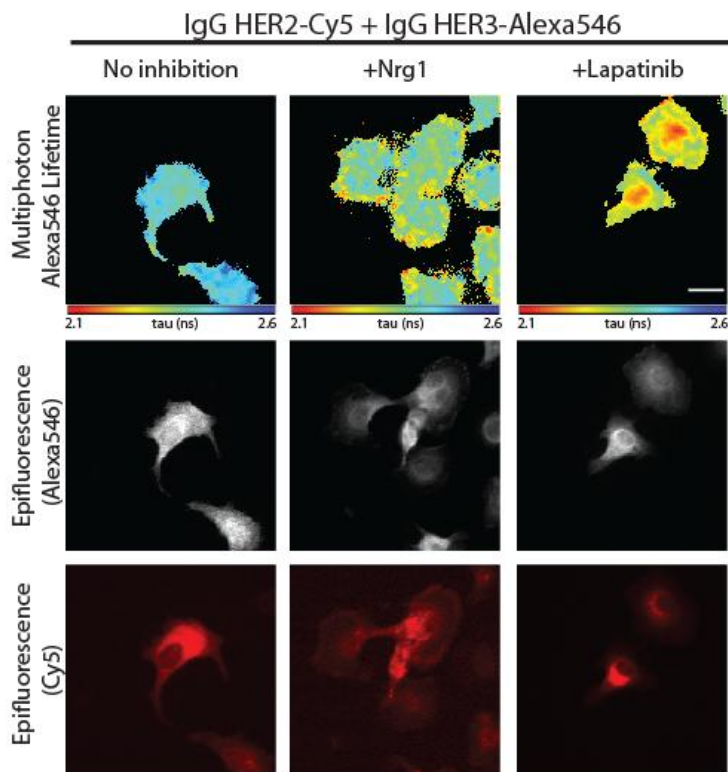
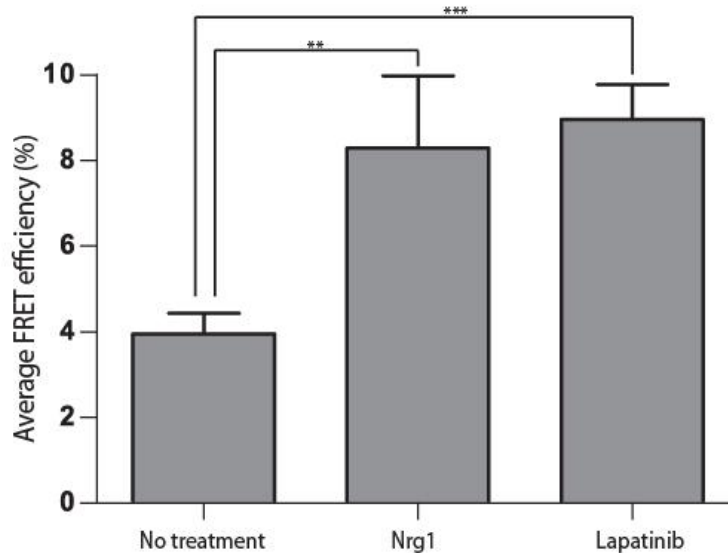
A**B**

Figure 5. 8 Measurement of HER2:HER3 dimerisation on treatment with lapatinib and NRG1

(A) The upper panel shows untransfected SK-Br-3 cells which were seeded for 24 hours, treated with NRG1 or lapatinib and stained with both anti-HER2 IgG-Cy3 and anti-HER3 IgG Cy2. Both these antibodies had been donated by Prof Yarden. Cells were fixed and processed for FRET/FLIM analysis. Scale bar represents 5 μ m. (B) Bar graph shows cumulative analysis of FRET efficiency, calculated as described previously. 20-25 points were taken for each condition. Error bars represent SEM, values for p are <0.001(***) or <0.01(**) calculated by one way ANOVA.

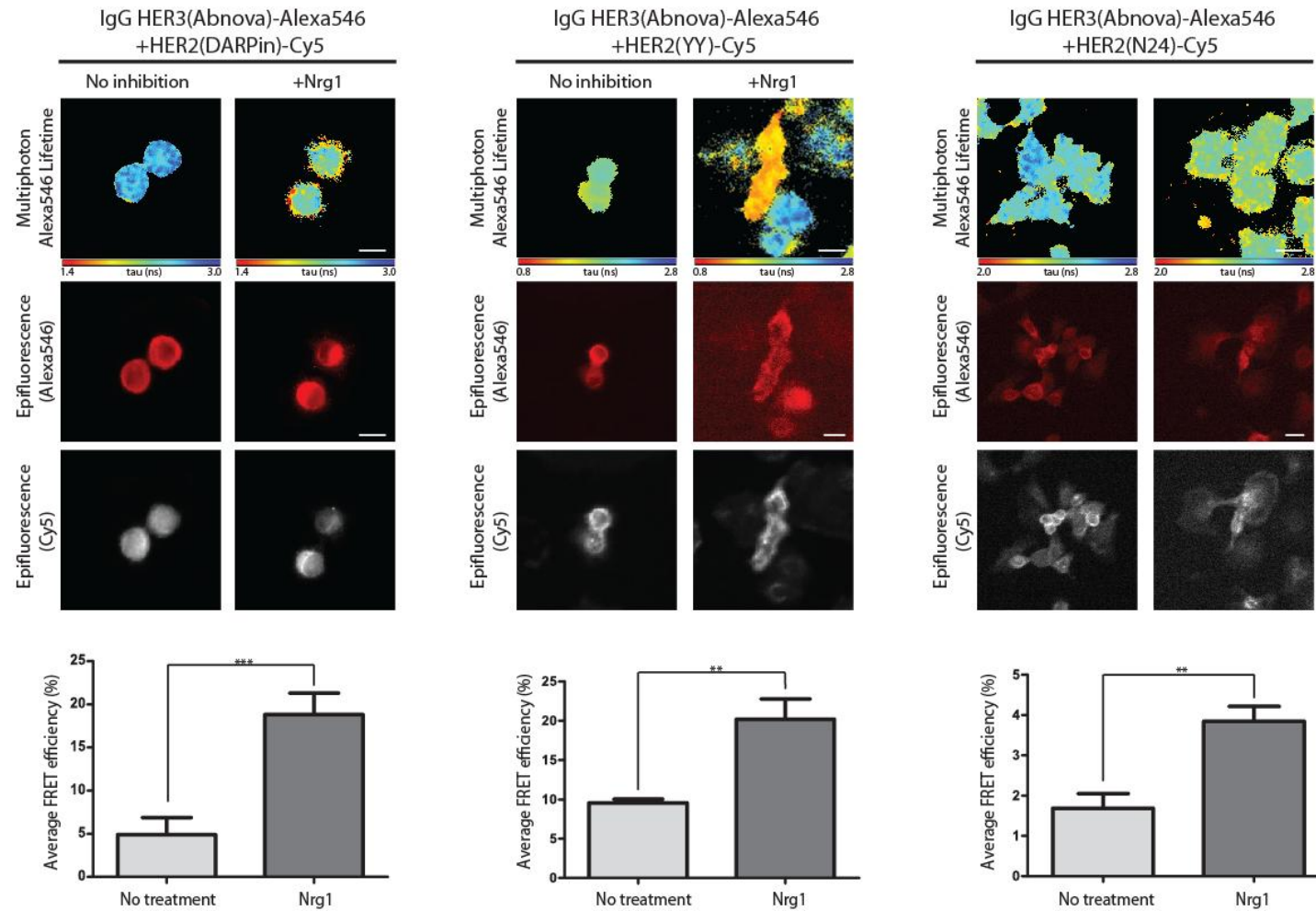


Figure 5.9 Degree of HER2:HER3 dimerisation in SK-Br-3 cells measured by FRET/FLIM, using different antibodies

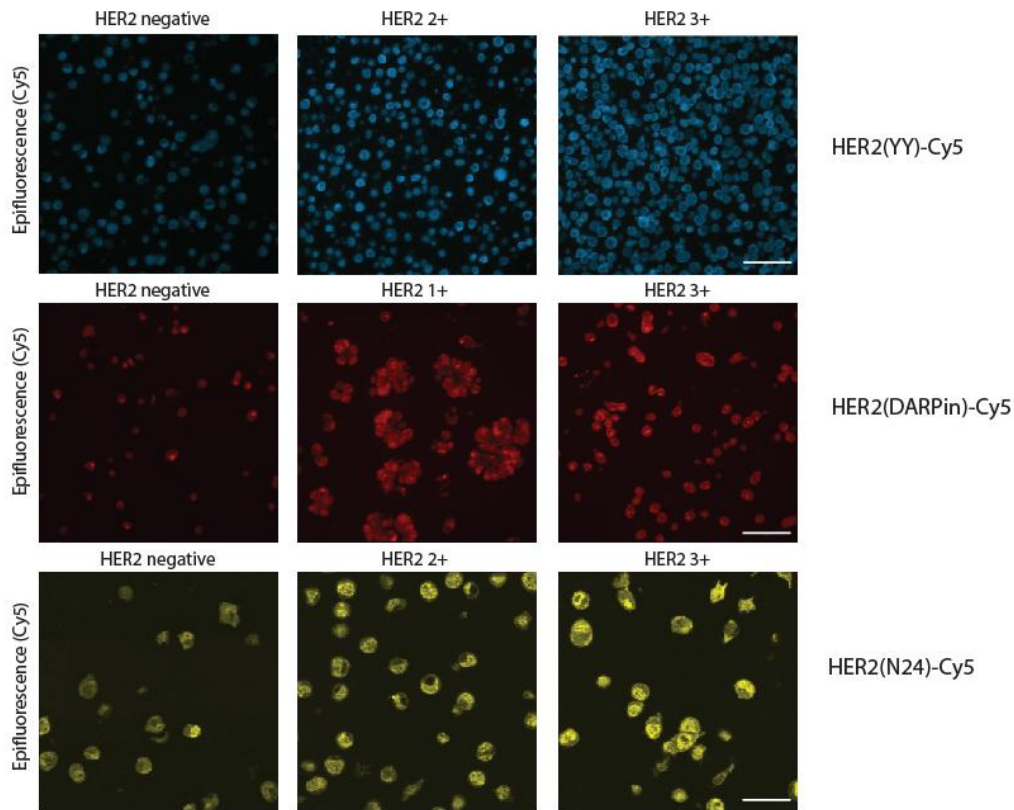
SK-BR-3 cells were plated on 24 well coverslips and transfected with HER3-HA and HER2-HA for 24 hours. Cells were treated with NRG1 (50ng/ml) for 15 minutes prior to fixation and processing for FRET/FLIM analysis. Scale bars represent 5µm. Lower panels show cumulative analysis of FRET efficiency, calculated as described previously, for each antibody pair. 20-30 points were taken for each condition. Error bars represent SEM, values for p are <0.001(***) or <0.01(**).

5.2.4 Validation of fluorophore-conjugated antibodies in formalin fixed, paraffin-embedded cell pellets

Although HER2 expression is routinely assessed in breast tumour samples, the same is not true of HER3. Initially, it became necessary to devise a method of validating the fluorophore-conjugated antibodies in FFPE material prior to application to archived tumour tissue. Therefore, we developed a method for the production of cell pellets consisting of SK-BR-3 cells which endogenously overexpress HER2 and HER3, but were also transiently transfected with HER3-HA. **Figure 5. 10A** and **B** demonstrate validation of the fluorophore-conjugated antibodies/DARPin to HER2 and HER3, in FFPE cell pellets. Three cell lines which overexpress a spectrum of HER2 protein, from none (0, negative) to strongly positive (3+) were used to test the HER2 antibodies. As such a spectrum was not available for HER3, HER3-HA was transiently transfected into SK-BR-3 cells prior to processing into cell pellets. Both HER2(YY)-Cy5 and HER2(DARPin)-Cy5 demonstrated a differential staining pattern between strongly positive and negative cell pellets (**Figure 5. 10A**, upper panels) with an increase in intensity and membranous staining in the strongly positive cell lines. However, antibody staining with HER2(N24)-Cy5 seemed fairly non-specific, with no specific membrane staining in the strongly positive cell line. Hence this antibody was excluded from further optimization. Both HER2(YY)-Cy5 and HER2(DARPin)-Cy5 were tested in an available tissue composite control block which contained archived tumour tissue expressing a spectrum of HER2 proteins (**Figure 5. 11**). Both antibodies demonstrate higher intensity and more membranous staining in tissue which is strongly positive for HER2 (3+) as opposed to negative or weakly positive (0 or 1-2+).

In the case of HER3 (**Figure 5. 10B**), the fluorophore-conjugated M01 antibody demonstrates an intracellular distribution of HER3, with some areas of higher intensity staining which are likely to represent transfected HER3-HA (yellow arrows). However the antibody donated by Prof Yarden no longer recognizes the antigen in FFPE cells. Indirect antibody labeling (RTJ2) highlights transiently transfected HER3-HA, demonstrated by both by immunofluorescence and immunohistochemistry (IHC) with DAB staining. The transfection efficiency appears to be around 10-20% with the transfected cells demonstrating a much higher intensity stain and a more membranous distribution (yellow arrows) compared to endogenously expressed HER3 (white arrows). From these tests in cell pellets, HER2(YY)-Cy5, HER2(DARPin)-Cy5 and HER3(M01)-Alexa546 were chosen for testing for FRET/FLIM in cell pellets.

A HER2 antibodies applied to cell pellets endogenously expressing HER2



B HER3 antibodies applied to cell pellets overexpressing HER3-HA

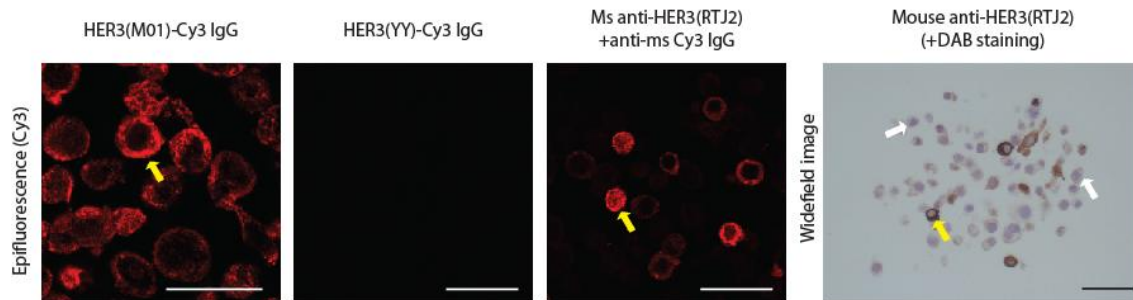


Figure 5. 10 Assessment of fluorophore-conjugated antibodies in PPFE cell pellets

(A) A block containing cell pellets from 3 different cell lines was available, containing MCF-7 cells (HER2 negative/0), BT474 (HER2 3+), and either MDA-MB-453 or MDA-MB-175 (2+ or 1+ respectively). Three antibodies were assessed on these blocks to demonstrate the spectrum of staining from negative to highly positive. All antibodies differentiated between HER2 negative and strongly positive cells. (B) Three fluorescently labelled antibodies to HER3 were tested on cell pellets of SK-Br-3 cells, transfected with HER3-HA, as a similar block was not available for HER3. Although both HER3(M01) and (RTJ2) identified HER3 protein, either endogenous or transfected, the HER3(YV) antibody did not. IHC image of HER3(RTJ2) antibody with DAB staining on the far right demonstrates HER3 distribution for both transfected (yellow arrows) and endogenous protein (white arrows). Scale bars represent 50µm.

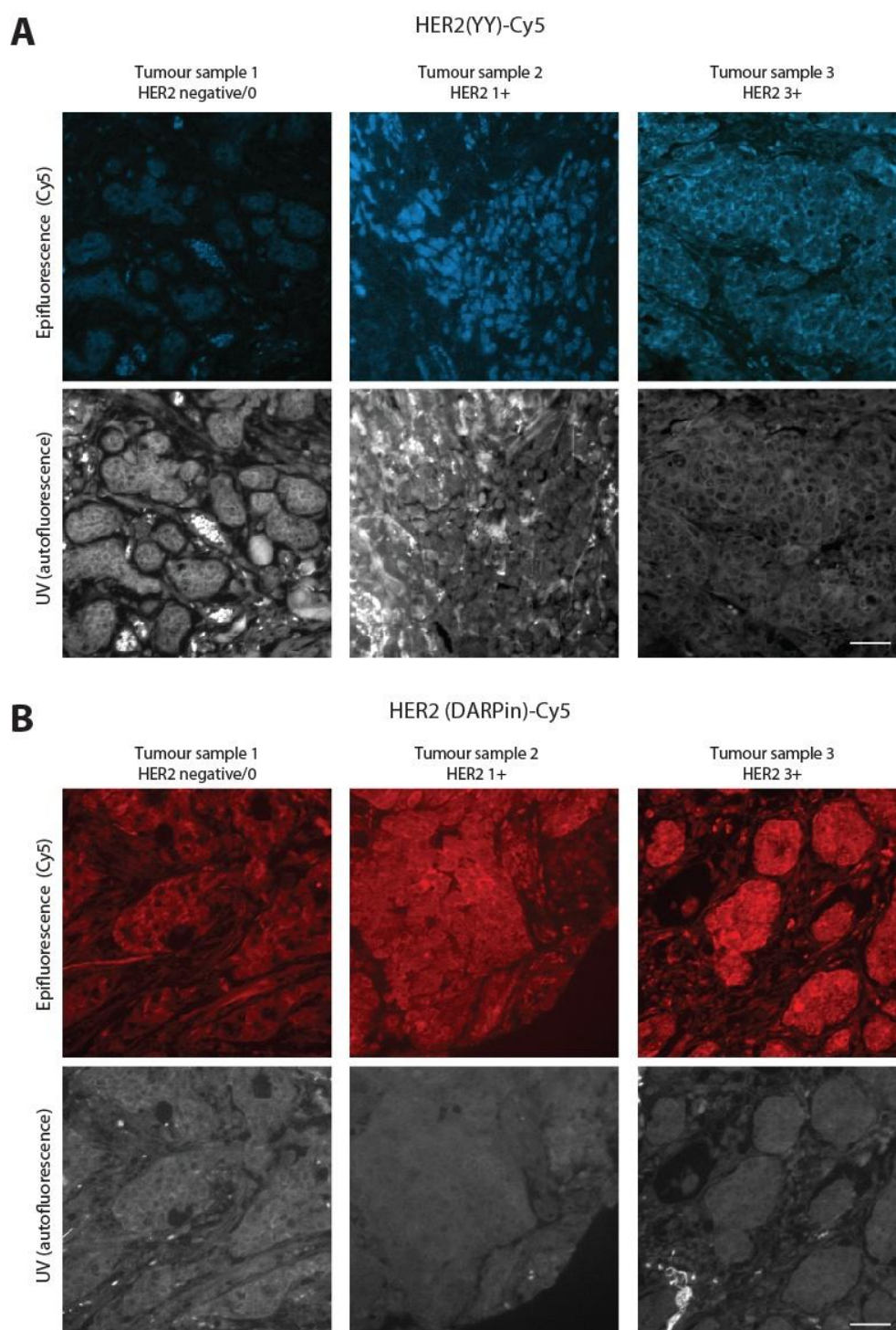


Figure 5. 11 HER2 antibody and DARPin staining of HER2 overexpressing tumour tissue

Sections from a tumour block containing tumour tissues expressing various levels of HER2 protein, were used to test fluorescently labelled HER2(Y_Y)-Cy5(A) and HER2 (DARPin)-Cy5 (B). Both agents demonstrate high intensity membranous staining for HER2 protein in HER2 strongly positive (3+) tissue compared to HER2 negative (0), as assessed by the Hercep Test. The distribution of HER2(Y_Y)-Cy5 and HER2(DARPin)-Cy5 in low expressing tissue (1+) was variable, although the same tumours had not been assessed for both agents. Scale bar represents 50µm.

5.2.5 FRET/FLIM measurement of HER2:HER3 dimers in FFPE cell pellets

In order to validate the FRET/FLIM assay in FFPE material, two sets of cell pellets were constructed, one stimulated with ligand, and one unstimulated. These pellets were anonymised prior to application of the antibodies to both pellets, simultaneously. These pellets were then processed for FLIM in order to select a pair of antibodies which reliably differentiated HER2:HER3 interaction between stimulated and non stimulated cells (**Figure 5. 12**). Of the antibodies tested, the only successful pairing was HER2(DARPin)-Cy5 and HER3(M01)-Alexa546.

As can be seen from the histogram in **Figure 5. 12B**, the level of FRET efficiency observed in FFPE pellets compared to cell lines (**Figure 5. 8** and **Figure 5. 9**) at baseline is slightly reduced, and the interaction noted on ligand treatment is significantly reduced. This is likely to be due to background fluorescence or 'autofluorescence' from the FFPE pellet diluting the signal. Furthermore, processing of the cells after stimulation may not preserve the protein:protein interactions efficiently. Although the signal from HER2(DARPin)-Cy5 may demonstrate some non-specific cytoplasmic staining of background, on examination of the pseudocolour lifetime images, FRET/FLIM appears to occur on membranous regions of the cells, especially after ligand treatment, as expected (white arrows). Therefore, we have validated our FRET/FLIM assay in formalin fixed paraffin-embedded tissue, and shown differentiation between the extent of HER2:HER3 dimerisation with and without ligand, as a positive control. The final optimisation step is the application of this assay to FFPE archived tumour tissue.

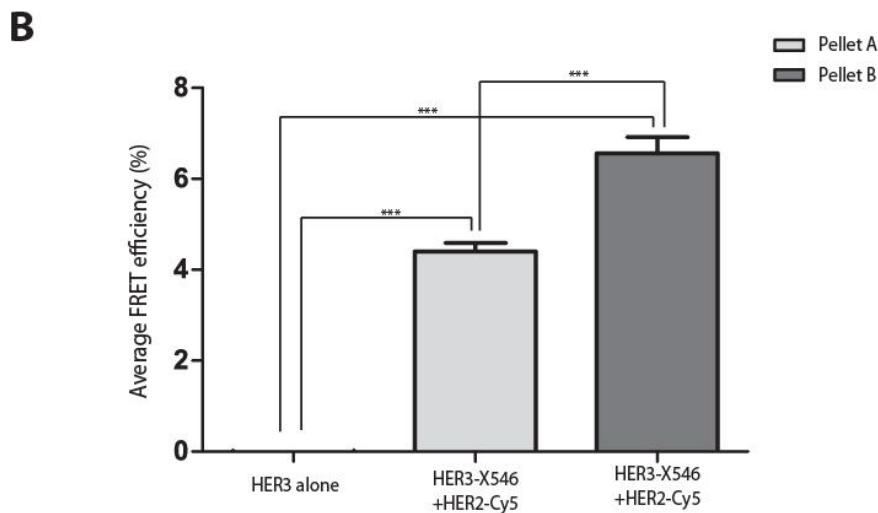
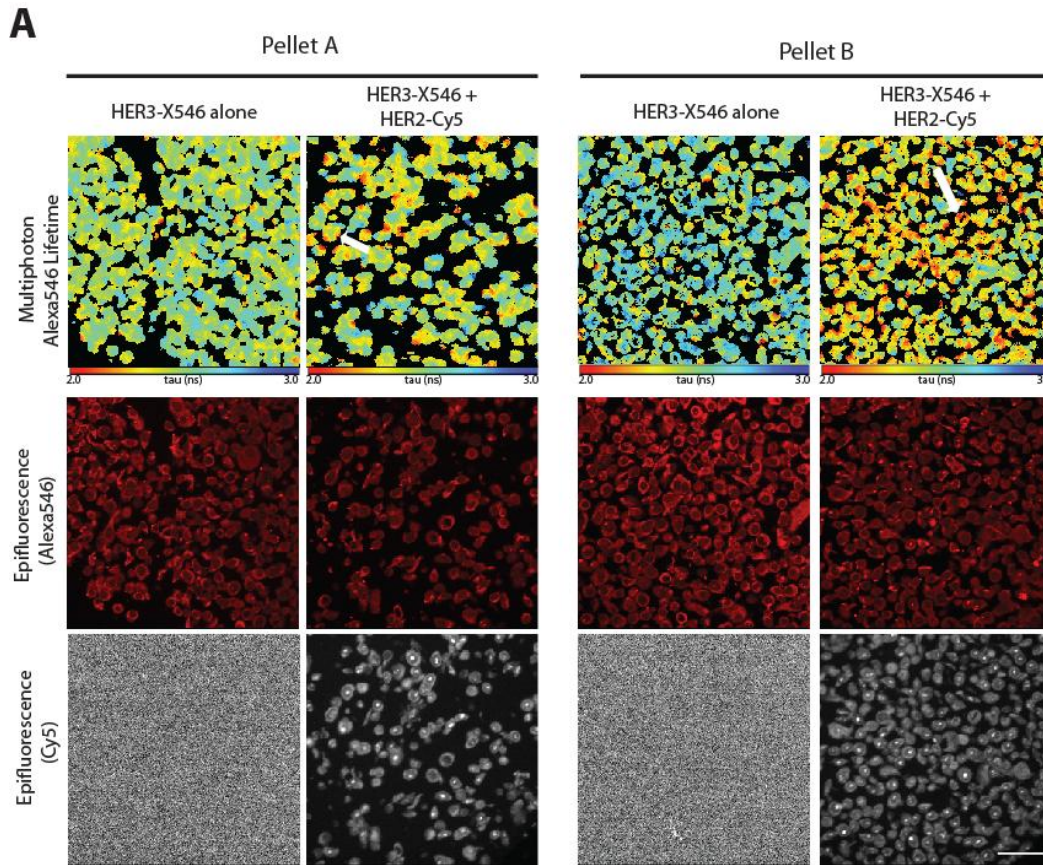


Figure 5. 12 HER2:HER3 dimerisation measured in cell pellets, as measured by FRET/FLIM

(A) Images from FFPE cell pellets of SK-Br-3 cells are shown. Cells for Pellet B were treated with neuregulin (50ng/ml) for 15 minutes prior to fixation; cells for pellet A were untreated. The cells were processed for the manufacture of cell pellets as described in Materials and Methods. Sections were dewaxed and antigen retrieval was carried out as per routine for FFPE tumour tissue, followed by processing for IF. The operator was blinded to the identity of each pellet during image acquisition and analysis. White scale bar represents 50 μ m. (B) Cumulative analysis of FRET efficiencies, calculated as described previously, are shown in a bar graph. 5 points were taken from each tumour specimen. Error bars represent SEM, values for p are <0.001(***)

5.2.6 FRET/FLIM measurement of HER2:HER3 dimers in FFPE tumour tissue

Once our FRET/FLIM assay had been validated in cell pellets, it was then applied to FFPE tumour tissue in order to assess the spectrum of HER2:HER3 dimers detectable. Therefore, we used a section from a composite block of four tumour tissues, each expressing various levels of HER2 protein (3+, 2+, 1+ and 0 or negative, as scored using the Hercep Test). Of note, the level of HER3 protein expression in each tumour tissue had not been previously documented, and of course is highly relevant within our assay. The bar graph in **Figure 5.13B** shows the range of lifetimes detected in these tissues, which did not entirely correlate with the IHC scoring of HER2. An antibody raised against an intracellular epitope of HER3, 2F12, kindly validated by Dr Gregory Weitsman, was used to control for any non-specific binding of HER2(DARPin)-Cy5. As the DARPin binds to an extracellular epitope of HER2, and 2F12, to an intracellular epitope, little change in fluorescent lifetime of HER3(2F12)-X546 is expected as the fluorophores are too far apart for FRET to occur. In order to illustrate this point, the mean lifetimes and FRET efficiencies for the 4 tissues for both HER3(M01)-X546 and HER3(2F12)-X546 are illustrated in the bar chart.

Within the group of tissues assessed with the validated HER2:HER3 assay, using HER3(M01)-X546, a variety of fluorescent lifetimes were noted, with a shorter lifetime, indicating increased FRET efficiency. However, the mean lifetimes from HER3(2F12)-X546 did not differ significantly across the tissues. Although our assay demonstrates no FRET efficiency in the HER2 negative tissue specimen, HER2:HER3 dimer formation within tissues which are classified as HER2 'positive' is heterogeneous. For instance, the FRET efficiency detected in HER2 1+ and HER2 3+ tissue is, on average 6.5-7%, and is significantly higher than that seen in HER2 2+ or HER2 negative tissue. No significant difference was detected between the lifetimes in the HER2 1+ and HER2 3+ samples. This result indicates that HER2:HER3 dimer formation may exist in tumour which are usually classified as HER2 'negative' by the Hercep test, as well as in HER2 'positive' tumours. These results are preliminary and a full evaluation of this assay across a much larger cohort of tumour tissues is required.

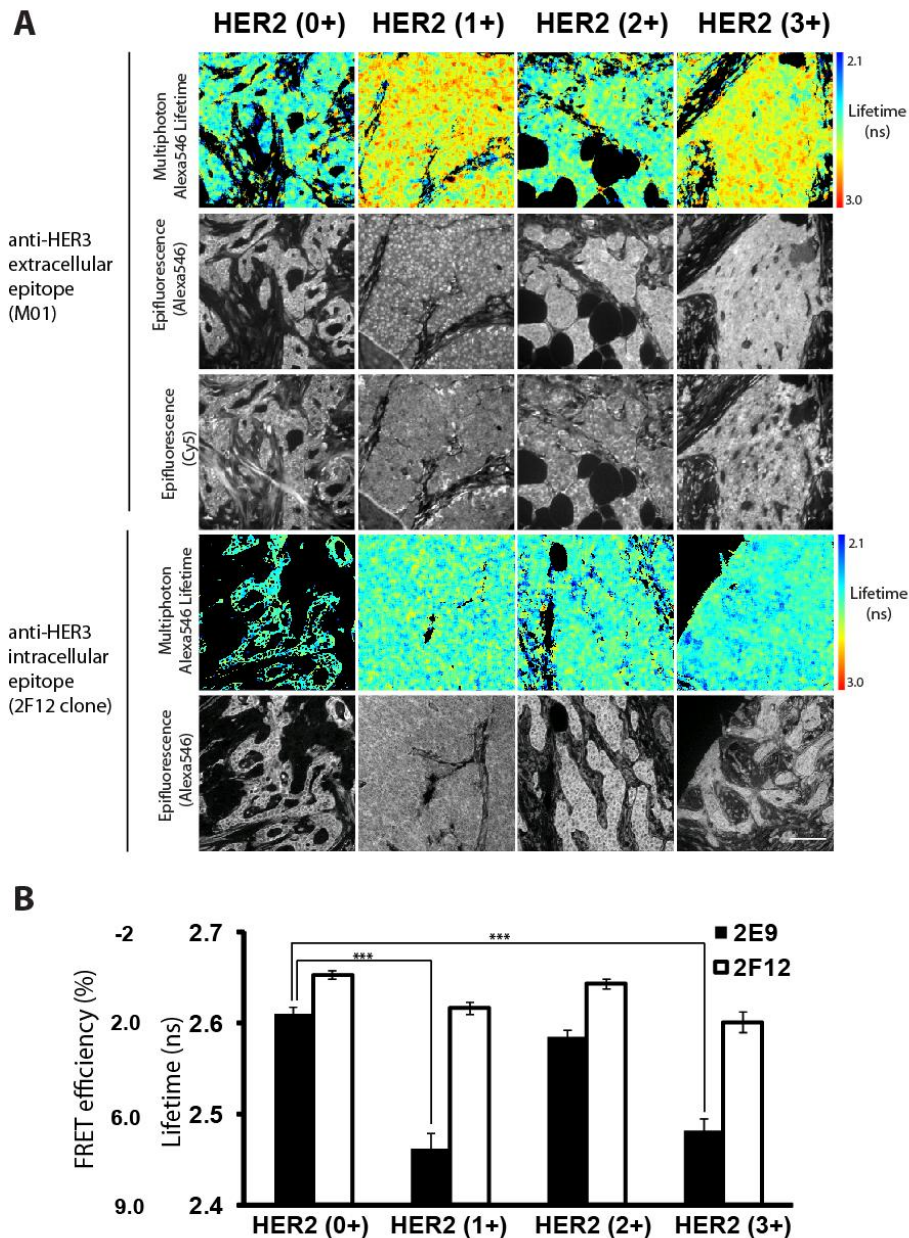


Figure 5. 13 HER2:HER3 dimerisation in tumour tissues expressing various levels of HER2 protein

(A) FRET images from formalin-fixed paraffin-embedded invasive ductal breast tumour samples within a composite block, stained with HER2(DARPin)-Cy5 and either anti-HER3(M01)-Alexa546 or anti-HER3(2F12)-Alexa546. The latter was used as negative control since the epitope recognised is on the cytoplasmic portion of HER3 whereas the HER2 DARPin recognises an extracellular epitope on HER2³⁷². White bar represents 50µm. (B) Both FRET efficiency and lifetime are represented on the scale to the left of the bar chart. FRET efficiency = $1 - \text{lifetime}$ or $\tau(\text{DA}) / \tau(\text{control})$ where $\tau(\text{DA})$ is the lifetime of anti-HER3(2E9)-Alexa546 in the presence of anti-HER2 DARPin-Cy5, whereas $\tau(\text{control})$ was that of anti-HER3(2F12)-Alexa546 in the presence of anti-HER2 DARPin-Cy5. The quantification of FRET by FLIM was pioneered by our group more than a decade ago³⁵⁴. Detailed methodology pertaining to cell staining with fluorophore-conjugated antibodies, imaging protocols and analysis algorithms are published^{117,373,374}. Red and blue pixels on the pseudocolour tumour image = low lifetime/high FRET efficiency and high lifetime/low FRET efficiency, respectively. The tumour tissues express various levels of HER2 protein, as scored by immunohistochemistry, ranging from highly positive (3+) to negative (0), according to the Hercep scoring system. Cumulative analysis of FRET efficiency based on fluorescent lifetimes is shown in a bar graph in the (B). Error bars represent SEM and p values are <0.001 (***)

5.2.7 Development of a method for measurement of protein:protein interactions in isolated tumour cells

In order to develop an assay which can predict tumour response to targeted therapies, multiple tumour biopsies are ideally required both in the process of validation and for monitoring during ongoing treatment. However, the acquisition of fresh tumour tissue on recurrence or from metastatic sites is often difficult, unfeasible and confers patient morbidity. Circulating tumour cells (CTCs) have been used as surrogate biomarker and presence of a high number of these cells are associated with a poor prognosis³⁷⁵. However, the baseline count of CTCs was not prognostic in patients who were HER2 positive. In this case delineation of protein expression and interaction in these cells may be associated with prognosis and/or predictive of response to HER2-targeted treatment. Therefore, in addition to the quantification of protein:protein interaction in primary tissue, we sought to optimize the assay for use on isolated tumour cells aspirated from distant sites such as lymph nodes, which may also be applied to isolated circulating tumour cells.

We are developing a protocol in order to combine information from pre-procedural ¹⁸F-FDG-PET scans with real time endobronchial ultrasound guided transbronchial fine needle aspiration (EBUS-TBNA) of mediastinal and hilar lymph nodes in non-small cell lung cancer (**Figure 5. 14**). An ongoing collaboration with a group performing EBUS for diagnostic and research purposes, allowed access to lymph node aspirates from malignant and benign lymph nodes in order to refine our protocol. The protocol for isolation of epithelial cells from lymph node aspirates was optimised, by increasing cell yield from the lymph node aspirate, immediately transferring the aspirate to ice for transport followed by cytopsin of cells onto a slide for staining, with or without red cell lysis, in order to reduce background signal. **Figure 5. 14** demonstrates an example of the application of this protocol, using a FRET/FLIM assay for HER1 ubiquitination which I had previously developed, as a post-translational modification which may be relevant in isolated lung cancer cells. This assay is of relevance in lung tumours as HER1 is an important target for novel therapies, e.g. gefitinib or erlotinib, and ubiquitination of this receptor is associated with downregulation and degradation of HER1^{157,358,359}.

In this example, the ¹⁸F-FDG-PET scan carried out at diagnosis shows a left sided thoracic malignancy, highlighted in black on the PET scan and in orange in the co-registration scan. An enlarged lymph node is seen on the CT scan but does not show increased FDG avidity (white arrow in the co-registration scan). This lymph node was biopsied using EBUS-TBNA and haematoxylin and eosin (H&E) images demonstrate malignant infiltration of the node.

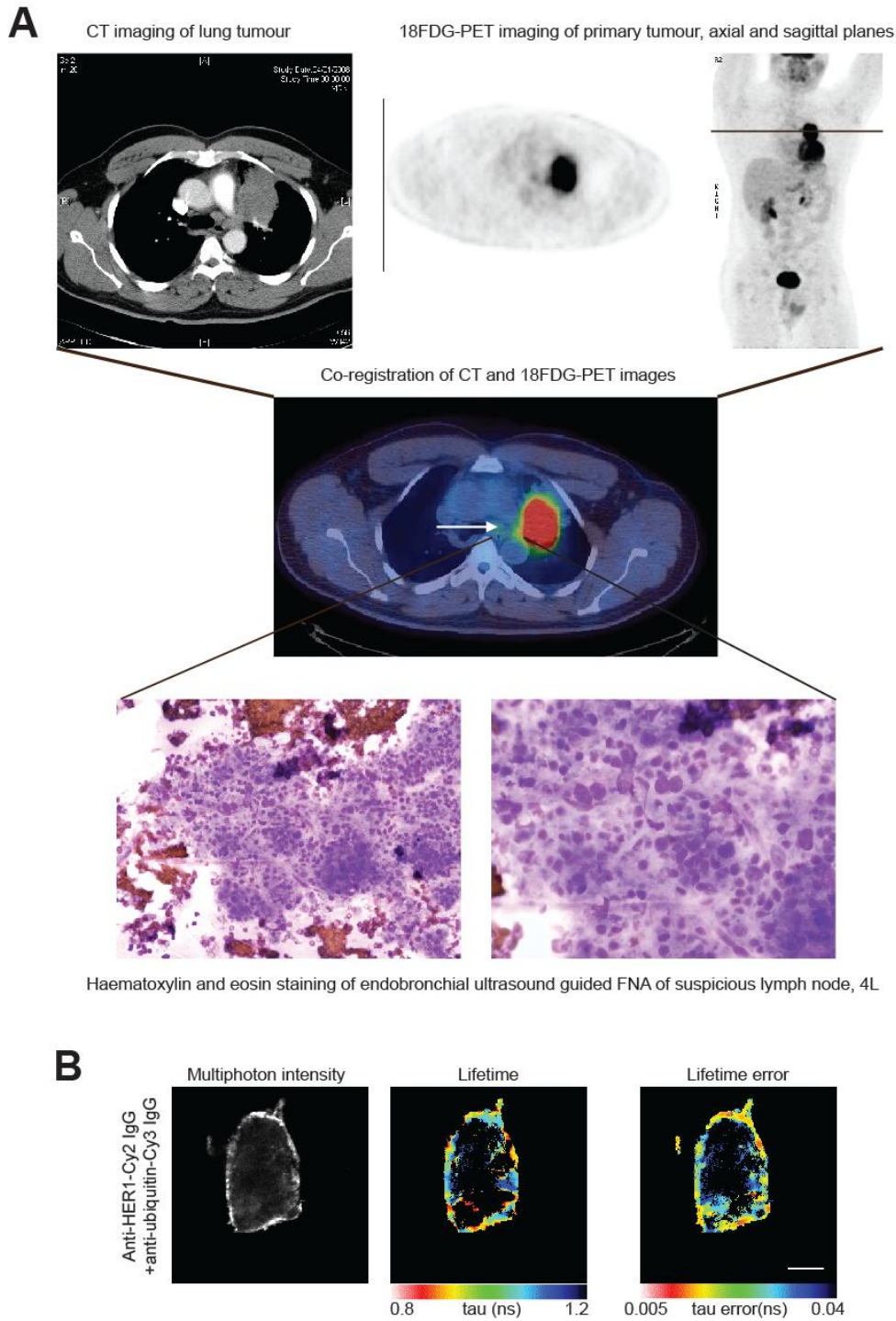


Figure 5. 14 Extraction of tumour cells from endobronchial ultrasound guided lymph node aspiration

(A) Co-registration of images from CT and ^{18}F -FDG-PET combines spatial resolution of CT with the functional capacity of PET in order to stage this patient with non-small cell lung cancer. The middle image shows FDG uptake in the left upper lobe primary tumour (red spot) and very low FDG uptake in an adjacent left paratracheal lymph node, as demonstrated by the white arrow. The low FDG uptake in left paratracheal lymph node was not deemed to be significant but EBUS-guided transbronchial needle aspiration (TBNA) showed evidence of metastatic infiltration by non-small cell lung cancer (NSCLC). The H&E images show a mixed population of lymphocytes, but with a few groups of atypical cells. Within these cells, a high nuclear to cytoplasmic ratio, angulated and prominent nucleoli suggest malignant transformation.

Figure 5.14 legend ctd:

(B) FRET/FLIM assays are performed on samples obtained by EBUS-TBNA. HER1 ubiquitination is assessed by measuring FRET between anti-HER1-Cy2 IgG and anti-ubiquitin-Cy3 IgG. Interaction between Cy2 and Cy3 results in a shortening of the lifetime of Cy2, as seen in the pseudocolour lifetime image. FRET efficiency was calculated using the following equation in each pixel and averaged per each cell. FRET efficiency = $1 - \tau_{da}/\tau_{control}$, where τ_{da} is the lifetime of cells stained with both anti-HER1-Cy2 IgG and anti-ubiquitin-Cy3 IgG and $\tau_{control}$ is the mean anti-HER1-Cy2 lifetime measured in the absence of acceptor. The lifetime error image on the far right illustrates the small error margins associated with this approach. Analysis was done using Bayesian fitting methods³⁷⁶. Scale bar represents 5 μ m.

We have demonstrated the feasibility of delineation of protein interactions or post-translational modifications, such as HER1 ubiquitination (**Figure 5. 14B**) within these metastatic tumour cells from a non-FDG avid lymph node, which may be different to those seen in the primary FDG-avid tumour. In a similar manner, the HER2:HER3 assay developed herein could be applied to metastatic tumour cells from breast cancer patients, e.g. by collection of circulating tumour cells or from lymph node fine-needle aspirates, to better profile both the primary and metastatic tumour.

5.3 Discussion

Despite the challenges and pitfalls of translation of a cell-based FRET/FLIM assay for use in human tissue, we have quantified, for the first time, HER2:HER3 interaction in FFPE tumour samples. A panel of antibodies were screened and optimised, and FFPE cell pellets created to further test these antibodies. Preclinical validation of this assay confirmed an increase in HER2:HER3 dimer formation upon treatment with the ligand, neuregulin, compared to baseline, in FFPE cell pellets. Currently, the only other method for the assessment of protein interaction between HER2 and HER3 in tumour tissue is *in situ* proximity ligation assay (PLA)³⁴⁵. However, this method does exhibit some technological flaws. The maximum degree of resolution of this assay is approximately 40nm, due to the constraints of antibody formation and DNA hybridisation, which entails the distance between proteins in clusters or an oligomer, but not necessarily within a dimer. FRET/FLIM assays provide a higher degree of resolution, of less than 10nm, thus allowing quantification of protein dimerisation. Furthermore, the PLA technique described in this example is an intensity-based assay, so that overexpression of HER2, a known prognostic factor, will result in high signal intensity and interpretation of homodimer formation if the receptors are situated in clusters. Therefore, it is difficult to extract the prognostic significance of results obtained with PLA, from the highly prognostic value of HER2 overexpression alone. In design, our FRET/FLIM assay is more specific, in terms of measuring HER2:HER3 dimerisation not oligomerisation, and less likely to be biased by HER2 amplification.

Within our cohort of patients we have shown that there is a trend for HER2 overexpression by IHC to be prognostic of a poor outcome both for DMFS and OS. However, this is not statistically significant and HER3 overexpression is not prognostic of outcome. The lack of statistical significance is likely to be due to the small event numbers. Although the cohort contains 220 patients, only 110 and 125 patients were used in the survival analysis for HER2 and HER3 respectively. Within this subset of patients, only 22 and 28 events occurred in, for example, the overall survival analysis for HER2 and HER3 overexpression, respectively. Therefore larger patient numbers, and hence a larger number of events would be required to achieve statistical significance. Furthermore, the assessment of HER3 overexpression by IHC is not yet standardised, either for the antibodies applied or the scoring method used, and is difficult to quantify. These factors are likely to play a large part in the variation in results seen here and in the literature.

Our FRET/FLIM assay quantifying HER2:HER3 dimer formation may potentially improve prediction of outcome, and predict for response to HER2-targeted drugs. For instance, tumours expressing both phosphorylated HER2 and HER3 have been shown to be

predictive for response to lapatinib in a cohort of patients with advanced inflammatory breast cancer³¹⁷. This finding suggests that patients with a higher level of pre-formed dimers of HER2 and HER3, may be more likely to respond to lapatinib, and requires testing in prospective clinical studies.

Assessment of HER2 heterodimer formation may be able to identify a subset of patients who are not classified as HER2 positive but may still benefit from HER2-targeted treatment. In a recent study of postmenopausal, ER-positive tumours, treatment with lapatinib and letrozole for HER2 negative tumours which relapse early (<6months of tamoxifen treatment), has been shown to produce a trend to improved progression-free survival and clinical benefit rate although this is not statistically significant³¹⁸. We have shown here, for the first time that heterodimers of HER2 and HER3 may be present in tumour samples where HER2 is not classically overexpressed, as well as in samples which are strongly positive for HER2 (**Figure 5. 13**). For instance, a tumour sample scored as expressing a low level of HER2 receptor (1+) demonstrated the same degree of dimer formation as one scored as expressing a very high level of HER2 (3+), which was significantly higher than that seen in a moderately expressing tumour (HER2 (2+)). One explanation of this phenomenon is that those tumours expressing a high level of HER2 exhibit a higher level of HER2 homodimerisation compared to a lower scoring tumour, which may be more likely to form the HER2:HER3 heterodimer. As HER3 heterodimer induced signaling and proliferation is thought to be the most potent³³⁰, with increased recycling of heterodimers compared to homodimers²⁸¹, the mitogenic capacity of both these tumour samples may be equivalent. This would indicate that both would benefit from HER2-targeted therapy, whereas in clinical practice, only the highly overexpressing tumour would be prescribed such therapy. Of course the results presented here are very preliminary, on only four tumour samples and require validation across both retrospective and prospective clinical trials prior to a change in clinical practice. In the first instance, we are planning to apply this assay to the Guy's cohort of METABRIC samples in order to test the hypothesis that HER2:HER3 heterodimer formation does not correlate with HER2 overexpression and may be prognostic of clinical outcome.

Although our assay has great potential in providing an improved prognostic and predictive tool, development of this tool has been fraught with many challenges and has been significantly delayed. First, it was necessary to select antibodies which could be viable for use in tumour tissue. Although many HER2 antibodies have been identified and validated for use in immunohistochemistry, the pool for selection of antibodies raised against HER3 is significantly smaller, with few having been validated in the literature^{333,336,338,339}. Furthermore, the conjugation of fluorophores to the antibodies of choice was a stringent process which required the antibody to be provided without routine carrier proteins, such as bovine serum

albumin (BSA), to avoid non-specific labeling of albumin. Antibody ultra-filtration and fluorophore conjugation at a variety of pH levels may render the antibody non-specific, as seen with a HER2 antibody (**Figure 5. 5**) and the HER3 antibody (RTJ2, **Figure 5. 7**), best characterised for use in IHC. The process of conjugation may be contaminated by any additional free lysines which may be present within the antibody solution, resulting in conjugation of these lysines with the fluorophore and non-specific staining of tissue from these products.

As we have noted from our cell-based assay stoichiometry between the bound fluorophore-conjugated antibodies must be optimal in order for FRET to occur. This phenomenon explains the variation seen in FRET efficiency between the examples of different fluorescently labeled conjugates shown in **Figure 5. 9** (not all antibody pairs tested were shown here). The conjugation of small proteins such as DARPins added a further dimension as these molecules are significantly smaller than antibodies, thus potentially reducing distances over which FRET may occur. However, fluorescently-labeled DARPins are transiently unstable, thus requiring careful storage and repeated conjugation of fresh DARPins with fluorophores was necessary. As, the acceptor fluorophore was required to be in excess of the donor fluorophore, HER2 was chosen as the acceptor as expression of this protein is routinely assessed in the staging of breast tumours, allowing the selection of HER2-positive tumour cases as controls.

Aside from the challenges in finding the optimal antibody pair for our FRET/FLIM assay, we faced further issues related to the tissue itself. It is well established that tumour tissues exhibit 'auto-fluorescence' which may vary from benign tissues, and may in itself be used as a mechanism for differentiating benign and malignant specimens³⁷⁷⁻³⁷⁹. Furthermore, the preparation of tissue in formalin leads to dehydration and thus, significant changes to auto-fluorescence³⁸⁰. We defined the lifetime of tissue auto-fluorescence as short but variable, by analysing unstained equivalent FFPE samples. We attempted to circumvent this issue by selecting fluorophores with longer fluorescent lifetimes, such as Cy3 and Cy5 compared to Cy2. However, some dilution of signal due to auto-fluorescence is unavoidable, and explains, in part the difference in FRET efficiency detected between FFPE cell pellets and cells in vitro (**Figure 5. 12** and **Figure 5. 9** respectively).

This degree of contamination due to 'auto-fluorescence' may be reduced by using fresh frozen tumour samples or isolated tumour cells. As the majority of tumour specimens are processed in formalin and paraffin, with a smaller proportion having equivalent fresh frozen sections, an assay which is limited for use in frozen sections, would not be as generally applicable as one which is successful in FFPE material. Optimisation of our assay in FFPE

material also lends the assay for use in screening of multiple specimens from tissue microarrays, which can contain over 100 tumour cores per section. This HER2:HER3 assay will now be applied to TMAs from the METABRIC cohort of patients in order to assess its prognostic capacity. Gene expression data from this cohort is available. Hence data from protein:protein interactions, gene expression and traditional clinico-pathological variables will be combined in an aim to improve upon current methods of prognosis.

Within this work, we also begin to address the relevance of tumour heterogeneity in developing fully inclusive prognostic and predictive tools. Expression profiles of, for example, HER2, vary both within the primary tumour and between the primary and metastatic site³⁶⁶, but the clinical significance of this is unknown. Identification of HER2 expression and/or dimerisation with HER3 on circulating tumour cells in patients without distant metastases may provide vital additional information in the staging of patients with local disease. In order to assess treatment response, repeated biopsies may be necessary at different time points to obtain surrogate markers for treatment response. However, this approach confers morbidity to patients in the attempt to access cancer tissues or cells, and may not be acceptable or feasible. A non-invasive method of imaging is routinely used in this case, e.g. MRI scans in the assessment of tumour response to neoadjuvant chemotherapy, but is not feasible for all patients receiving treatment. Imaging based on ionising radiation, such as X-ray, CT, and PET may lead to unacceptable levels of radiation exposure.

In the era of drugs targeted against specific molecular pathways, it is imperative that we develop methods of imaging at the molecular scale, such as FRET/FLIM, in order to select appropriate initial therapy and accurately assess on-target drug effects. Such technology has the potential to reduce drug costs and patient morbidity. For example, ¹⁸F-FDG-PET scanning has been shown to improve selection of patients for hepatic surgery of colorectal liver metastases³⁸¹. This study demonstrated a risk reduction in the number of futile laparotomies from 45% to 28% using PET/CT compared to CT, potentially saving costs of surgical interventions, inpatient stays and patient morbidity. In order to maximise predictive capacity, the issue of heterogeneity of the malignant profile in primary and metastatic tumour cells must be addressed.

We have demonstrated the feasibility of application of a FRET/FLIM assay to tumour cells from distant tumour sites in order to profile the malignant proteome of the escaped cells (**Figure 5. 14**). Smears and cell block preparations of EBUS-TBNA aspirates can be screened for HER1 mutations that can render the tumour drug resistant, such as the T790M mutation which can confer gefitinib resistance; as well as for quantifying protein-protein interaction of interest, e.g. HER1 ubiquitination. This technique was used to examine

signaling events at a site which was suspicious on routine imaging with CT but negative on functional imaging with ^{18}F FDG-PET. The success of treatment strategies may be monitored (both spatially and temporally) by the changes in specific tumour cell mechanisms. In the future, molecular imaging may be carried out on image-guided biopsy material, in order to apply the right treatment regimen to the right patient at the right time. The main challenge to this strategy would be the difficulty in choosing the site for biopsy and the need to minimise multiple biopsies, and hence the need to improve the accuracy of currently available image-guidance techniques. In part, this challenge could be addressed by examining circulating tumour cells (CTCs) which may be obtained in a less invasive way (discussed further in **Chapter 6**).

Tumour heterogeneity and a differential response to treatment represent a few of many characteristics influencing the eventual tumour phenotype, and thus, response to cancer therapeutics. Whole body imaging is the only technique currently available for the study of both primary tumour and metastases, both at diagnosis and to monitor response to treatment, but may not provide vital information at the molecular level. Image-guided biopsy, co-registration of complementary imaging modalities and appropriate biomarker choice may provide optimal risk stratification and help overcome these challenges. Prospective trials with biomarker end-points are required to map the tumour phenotype. Clinical outcome and response to treatment has a complex and multifaceted relationship to genotype and gene expression, dysregulation of signaling pathways *via* gene expression, protein activity, protein-protein interactions and tumour phenotypic traits. It may be possible to extract this data from patients using a combination of techniques, including molecular imaging of protein-protein interactions, assessment of gene expression and functional whole body imaging. We have set up such a pilot study in order to attempt to establish the multi-parameter dataset required to predict response to treatment. However, the real challenge is to integrate datasets from each observable level of variation, from genotype to tumour phenotype, in order to inform clinical management for the individual patient.

Chapter 6: Summary and Future Directions

6.1 Summary

The advent of targeted therapy has brought major improvements in clinical outcome for cancer patients. For example, the TKI imatinib is specific to the bcr-abl fusion protein, and when administered in patients with chronic myelogenous leukaemia (CML) which produces this protein, clinical remission rates of 90% are achieved³⁸². However, the promise of targeted agents has not been realised to same extent for all TKIs, in part due to the lack of patient selection based upon molecular profiling. For instance, the HER1 TKIs, erlotinib and gefitinib produce response rates of less than 10% in unselected populations and overexpression of HER1 does not correlate with response to treatment^{322,323}. Investigation of somatic gain-of-function mutations in HER1, led to the discovery of a missense mutation L858R in the HER1 activation loop which facilitates gefitinib binding^{383,384}. This and other activating mutations are correlated with a much improved response rate to TKI therapy, and have helped revolutionise treatment regimens for non-small cell lung cancer patients. By analysing the relationship between structure and activity of HER1, bound to TKIs, a better understanding of sensitivity and mechanisms of resistance to these drugs has evolved. In the case of lapatinib, response rates are 40% in metastatic breast cancer patients. In the hope to understand the effects of lapatinib upon HER2 and the ensuing molecular events, I have quantified HER2:HER3 interactions within a structural context, using FRET/FLIM technology, which was translated for use in patient tumour tissue.

Within this thesis, I have demonstrated the differential effects of various TKIs upon HER2:HER3 heterodimer formation, quantifying lapatinib-induced dimerisation as greater than that induced by TKIs binding to the active form of receptor, in contrast with lapatinib, which binds to the inactive form. We have developed, for the first time a model of the lapatinib-induced dimer, validated by a chemical biology approach using site-directed mutagenesis at the dimer interface. Lapatinib-induced dimer formation eventually leads to the development of resistance by the re-phosphorylation of HER3. I have used a novel mutation of HER2 to disrupt TKD-mediated dimer formation and attenuate the development of resistance, as well as emphasising the importance of the N-lobe of the TKD within this dimer. Furthermore, I have shown, for the first time that the structural integrity of HER3 is vital to the formation of this heterodimer. Hence, elucidation of the structural conformation of the lapatinib-induced HER2:HER3 dimer has led to the discovery of strategies to target the

intracellular dimerisation interface, and hence provided biological insights into novel, viable drug targets which could circumvent dimer-mediated resistance.

The clarification of the cell biology has helped to highlight the HER2:HER3 dimer as highly relevant for assessment in clinical tumour samples by FRET/FLIM, in order to create a novel prognostic or predictive biomarker. As we have shown HER2:HER3 dimer formation to be key to HER recycling and the development of resistance to lapatinib, the FRET/FLIM assay may be particularly of use in the delineation of mechanisms of resistance in tumour recurrence. We have faced many technical challenges in the optimisation of this assay, as described in Chapter 5, some of which still remain. For instance, further work needs to be carried out in the delineation of auto-fluorescence in tissue in order to devise strategies to eliminate signal dilution. However, we have shown for the first time, HER2:HER3 dimers of varying extent in a variety of breast tumour tissues. A significant amount of work remains to be carried out in order to fully validate this assay and define its clinical utility.

6.2 Future directions

Quantification of HER2:HER3 dimer formation as a prognostic biomarker is currently being tested within our group. The FRET/FLIM assay is being applied to TMAs from the METABRIC dataset, initially profiled in Chapter 5, to correlate dimer formation with clinical outcome in terms of disease recurrence or disease-related death. In order to maximise prognostic capacity, it is important to fully profile the tumour within its milieu. The combination of data from gene derived signatures and clinico-pathological factors together with output from our proteomic based assay should provide a better prognostic model for outcome. This hypothesis will now be tested in the group as data from all three sources are available for the METABRIC patient cohort. Further improvements in protein-based biomarkers are being sought by examining protein network maps to highlight interactions between key nodes of relevance to HER2. Simultaneously, we aim to better describe the tumour microenvironment and immune response in order to fully profile, not only the tumour itself, but also external factors which may be relevant to metastasis. Integration of the terabytes of data that are likely to be generated using this strategy is likely to pose a real challenge and will require high powered bioinformatics and computational modeling. Furthermore, once validated, high-throughput technology will have to be developed to facilitate the use of these assays in clinical practice.

Although prognostic tools already exist, we hope to improve upon prediction of outcome by these methods. However, the tools for prediction of response to treatment for targeted drugs are severely lacking and it is in this arena that I hope our assay will be of most benefit.

Firstly, validation of the assay must be carried out in a population treated with a HER2-targeted agent, either retrospectively or prospectively or both. Due to the time of patient recruitment, few patients within the METABRIC cohort would have received treatment with trastuzumab and none would have received lapatinib, eliminating this group from assessing predictive capacity for our HER2-based FRET/FLIM assay. However our group is attempting to obtain access to tissue samples from previous studies assessing lapatinib response, in order to correlate HER2:HER3 dimer formation to response. We will also try to address the hypothesis that even those tumours which are HER2 negative may respond to HER2-targeted treatment if the oncogenic pathway is heterodimer formation between low levels of HER2 and HER3, by quantifying HER2:HER3 dimerisation in all tumours within this cohort.

Further validation of this assay in the prospective setting is required. Neoadjuvant clinical trials provide an opportunity to use complete tumour eradication (pathological complete response, pCR) as a surrogate end-point in order to assess predictive capacity of biomarkers. Although pCR has not yet been validated as a surrogate end-point for overall survival, it is used in neoadjuvant studies in order to gauge the potential of a new drug, correlate biopsy-derived potential biomarkers with outcome and to inform on the design of much larger, more time-consuming and expensive adjuvant studies. For instance, incorporation of pertuzumab, a humanised monoclonal antibody against the dimerisation domain of HER2, into standard neoadjuvant chemotherapy, has recently demonstrated the next incremental benefits in the early treatment of HER2+ve patients when compared to trastuzumab, a monoclonal antibody targeting an alternative extracellular domain of HER2. Upon pertuzumab treatment, critical proteomic events such as HER2:HER3 receptor dimerisation, allosteric activation, initiation of further downstream signalling and cell proliferation, are prevented, leading to an improvement in pathological complete response from 29% (trastuzumab and docetaxel) to 45.8% (pertuzumab, trastuzumab and docetaxel)⁴².

With current therapies we can see a clinical benefit in the region of 30% in terms of pCR, on the use of trastuzumab and chemotherapy⁴²⁻⁴⁴. A significant improvement has been made on the addition of pertuzumab. However, if we are to make incremental clinical gains for patients, we need to address the functional state of the protein network for relevant oncogenic protein such as HER2 and HER3, on an individual basis, especially if we are to realise the potential of treatment with targeted therapies alone³⁸⁵. Treatment with pertuzumab and trastuzumab without chemotherapy, results in complete tumour eradication, i.e. pCR of 17% which is very promising but currently unacceptable when compared to standard chemotherapy. However, validated biomarkers may highlight selected patients who may yet benefit from lapatinib treatment. The neoadjuvant study I-SPY1, demonstrated

improved prediction of disease free survival using gene expression signatures compared to clinic-pathological variables and pCR in a subset of patients who did not receive trastuzumab³⁸⁶. However trial exemplifies the lack of a good predictive biomarker for pCR. Nine potential biomarkers, including clinco-pathological variables and a variety of gene expression signatures, were tested but very little consistency was found in the prediction of response to therapy. A good signature for accurate prediction of pCR in all groups does not yet exist and hence, the search for biomarkers continues.

Profiling protein-protein interactions such as HER2-HER3 dimerisation, in combination with current biomarkers, may lead better prediction of pCR. I have completed the initial stages of setting up a prospective neoadjuvant clinical trial in order to test whether HER2:HER3 dimer formation alongside functional imaging with FDG- and FLT-PET could improve prediction of response to HER2-targeted treatment (trial schema, Figure 6.1, Table 6.1 and full documentation, **Appendix 1**). As recent evidence has shown that no benefit to the substitution of trastuzumab with lapatinib in the neoadjuvant treatment of HER2 positive tumours³⁸⁷, within our clinical trial, we propose to use the standard regime of trastuzumab and taxane chemotherapy, as well as anthracycline based combination chemotherapy. Both fresh frozen and FFPE samples will be taken at the indicated time-points in order to obtain both gene expression data and to assess a variety of protein:protein interactions, including HER2:HER3 dimer formation. We also aim to answer some of the questions raised within this thesis regarding tissue heterogeneity by combining imaging modalities to fully profile the tumour.

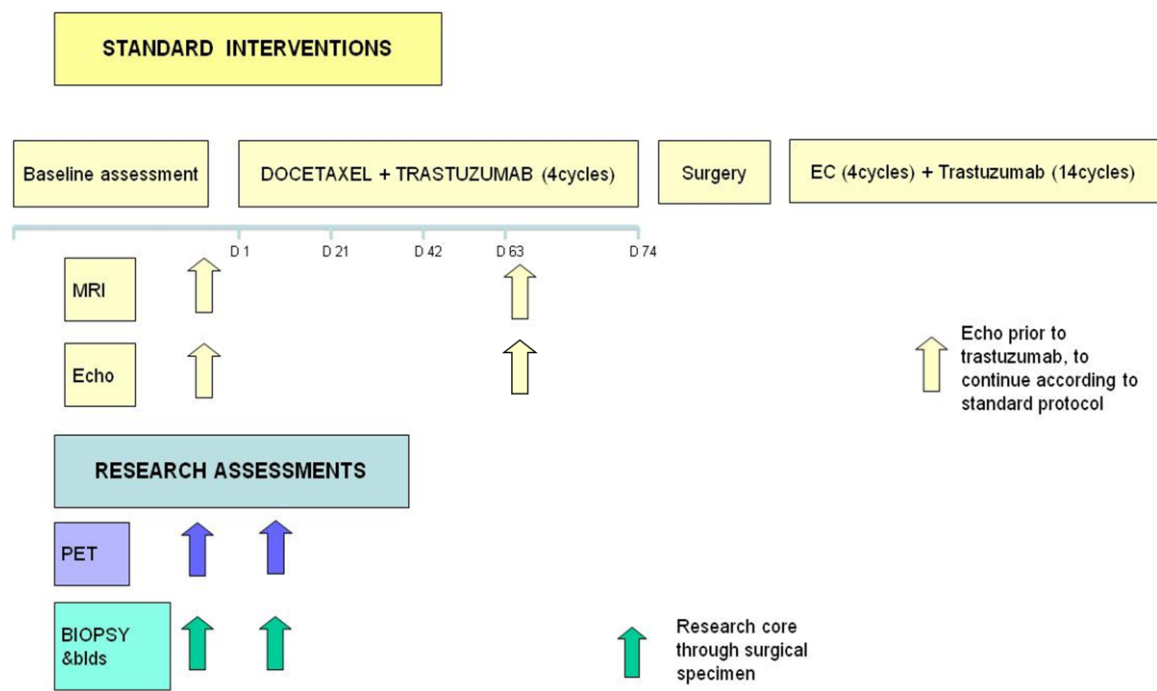


Figure 6. 1 Neoadjuvant clinical trial schema

Primary Objective	Endpoint
To correlate PET imaging response in breast and axillary lymph nodes with residual cancer burden (RCB) at definitive surgery	Correlation of SUV response for each tracer with residual cancer burden (RCB) in breast and axilla

Secondary Objective	Endpoint
To evaluate optical proteomic profiling of HER2 and related protein interactions in primary tissue and circulating tumour cells as a method for predicting response to targeted treatment and chemotherapy	Correlation of outcome from optical proteomic profile with [¹⁸ F]-FLT and FDG, conventional MRI RECIST response criteria, RCB and pathological response to treatment from surgical specimen
To evaluate PET imaging using the tracers [¹⁸ F]-FLT and FDG as a method for evaluating response to systemic therapy in HER2 positive breast cancer	Correlation of SUV response for each tracer with conventional MRI RECIST response assessment
To correlate PET imaging response with biopsy derived proliferation biomarkers	Correlation with % cell positive for proliferation markers ki 67 (MIB-1), geminin, mcms and mRNA expression markers of proliferation genes (if present)
Non invasive assessment of Ki and K1 from this dataset	The dynamic analyses will use an input function derived from the aorta of heart of both to derive rate constants Ki and K1, measurements transport and phosphorylation for both tracers
To obtain performance estimates for the ability of the tracers FDG and FLT to report MRI response	Evaluate the ability of FDG and FLT tracers to predict RCB
To assess nodal imaging response using PET imaging	Correlate with standard imaging response in nodes, SUV response in breast.
To assess the safety of fluorothymidine in patients with breast cancer.	Determining the causality of each adverse event to the two agents, and grading AE severity according to NCI CTCAE version 4.0.

Table 6. 1 Clinical trial primary and secondary end-points

In collaboration with Prof Michel O'Doherty (Nuclear Medicine) and Dr Jennie Glendenning (Clinical Oncology) we hope to incorporate functional imaging with both ^{18}F -FDG- and ^{18}F -FLT-PET scanning to define tumour changes after one cycle and four cycles of trastuzumab with chemotherapy, with corresponding tumour biopsies for FRET/FLIM imaging, as shown in **Figure 6. 1**. Furthermore, we aim to collect blood samples for assessment of number of circulating tumour cells (CTCs) and to test feasibility of quantification of protein:protein interactions on these cells. The current validated methods for detection of CTCs rely on blood or bone sampling prior to immunocytochemical or molecular analysis³⁸⁸. Bone marrow involvement delineates the metastatic group more accurately in breast cancer patients, but bone marrow biopsy is invasive and the cells obtained are often not viable³⁸⁹. CTCs in the blood have been identified by a variety of immunological approaches, including identification of epithelium-specific antigens, e.g. cytoskeleton-associated cytokeratins, surface adhesion molecules, or growth factor receptors, and by molecular PCR-based techniques. The presence or absence of CTCs in the blood both before and after treatment has been shown to correlate with treatment response^{390,391}. Furthermore, the presence or absence of radiological signs of disease progression can be combined with CTC counts in the blood to improve the prediction of overall survival in metastatic breast cancer patients undergoing therapy³⁹¹. Since we would ultimately like to derive tools that can monitor patients non-invasively and can, in the future, inform on treatment stratification strategies for tumour progression on treatment, an important part of any prospective trial will therefore also be to establish the relationship between non-invasive (e.g. radionuclide) imaging-derived parameters and the molecular parameters derived from biopsies.

In summary we aim to produce the best possible biomarkers for both prognostication and prediction of response to treatment in order to minimise patient morbidity, toxicities and financial burden. Development of minimally invasive methods of obtaining tumour cells for imaging are necessary for tumour surveillance, both during and after treatment. The eventual goal is to select the right drug for the right patient at the right time.

References

1. Fruhwirth, G.O. et al. How Förster resonance energy transfer imaging improves the understanding of protein interaction networks in cancer biology. *Chemphyschem* **12**, 442-61 (2011).
2. Kelleher, M.T. et al. The potential of optical proteomic technologies to individualize prognosis and guide rational treatment for cancer patients. *Target Oncol* **4**, 235 - 252 (2009).
3. Patel, G.S. et al. The challenges of integrating molecular imaging into the optimization of cancer therapy. *Integr Biol (Camb)* **3**, 603-31 (2011).
4. Office for National Statistics (2011).
5. Zhao, L. & Vogt, P.K. Class I PI3K in oncogenic cellular transformation. *Oncogene* **27**, 5486-96 (2008).
6. Burke, W.M. et al. Inhibition of constitutively active Stat3 suppresses growth of human ovarian and breast cancer cells. *Oncogene* **20**, 7925-7934 (2001).
7. Pawson, T. & Kofler, M. Kinome signaling through regulated protein-protein interactions in normal and cancer cells. *Curr Opin Cell Biol* **21**, 147-53 (2009).
8. Di Fiore, P.P., Segatto, O., Taylor, W.G., Aaronson, S.A. & Pierce, J.H. EGF receptor and erbB-2 tyrosine kinase domains confer cell specificity for mitogenic signaling. *Science* **248**, 79-83 (1990).
9. Dougall, W.C., Qian, X. & Greene, M.I. Interaction of the neu/p185 and EGF receptor tyrosine kinases: implications for cellular transformation and tumor therapy. *J Cell Biochem* **53**, 61-73 (1993).
10. Mortality Statistics: Deaths Registered in England and Wales *Office of National Statistics* (2010).
11. Kingsmore, D., Ssemwogerere, A., Hole, D. & Gillis, C. Specialisation and breast cancer survival in the screening era. *Br J Cancer* **88**, 1708-12 (2003).
12. MacGregor, J.I. & Jordan, V.C. Basic guide to the mechanisms of antiestrogen action. *Pharmacological Reviews* **50**, 151-196 (1998).
13. Clarke, M. et al. Tamoxifen for early breast cancer: An overview of the randomised trials. *Lancet* **351**, 1451-1467 (1998).
14. Forbes, J.F. et al. Effect of anastrozole and tamoxifen as adjuvant treatment for early-stage breast cancer: 100-month analysis of the ATAC trial. *Lancet Oncol* **9**, 45-53 (2008).
15. Regan, M.M. et al. Assessment of letrozole and tamoxifen alone and in sequence for postmenopausal women with steroid hormone receptor-positive breast cancer: the BIG 1-98 randomised clinical trial at 8.1 years median follow-up. *Lancet Oncol* **12**, 1101-8 (2011).
16. Goss, P.E. Letrozole in the extended adjuvant setting: MA.17. *Breast Cancer Res Treat* **105 Suppl 1**, 45-53 (2007).
17. Effects of chemotherapy and hormonal therapy for early breast cancer on recurrence and 15-year survival: an overview of the randomised trials. *Lancet* **365**, 1687-717 (2005).
18. Sorlie, T. et al. Gene expression patterns of breast carcinomas distinguish tumor subclasses with clinical implications. *Proc Natl Acad Sci U S A* **98**, 10869-74 (2001).
19. Albain, K.S. et al. Prognostic and predictive value of the 21-gene recurrence score assay in postmenopausal women with node-positive, oestrogen-receptor-positive breast cancer on chemotherapy: a retrospective analysis of a randomised trial. *Lancet Oncol* **11**, 55-65 (2010).
20. Peto, R. et al. Comparisons between different polychemotherapy regimens for early breast cancer: meta-analyses of long-term outcome among 100,000 women in 123 randomised trials. *Lancet* **379**, 432-44 (2012).
21. De Laurentiis, M. et al. Taxane-based combinations as adjuvant chemotherapy of early breast cancer: A meta-analysis of randomized trials. *Journal of Clinical Oncology* **26**, 44-53 (2008).
22. Green, M.H., G. *Breast Cancer : M.D Anderson Cancer Care Series*, (Springer-Verlag, New York, 2001).
23. Gennari, A. et al. HER2 status and efficacy of adjuvant anthracyclines in early breast cancer: a pooled analysis of randomized trials. *J Natl Cancer Inst* **100**, 14-20 (2008).
24. Pinder, M.C., Duan, Z., Goodwin, J.S., Hortobagyi, G.N. & Giordano, S.H. Congestive heart failure in older women treated with adjuvant anthracycline chemotherapy for breast cancer. *J Clin Oncol* **25**, 3808-15 (2007).
25. De Laurentiis, M. et al. Taxane-based combinations as adjuvant chemotherapy of early breast cancer: a meta-analysis of randomized trials. *J Clin Oncol* **26**, 44-53 (2008).
26. Slamon, D.J. et al. Human-Breast Cancer - Correlation of Relapse and Survival with Amplification of the Her-2 Neu Oncogene. *Science* **235**, 177-182 (1987).

27. Yarden, Y. & Sliwkowski, M.X. Untangling the ErbB signalling network. *Nature Reviews Molecular Cell Biology* **2**, 127-137 (2001).
28. Wolff, A.C. et al. American Society of Clinical Oncology/College of American Pathologists guideline recommendations for human epidermal growth factor receptor 2 testing in breast cancer. *Journal of Clinical Oncology* **25**, 118-145 (2007).
29. Romond, E.H. et al. Trastuzumab plus adjuvant chemotherapy for operable HER2-positive breast cancer. *New England Journal of Medicine* **353**, 1673-1684 (2005).
30. Piccart-Gebhart, M.J. et al. Trastuzumab after adjuvant chemotherapy in HER2-positive breast cancer. *New England Journal of Medicine* **353**, 1659-1672 (2005).
31. Slamon, D. et al. Phase III randomized trial comparing doxorubicin and cyclophosphamide followed by docetaxel (AC (R) T) with doxorubicin and cyclophosphamide followed by docetaxel and trastuzumab (AC (R) TH) with docetaxel, carboplatin and trastuzumab (TCH) in HER2 positive early breast cancer patients: BCIRG 006 study. *Breast Cancer Research and Treatment* **94**, S5-S5 (2005).
32. Joensuu, H. et al. Adjuvant docetaxel or vinorelbine with or without trastuzumab for breast cancer. *New England Journal of Medicine* **354**, 809-820 (2006).
33. Spielmann, M. et al. 3-year follow-up of trastuzumab following adjuvant chemotherapy in node positive HER2-positive breast cancer patients: results of the PACS-04 trial. *Breast Cancer Research and Treatment* **106**, S19-S19 (2007).
34. Vogel, C. et al. First-line, single-agent Herceptin (R) (trastuzumab) in metastatic breast cancer: a preliminary report. *European Journal of Cancer* **37**, S25-S29 (2001).
35. Slamon, D.J. et al. Use of chemotherapy plus a monoclonal antibody against HER2 for metastatic breast cancer that overexpresses HER2. *New England Journal of Medicine* **344**, 783-792 (2001).
36. Bedard, P.L., de Azambuja, E. & Cardoso, F. Beyond Trastuzumab: Overcoming Resistance to Targeted HER-2 Therapy in Breast Cancer. *Current Cancer Drug Targets* **9**, 148-162 (2009).
37. Geyer, C.E. et al. Lapatinib plus capecitabine for HER2-positive advanced breast cancer. *New England Journal of Medicine* **355**, 2733-2743 (2006).
38. Gianni, L. et al. Neoadjuvant chemotherapy with trastuzumab followed by adjuvant trastuzumab versus neoadjuvant chemotherapy alone, in patients with HER2-positive locally advanced breast cancer (the NOAH trial): a randomised controlled superiority trial with a parallel HER2-negative cohort. *Lancet* **375**, 377-84 (2010).
39. Untch, M. et al. Neoadjuvant treatment with trastuzumab in HER2-positive breast cancer: results from the GeparQuattro study. *J Clin Oncol* **28**, 2024-31 (2010).
40. Coudert, B.P. et al. Multicenter phase II trial of neoadjuvant therapy with trastuzumab, docetaxel, and carboplatin for human epidermal growth factor receptor-2-overexpressing stage II or III breast cancer: results of the GETN(A)-1 trial. *J Clin Oncol* **25**, 2678-84 (2007).
41. Buzdar, A.U. et al. Significantly higher pathologic complete remission rate after neoadjuvant therapy with trastuzumab, paclitaxel, and epirubicin chemotherapy: results of a randomized trial in human epidermal growth factor receptor 2-positive operable breast cancer. *J Clin Oncol* **23**, 3676-85 (2005).
42. Gianni, L. et al. Efficacy and safety of neoadjuvant pertuzumab and trastuzumab in women with locally advanced, inflammatory, or early HER2-positive breast cancer (NeoSphere): a randomised multicentre, open-label, phase 2 trial. *Lancet Oncol* **13**, 25-32 (2012).
43. Baselga, J. et al. Lapatinib with trastuzumab for HER2-positive early breast cancer (NeoALTTO): a randomised, open-label, multicentre, phase 3 trial. *Lancet* **379**, 633-40 (2012).
44. Untch, M. et al. Lapatinib versus trastuzumab in combination with neoadjuvant anthracycline-taxane-based chemotherapy (GeparQuinto, GBG 44): a randomised phase 3 trial. *Lancet Oncol* **13**, 135-44 (2012).
45. Fisher, B. et al. Relation of Number of Positive Axillary Nodes to the Prognosis of Patients with Primary Breast-Cancer - an Nsabp Update. *Cancer* **52**, 1551-1557 (1983).
46. Elston, C.W. & Ellis, I.O. Pathological Prognostic Factors in Breast-Cancer .1. The Value of Histological Grade in Breast-Cancer - Experience from a Large Study with Long-Term Follow-Up. *Histopathology* **19**, 403-410 (1991).
47. Hanrahan, E.O. et al. Outcome and prognostic factors among patients with node-negative invasive breast carcinoma that is one centimeter or less in size (stage I; T1a,b NO MO): the University of Texas M. D. Anderson Cancer Center experience. *Breast Cancer Research and Treatment* **94**, S124-S124 (2005).
48. Fisher, B., Redmond, C., Fisher, E.R. & Caplan, R. Relative Worth of Estrogen or Progesterone-Receptor and Pathologic Characteristics of Differentiation as Indicators of Prognosis in Node Negative Breast-Cancer Patients - Findings from National Surgical Adjuvant Breast and Bowel Project Protocol B-06. *Journal of Clinical Oncology* **6**, 1076-1087 (1988).

49. Muss, H.B. et al. C-ErbB-2 Expression and Response to Adjuvant Therapy in Women with Node-Positive Early Breast-Cancer. *New England Journal of Medicine* **330**, 1260-1266 (1994).
50. Rubens, R.D. Age and the Treatment of Breast-Cancer. *Journal of Clinical Oncology* **11**, 3-4 (1993).
51. Galea, M.H., Blamey, R.W., Elston, C.E. & Ellis, I.O. The Nottingham Prognostic Index in Primary Breast-Cancer. *Breast Cancer Research and Treatment* **22**, 207-219 (1992).
52. Ravdin, P.M. et al. Computer program to assist in making decisions about adjuvant therapy for women with early breast cancer. *Journal of Clinical Oncology* **19**, 980-991 (2001).
53. Mook, S. et al. Calibration and discriminatory accuracy of prognosis calculation for breast cancer with the online Adjuvant! program: a hospital-based retrospective cohort study. *Lancet Oncol* **10**, 1070-6 (2009).
54. Goldhirsch, A. et al. Meeting highlights: International Expert Consensus on the Primary Therapy of Early Breast Cancer 2005. *Annals of Oncology* **16**, 1569-1583 (2005).
55. Goldhirsch, A. et al. Thresholds for therapies: highlights of the St Gallen International Expert Consensus on the primary therapy of early breast cancer 2009. *Ann Oncol* **20**, 1319-29 (2009).
56. Eifel, P. et al. National Institutes of Health Consensus Development Conference Statement: adjuvant therapy for breast cancer, November 1-3, 2000. *J Natl Cancer Inst* **93**, 979-89 (2001).
57. Hernandez-Aya, L.F. et al. Nodal status and clinical outcomes in a large cohort of patients with triple-negative breast cancer. *J Clin Oncol* **29**, 2628-34 (2011).
58. Wo, J.Y., Chen, K., Neville, B.A., Lin, N.U. & Punglia, R.S. Effect of very small tumor size on cancer-specific mortality in node-positive breast cancer. *J Clin Oncol* **29**, 2619-27 (2011).
59. van't Veer, L.J. et al. Gene expression profiling predicts clinical outcome of breast cancer. *Nature* **415**, 530-536 (2002).
60. Paik, S. et al. A multigene assay to predict recurrence of tamoxifen-treated, node-negative breast cancer. *N Engl J Med* **351**, 2817-26 (2004).
61. Buyse, M. et al. Validation and clinical utility of a 70-gene prognostic signature for women with node-negative breast cancer. *J Natl Cancer Inst* **98**, 1183-92 (2006).
62. Gray, J. & Druker, B. Genomics: the breast cancer landscape. *Nature* **486**, 328-9 (2012).
63. Schulze, A. & Downward, J. Navigating gene expression using microarrays--a technology review. *Nat Cell Biol* **3**, E190-5 (2001).
64. Perou, C.M. et al. Molecular portraits of human breast tumours. *Nature* **406**, 747-52 (2000).
65. Venet, D., Dumont, J.E. & Detours, V. Most random gene expression signatures are significantly associated with breast cancer outcome. *PLoS Comput Biol* **7**, e1002240 (2011).
66. Haibe-Kains, B. et al. Comparison of prognostic gene expression signatures for breast cancer. *BMC Genomics* **9**, 394 (2008).
67. Prat, A. et al. Concordance among gene expression-based predictors for ER-positive breast cancer treated with adjuvant tamoxifen. *Ann Oncol* (2012).
68. Chi, J.T. et al. Gene expression programs in response to hypoxia: cell type specificity and prognostic significance in human cancers. *PLoS Med* **3**, e47 (2006).
69. Potti, A. et al. Genomic signatures to guide the use of chemotherapeutics. *Nat Med* **12**, 1294-300 (2006).
70. Liu, R. et al. The prognostic role of a gene signature from tumorigenic breast-cancer cells. *N Engl J Med* **356**, 217-26 (2007).
71. Chang, H.Y. et al. Gene expression signature of fibroblast serum response predicts human cancer progression: similarities between tumors and wounds. *PLoS Biol* **2**, E7 (2004).
72. Massague, J. Sorting out breast-cancer gene signatures. *N Engl J Med* **356**, 294-7 (2007).
73. Michiels, S., Koscielny, S. & Hill, C. Prediction of cancer outcome with microarrays: a multiple random validation strategy. *Lancet* **365**, 488-92 (2005).
74. Fan, C. et al. Concordance among gene-expression-based predictors for breast cancer. *N Engl J Med* **355**, 560-9 (2006).
75. Boutros, P.C. et al. Prognostic gene signatures for non-small-cell lung cancer. *Proc Natl Acad Sci U S A* **106**, 2824-8 (2009).
76. Popovici, V. et al. Effect of training-sample size and classification difficulty on the accuracy of genomic predictors. *Breast Cancer Res* **12**, R5 (2010).
77. Miller, L.D. et al. Optimal gene expression analysis by microarrays. *Cancer Cell* **2**, 353-61 (2002).
78. Ein-Dor, L., Zuk, O. & Domany, E. Thousands of samples are needed to generate a robust gene list for predicting outcome in cancer. *Proc Natl Acad Sci U S A* **103**, 5923-8 (2006).
79. Kim, S.Y. Effects of sample size on robustness and prediction accuracy of a prognostic gene signature. *BMC Bioinformatics* **10**, 147 (2009).

80. Starmans, M.H., Fung, G., Steck, H., Wouters, B.G. & Lambin, P. A simple but highly effective approach to evaluate the prognostic performance of gene expression signatures. *PLoS One* **6**, e28320 (2011).
81. Ntzani, E.E. & Ioannidis, J.P. Predictive ability of DNA microarrays for cancer outcomes and correlates: an empirical assessment. *Lancet* **362**, 1439-44 (2003).
82. Dupuy, A. & Simon, R.M. Critical review of published microarray studies for cancer outcome and guidelines on statistical analysis and reporting. *J Natl Cancer Inst* **99**, 147-57 (2007).
83. van de Vijver, M.J. et al. A gene-expression signature as a predictor of survival in breast cancer. *N Engl J Med* **347**, 1999-2009 (2002).
84. Bueno-de-Mesquita, J.M. et al. Validation of 70-gene prognosis signature in node-negative breast cancer. *Breast Cancer Res Treat* **117**, 483-95 (2009).
85. Glas, A.M. et al. Converting a breast cancer microarray signature into a high-throughput diagnostic test. *BMC Genomics* **7**, 278 (2006).
86. Wittner, B.S. et al. Analysis of the MammaPrint breast cancer assay in a predominantly postmenopausal cohort. *Clin Cancer Res* **14**, 2988-93 (2008).
87. Knauer, M. et al. Identification of a low-risk subgroup of HER-2-positive breast cancer by the 70-gene prognosis signature. *Br J Cancer* **103**, 1788-93 (2010).
88. Bueno-de-Mesquita, J.M., Sonke, G.S., van de Vijver, M.J. & Linn, S.C. Additional value and potential use of the 70-gene prognosis signature in node-negative breast cancer in daily clinical practice. *Ann Oncol* **22**, 2021-30 (2011).
89. Modlich, O. & Bojar, H. Can a 70-gene signature provide useful prognostic information in patients with node-negative breast cancer? *Nat Clin Pract Oncol* **4**, 216-7 (2007).
90. Bogaerts, J. et al. Gene signature evaluation as a prognostic tool: challenges in the design of the MINDACT trial. *Nat Clin Pract Oncol* **3**, 540-51 (2006).
91. Cardoso, F. et al. Clinical application of the 70-gene profile: the MINDACT trial. *J Clin Oncol* **26**, 729-35 (2008).
92. Esteva, F.J. et al. Prognostic role of a multigene reverse transcriptase-PCR assay in patients with node-negative breast cancer not receiving adjuvant systemic therapy. *Clin Cancer Res* **11**, 3315-9 (2005).
93. Goldstein, L.J. et al. Prognostic utility of the 21-gene assay in hormone receptor-positive operable breast cancer compared with classical clinicopathologic features. *J Clin Oncol* **26**, 4063-71 (2008).
94. Sparano, J.A. & Paik, S. Development of the 21-gene assay and its application in clinical practice and clinical trials. *J Clin Oncol* **26**, 721-8 (2008).
95. Blows, F.M. et al. Subtyping of Breast Cancer by Immunohistochemistry to Investigate a Relationship between Subtype and Short and Long Term Survival: A Collaborative Analysis of Data for 10,159 Cases from 12 Studies. *PLoS Med* **7**, e1000279 (2010).
96. Vassilev, L.T. et al. In vivo activation of the p53 pathway by small-molecule antagonists of MDM2. *Science* **303**, 844-8 (2004).
97. Tovar, C. et al. Small-molecule MDM2 antagonists reveal aberrant p53 signaling in cancer: implications for therapy. *Proc Natl Acad Sci U S A* **103**, 1888-93 (2006).
98. Arkin, M.R. & Wells, J.A. Small-molecule inhibitors of protein-protein interactions: progressing towards the dream. *Nat Rev Drug Discov* **3**, 301-17 (2004).
99. Chuang, H.Y., Lee, E., Liu, Y.T., Lee, D. & Ideker, T. Network-based classification of breast cancer metastasis. *Mol Syst Biol* **3**, 140 (2007).
100. Taylor, I.W. et al. Dynamic modularity in protein interaction networks predicts breast cancer outcome. *Nat Biotechnol* **27**, 199-204 (2009).
101. Chen, J. et al. Protein interaction network underpins concordant prognosis among heterogeneous breast cancer signatures. *J Biomed Inform* **43**, 385-96 (2010).
102. Hollingsworth, M.A. & Swanson, B.J. Mucins in cancer: Protection and control of the cell surface. *Nature Reviews Cancer* **4**, 45-60 (2004).
103. Hicke, L. Protein regulation by monoubiquitin. *Nature Reviews Molecular Cell Biology* **2**, 195-201 (2001).
104. Srinivas, P.R., Verma, M., Zhao, Y. & Srivastava, S. Proteomics for cancer biomarker discovery. *Clin Chem* **48**, 1160-9. (2002).
105. McClelland, C.M. & Gullick, W.J. Proteomic identification of secreted proteins as surrogate markers for signal transduction inhibitor activity. *Br J Cancer* **96**, 284-9 (2007).
106. Gavin, A.C. et al. Functional organization of the yeast proteome by systematic analysis of protein complexes. *Nature* **415**, 141-7 (2002).
107. Phizicky, E., Bastiaens, P.I., Zhu, H., Snyder, M. & Fields, S. Protein analysis on a proteomic scale. *Nature* **422**, 208-15 (2003).

108. Abd El-Rehim, D.M. et al. High-throughput protein expression analysis using tissue microarray technology of a large well-characterised series identifies biologically distinct classes of breast cancer confirming recent cDNA expression analyses. *International Journal of Cancer* **116**, 340-350 (2005).
109. Lakowicz, J.R. *Principles of Fluorescence Spectroscopy*, (Kluwer Academic/Plenum, New York, 2006).
110. Legg, J.W., Lewis, C.A., Parsons, M., Ng, T. & Isacke, C.M. A novel PKC-regulated mechanism controls CD44-ezrin association and directional cell motility. *Nature Cell Biology* **4**, 399-407 (2002).
111. Ng, T. et al. Ezrin is a downstream effector of trafficking PKC-integrin complexes involved in the control of cell motility. *Embo Journal* **20**, 2723-2741 (2001).
112. Ng, T. et al. Imaging protein kinase C alpha activation in cells. *Science* **283**, 2085-2089 (1999).
113. Ganesan, S., Ameer-beg, S.M., Ng, T.T.C., Vojnovic, B. & Wouters, F.S. A dark yellow fluorescent protein (YFP)-based Resonance Energy-Accepting Chromoprotein (REACH) for Forster resonance energy transfer with GFP. *Proceedings of the National Academy of Sciences of the United States of America* **103**, 4089-4094 (2006).
114. Peter, M. et al. Multiphoton-FLIM quantification of the EGFP-mRFP1 FRET pair for localization of membrane receptor-kinase interactions. *Biophysical Journal* **88**, 1224-1237 (2005).
115. Morris, J.R. et al. The SUMO modification pathway is involved in the BRCA1 response to genotoxic stress. *Nature* **462**, 886-90 (2009).
116. Peter, M. et al. Multiphoton-FLIM quantification of the EGFP-mRFP1 FRET pair for localization of membrane receptor-kinase interactions. *Biophys J* **88**, 1224-37 (2005).
117. Festy, F., Ameer-Beg, S.M., Ng, T. & Suhling, K. Imaging proteins in vivo using fluorescence lifetime microscopy. *Mol Biosyst* **3**, 381-91 (2007).
118. Peter, M. & Ameer-Beg, S.M. Imaging molecular interactions by multiphoton FLIM. *Biol Cell* **96**, 231-6 (2004).
119. Bastiaens, P.I. & Squire, A. Fluorescence lifetime imaging microscopy: spatial resolution of biochemical processes in the cell. *Trends Cell Biol* **9**, 48-52 (1999).
120. Wouters, F.S., Verveer, P.J. & Bastiaens, P.I. Imaging biochemistry inside cells. *Trends Cell Biol* **11**, 203-11 (2001).
121. Kong, A. et al. Prognostic value of an activation state marker for epidermal growth factor receptor in tissue microarrays of head and neck cancer. *Cancer Res* **66**, 2834-43 (2006).
122. Keese, M. et al. Imaging epidermal growth factor receptor phosphorylation in human colorectal cancer cells and human tissues. *J Biol Chem* **280**, 27826-31 (2005).
123. Itoh, R.E. et al. A FRET-based probe for epidermal growth factor receptor bound non-covalently to a pair of synthetic amphipathic helices. *Experimental Cell Research* **307**, 142-152 (2005).
124. Kong, A. et al. Activation of alternative HER receptors mediates resistance to EGFR tyrosine kinase inhibitors in breast cancer cells. *Ejc Supplements* **6**, 9-9 (2008).
125. Schreiber, A.B., Libermann, T.A., Lax, I., Yarden, Y. & Schlessinger, J. Biological Role of Epidermal Growth Factor-Receptor Clustering - Investigation with Monoclonal Anti-Receptor Antibodies. *Journal of Biological Chemistry* **258**, 846-853 (1983).
126. Schlessinger, J. Ligand-induced, receptor-mediated dimerization and activation of EGF receptor. *Cell* **110**, 669-672 (2002).
127. Jura, N. et al. Mechanism for Activation of the EGF Receptor Catalytic Domain by the Juxtamembrane Segment (vol 137, pg 1293, 2009). *Cell* **138**, 604-604 (2009).
128. Bublil, E.M. & Yarden, Y. The EGF receptor family: spearheading a merger of signaling and therapeutics. *Current Opinion in Cell Biology* **19**, 124-134 (2007).
129. Alvarado, D., Klein, D.E. & Lemmon, M.A. ErbB2 resembles an autoinhibited invertebrate epidermal growth factor receptor. *Nature* **461**, 287-U172 (2009).
130. Garrett, T.P.J. et al. Crystal structure of a truncated epidermal growth factor receptor extracellular domain bound to transforming growth factor alpha. *Cell* **110**, 763-773 (2002).
131. Ogiso, H. et al. Crystal structure of the complex of human epidermal growth factor and receptor extracellular domains. *Cell* **110**, 775-787 (2002).
132. Ferguson, K.M. et al. EGF activates its receptor by removing interactions that autoinhibit ectodomain dimerization. *Molecular Cell* **11**, 507-517 (2003).
133. Schlessinger, J. Cell signaling by receptor tyrosine kinases. *Cell* **103**, 211-225 (2000).
134. Baselga, J. & Swain, S.M. Novel anticancer targets: revisiting ERBB2 and discovering ERBB3. *Nature Reviews Cancer* **9**, 463-475 (2009).
135. Jorissen, R.N. et al. Epidermal growth factor receptor: mechanisms of activation and signalling. *Experimental Cell Research* **284**, 31-53 (2003).
136. Olayioye, M.A., Neve, R.M., Lane, H.A. & Hynes, N.E. The ErbB signaling network: receptor heterodimerization in development and cancer. *Embo Journal* **19**, 3159-3167 (2000).

137. Citri, A. & Yarden, Y. EGF-ERBB signalling: towards the systems level. *Nature Reviews Molecular Cell Biology* **7**, 505-516 (2006).
138. Haj, F.G., Verveer, P.J., Squire, A., Neel, B.G. & Bastiaens, P.I.H. Imaging sites of receptor dephosphorylation by PTP1B on the surface of the endoplasmic reticulum. *Science* **295**, 1708-1711 (2002).
139. Vermeij, J. et al. Genomic activation of the EGFR and HER2-neu genes in a significant proportion of invasive epithelial ovarian cancers. *Bmc Cancer* **8**, - (2008).
140. Jaehne, J. et al. Expression of Her2/Neu Oncogene Product P185 in Correlation to Clinicopathological and Prognostic Factors of Gastric-Carcinoma. *Journal of Cancer Research and Clinical Oncology* **118**, 474-479 (1992).
141. Cornolti, G. et al. Amplification and overexpression of HER2/neu gene and HER2/neu protein in salivary duct carcinoma of the parotid gland. *Archives of Otolaryngology-Head & Neck Surgery* **133**, 1031-1036 (2007).
142. Wang, S.Z.E. et al. HER2 kinase domain mutation results in constitutive phosphorylation and activation of HER2 and EGFR and resistance to EGFR tyrosine kinase inhibitors. *Cancer Cell* **10**, 25-38 (2006).
143. Hynes, N.E. & Lane, H.A. ERBB receptors and cancer: The complexity of targeted inhibitors (vol 5, pg 341, 2005). *Nature Reviews Cancer* **5**, - (2005).
144. Bose, R. & Zhang, X.W. The ErbB kinase domain: Structural perspectives into kinase activation and inhibition. *Experimental Cell Research* **315**, 649-658 (2009).
145. Shigematsu, H. & Gazdar, A.F. Somatic mutations of epidermal growth factor receptor signaling pathway in lung cancers. *International Journal of Cancer* **118**, 257-262 (2006).
146. Bose, R. et al. Phosphoproteomic analysis of Her2/neu signaling and inhibition. *Proceedings of the National Academy of Sciences of the United States of America* **103**, 9773-9778 (2006).
147. Mukherji, M., Brill, L.M., Ficarro, S.B., Hampton, G.M. & Schultz, P.G. A phosphoproteomic analysis of the ErbB2 receptor tyrosine kinase signaling pathways. *Biochemistry* **45**, 15529-15540 (2006).
148. Wolf-Yadlin, A. et al. Effects of HER2 overexpression on cell signaling networks governing proliferation and migration. *Molecular Systems Biology*, - (2006).
149. Zhang, X.W., Gureasko, J., Shen, K., Cole, P.A. & Kuriyan, J. An allosteric mechanism for activation of the kinase domain of epidermal growth factor receptor. *Cell* **125**, 1137-1149 (2006).
150. Sorkin, A. & Goh, L.K. Endocytosis and intracellular trafficking of ErbBs. *Experimental Cell Research* **315**, 683-696 (2009).
151. Beguinot, L., Lyall, R.M., Willingham, M.C. & Pastan, I. Down-Regulation of the Epidermal Growth-Factor Receptor in Kb Cells Is Due to Receptor Internalization and Subsequent Degradation in Lysosomes. *Proceedings of the National Academy of Sciences of the United States of America-Biological Sciences* **81**, 2384-2388 (1984).
152. Stoscheck, C.M. & Carpenter, G. Down Regulation of Epidermal Growth-Factor Receptors - Direct Demonstration of Receptor Degradation in Human-Fibroblasts. *Journal of Cell Biology* **98**, 1048-1053 (1984).
153. Stoscheck, C.M. & Carpenter, G. Characteristics of Antibodies to the Epidermal Growth-Factor Receptor Kinase. *Archives of Biochemistry and Biophysics* **227**, 457-468 (1983).
154. Wiley, H.S. et al. The Role of Tyrosine Kinase-Activity in Endocytosis, Compartmentation, and down-Regulation of the Epidermal Growth-Factor Receptor. *Journal of Biological Chemistry* **266**, 11083-11094 (1991).
155. Resat, H., Ewald, J.A., Dixon, D.A. & Wiley, H.S. An integrated model of epidermal growth factor receptor trafficking and signal transduction. *Biophysical Journal* **85**, 730-743 (2003).
156. Austin, C.D. et al. Endocytosis and sorting of ErbB2 and the site of action of cancer therapeutics trastuzumab and geldanamycin. *Molecular Biology of the Cell* **15**, 5268-5282 (2004).
157. Mosesson, Y., Mills, G.B. & Yarden, Y. Derailed endocytosis: an emerging feature of cancer. *Nature Reviews Cancer* **8**, 835-850 (2008).
158. Huang, F.T., Khvorova, A., Marshall, W. & Sorkin, A. Analysis of clathrin-mediated endocytosis of epidermal growth factor receptor by RNA interference. *Journal of Biological Chemistry* **279**, 16657-16661 (2004).
159. Motley, A., Bright, N.A., Seaman, M.N.J. & Robinson, M.S. Clathrin-mediated endocytosis in AP-2-depleted cells. *Journal of Cell Biology* **162**, 909-918 (2003).
160. Goldstein, J.L., Anderson, R.G.W. & Brown, M.S. Coated Pits, Coated Vesicles, and Receptor-Mediated Endocytosis. *Nature* **279**, 679-685 (1979).
161. Lenferink, A.E.G. et al. Differential endocytic routing of homo- and hetero-dimeric ErbB tyrosine kinases confers signaling superiority to receptor heterodimers. *Embo Journal* **17**, 3385-3397 (1998).
162. Pickart, C.M. Ubiquitin enters the new millennium. *Molecular Cell* **8**, 499-504 (2001).

163. Hoeller, D. & Dikic, I. Targeting the ubiquitin system in cancer therapy. *Nature* **458**, 438-444 (2009).
164. Wong, B.R. et al. Drug discovery in the ubiquitin regulatory pathway. *Drug Discovery Today* **8**, 746-754 (2003).
165. Levkowitz, G. et al. c-Cbl/Sli-1 regulates endocytic sorting and ubiquitination of the epidermal growth factor receptor. *Genes & Development* **12**, 3663-3674 (1998).
166. Xu, W.P. et al. Chaperone-dependent E3 ubiquitin ligase CHIP mediates a degradative pathway for c-ErbB2 Neu. *Proceedings of the National Academy of Sciences of the United States of America* **99**, 12847-12852 (2002).
167. Cao, Z.W., Wu, X.L., Yen, L., Sweeney, C. & Carraway, K.L. Neuregulin-induced ErbB3 downregulation is mediated by a protein stability cascade involving the E3 ubiquitin ligase Nrdp1. *Molecular and Cellular Biology* **27**, 2180-2188 (2007).
168. Omerovic, J. et al. The E3 ligase Aip4/Itch ubiquitinates and targets ErbB-4 for degradation. *Faseb Journal* **21**, 2849-2862 (2007).
169. Worthylake, R. & Wiley, H.S. Structural aspects of the epidermal growth factor receptor required for transmodulation of erbB-2/neu. *Journal of Biological Chemistry* **272**, 8594-8601 (1997).
170. Li, X. et al. Degradation of HER2 by cbl-based chimeric ubiquitin Ligases. *Cancer Research* **67**, 8716-8724 (2007).
171. Klapper, L.N., Waterman, H., Sela, M. & Yarden, Y. Tumor-inhibitory antibodies to HER-2/ErbB-2 may act by recruiting c-Cbl and enhancing ubiquitination of HER-2. *Cancer Research* **60**, 3384-3388 (2000).
172. Muthuswamy, S.K., Gilman, M. & Brugge, J.S. Controlled dimerization of ErbB receptors provides evidence for differential signaling by homo- and heterodimers. *Molecular and Cellular Biology* **19**, 6845-6857 (1999).
173. Magnifico, A. et al. Protein kinase c alpha determines HER2 fate in breast carcinoma cells with HER2 protein overexpression without gene amplification. *Cancer Research* **67**, 5308-5317 (2007).
174. Bao, J. et al. Threonine phosphorylation diverts internalized epidermal growth factor receptors from a degradative pathway to the recycling endosome. *Journal of Biological Chemistry* **275**, 26178-26186 (2000).
175. Holbro, T. et al. The ErbB2/ErbB3 heterodimer functions as an oncogenic unit: ErbB2 requires ErbB3 to drive breast tumor cell proliferation. *Proceedings of the National Academy of Sciences of the United States of America* **100**, 8933-8938 (2003).
176. Tzahar, E. et al. A hierarchical network of interreceptor interactions determines signal transduction by neu differentiation factor/neuregulin and epidermal growth factor. *Molecular and Cellular Biology* **16**, 5276-5287 (1996).
177. Hellyer, N.J., Cheng, K. & Koland, J.G. ErbB3 (HER3) interaction with the p85 regulatory subunit of phosphoinositide 3-kinase. *Biochemical Journal* **333**, 757-763 (1998).
178. Wehrman, T.S. et al. System for quantifying dynamic protein interactions defines a role for Herceptin in modulating ErbB2 interactions. *Proceedings of the National Academy of Sciences of the United States of America* **103**, 19063-19068 (2006).
179. Musolino, A. et al. Immunoglobulin G fragment C receptor polymorphisms and clinical efficacy of trastuzumab-based therapy in patients with HER-2/neu-positive metastatic breast cancer. *Journal of Clinical Oncology* **26**, 1789-1796 (2008).
180. Molina, M.A. et al. Trastuzumab (Herceptin), a humanized anti-HER2 receptor monoclonal antibody, inhibits basal and activated HER2 ectodomain cleavage in breast cancer cells. *Cancer Research* **61**, 4744-4749 (2001).
181. Scaltriti, M. et al. Expression of p95HER2, a truncated form of the HER2 receptor, and response to anti-HER2 therapies in breast cancer. *Journal of the National Cancer Institute* **99**, 628-638 (2007).
182. Nagata, Y. et al. PTEN activation contributes to tumor inhibition by trastuzumab, and loss of PTEN predicts trastuzumab resistance in patients. *Cancer Cell* **6**, 117-127 (2004).
183. Lu, Y.H., Zi, X.L., Zhao, Y.H., Mascarenhas, D. & Pollak, M. Insulin-like growth factor-I receptor signaling and resistance to trastuzumab (Herceptin). *Journal of the National Cancer Institute* **93**, 1852-1857 (2001).
184. Lee-Hoeflich, S.T. et al. A central role for HER3 in HER2-amplified breast cancer: implications for targeted therapy. *Cancer Research* **68**, 5878-5887 (2008).
185. Portera, C.C. et al. Cardiac toxicity and efficacy of trastuzumab combined with pertuzumab in patients with human epidermal growth factor receptor 2-positive metastatic breast cancer (vol 14, pg 2710, 2008). *Clinical Cancer Research* **14**, 3641-3641 (2008).
186. Blackburn, E. et al. A monoclonal antibody to the human HER3 receptor inhibits Neuregulin 1-beta binding and co-operates with Herceptin in inhibiting the growth of breast cancer derived cell lines. *Breast Cancer Res Treat* **134**, 53-9 (2012).

187. Schoeberl, B. et al. An ErbB3 antibody, MM-121, is active in cancers with ligand-dependent activation. *Cancer Res* **70**, 2485-94 (2010).
188. van der Horst, E.H., Murgia, M., Treder, M. & Ullrich, A. Anti-HER-3 MAbs inhibit HER-3-mediated signaling in breast cancer cell lines resistant to anti-HER-2 antibodies. *Int J Cancer* **115**, 519-27 (2005).
189. Wood, E.R. et al. A unique structure for epidermal growth factor receptor bound to GW572016 (Lapatinib): Relationships among protein conformation, inhibitor off-rate, and receptor activity in tumor cells. *Cancer Research* **64**, 6652-6659 (2004).
190. Stamos, J., Sliwkowski, M.X. & Eigenbrot, C. Structure of the epidermal growth factor receptor kinase domain alone and in complex with a 4-anilinoquinazoline inhibitor. *Journal of Biological Chemistry* **277**, 46265-46272 (2002).
191. Yun, C.H. et al. Structures of lung cancer-derived EGFR mutants and inhibitor complexes: Mechanism of activation and insights into differential inhibitor sensitivity. *Cancer Cell* **11**, 217-227 (2007).
192. Sergina, N.V. et al. Escape from HER-family tyrosine kinase inhibitor therapy by the kinase-inactive HER3. *Nature* **445**, 437-441 (2007).
193. Hickinson, D.M. et al. AZD8931, an equipotent, reversible inhibitor of signaling by epidermal growth factor receptor, ERBB2 (HER2), and ERBB3: a unique agent for simultaneous ERBB receptor blockade in cancer. *Clin Cancer Res* **16**, 1159-69 (2010).
194. Papatheodorou, I. et al. A metadata approach for clinical data management in translational genomics studies in breast cancer. *BMC Med Genomics* **2**, 66 (2009).
195. Jura, N. et al. Mechanism for activation of the EGF receptor catalytic domain by the juxtamembrane segment. *Cell* **137**, 1293-307 (2009).
196. Wood, E.R. et al. A unique structure for epidermal growth factor receptor bound to GW572016 (Lapatinib): relationships among protein conformation, inhibitor off-rate, and receptor activity in tumor cells. *Cancer Res* **64**, 6652-9 (2004).
197. Jura, N., Shan, Y., Cao, X., Shaw, D.E. & Kuriyan, J. Structural analysis of the catalytically inactive kinase domain of the human EGF receptor 3. *Proc Natl Acad Sci U S A* **106**, 21608-13 (2009).
198. Simossis, V.A., Kleinjung, J. & Heringa, J. Homology-extended sequence alignment. *Nucleic Acids Res* **33**, 816-24 (2005).
199. Sali, A. & Blundell, T.L. Comparative protein modelling by satisfaction of spatial restraints. *J Mol Biol* **234**, 779-815 (1993).
200. Barber, P., S. M. Ameer-Beg, J. Gilbey, R. J. Edens, I. Ezike, and B. Vojnovic. Global and pixel kinetic data analysis for FRET detection by multi-photon time-domain FLIM. *Proc. SPIE* 171-181 (2005).
201. Terry Therneau, o.S.-R.p.b.T.L. survival: Survival analysis, including penalised likelihood. 2.36-14 edn (2012).
202. Team, R.D.C. R: A language and environment for statistical computing. *R Foundation for Statistical Computing* (2011).
203. Burgess, A.W. et al. An open-and-shut case? Recent insights into the activation of EGF/ErbB receptors. *Mol Cell* **12**, 541-52 (2003).
204. Bouyain, S., Longo, P.A., Li, S., Ferguson, K.M. & Leahy, D.J. The extracellular region of ErbB4 adopts a tethered conformation in the absence of ligand. *Proc Natl Acad Sci U S A* **102**, 15024-9 (2005).
205. Lemmon, M.A. Ligand-induced ErbB receptor dimerization. *Exp Cell Res* **315**, 638-48 (2009).
206. Aertgeerts, K. et al. Structural analysis of the mechanism of inhibition and allosteric activation of the kinase domain of HER2 protein. *J Biol Chem* **286**, 18756-65 (2011).
207. Yarden, Y. & Schlessinger, J. Self-phosphorylation of epidermal growth factor receptor: evidence for a model of intermolecular allosteric activation. *Biochemistry* **26**, 1434-42 (1987).
208. Ferguson, K.M. et al. EGF activates its receptor by removing interactions that autoinhibit ectodomain dimerization. *Mol Cell* **11**, 507-17 (2003).
209. Garrett, T.P. et al. The crystal structure of a truncated ErbB2 ectodomain reveals an active conformation, poised to interact with other ErbB receptors. *Mol Cell* **11**, 495-505 (2003).
210. Mendrola, J.M., Berger, M.B., King, M.C. & Lemmon, M.A. The single transmembrane domains of ErbB receptors self-associate in cell membranes. *J Biol Chem* **277**, 4704-12 (2002).
211. Shan, Y. et al. Oncogenic Mutations Counteract Intrinsic Disorder in the EGFR Kinase and Promote Receptor Dimerization. *Cell* **149**, 860-70 (2012).
212. Red Brewer, M. et al. The juxtamembrane region of the EGF receptor functions as an activation domain. *Mol Cell* **34**, 641-51 (2009).
213. Yarden, Y. Biology of HER2 and Its Importance in Breast Cancer. *Oncology* **61**, 1-13 (2001).

214. Brewer, M.R. et al. The Juxtamembrane Region of the EGF Receptor Functions as an Activation Domain. *Molecular Cell* **34**, 641-651 (2009).
215. Wang, Z. et al. Mechanistic insights into the activation of oncogenic forms of EGF receptor. *Nat Struct Mol Biol* **18**, 1388-93 (2011).
216. Low-Nam, S.T. et al. ErbB1 dimerization is promoted by domain co-confinement and stabilized by ligand binding. *Nat Struct Mol Biol* **18**, 1244-9 (2011).
217. Fleishman, S.J., Schlessinger, J. & Ben-Tal, N. A putative molecular-activation switch in the transmembrane domain of erbB2. *Proc Natl Acad Sci U S A* **99**, 15937-40 (2002).
218. Bargmann, C.I., Hung, M.C. & Weinberg, R.A. Multiple independent activations of the neu oncogene by a point mutation altering the transmembrane domain of p185. *Cell* **45**, 649-57 (1986).
219. Sternberg, M.J. & Gullick, W.J. A sequence motif in the transmembrane region of growth factor receptors with tyrosine kinase activity mediates dimerization. *Protein Eng* **3**, 245-8 (1990).
220. Xie, D. et al. Population-based, case-control study of HER2 genetic polymorphism and breast cancer risk. *J Natl Cancer Inst* **92**, 412-7 (2000).
221. Smirnova, T. et al. Phosphoinositide 3-kinase signaling is critical for ErbB3-driven breast cancer cell motility and metastasis. *Oncogene* (2011).
222. Bessman, N.J. & Lemmon, M.A. Finding the missing links in EGFR. *Nat Struct Mol Biol* **19**, 1-3 (2012).
223. Shi, F., Telesco, S.E., Liu, Y., Radhakrishnan, R. & Lemmon, M.A. ErbB3/HER3 intracellular domain is competent to bind ATP and catalyze autophosphorylation. *Proc Natl Acad Sci U S A* **107**, 7692-7 (2010).
224. Nazarian, R. et al. Melanomas acquire resistance to B-RAF(V600E) inhibition by RTK or N-RAS upregulation. *Nature* **468**, 973-7 (2010).
225. Poulikakos, P.I., Zhang, C., Bollag, G., Shokat, K.M. & Rosen, N. RAF inhibitors transactivate RAF dimers and ERK signalling in cells with wild-type BRAF. *Nature* **464**, 427-30 (2010).
226. Cameron, A.J., Escribano, C., Saurin, A.T., Kosteletzky, B. & Parker, P.J. PKC maturation is promoted by nucleotide pocket occupation independently of intrinsic kinase activity. *Nat Struct Mol Biol* **16**, 624-30 (2009).
227. Zeqiraj, E. et al. ATP and MO25alpha regulate the conformational state of the STRADalpha pseudokinase and activation of the LKB1 tumour suppressor. *PLoS Biol* **7**, e1000126 (2009).
228. Cameron, A.J. Occupational hazards: allosteric regulation of protein kinases through the nucleotide-binding pocket. *Biochem Soc Trans* **39**, 472-6 (2011).
229. Fan, Y.X. et al. Mutational activation of ErbB2 reveals a new protein kinase autoinhibition mechanism. *J Biol Chem* **283**, 1588-96 (2008).
230. Wakeling, A.E. et al. ZD1839 (Iressa): an orally active inhibitor of epidermal growth factor signaling with potential for cancer therapy. *Cancer Res* **62**, 5749-54 (2002).
231. Liu, Y. & Gray, N.S. Rational design of inhibitors that bind to inactive kinase conformations. *Nat Chem Biol* **2**, 358-64 (2006).
232. Yun, C.H. et al. Structures of lung cancer-derived EGFR mutants and inhibitor complexes: mechanism of activation and insights into differential inhibitor sensitivity. *Cancer Cell* **11**, 217-27 (2007).
233. Eck, M.J. & Yun, C.H. Structural and mechanistic underpinnings of the differential drug sensitivity of EGFR mutations in non-small cell lung cancer. *Biochim Biophys Acta* **1804**, 559-66 (2010).
234. Bublil, E.M. et al. Kinase-mediated quasi-dimers of EGFR. *FASEB J* **24**, 4744-55 (2010).
235. Jackman, D.M. et al. Exon 19 deletion mutations of epidermal growth factor receptor are associated with prolonged survival in non-small cell lung cancer patients treated with gefitinib or erlotinib. *Clin Cancer Res* **12**, 3908-14 (2006).
236. Riely, G.J. et al. Clinical course of patients with non-small cell lung cancer and epidermal growth factor receptor exon 19 and exon 21 mutations treated with gefitinib or erlotinib. *Clin Cancer Res* **12**, 839-44 (2006).
237. Shah, S.P. et al. Mutational evolution in a lobular breast tumour profiled at single nucleotide resolution. *Nature* **461**, 809-13 (2009).
238. Wang, S.E. et al. HER2 kinase domain mutation results in constitutive phosphorylation and activation of HER2 and EGFR and resistance to EGFR tyrosine kinase inhibitors. *Cancer Cell* **10**, 25-38 (2006).
239. Shigematsu, H. et al. Somatic mutations of the HER2 kinase domain in lung adenocarcinomas. *Cancer Res* **65**, 1642-6 (2005).
240. Lee, J.W. et al. Somatic mutations of ERBB2 kinase domain in gastric, colorectal, and breast carcinomas. *Clin Cancer Res* **12**, 57-61 (2006).
241. Stephens, P. et al. Lung cancer: intragenic ERBB2 kinase mutations in tumours. *Nature* **431**, 525-6 (2004).

242. Gazdar, A.F., Shigematsu, H., Herz, J. & Minna, J.D. Mutations and addiction to EGFR: the Achilles 'heal' of lung cancers? *Trends Mol Med* **10**, 481-6 (2004).
243. Scaltriti, M. et al. Clinical benefit of lapatinib-based therapy in patients with human epidermal growth factor receptor 2-positive breast tumors coexpressing the truncated p95HER2 receptor. *Clin Cancer Res* **16**, 2688-95 (2010).
244. Scaltriti, M. et al. Lapatinib, a HER2 tyrosine kinase inhibitor, induces stabilization and accumulation of HER2 and potentiates trastuzumab-dependent cell cytotoxicity. *Oncogene* **28**, 803-14 (2009).
245. Agus, D.B. et al. Targeting ligand-activated ErbB2 signaling inhibits breast and prostate tumor growth. *Cancer Cell* **2**, 127-37 (2002).
246. Kim, H.H., Vijapurkar, U., Hellyer, N.J., Bravo, D. & Koland, J.G. Signal transduction by epidermal growth factor and heregulin via the kinase-deficient ErbB3 protein. *Biochem J* **334** (Pt 1), 189-95 (1998).
247. Perera, S.A. et al. HER2YVMA drives rapid development of adenosquamous lung tumors in mice that are sensitive to BIBW2992 and rapamycin combination therapy. *Proc Natl Acad Sci U S A* **106**, 474-9 (2009).
248. Kleinjung, J. & Fraternali, F. POPSCOMP: an automated interaction analysis of biomolecular complexes. *Nucleic Acids Res* **33**, W342-6 (2005).
249. Hoffmann, C. et al. A FIAsh-based FRET approach to determine G protein-coupled receptor activation in living cells. *Nat Methods* **2**, 171-6 (2005).
250. Sanchez-Martin, M. & Pandiella, A. Differential action of small molecule HER kinase inhibitors on receptor heterodimerization: therapeutic implications. *Int J Cancer* **131**, 244-52 (2012).
251. Mi, L.Z. et al. Simultaneous visualization of the extracellular and cytoplasmic domains of the epidermal growth factor receptor. *Nat Struct Mol Biol* **18**, 984-9 (2011).
252. Macdonald-Obermann, J.L. & Pike, L.J. The Intracellular Juxtamembrane Domain of the Epidermal Growth Factor (EGF) Receptor Is Responsible for the Allosteric Regulation of EGF Binding. *Journal of Biological Chemistry* **284**, 13570-13576 (2009).
253. Okuzumi, T. et al. Inhibitor hijacking of Akt activation. *Nat Chem Biol* **5**, 484-93 (2009).
254. Rusnak, D.W. et al. The effects of the novel, reversible epidermal growth factor receptor/ErbB-2 tyrosine kinase inhibitor, GW2016, on the growth of human normal and tumor-derived cell lines in vitro and in vivo. *Mol Cancer Ther* **1**, 85-94 (2001).
255. Li, J. et al. Lapatinib, a preventive/therapeutic agent against mammary cancer, suppresses RTK-mediated signaling through multiple signaling pathways. *Cancer Prev Res (Phila)* **4**, 1190-7 (2011).
256. Spector, N.L. et al. Study of the biologic effects of lapatinib, a reversible inhibitor of ErbB1 and ErbB2 tyrosine kinases, on tumor growth and survival pathways in patients with advanced malignancies. *J Clin Oncol* **23**, 2502-12 (2005).
257. Kostyal, D. et al. Trastuzumab and lapatinib modulation of HER2 tyrosine/threonine phosphorylation and cell signaling. *Med Oncol* (2011).
258. Xia, W. et al. Anti-tumor activity of GW572016: a dual tyrosine kinase inhibitor blocks EGF activation of EGFR/erbB2 and downstream Erk1/2 and AKT pathways. *Oncogene* **21**, 6255-63 (2002).
259. Dolloff, N.G. et al. Off-target lapatinib activity sensitizes colon cancer cells through TRAIL death receptor up-regulation. *Sci Transl Med* **3**, 86ra50 (2011).
260. Tanizaki, J. et al. Roles of BIM induction and survivin downregulation in lapatinib-induced apoptosis in breast cancer cells with HER2 amplification. *Oncogene* **30**, 4097-106 (2011).
261. Cook, R.S. et al. ErbB3 ablation impairs PI3K/Akt-dependent mammary tumorigenesis. *Cancer Res* **71**, 3941-51 (2011).
262. Amin, D.N. et al. Resiliency and vulnerability in the HER2-HER3 tumorigenic driver. *Sci Transl Med* **2**, 16ra7 (2010).
263. Garrett, J.T. et al. Transcriptional and posttranslational up-regulation of HER3 (ErbB3) compensates for inhibition of the HER2 tyrosine kinase. *Proc Natl Acad Sci U S A* **108**, 5021-6 (2011).
264. Hudziak, R.M. et al. p185HER2 monoclonal antibody has antiproliferative effects in vitro and sensitizes human breast tumor cells to tumor necrosis factor. *Mol Cell Biol* **9**, 1165-72 (1989).
265. Sorkin, A., Di Fiore, P.P. & Carpenter, G. The carboxyl terminus of epidermal growth factor receptor/erbB-2 chimerae is internalization impaired. *Oncogene* **8**, 3021-8 (1993).
266. Waterman, H., Sabanai, I., Geiger, B. & Yarden, Y. Alternative intracellular routing of ErbB receptors may determine signaling potency. *J Biol Chem* **273**, 13819-27 (1998).
267. Baulida, J., Kraus, M.H., Alimandi, M., Di Fiore, P.P. & Carpenter, G. All ErbB receptors other than the epidermal growth factor receptor are endocytosis impaired. *J Biol Chem* **271**, 5251-7 (1996).
268. Sak, M.M. et al. The oncoprotein ErbB3 is endocytosed in the absence of added ligand in a clathrin-dependent manner. *Carcinogenesis* **33**, 1031-9 (2012).

269. Baulida, J. & Carpenter, G. Heregulin degradation in the absence of rapid receptor-mediated internalization. *Exp Cell Res* **232**, 167-72 (1997).
270. Waterman, H., Alroy, I., Strano, S., Seger, R. & Yarden, Y. The C-terminus of the kinase-defective neuregulin receptor ErbB-3 confers mitogenic superiority and dictates endocytic routing. *EMBO J* **18**, 3348-58 (1999).
271. Wang, Z.X., Zhang, L.F., Yeung, T.K. & Chen, X.M. Endocytosis deficiency of epidermal growth factor (EGF) receptor-ErbB2 heterodimers in response to EGF stimulation. *Molecular Biology of the Cell* **10**, 1621-1636 (1999).
272. Longva, K.E., Pedersen, N.M., Haslekas, C., Stang, E. & Madhus, I.H. Herceptin-induced inhibition of ErbB2 signaling involves reduced phosphorylation of Akt but not endocytic down-regulation of ErbB2. *International Journal of Cancer* **116**, 359-367 (2005).
273. Harari, D. & Yarden, Y. Molecular mechanisms underlying ErbB2/HER2 action in breast cancer. *Oncogene* **19**, 6102-14 (2000).
274. Hommelgaard, A.M., Lerdrup, M. & van Deurs, B. Association with membrane protrusions makes ErbB2 an internalization-resistant receptor. *Mol Biol Cell* **15**, 1557-67 (2004).
275. Marmor, M.D. & Yarden, Y. Role of protein ubiquitylation in regulating endocytosis of receptor tyrosine kinases. *Oncogene* **23**, 2057-70 (2004).
276. Maxfield, F.R. & McGraw, T.E. Endocytic recycling. *Nat Rev Mol Cell Biol* **5**, 121-32 (2004).
277. Lawe, D.C. et al. Sequential roles for phosphatidylinositol 3-phosphate and Rab5 in tethering and fusion of early endosomes via their interaction with EEA1. *J Biol Chem* **277**, 8611-7 (2002).
278. McBride, H.M. et al. Oligomeric complexes link Rab5 effectors with NSF and drive membrane fusion via interactions between EEA1 and syntaxin 13. *Cell* **98**, 377-86 (1999).
279. Worthylake, R., Opresko, L.K. & Wiley, H.S. ErbB-2 amplification inhibits down-regulation and induces constitutive activation of both ErbB-2 and epidermal growth factor receptors. *J Biol Chem* **274**, 8865-74 (1999).
280. Basu, S.K., Goldstein, J.L., Anderson, R.G. & Brown, M.S. Monensin interrupts the recycling of low density lipoprotein receptors in human fibroblasts. *Cell* **24**, 493-502 (1981).
281. Lenferink, A.E. et al. Differential endocytic routing of homo- and hetero-dimeric ErbB tyrosine kinases confers signaling superiority to receptor heterodimers. *EMBO J* **17**, 3385-97 (1998).
282. Puri, C. et al. Relationships between EGFR signaling-competent and endocytosis-competent membrane microdomains. *Mol Biol Cell* **16**, 2704-18 (2005).
283. Wiley, H.S. Trafficking of the ErbB receptors and its influence on signaling. *Exp Cell Res* **284**, 78-88 (2003).
284. Carpentier, J.L., White, M.F., Orci, L. & Kahn, R.C. Direct visualization of the phosphorylated epidermal growth factor receptor during its internalization in A-431 cells. *J Cell Biol* **105**, 2751-62 (1987).
285. Vieira, A.V., Lamaze, C. & Schmid, S.L. Control of EGF receptor signaling by clathrin-mediated endocytosis. *Science* **274**, 2086-9 (1996).
286. Teis, D. et al. p14-MP1-MEK1 signaling regulates endosomal traffic and cellular proliferation during tissue homeostasis. *J Cell Biol* **175**, 861-8 (2006).
287. Jallal, B., Schlessinger, J. & Ullrich, A. Tyrosine phosphatase inhibition permits analysis of signal transduction complexes in p185HER2/neu-overexpressing human tumor cells. *J Biol Chem* **267**, 4357-63 (1992).
288. Brown, V.I. et al. Demonstration by two-color flow cytometry that tyrosine kinase activity is required for down-modulation of the oncogenic neu receptor. *DNA Cell Biol* **13**, 193-209 (1994).
289. Chung, B.M. et al. Aberrant trafficking of NSCLC-associated EGFR mutants through the endocytic recycling pathway promotes interaction with Src. *BMC Cell Biol* **10**, 84 (2009).
290. Austin, C.D. et al. Endocytosis and sorting of ErbB2 and the site of action of cancer therapeutics trastuzumab and geldanamycin. *Mol Biol Cell* **15**, 5268-82 (2004).
291. Grovdal, L.M. et al. EGF receptor inhibitors increase ErbB3 mRNA and protein levels in breast cancer cells. *Cell Signal* **24**, 296-301 (2012).
292. Marx, C., Held, J.M., Gibson, B.W. & Benz, C.C. ErbB2 Trafficking and Degradation Associated with K48 and K63 Polyubiquitination. *Cancer Research* **70**, 3709-3717 (2010).
293. Mimnaugh, E.G., Chavany, C. & Neckers, L. Polyubiquitination and proteasomal degradation of the p185c-erbB-2 receptor protein-tyrosine kinase induced by geldanamycin. *J Biol Chem* **271**, 22796-801 (1996).
294. Tikhomirov, O. & Carpenter, G. Geldanamycin induces ErbB-2 degradation by proteolytic fragmentation. *J Biol Chem* **275**, 26625-31 (2000).

295. Ehrlich, E.S. et al. Regulation of Hsp90 client proteins by a Cullin5-RING E3 ubiquitin ligase. *Proceedings of the National Academy of Sciences of the United States of America* **106**, 20330-20335 (2009).
296. Burris, H.A., 3rd et al. Phase I safety, pharmacokinetics, and clinical activity study of lapatinib (GW572016), a reversible dual inhibitor of epidermal growth factor receptor tyrosine kinases, in heavily pretreated patients with metastatic carcinomas. *J Clin Oncol* **23**, 5305-13 (2005).
297. Neve, R.M. et al. A collection of breast cancer cell lines for the study of functionally distinct cancer subtypes. *Cancer Cell* **10**, 515-27 (2006).
298. Wells, A. EGF receptor. *Int J Biochem Cell Biol* **31**, 637-43 (1999).
299. Yarden, Y. The EGFR family and its ligands in human cancer: signalling mechanisms and therapeutic opportunities. *Eur J Cancer* **37 Suppl 4**, S3-8 (2001).
300. Wu, Y., Shang, X., Sarkissyan, M., Slamon, D. & Vadgama, J.V. FOXO1A is a target for HER2-overexpressing breast tumors. *Cancer Res* **70**, 5475-85 (2010).
301. Nishi, T. & Forgac, M. The vacuolar (H⁺)-ATPases--nature's most versatile proton pumps. *Nat Rev Mol Cell Biol* **3**, 94-103 (2002).
302. Baravalle, G. et al. Transferrin recycling and dextran transport to lysosomes is differentially affected by bafilomycin, nocodazole, and low temperature. *Cell Tissue Res* **320**, 99-113 (2005).
303. van Weert, A.W., Dunn, K.W., Geuze, H.J., Maxfield, F.R. & Stoorvogel, W. Transport from late endosomes to lysosomes, but not sorting of integral membrane proteins in endosomes, depends on the vacuolar proton pump. *J Cell Biol* **130**, 821-34 (1995).
304. Ceresa, B.P. Regulation of EGFR endocytic trafficking by rab proteins. *Histol Histopathol* **21**, 987-93 (2006).
305. Wilson, T.R., Lee, D.Y., Berry, L., Shames, D.S. & Settleman, J. Neuregulin-1-mediated autocrine signaling underlies sensitivity to HER2 kinase inhibitors in a subset of human cancers. *Cancer Cell* **20**, 158-72 (2011).
306. Faure, R., Baquiran, G., Bergeron, J.J. & Posner, B.I. The dephosphorylation of insulin and epidermal growth factor receptors. Role of endosome-associated phosphotyrosine phosphatase(s). *J Biol Chem* **267**, 11215-21 (1992).
307. Reynolds, A.R., Tischer, C., Verveer, P.J., Rocks, O. & Bastiaens, P.I. EGFR activation coupled to inhibition of tyrosine phosphatases causes lateral signal propagation. *Nat Cell Biol* **5**, 447-53 (2003).
308. Mollenhauer, H.H., Morre, D.J. & Rowe, L.D. Alteration of intracellular traffic by monensin; mechanism, specificity and relationship to toxicity. *Biochim Biophys Acta* **1031**, 225-46 (1990).
309. Kong, A. et al. HER2 oncogenic function escapes EGFR tyrosine kinase inhibitors via activation of alternative HER receptors in breast cancer cells. *PLoS One* **3**, e2881 (2008).
310. Engelman, J.A. et al. MET amplification leads to gefitinib resistance in lung cancer by activating ERBB3 signaling. *Science* **316**, 1039-43 (2007).
311. Chen, C.T. et al. MET activation mediates resistance to lapatinib inhibition of HER2-amplified gastric cancer cells. *Mol Cancer Ther* **11**, 660-9 (2012).
312. Liu, L. et al. Novel mechanism of lapatinib resistance in HER2-positive breast tumor cells: activation of AXL. *Cancer Res* **69**, 6871-8 (2009).
313. Gallardo, A. et al. Increased signalling of EGFR and IGF1R, and deregulation of PTEN/PI3K/Akt pathway are related with trastuzumab resistance in HER2 breast carcinomas. *Br J Cancer* **106**, 1367-73 (2012).
314. Cai, Z. et al. Differential binding patterns of monoclonal antibody 2C4 to the ErbB3-p185her2/neu and the EGFR-p185her2/neu complexes. *Oncogene* **27**, 3870-4 (2008).
315. Junttila, T.T. et al. Ligand-independent HER2/HER3/PI3K complex is disrupted by trastuzumab and is effectively inhibited by the PI3K inhibitor GDC-0941. *Cancer Cell* **15**, 429-40 (2009).
316. Rusnak, D.W. et al. Assessment of epidermal growth factor receptor (EGFR, ErbB1) and HER2 (ErbB2) protein expression levels and response to lapatinib (Tykerb, GW572016) in an expanded panel of human normal and tumour cell lines. *Cell Prolif* **40**, 580-94 (2007).
317. Johnston, S. et al. Phase II study of predictive biomarker profiles for response targeting human epidermal growth factor receptor 2 (HER-2) in advanced inflammatory breast cancer with lapatinib monotherapy. *J Clin Oncol* **26**, 1066-72 (2008).
318. Johnston, S. et al. Lapatinib combined with letrozole versus letrozole and placebo as first-line therapy for postmenopausal hormone receptor-positive metastatic breast cancer. *J Clin Oncol* **27**, 5538-46 (2009).
319. Arteaga, C.L. & Baselga, J. Tyrosine kinase inhibitors: why does the current process of clinical development not apply to them? *Cancer Cell* **5**, 525-31 (2004).
320. DiMasi, J.A., Hansen, R.W. & Grabowski, H.G. The price of innovation: new estimates of drug development costs. *J Health Econ* **22**, 151-85 (2003).

321. Toschi, L. & Cappuzzo, F. Understanding the new genetics of responsiveness to epidermal growth factor receptor tyrosine kinase inhibitors. *Oncologist* **12**, 211-20 (2007).
322. Cappuzzo, F. et al. Gefitinib in pretreated non-small-cell lung cancer (NSCLC): analysis of efficacy and correlation with HER2 and epidermal growth factor receptor expression in locally advanced or metastatic NSCLC. *J Clin Oncol* **21**, 2658-63 (2003).
323. Parra, H.S. et al. Analysis of epidermal growth factor receptor expression as a predictive factor for response to gefitinib ('Iressa', ZD1839) in non-small-cell lung cancer. *Br J Cancer* **91**, 208-12 (2004).
324. Teng, M.W., Swann, J.B., Koebel, C.M., Schreiber, R.D. & Smyth, M.J. Immune-mediated dormancy: an equilibrium with cancer. *J Leukoc Biol* **84**, 988-93 (2008).
325. Gerlinger, M. et al. Intratumor heterogeneity and branched evolution revealed by multiregion sequencing. *N Engl J Med* **366**, 883-92 (2012).
326. Gullick, W.J. et al. c-erbB-2 protein overexpression in breast cancer is a risk factor in patients with involved and uninvolved lymph nodes. *Br J Cancer* **63**, 434-8 (1991).
327. Slamon, D.J. et al. Human breast cancer: correlation of relapse and survival with amplification of the HER-2/neu oncogene. *Science* **235**, 177-82 (1987).
328. Ross, J.S. & Fletcher, J.A. The HER-2/neu oncogene in breast cancer: prognostic factor, predictive factor, and target for therapy. *Stem Cells* **16**, 413-28 (1998).
329. Nahta, R., Yu, D., Hung, M.C., Hortobagyi, G.N. & Esteva, F.J. Mechanisms of disease: understanding resistance to HER2-targeted therapy in human breast cancer. *Nat Clin Pract Oncol* **3**, 269-80 (2006).
330. Citri, A., Skaria, K.B. & Yarden, Y. The deaf and the dumb: the biology of ErbB-2 and ErbB-3. *Exp Cell Res* **284**, 54-65 (2003).
331. Frogne, T., Laenkholm, A.V., Lyng, M.B., Henriksen, K.L. & Lykkesfeldt, A.E. Determination of HER2 phosphorylation at tyrosine 1221/1222 improves prediction of poor survival for breast cancer patients with hormone receptor-positive tumors. *Breast Cancer Res* **11**, R11 (2009).
332. Sassen, A. et al. Cytogenetic analysis of HER1/EGFR, HER2, HER3 and HER4 in 278 breast cancer patients. *Breast Cancer Res* **10**, R2 (2008).
333. Tovey, S.M. et al. Outcome and human epidermal growth factor receptor (HER) 1-4 status in invasive breast carcinomas with proliferation indices evaluated by bromodeoxyuridine labelling. *Breast Cancer Res* **6**, R246-51 (2004).
334. Tsutsui, S. et al. Prognostic value of the combination of epidermal growth factor receptor and c-erbB-2 in breast cancer. *Surgery* **133**, 219-21 (2003).
335. Witton, C.J., Reeves, J.R., Going, J.J., Cooke, T.G. & Bartlett, J.M. Expression of the HER1-4 family of receptor tyrosine kinases in breast cancer. *J Pathol* **200**, 290-7 (2003).
336. Abd El-Rehim, D.M. et al. Expression and co-expression of the members of the epidermal growth factor receptor (EGFR) family in invasive breast carcinoma. *Br J Cancer* **91**, 1532-42 (2004).
337. Prigent, S.A. et al. Expression of the c-erbB-3 protein in normal human adult and fetal tissues. *Oncogene* **7**, 1273-8 (1992).
338. Lemoine, N.R. et al. Expression of the ERBB3 gene product in breast cancer. *Br J Cancer* **66**, 1116-21 (1992).
339. Travis, A. et al. C-erbB-3 in human breast carcinoma: expression and relation to prognosis and established prognostic indicators. *Br J Cancer* **74**, 229-33 (1996).
340. Lee, H. & Mairle, N.J. Isolation and characterization of four alternate c-erbB3 transcripts expressed in ovarian carcinoma-derived cell lines and normal human tissues. *Oncogene* **16**, 3243-52 (1998).
341. Srinivasan, R. et al. Intracellular expression of the truncated extracellular domain of c-erbB-3/HER3. *Cell Signal* **13**, 321-30 (2001).
342. Funayama, T. et al. Overexpression of c-erbB-3 in various stages of human squamous cell carcinomas. *Oncology* **55**, 161-7 (1998).
343. Shi, Y. et al. A novel proximity assay for the detection of proteins and protein complexes: quantitation of HER1 and HER2 total protein expression and homodimerization in formalin-fixed, paraffin-embedded cell lines and breast cancer tissue. *Diagn Mol Pathol* **18**, 11-21 (2009).
344. Larson, J.S. et al. Analytical Validation of a Highly Quantitative, Sensitive, Accurate, and Reproducible Assay (HERmark) for the Measurement of HER2 Total Protein and HER2 Homodimers in FFPE Breast Cancer Tumor Specimens. *Patholog Res Int* **2010**, 814176 (2010).
345. Spears, M. et al. In situ detection of HER2:HER2 and HER2:HER3 protein-protein interactions demonstrates prognostic significance in early breast cancer. *Breast Cancer Res Treat* **132**, 463-70 (2012).
346. Soderberg, O. et al. Characterizing proteins and their interactions in cells and tissues using the in situ proximity ligation assay. *Methods* **45**, 227-32 (2008).
347. Soderberg, O. et al. Direct observation of individual endogenous protein complexes in situ by proximity ligation. *Nat Methods* **3**, 995-1000 (2006).

348. Kerppola, T.K. Complementary methods for studies of protein interactions in living cells. *Nat Methods* **3**, 969-71 (2006).
349. Ting, A.Y., Kain, K.H., Klemke, R.L. & Tsien, R.Y. Genetically encoded fluorescent reporters of protein tyrosine kinase activities in living cells. *Proc Natl Acad Sci U S A* **98**, 15003-8 (2001).
350. Zhang, J., Campbell, R.E., Ting, A.Y. & Tsien, R.Y. Creating new fluorescent probes for cell biology. *Nat Rev Mol Cell Biol* **3**, 906-18 (2002).
351. Sekar, R.B. & Periasamy, A. Fluorescence resonance energy transfer (FRET) microscopy imaging of live cell protein localizations. *J Cell Biol* **160**, 629-33 (2003).
352. Legg, J.W., Lewis, C.A., Parsons, M., Ng, T. & Isacke, C.M. A novel PKC-regulated mechanism controls CD44 ezrin association and directional cell motility. *Nat Cell Biol* **4**, 399-407 (2002).
353. Ng, T. et al. Ezrin is a downstream effector of trafficking PKC-integrin complexes involved in the control of cell motility. *EMBO J* **20**, 2723-41 (2001).
354. Ng, T. et al. Imaging protein kinase C α activation in cells. *Science* **283**, 2085-9 (1999).
355. Fruhwirth, G. et al. Deep-tissue multiphoton fluorescence lifetime microscopy for intravital imaging of protein-protein interactions. in *SPIE BIOS/Photonics West 2009* Vol. 7183 (eds Periasamy, A. & So, P.T.C.) 71830-71839 (2009).
356. Zhou, F., Xing, D., Wu, S. & Chen, W.R. Intravital imaging of tumor apoptosis with FRET probes during tumor therapy. *Mol Imaging Biol* **12**, 63-70.
357. Ho-Pun-Cheung, A. et al. Quantification of HER Expression and Dimerization in Patients' Tumor Samples Using Time-Resolved Forster Resonance Energy Transfer. *PLoS One* **7**, e37065 (2012).
358. Citri, A. et al. Drug-induced ubiquitylation and degradation of ErbB receptor tyrosine kinases: implications for cancer therapy. *EMBO J* **21**, 2407-17 (2002).
359. Shtiegman, K. et al. Defective ubiquitinylation of EGFR mutants of lung cancer confers prolonged signaling. *Oncogene* (2007).
360. Fruhwirth, G.O. et al. Fluorescence lifetime endoscopy using TCSPC for the measurement of FRET in live cells. *Opt Express* **18**, 11148-58 (2010).
361. Pierre, S. & Scholich, K. Toponomics: studying protein-protein interactions and protein networks in intact tissue. *Mol Biosyst* **6**, 641-7 (2010).
362. Nik-Zainal, S. et al. Mutational processes molding the genomes of 21 breast cancers. *Cell* **149**, 979-93 (2012).
363. Nik-Zainal, S. et al. The life history of 21 breast cancers. *Cell* **149**, 994-1007 (2012).
364. Allred, D.C. et al. Ductal carcinoma in situ and the emergence of diversity during breast cancer evolution. *Clin Cancer Res* **14**, 370-8 (2008).
365. Lenington, W.J., Jensen, R.A., Dalton, L.W. & Page, D.L. Ductal carcinoma in situ of the breast. Heterogeneity of individual lesions. *Cancer* **73**, 118-24 (1994).
366. Lower, E.E., Glass, E., Blau, R. & Harman, S. HER-2/neu expression in primary and metastatic breast cancer. *Breast Cancer Res Treat* **113**, 301-6 (2009).
367. Brunelli, M. et al. Genotypic intratumoral heterogeneity in breast carcinoma with HER2/neu amplification: evaluation according to ASCO/CAP criteria. *Am J Clin Pathol* **131**, 678-82 (2009).
368. Wilking, U. et al. HER2 status in a population-derived breast cancer cohort: discordances during tumor progression. *Breast Cancer Res Treat* (2010).
369. Wolff, A.C. et al. American Society of Clinical Oncology/College of American Pathologists guideline recommendations for human epidermal growth factor receptor 2 testing in breast cancer. *J Clin Oncol* **25**, 118-45 (2007).
370. O'Flynn, E.A., Wilson, A.R. & Michell, M.J. Image-guided breast biopsy: state-of-the-art. *Clin Radiol* **65**, 259-70.
371. Klaeser, B. et al. PET/CT-guided biopsies of metabolically active bone lesions: applications and clinical impact. *Eur J Nucl Med Mol Imaging*.
372. Steiner, D., Forrer, P. & Pluckthun, A. Efficient selection of DARPins with sub-nanomolar affinities using SRP phage display. *J Mol Biol* **382**, 1211-27 (2008).
373. Parsons, M. & Ng, T. Intracellular coupling of adhesion receptors: molecular proximity measurements. *Methods Cell Biol* **69**, 261-78 (2002).
374. Barber, P.R., et al. . Multiphoton time-domain fluorescence lifetime imaging microscopy: practical application to protein-protein interactions using global analysis. *J R Soc Interface* S93-S105 (2009).
375. Giuliano, M. et al. Circulating tumor cells as prognostic and predictive markers in metastatic breast cancer patients receiving first-line systemic treatment. *Breast Cancer Res* **13**, R67 (2011).
376. Mark I. Rowley, P.R.B., Anthony Coolen, Borivoj Vojnovic. Bayesian analysis of fluorescence lifetime imaging data. in *BIOS, SPIE Photonics West Paper 7903-74* (The Moscone Center, San Francisco, California, USA, 2011).

377. Fitzmaurice, M. Principles and pitfalls of diagnostic test development: implications for spectroscopic tissue diagnosis. *J Biomed Opt* **5**, 119-30 (2000).
378. Wagnieres, G.A., Star, W.M. & Wilson, B.C. In vivo fluorescence spectroscopy and imaging for oncological applications. *Photochem Photobiol* **68**, 603-32 (1998).
379. Ramanujam, N. Fluorescence spectroscopy of neoplastic and non-neoplastic tissues. *Neoplasia* **2**, 89-117 (2000).
380. Huang, Z. et al. Effect of formalin fixation on the near-infrared Raman spectroscopy of normal and cancerous human bronchial tissues. *Int J Oncol* **23**, 649-55 (2003).
381. Ruers, T.J. et al. Improved selection of patients for hepatic surgery of colorectal liver metastases with (18)F-FDG PET: a randomized study. *J Nucl Med* **50**, 1036-41 (2009).
382. O'Brien, S.G. et al. Imatinib compared with interferon and low-dose cytarabine for newly diagnosed chronic-phase chronic myeloid leukemia. *N Engl J Med* **348**, 994-1004 (2003).
383. Paez, J.G. et al. EGFR mutations in lung cancer: correlation with clinical response to gefitinib therapy. *Science* **304**, 1497-500 (2004).
384. Lynch, T.J. et al. Activating mutations in the epidermal growth factor receptor underlying responsiveness of non-small-cell lung cancer to gefitinib. *N Engl J Med* **350**, 2129-39 (2004).
385. Krop, I. & Winer, E.P. Further progress in HER2-directed therapy. *Lancet Oncol* **13**, 2-3 (2012).
386. Esserman, L.J. et al. Chemotherapy response and recurrence-free survival in neoadjuvant breast cancer depends on biomarker profiles: results from the I-SPY 1 TRIAL (CALGB 150007/150012; ACRIN 6657). *Breast Cancer Res Treat* **132**, 1049-62 (2012).
387. Robidoux, A., Tang, G., Priya Rastogi, Charles E. Geyer & Azar, C.A. Evaluation of lapatinib as a component of neoadjuvant therapy for HER2+ operable breast cancer: NSABP protocol B-41. *J Clin Oncol* **30** (suppl; abstr **LBA506**)(2012).
388. Pantel, K., Brakenhoff, R.H. & Brandt, B. Detection, clinical relevance and specific biological properties of disseminating tumour cells. *Nat Rev Cancer* **8**, 329-40 (2008).
389. Braun, S. et al. A pooled analysis of bone marrow micrometastasis in breast cancer. *N Engl J Med* **353**, 793-802 (2005).
390. Nagrath, S. et al. Isolation of rare circulating tumour cells in cancer patients by microchip technology. *Nature* **450**, 1235-9 (2007).
391. Budd, G.T. et al. Circulating tumor cells versus imaging--predicting overall survival in metastatic breast cancer. *Clin Cancer Res* **12**, 6403-9 (2006).

Appendix

Protocol Title:

A randomised phase II trial of [^{18}F]fluorothymidine and the standard tracer [^{18}F]Fluorodeoxyglucose in the assessment of HER2-targeted and systemic therapy response in HER2-positive breast cancer and their utility compared to conventional MRI imaging response and biopsy derived biomarkers.

Trial Identifiers: HER2PET01

EudraCT number: 2012-004028-39

Chief Investigator

Prof Paul Ellis

Address

Department of Oncology
Oncology Management Offices
F04 Bermondsey Wing
Guys Hospital
Great Maze Pond
London, SE1 9RT
Tel: 020-7188-4253
Fax: 020-7188-4271
Email: paul.ellis@gstt.nhs.uk

Chief Scientific Officer

Prof Tony Ng

Richard Dimpleby Dept and Randall
Division of Cancer Studies
King's College London
Room 2.32, Second Floor,
New Hunts House
London SE1 1UL
Tel: 020-7188-8056
Email: tony.ng@kcl.ac.uk

Co-Sponsors

Kings College London/Guy's and St. Thomas' NHS Foundation Trust

Address

King's Health Partners Clinical Trials
Office
16th floor Guy's Tower
London, SE1 9RT
Tel: 020-7188-5732
Fax: 020-7188-8330
Email: jackie.pullen@kcl.ac.uk

CONFIDENTIAL**PARTICIPATING INVESTIGATORS AT THE CENTRES**

Participating Centre:	Guy's and St. Thomas' NHS Foundation Trust (GSTT)
Clinical PET Specialist	Prof. Michael O'Doherty PET Imaging Centre St.Thomas' Hospital Lambeth Palace Road London SE1 7EH Tel: 020-7188-4988 Fax: 020-7620-0790 Email: michael.o'doherty@kcl.ac.uk
Clinical PET Specialist	Dr Sally Barrington PET Imaging Centre St.Thomas' Hospital Lambeth Palace Road London SE1 7EH Tel: 020-7188-4988 Fax: 020-7620-0790 Email: sally.barrington@kcl.ac.uk
Chief Surgeon	Prof Arnie Purushotrum Consultant Breast Surgeon F03 Bermondsey Wing Guys Hospital Great Maze Pond London SE1 9RT Tel : 020-7188-3027 Email : arnie.purushotham@kcl.ac.uk
Oncologist	Prof Paul Ellis Department of Oncology Oncology Management Offices F04 Bermondsey Wing Guys Hospital Great Maze Pond London, SE1 9RT Tel: 020-7188-4253 (Ext:84253) Fax: 020-7188- 4271 Email: paul.ellis@gstt.nhs.uk
Oncologist	Prof. Andrew Tutt Department of Oncology Guys Hospital Great Maze Pond London, SE1 9RT Tel: 020-7188-9881 Fax:020-7188- 3666 Email: andrew.tutt@kcl.ac.uk
Oncologist	Dr Jennifer Glendenning

CONFIDENTIAL

Department of Oncology
Guys Hospital
Great Maze Pond
London SE1 9RT
Tel 020-7188-9881
Email:
jennifer.glendenning@gstt.nhs.uk

Oncologist

Dr Gargi Patel
Richard Dimbleby Dept and Randall
Division of Cancer Studies
Room 2.32, New Hunts House
Kings College London
Guy's Campus
London SE1 9RT
Tel: 020-7848-6174
Email: gargi.patel@kcl.ac.uk

Oncologist

Dr Alison Jones
University College London Hospital
235 Euston Road
London NW1 2BU
Tel : 020-7380-9072
Email : alison.jones@uclh.nhs.uk

Radiologist

Dr Jyoti Parikh
Department of Radiology
Guys Hospital
Great Maze Pond
London SE1 9RT
Tel 020-7188-4113
Email: jyoti.parikh@gstt.nhs.uk

Radiologist

Dr Vicky Goh
Department of Radiology
Guys Hospital
Great Maze Pond
London SE1 9RT
Tel 020-7188-188 5550
Email: vicky.goh@kcl.ac.uk

Histopathologist

Prof. Sarah Pinder
Department of Histopathology
Guys Hospital
Great Maze Pond
London SE1 9RT
Tel 020 7188 4260

**Breast tissue & data bank
manager**

Dr Cheryl Gillett
Guys Hospital
Great Maze Pond
London SE1 9RT
Tel 020-7188-0874
cheryl.gillet@kcl.ac.uk

CONFIDENTIAL

PET Radiochemist:

Dr Marcel Cleij
PET Imaging Centre
St.Thomas' Hospital
Lambeth Palace Road
London SE1 7EH
Tel: 020-7188-4988
Email: marcel.cleij@kcl.ac.uk

PET Scientific director:

Prof Paul Marsden
PET Imaging Centre
St.Thomas' Hospital
Lambeth Palace Road
London SE1 7EH
Tel: 020-7188-4988
Email: paul.marsden@kcl.ac.uk

Statistician

Mrs. Lucy Kilburn
The Institute of Cancer Research,
Sir Richard Doll Building
15 Cotswold Rd, Belmont,
Sutton,
Surrey SM2 5NG
Tel: 020 8722 4080
Fax: 020 8770 7876
Email: Lucy.Kilburn@icr.ac.uk

TABLE OF CONTENTS

Title Page	1
Investigators and sponsor	1
Table of Contents	5
List of abbreviations and definition of terms	8
Protocol Signatures	9
PROTOCOL SUMMARY	202
1.1 FULL TITLE	202
1.1.1 Short Title	202
1.2 CLINICAL TRIAL OBJECTIVES AND ENDPOINTS	202
1.2.1 Primary Objectives and Endpoints	202
1.2.2 Secondary Objectives and Endpoints	202
1.3 DESIGN	203
1.4 TRIAL INTERVENTIONS.....	203
1.5 PET TRACER ADMINISTRATION SCHEDULE.....	204
1.6 TREATMENT GROUP	205
1.7 TRIAL TIMELINES AND ACCRUAL RATE	205
2. INTRODUCTION AND TRIAL RATIONALE	205
2.1 BACKGROUND	205
2.1.1 Rationale for developing functional imaging in breast cancers	205
2.1.2 Positron emission tomography (PET)	206
2.1.3 Tumour tissue derived biomarker studies	206
2.1.4 Chemotherapy	208
2.2 INVESTIGATIONAL MEDICINAL PRODUCT: : [¹⁸ F]-FLUOROTHYRIDINE ([¹⁸ F]-FLT)	210
2.2.1 Structure of [¹⁸ F]-FLT	210
2.2.2 Mechanism of action of [¹⁸ F]-FLT tracer	210
2.2.3 Pre-clinical experience	211
2.2.4 CLINICAL EXPERIENCE	211
2.3 INVESTIGATIONAL MEDICINAL PRODUCT: [¹⁸ F]FLUORODEOXYGLUCOSE ([¹⁸ F]-FDG).....	214
2.4 RATIONAL FOR PROPOSED STUDY	214
3 TRIAL DESIGN	214
3.1 CLINICAL TRIAL OBJECTIVES AND ENDPOINTS	214
3.1.1 Primary objectives and endpoints	214
3.1.2 Secondary objectives and endpoints	214
3.2 DESIGN OF THE CLINICAL TRIAL.....	216
3.2.1 Study Schema	216
3.2.2 Patient recruitment	217
3.3 FUNCTIONAL IMAGING	217
3.3.1. Patients allocated to FDG PET-CT	217
3.3.2. Patients allocated to FLT PET-CT	218
3.4 BIOPSY ANALYSES	218
4 PATIENT SELECTION	219
4.1 ELIGIBILITY CRITERIA	219
4.1.1 Inclusion Criteria:	219
4.1.2 Exclusion Criteria:	220
4.2 PATIENT REGISTRATION	221
5 TREATMENT	221
5.1 PET IMAGING	221
5.1.1 Radiation Dose and Schedule	221
5.1.2 Risk assessment	221
5.1.3 Post scan follow-Up	221
5.1.4 Replacement of Patients	222

CONFIDENTIAL

5.1.5 Modifications to the Imaging Schedule	222
5.2 CHEMOTHERAPY.....	222
5.2.1 Chemotherapy dose and dose modifications	222
5.3 TRASTUZUMAB/HERCEPTIN DOSE AND DOSE MODIFICATIONS	222
5.4 CONCOMITANT MEDICATION AND TREATMENT	223
6 PHARMACEUTICAL INFORMATION.....	223
6.1 [¹⁸ F]-FLUOROTHYMININE.....	223
6.1.1 Supply of [¹⁸ F]-fluorothymidine	223
6.1.2 Formulation of [¹⁸ F]-FLT	223
6.1.3 [¹⁸ F]-FLT Storage and Labelling	224
6.2 [¹⁸ F]-FLUORODEOXYGLUCOSE ([¹⁸ F]-FDG)	224
6.3 [¹⁸ F]-FLT AND [¹⁸ F]-FDG TRACER ADMINISTRATION	224
6.4 IMP ACCOUNTABILITY	225
7 INVESTIGATIONS SCHEDULE.....	225
7.1 BASELINE- PRE IMAGING EVALUATIONS	225
7.1.1 Obtaining Written Informed Consent	226
7.2. EVALUATIONS DURING THE STUDY	227
7.2.1 Prechemotherapy Study Imaging and Biopsy (d-10 to d1)	227
7.2.1.1 PET imaging	227
7.2.1.2 Biopsy	227
7.2.2 Study evaluations after cycle 1 chemotherapy/trastuzumab (day 17±3)	228
7.2.2.1 PET imaging	228
7.2.2.2 Biopsy	228
7.3 CYCLE 2 TO END OF STUDY	228
7.3.1 Definitive surgery	229
7.4 POST STUDY FOLLOW-UP	229
SCHEDULE OF EVENTS	230
8 ASSESSMENT OF SAFETY	231
8.1 ADVERSE EVENT DEFINITIONS	231
8.1.1 Adverse Event	231
8.1.2 Serious adverse events (SAEs)	231
8.2 Reporting Responsibilities	231
8.2.1 Events exempt from being reported as SAEs to KHPCTO	232
8.3 RECORDING OF ADVERSE EVENTS AND SERIOUS ADVERSE EVENTS IN ECRFs.....	232
8.4 FOLLOW-UP OF ADVERSE EVENTS.....	232
8.5 ETHICS AND REGULATORY APPROVAL.....	233
8.6 PREGNANCY.....	233
9 ASSESSMENT OF IMAGING TECHNIQUES.....	234
9.1 TIMING AND TYPE OF IMAGING ASSESSMENTS.....	234
9.1.1 Baseline Evaluations	234
9.1.2 Interpretation of Imaging Data	234
10 PATIENT WITHDRAWAL BEFORE COMPLETION OF STUDY SCHEDULE.....	235
11 DEFINING THE END OF STUDY.....	235
12 DATA ANALYSIS AND STATISTICAL CONSIDERATIONS.....	236
12.1 SAMPLE SIZE	236
12.2 INTERIM ASSESSMENT.....	236
12.3 PRESENTATION OF DATA	236
12.5 TOXICITY	237
13 ADMINISTRATION	237
13.1 COMPLETION OF THE ECRF	237
13.2 QUALITY ASSURANCE	237
13.3 DATA HANDLING	238
13.4 CLINICAL STUDY REPORT	238

CONFIDENTIAL

13.5 INDEMNITY..... 238
13.6 PUBLICATION POLICY AND PRESS RELEASES 238
13.7 FINANCE..... 238
14 REFERENCES..... 239
15 APPENDICES..... 253
15.1 APPENDIX 1: WHO PERFORMANCE SCALE 253
15.2 APPENDIX 2: DECLARATION OF HELSINKI 254
15.3 APPENDIX 3:..... 258
EXAMPLE PET REPORTING SCORING SHEETS FOR BREAST CANCER 258

CONFIDENTIAL

LIST OF ABBREVIATIONS AND DEFINITION OF TERMS

	Abbreviation	Definition
A	ABPI	Association of the British Pharmaceutical Industry
	AE	adverse event
	ALP	alkaline phosphatase
	ALT	alanine aminotransferase
	ARSAC	Administration of Radioactive Substances Advisory Committee
	AST	aspartate aminotransferase
B	BP	blood pressure
C	^o C	degrees Celsius
	CDM	Clinical Data Manager
	CI	Chief Investigator
	CIN	cervical intra-epithelial neoplasia
	CIRB	Central Institutional Review Board
	CRA	Clinical Research Associate
	CT	computerised tomography
	CTA	clinical trial authorisation
	CTC	circulating tumour cell
	CTCAE	Common Terminology Criteria for Adverse Events
	D	Day
DW		Diffusion weighted
E	EC	Epirubicin and cyclophosphamide
	ECG	Electrocardiogram
	eCRF	electronic case report form
	EDC	electronic data capture
	EGFR	epidermal growth factor receptor
	ER	oestrogen receptor
	EU GMP	European Union Good Manufacturing Practice (EU directive 2003/94/EC)
F	FDG	Fluorodeoxyglucose
	FEC	5-fluorouracil, epirubicin and cyclophosphamide
	FFPE	formalin-fixed paraffin-embedded
	FLIM	fluorescence lifetime imaging microscopy
	FLT	Fluoro-L-thymidine
	FNA	fine needle aspirate
	FRET	Förster resonance energy transfer
	[18]F	radioisotope of fluorine
G	GBq	Gigabecquerel
	GCP	Good Clinical Practice
H	Hb	Haemoglobin
	HER2	Human epidermal growth factor receptor 2
	HTA	Human Tissue Authority
I	ICH GCP	International Conference on Harmonisation of Good Clinical Practice
	IMAGINT	HER imaging and molecular interaction mapping in breast cancer
	IMP	investigational medicinal product

CONFIDENTIAL

	IRMER IRR99 ITF IUPAC	Ionising Radiation (Medical Exposure) Regulations Ionising Radiation Regulations (1999) Investigator Trial File International Union of Pure and Applied Chemistry
J	KHPCTO	King's Health Partners Clinical Trials Office
L	LD50 LVEF	lethal dose for 50% of sample population left ventricular ejection fraction
M	MBq MCM MDT MHRA MIA(IMP) MRI mSv MUGA	Megabecquerel Minichromosome maintenance (complex) multi-disciplinary team Medicines and Healthcare products Regulations Agency Manufacturer's Authorisation for Investigational Medicinal Products magnetic resonance imaging millisievert Multi-gated acquisition scan
N	NCI NPV	National Cancer Institute negative predicted value
P	pCR PET PET CT PPV	pathological complete response positron emission tomography positron emission tomography combined with computerised tomography positive predictive value
Q	QP	Qualified Person
R	RCB REC RECIST	Residual cancer burden Research Ethics Committee Response evaluation criteria in solid tumours
S	SAE SDV SOP SUSAR SUV	serious adverse event source data verification standard operating procedure suspected unexpected serious adverse (drug) reaction standardised uptake value
T	TNM TUNEL	Tumour (lymph) Nodes Metastases classification terminal deoxynucleotidyl transferase dUTP nick end labeling
U	ULN USM	upper limit of normal urgent safety measures
W	WHO	World Health Organisation

PROTOCOL signatures

Chief Investigator

Name: Prof Paul Ellis

Signature:

Date:

CONFIDENTIAL

PROTOCOL SUMMARY

1.1 Full Title

A randomised Phase II trial of [18F]-fluorothymidine and the standard tracer [18F]Fluorodeoxyglucose in the assessment of systemic therapy response in HER2 positive breast cancer and its utility compared to FDG PET, conventional imaging response and biopsy derived biomarkers.

1.1.1 SHORT TITLE

[18]FLT- and [18]FDG-PET as imaging biomarkers for the response to neoadjuvant treatment in HER2 positive breast cancer.

1.2 Clinical Trial Objectives and Endpoints

1.2.1 PRIMARY OBJECTIVES AND ENDPOINTS

Primary Objective	Endpoint
To correlate PET imaging response in breast and axillary lymph nodes with residual cancer burden (RCB) at definitive surgery	Correlation of SUV response for each tracer with residual cancer burden (RCB) in breast and axilla

1.2.2 SECONDARY OBJECTIVES AND ENDPOINTS

Secondary Objective	Endpoint
To evaluate optical proteomic profiling of HER2 and related protein interactions in primary tissue and circulating tumour cells as a method for predicting response to targeted treatment and chemotherapy	Correlation of outcome from optical proteomic profile with [18F]-FLT and FDG, conventional MRI RECIST response criteria, RCB and pathological response to treatment from surgical specimen
To evaluate PET imaging using the tracers [18F]-FLT and FDG as a method for evaluating response to systemic therapy in HER2 positive breast cancer	Correlation of SUV response for each tracer with conventional MRI RECIST response assessment
To correlate PET imaging response with biopsy derived proliferation biomarkers	Correlation with % cell positive for proliferation markers ki 67 (MIB-1), geminin, mcms and mRNA expression markers of proliferation genes (if present)
Non invasive assessment of binding affinity (K _i and K ₁) from this dataset	The dynamic analyses will use an input function derived from the aorta of heart of both to derive rate constants K _i and K ₁ , measurements transport and phosphorylation for both tracers
To obtain performance estimates for the	Evaluate the ability of FDG and

CONFIDENTIAL

ability of the tracers FDG and FLT to report MRI response	FLT tracers to predict RCB
To assess nodal imaging response using PET imaging	Correlate with standard imaging response in nodes, SUV response in breast.
To assess the safety of fluorothymidine in patients with breast cancer.	Determining the causality of each adverse event to the two agents, and grading AE severity according to NCI CTCAE version 4.0.

1.3 Design

This is a multi-centre, non-therapeutic Phase II trial directly evaluating PET imaging using [¹⁸F]-thymidine and FDG tracers, and proteomic biomarkers as a predictor for breast cancer response to standard neo-adjuvant chemotherapy.

Eligible patients will have ER negative and HER2 positive phenotypic receptor expression and require neoadjuvant chemotherapy. Neoadjuvant chemotherapy will consist of 4 cycles of trastuzumab/docetaxel followed by definitive surgery, and then further chemotherapy with 4 cycles of epirubicin and cyclophosphamide (EC) as outlined in section 5.2. Patients will undergo imaging evaluation as per standard, prior to surgery, as well as FLT and FDG PET-CT.

1.4 Trial interventions

Patients who consent to the study will be randomised and followed using one of two tracers, the IMP FLT and the IMP FDG at baseline and following their first trastuzumab/docetaxel administration at day 17±3. All participants will have a research core biopsy performed prior to chemotherapy, following their day 17±3 PET scan and through the definitive resection specimen at the time of surgery. All research scans will be performed prior to their research core biopsy.

Functional imaging results will be compared to standard imaging and pathological assessments of response to chemotherapy. All routine scans will be in accordance with departmental standard practice using contrast enhanced breast MRI using an image acquisition protocol which includes DW at baseline and after 3 cycles and will be reported according to RECIST criteria.

The following PET imaging evaluations will be performed:

- Changes in PET tracer uptake after 1 cycle of standard neoadjuvant chemotherapy will be correlated to subsequent ‘gold-standard’ cross-sectional imaging response using MRI after the 3rd chemotherapy cycle.
- Dynamic FDG and FLT PET CT scans will be performed to assess the uptake over time in this breast cancer sub-type and determine the optimum imaging time for FDG response assessment.
- Correlation of SUV response in the nodes with standard cross-sectional imaging, SUV response in the breast primary and the degree of response of nodal disease (if present) at definitive surgery
- Correlate PET imaging response for both tracers with residual cancer burden (RCB) at definitive surgery
- Dynamic analysis using an input function derived from the aorta or the heart or both to derive rate constants Ki and k1, measurements of transport of and phosphorylation for both tracers

CONFIDENTIAL

- Patients receiving the both tracers will be followed for reporting of adverse events (AEs) from when the informed consent is signed until their post-imaging telephone assessment after administration of the tracer.. If there is any doubt with the telephone conversation the patient will be seen by the oncologist /treating physician. If there are AEs that occur while the patient is on study which are attributed to the tracer, and which are still present at the post study discussion, the patient will be followed monthly by their oncologist / treating physician until resolution or stabilisation of these events.

Participants in this study will have biopsies performed at baseline prior to chemotherapy (both paraffin-fixed formalin-embedded and fresh frozen) after first trastuzumab/docetaxel administration following day 17(+/-3) PET scan and through the definitive surgical specimen at completion of 4 cycles of neoadjuvant chemotherapy.

These tissues will be used to assess response to the targeted agent as well as chemotherapy, and correlate with functional imaging through:

- HER2-HER3 interactions
- Further assessment of protein-protein interactions related to metastases, such as cofilin activation and interaction of protein kinase C and ezrin
- Proliferation index ki-67
- S phase specific replication marker geminin, MCM replication fork licensing factors and mRNA expression markers of proliferation genes
- Biomarkers of apoptosis (terminal transferase uridyl nick-end labelling assay)
- Glucose uptake biomarkers (Glut 1 receptor), and
- Tumour genotype

These assays will be applied to the diagnostic and research pre-chemotherapy core, post cycle 1 research core and on cores through the definitive surgical specimen. These changes will be correlated with changes in SUV uptake on PET scan using both tracers. Both biopsy and imaging assessments will be correlated with gold standard cross-sectional imaging response using MRI and pathological response (RCB) score following definitive surgery.

1.5 PET Tracer administration Schedule

At their PET study visits, participants allocated to receive FDG tracer will have 200 MBq of [¹⁸F]-Fluorodeoxyglucose administered via intravenous injection (time = T₀).

A dynamic scan will be performed over the breast primary for 100 minutes and then two 10 minute local views over the whole breast and also incorporating the breast in the final scan. The first of these two scans will be at 120 to 130 min after FDG injection and the patient will remain on the couch for this scan. The second of these two scans will occur at 170-180 minutes and will require a further single bed position low dose CT scan and PET acquisition. Either the aorta or the heart or both will be within the field of view to allow the derivation of an input function to enable the non invasive assessment of Ki and k1 from this data set as well as SUVmax, mean and SUV peak (derived from a 1cm³ box drawn over the SUVmax area. Ten patients will have a single venous blood sample drawn for metabolites during the dynamic imaging through a single venous access allowing the analysis of metabolites for image data correction (3.3.1).

For participants allocated to receive FLT, 200 MBq (-10%) [¹⁸F]-fluorothymidine will be administered via intravenous injection (time = T₀). A dynamic scan will be performed over the primary for 100 minutes this single view will also include the axilla and a summed view at 90 – 100 minutes will be obtained from the dynamic data. Ten patients will have 5 venous blood samples drawn for metabolites during the dynamic imaging through a single venous access allowing the analysis of metabolites (the glucuronide form of FLT) for image data correction (3.3.2). Scans will be evaluated qualitatively, semi-quantitatively and quantitatively

CONFIDENTIAL

using a variety of measures including SUVmax and SUV peak. The input function will be derived from the aorta or the heart for non invasive assessment of Ki and k1 from this data.

1.6 Treatment Group

A total of 30 patients with ER negative, HER2 positive breast cancer will be enrolled for evaluation. Patients will have been seen by the treating oncologist who knows the patient has breast cancer and has recommended neoadjuvant chemotherapy as described in this protocol (see 5.3). The patient will then be asked if they wish to take part in the study.

1.7 Trial Timelines and Accrual Rate

It is anticipated that recruitment to the trial will be completed in 24 months.

2. INTRODUCTION AND TRIAL RATIONALE**2.1 Background**

Breast cancer is the most common female cancer. A subset express the human epidermal growth factor receptor 2, HER2 (ErbB2) receptor (15%). This study will focus on the ER-HER2 positive breast cancers. In these patients, despite the advent of treatment with the monoclonal antibody, trastuzumab/Herceptin and selection of HER2+ve tumours for therapy, response to treatment often remains suboptimal hence necessitating other ongoing clinical studies of combination regimens. There is a clear need to develop an early imaging surrogate for assessing tumour response to systemic therapies and facilitate assessment of novel therapeutics. Furthermore, there is a paucity of tools available for the assessment of the 'on-target' effects of these novel drugs. Development of biomarkers which can inform specifically on these effects may provide early proof of tumour response or drug resistance and could help tailor treatment regimens to individual patients.

2.1.1 Rationale for developing functional imaging in breast cancers

Neo-adjuvant breast cancer therapy typically requires at least 9-12 weeks of chemotherapy (3-4 cycles) before assessment of tumour shrinkage and surgical planning can occur. This would typically be with magnetic resonance cross-sectional imaging (MRI). Early identification of patients who will fail to benefit adequately from standard therapy is pivotal to improving outcomes for breast cancer patients. Changes seen on MRI during neoadjuvant chemotherapy are predictive of subsequent pathological response in HER2 + breast cancer (Loo et al, 2011). However, assessment is constrained by the significant time lag from start of therapy to measurable size reduction of the tumour. This is equivalent to about 3 cycles (each 21 days) of chemotherapy treatment. Biopsy-derived biomarkers, such as the Ki-67 proliferation index, may have prognostic and possible predictive potential for subsequent systemic therapy response (Yerushalmi 2010).

In cancers such as lymphoma, early PET scans after 1-2 cycles of therapy can identify those patients who are not benefiting at an early stage, thus informing transition to alternative treatment. This trial will determine if similar methods can be developed specifically for patients receiving chemotherapy for HER 2 positive breast cancer. Validating an optimal early imaging surrogate for tumour response will enable more rapid and tailored patient treatment decisions to be made in the future, hence preventing toxicity from ineffective chemotherapy and allow prompt transition to other treatments. This project will determine if PET functional imaging techniques can be developed specifically for patients receiving chemotherapy for HER2+ve breast cancer to detect drug induced changes in tumour metabolism which precede size change. If this is shown to be the case FDG or FLT imaging

CONFIDENTIAL

may be used in prospective trials testing early imaging response adaptive chemotherapy approaches in neoadjuvant chemotherapy for HER2+ve breast cancer.

2.1.2 Positron emission tomography (PET)

Positron emission tomography (PET) functional imaging detects drug induced changes in tumour metabolism which precede size change. We will compare the ability of the tracers 2-[fluorine18]fluoro-2-deoxy-D-glucose (FDG) 3'deoxy-3'-[18F]fluorothymidine (FLT) to provide an early means of determining whether chemotherapy is being effective or not.

2-[fluorine18]fluoro-2-deoxy-D-glucose (FDG) PET is the most commonly used PET tracer for staging in cancer. Although not routinely used in breast cancer FDG PET has been shown to correlate with uptake in the primary and has a sensitivity and specificity of 97% and 100% for detecting axillary nodal metastasis when compared with FNA cytology or sentinel lymph node biopsy (Straver, 2010). Preoperative FDG uptake has been demonstrated to correlate with prognosis in breast cancer and axillary nodal response to chemotherapy (Oshida, 2000, Straver, 2010). Following neoadjuvant chemotherapy the predictive value of early assessment of response with FDG using semi-quantitative assessment (Standardized Uptake Value, SUV) has been demonstrated and a threshold decrease of 45% identifies responders in ~73% patients. Uptake patterns differ with time according to histology, with uptake generally being lower in the receptor positive breast cancers than the triple negative subtypes and the optimal scan time in the different subsets remains undefined (Boerner 1999 Buck 2002, Basu 2007, Straver 2010).

FDG uptake non-specifically represents proliferation through an increase in general cell metabolism requiring glucose as an energy source. Uptake may be confounded by post therapy inflammation within the tumour or surrounding tissues thereby falsely indicating lack of response. Biological factors predicting enhanced baseline FDG uptake include higher proliferative index (ki-67), and negative receptor status (Buck 2002, Basu 2007, Straver 2010). The risk of underestimating tumour response is, therefore, greater in the oestrogen negative or HER2 positive subpopulations. Potentially the optimal imaging biomarker for early tumour response may derive from novel imaging strategies which have greater specificity for tumour metabolism and are not susceptible to inflammatory change. Proliferation can be assessed by the tracer 3'deoxy-3'-[18F]fluorothymidine (FLT). This is a structural analogue of thymidine which assesses DNA turnover by reflecting the use of thymidine.

FLT PET can be used as an imaging probe to assess *in vivo* cellular proliferation in malignant tumors. The diagnostic utility of FLT has been evaluated in a number of different primary tumour sites and correlation between uptake and proliferative activity (Ki-67) has been demonstrated. Although, FLT has been available for some years, data reporting its use in breast cancer is limited. In metastatic breast cancer changes in FLT uptake at 1-2 weeks following therapy (chemotherapy or endocrine) pre-date imaging and marker response (Kenny 2007, Pio 2006). Details of tumour subtype were not reported in either of these studies and FLT's ability to report tumour response in HER 2 positive breast cancer specifically remains unproven. However, given that an impact on proliferation would be rapidly expected following exposure to effective systemic therapy, there is a powerful rationale for believing that FLT PET may be the optimal biomarker for response prediction.

2.1.3 Tumour tissue derived biomarker studies

Unravelling the complexity of the macromolecular networks that drive biological function to derive clinically useful biomarkers, is arguably the most important challenge of post-genomic

CONFIDENTIAL

biology and medicine. Currently the molecular diagnostics developed for clinical use are based on detecting genetic changes (gene amplification/increased copy number, mutations) and genomic signatures derived from microarray analysis). The therapeutic responsiveness of cancers to HER-targeted therapies do not necessarily correlate with the receptor levels.

For instance, when trastuzumab/Herceptin is given as with chemotherapy for first-line treatment of HER2-overexpressing metastatic breast cancer, it is associated only with a 50% objective response rate (Slamon et al, 2001). Overexpression of HER2 alone does not promote cell division as effectively as HER2 coupled to HER3, via the PI3K/protein kinase B pathway. HER3 is the preferred dimerisation partner for HER2 and this heterodimer is believed to be the most active dimer, thus forming a key target for inhibition (Holbro, 2003, Tzahar, 1996). Proteomic assessment of this dimer may provide a predictive biomarker for response or resistance to HER targeted treatments. In addition to primary resistance, HER2+ breast cancer patients who initially respond can subsequently progress/relapse on trastuzumab treatment (acquired resistance). In the case of genetic mutations (e.g. *AKT1* and *PTEN*), the incidence in breast tumours is typically low. In a recently published series of hormone receptor positive breast tumours, the incidence of *AKT1* and *PTEN* mutations are reported at 1.4% and 2.3%, respectively (Stemke-Hale et al., 2008). The more common *PIK3CA* mutation (34.5%) was however not significantly correlated with any measured clinical variable (relapse-free survival or overall survival) (Stemke-Hale et al., 2008).

Studying protein function (in terms of activity and spatiotemporal location) will give a broader patient base to integrate into a metastatic signature, regardless of whether patients have germline or somatic mutations. For probing protein function in cancer tissues, we have now finalised a multivariate tumour invasion signature containing information that can classify breast cancer patients at an individualized level, by imaging in breast cancer tissue cores from 221 patients, the macromolecular interaction between activated protein kinase C (PKC) and ezrin, as well as cofilin activation status. Ezrin and cofilin are actin microfilament-associated proteins, which we and others have shown to be important mediators of breast cancer cell migration; and various clinical reports have highlighted the significant contribution of ezrin and cofilin to the clinical development of metastasis in cancers. The difference between patients according to this image-based protein function signature correlates significantly with the development of metastasis/time to metastasis (p-value ~ 0.008) (Kelleher et al., 2006; Kelleher et al., 2010; Kelleher et al., 2009; Patel et al., 2011). The assays/tools and algorithms that have been developed in this protein function-based metastatic signature will be complemented by our in-house assay that measures HER2/HER3 complex by Förster resonance energy transfer (FRET)/ fluorescence lifetime imaging microscopy (FLIM), then applied to the new EU FP7 programme: entitled 'HER imaging and molecular interaction mapping in breast cancer (IMAGINT)'.

Recent pre-clinical studies have demonstrated the significance of delineation of dimerisation of the HER family receptors in the modulation of targeted therapies using monoclonal antibodies. Gaborit et al used time-resolved FRET to quantify EGFR and HER2 dimers in ovarian tumour cell lines and in vivo in mouse models. Quantification of EGFR/HER2 heterodimers revealed perturbation of heterodimerisation on trastuzumab or cetuximab treatment and this effect correlated with clinical response to treatment in mouse models. Ghosh et al described inhibition of HER2 homodimer tumour cell line proliferation in vitro and a correlation between high HER2 homodimer expression at diagnostic biopsy and prolonged disease free, and overall survival in a cohort of HER2+ve breast cancer patients treated with trastuzumab. Lee-Hoeflich et al described a central role for the HER2/HER3 dimer in the pathogenesis of HER2+ve breast cancer as HER3 signalling was demonstrated to be vital to cell proliferation in HER2+ve cell lines, as opposed to EGFR related signalling. The HER2 oligomeric states have already been shown to be pertinent to predicting response to targeted treatment both in vitro and in vivo. We propose to use highly sensitive optical proteomic imaging with FRET/FLIM to profile HER2 dimerisation along side related metastatic protein

CONFIDENTIAL

interactions such as ezrin and cofilin, and to integrate this result with functional imaging with FDG- and FLT-PET in order to better predict outcome to targeted therapy.

In order to complement the assessment of pertinent protein-protein interactions in primary tissue, we aim to apply the proteomic biomarkers described above to circulating tumour cells (CTCs). We plan to identify and isolate circulating tumour cells using CellSearch (Veridex, Raritan, NJ), which is the most widely used technology for this application and has been used to show a negative correlation between CTC number and prognosis in metastatic breast cancer (Cristofanilli et al, Liu et al). However, the evaluation of CTCs as prognostic biomarkers has been hampered especially in early stage disease due to poor performance characteristics of the variety of assays which are available to detect CTCs (Rack et al, 2010).

Although the value of CTCs alone as biomarkers has yet to be demonstrated, we hope to evaluate not only the numbers of CTCs, but also protein function within CTCs, e.g. HER2-3 dimerisation, within the context of the primary tumour. This information will be integrated into the metastatic signature described above. We may then be able to evaluate the significance of protein-protein interactions/activation in potential metastatic cells as opposed to the primary tumour, in terms of prediction and prognostication.

Systemic imaging (e.g. PET-CT) allows whole body localisation and quantification of contrast agents (e.g. fluorodeoxyglucose, ¹⁸F-FDG and fluorothymidine, ¹⁸FLT) uptake but suffers from a lower sensitivity and spatial resolution in comparison with optical imaging. We will combine the high resolution tissue imaging techniques, offering molecular markers, with clinical bioimaging methods; a combination which will be truly complementary. It is expected that an integrated analysis of the datasets obtained for each patient will allow us to derive a new generation of biomarkers that can predict response to molecule-targeted treatments and have the potential for clinical validation and exploitation.

2.1.4 Chemotherapy

The neoadjuvant setting provides an excellent opportunity to investigate potential molecular predictors of response to targeted treatments, such as trastuzumab/Herceptin. This study is designed to optimise the validation of predictive biomarkers such as FDG/FLT-PET and biopsy derived assays of protein-protein interactions related to the targeted treatment, without affecting overall or disease-free survival. The chemotherapy drugs used have been widely studied in the adjuvant setting and have also been applied in the neoadjuvant setting as described below. Patients will receive the targeted agent (trastuzumab) first, with taxane chemotherapy for 4 cycles with biopsies before treatment and on completion of the first cycle of chemotherapy (to co-ordinate with PET imaging), in order to assess the biological 'on target' activity of trastuzumab. Following the first 4 cycles, patients will undergo definitive surgery to excise the tumour, from which pathological response will be assessed. Following surgery, patients will have a further 4 cycles of epirubicin and cyclophosphamide, without trastuzumab, to complete a standard number of chemotherapy cycles. Patients will then continue to complete one year of trastuzumab therapy.

In the case of HER2+ve tumours, the pivotal randomised controlled neoadjuvant trials examining the effect of the addition of trastuzumab to chemotherapy are summarised in the table below (Baselga et al 2012, Gianni et al 2012, Baselga et al 2010, Gianni et al 2010, Untch et al, 2010, Coudert et al, 2007, Buzdar et al 2005). These studies have established an improvement in pathological complete response rate on addition of trastuzumab to various neoadjuvant chemotherapy regimens. Gianni et al (NOAH, 2010) randomised patients to neoadjuvant chemotherapy with doxorubicin, paclitaxel, cyclophosphamide,

CONFIDENTIAL

methotrexate and fluorouracil, with or without the addition of concomitant trastuzumab for 1 year (in both the neoadjuvant and adjuvant setting). They demonstrated a significant improvement in 3 year event-free survival from 56% to 71% (HR 0.59, 95% CI 0.38–0.90]; p=0.013), and in pathological complete response rate (pCR) from 19% to 38%. Buzdar et al similarly reported an impressive improvement in pCR for patients treated with 8 cycles of neoadjuvant chemotherapy (taxane+FEC) +/- concomitant trastuzumab for 1 year, from 26% to 65.2%.

More recently, the Neo-ALLTO, NeoSphere and GeparQuinto studies have examined the effect of addition of further targeted therapies, i.e. lapatinib (an EGFR and HER2 tyrosine kinase inhibitor), and pertuzumab (a humanised monoclonal antibody directed at the dimerisation domain of HER2) to a 'control' arm of neoadjuvant trastuzumab and taxane, followed by definitive surgery, adjuvant anthracycline-based chemotherapy and adjuvant trastuzumab up to 1 year. Both studies demonstrated excellent pCR of 29% and 29.5%, and overall response rates of 81.4% and 70.5% respectively, in the arm containing taxane and trastuzumab alone. Furthermore, the taxane/trastuzumab regimen was very well tolerated. For example, within the NeoSphere study, the number of adverse events in this arm was 20 (107 patients), the most common of which was febrile neutropaenia (7%) as expected. Of the 106 patients eligible for this arm of treatment, only 3 patients did not proceed to surgery and adjuvant chemotherapy/trastuzumab, due to patient choice. There were no cardiac serious adverse event or toxic deaths in the neoadjuvant phase. Data from the GeparQuinto study demonstrated a pCR of 30.3% using 6 cycles of neoadjuvant anthracycline/taxane chemotherapy with concomitant trastuzumab versus the same chemotherapy with lapatinib, but adverse events were higher with 29.6% experiencing dyspnoea, 39.1% experiencing oedema and 14% of patients discontinuing chemotherapy.

These studies demonstrate neoadjuvant treatment with taxane and trastuzumab, followed by definitive surgery and adjuvant chemotherapy/trastuzumab as a feasible, tolerable regimen with comparable, if not improved outcomes to standard neoadjuvant therapy in terms of pCR. In addition, the NeoSphere study demonstrates an improvement in pCR with the addition of pertuzumab, an antibody which prevents HER2 dimerisation, to trastuzumab and taxane, thus highlighting the importance of quantification of HER2-HER3 dimerisation in tumour samples as proposed within this study.

We propose to administer docetaxel with trastuzumab for the first 4 cycles of treatment, thus employing the targeted agent first, in order to compare histopathological proteomic profiles and FLT/FDG-PET scans pre- and post-trastuzumab treatment, without the added biological effect anthracyclines. Primary use of 4 cycles of taxane and trastuzumab in the neoadjuvant setting in this protocol is in keeping with that administered in the NeoSphere and NeoALLTO trials. Furthermore, all the neoadjuvant trials listed in the table below administered at least 4 cycles of taxane as in our protocol. As per the Neo-ALLTO study, we have opted for adjuvant anthracycline followed by trastuzumab in order to avoid the cardiotoxicity of concomitant treatment. Hence trastuzumab will be recommenced after surgery to complete 1 year of treatment. In total, all patients receive a cumulative dose of anthracycline/taxane/trastuzumab which is equivalent to the majority of the neoadjuvant trials summarised here and our current standard of care. Therefore, overall survival and disease-free survival is not compromised within this study design.

Trial	Chemo regimen	pCR/DFS	Reference
NeoSphere	4#T+D vs	pCR: 29% vs	Gianni et al,

CONFIDENTIAL

	4#PER+T+D vs 4#PER+D vs 4#PER+T. Followed by surgery, then adj 3# FEC (except last group : 4#D+3#FEC)	45.8% vs 24% vs16.8%	Lancet Oncol Jan 2012; 25- 32
NeoALTTO	L+P vs T+P vs L+T+P (12 weeks of Paclitaxel)	pCR: 24.7% vs 29.5% vs 51.3%	Baselga et al Lancet Jan 2012
GeparQuinto	4#EC+T-4#D+T vs 4#EC+L-4#D+ L	pCR 30.3% vs 22.7%	Untch et al, Lancet Oncol Jan 2012
NOAH	3#AP-4#P-3CMF +/-T(33wks)	pCR: 38% vs 19%. 3-year event-free survival, 71% vs 56% without T; HR 0.59 p=0.013	Gianni et al Lancet 2010;375:377- 384
GeparQuattro	4#EC-4#D+T vs 4#EC-4#D+T+X (concurrent or sequential) (T=24wks vs 36wks respectively)	31.7% (vs 15.7% in HER2-ve pts)	Untch et al, JCO 2010;28:2024- 2031
GETN(A)-1	6#DCarbo+T (18wks)	43%	Coudert et al JCO 2007 25:2678-2684
Buzdar et al	4#P-4#FEC +/- concomitant T throughout (24wks)	65.2% vs 26%/ No recurrence at median follow up 16.3 mons vs 3 in chemo arm	Buzdar et al, JCO 2005 23:3676

A=Doxorubicin, Carbo=Carboplatin, C=Cyclophosphamide, D=Docetaxel, E=Epirubicin, F=5-fluorouracil, L=Lapatinib, M=Methotrexate, P=Paclitaxel, Per=Pertuzumab, T=Trastuzumab, X=Capecitabine, pCR-pathological complete response, DFS=disease-free survival

2.2 Investigational Medicinal Product : [¹⁸F]-fluorothymidine ([¹⁸F]-FLT)

Full details of the physical and chemical characteristics of the IMP [¹⁸F]-fluorothymidine, is provided in the Investigator's Brochure.

2.2.1 Structure of [¹⁸F]-FLT

The [¹⁸F]-fluorothymidine drug product is a mixture of radio-labelled fluorine-18 fluorothymidine and 'cold' Fluorothymidine. [See Section 6.1 Pharmaceutical Data.]

2.2.2 Mechanism of action of [¹⁸F]-FLT tracer

[¹⁸F]-fluorothymidine is a Positron Emission Tomography (PET) radiotracer is chemically altered thymidine with the addition of Fluorine-18. Thymidine is an essential component of DNA. [¹⁸F]-fluorothymidine monitors synthesis of DNA and hence proliferation of cancer cells in the body. It is not incorporated into DNA but does reflect the uptake of thymidine into cells and the cell pool of thymidine. It has particularly been studied in gliomas, oesophageal cancers, lymphomas, oropharyngeal cancers, lung cancer and breast cancer.

Radio-labelled [¹⁸F]-fluorothymidine metabolism has been evaluated as a cancer imaging agent, both pre-clinically and clinically. Radio-labelled thymidine clears rapidly and

CONFIDENTIAL

extensively from the blood after intravenous administration. The uptake is very low in normal tissues of the cerebral cortex, lung, heart and soft tissue in the oropharynx and normal breast tissue, allowing excellent differentiation of malignancies against these tissues. Highest uptake is observed in the liver and bone marrow and this does present a problem with identifying malignancy at these sites.

2.2.3 Pre-clinical experience

[¹⁸F]-fluorothymidine has been used in mice and rats to assess a variety of tumour models as described in the IB.

2.2.4 Clinical Experience

A summary of patient studies carried out using [¹⁸F]-fluorothymidine is provided in Table 1. There is one published toxicology study (Spence 2008) which did not raise any safety concerns. No safety concerns have been highlighted in any of the studies performed in the literature. At Guy's and St. Thomas' NHS Foundation Trust we have recruited 8 patients (with 3 or 4 repeat scans each) to a mechanistic study using [¹⁸F]-fluorothymidine in patients with head and neck cancer and lung cancer without incident to date.

CONFIDENTIAL

Disease studied	No. patients		Reference
GLIOMA			
	30	3 scans each	Schwarzenberg, 2012
	20		Hong, 2011
	18	3 scans each	Wardak, 2011
	15	3 scans each	Schiepers, 2010
	2	repeats	Galdiks, 2010
	11		Backes, 2009
	14		Price, 2009
	13		Ullrich, 2008
<i>Cancer and radionecrosis</i>	19		Spence, 2009 & 2008?
	18		Hatakeyama, 2008
	9		Schiepers, 2007
	21	3 scans each	Chen, 2007
	12		Muzi, 2006
	25		Saga, 2006
	10		Yamamoto, 2006
	23		Jacobs, 2005
	25		Chen, 2005
<i>Cancer and benign</i>	26		Choi, 2005
H & N			
	10	3 scans each	Troost, 2010
	17		Troost, 2010
	43		Hoshikawa, 2011
	14	(2 scans,)	Menda, 2010
	8	(2 scans each)	Menda, 2009
	6	2 scans each	de Langen, 2009
	10		Troost, 2007
	11		Cobben, 2004
GERM CELL TUMOUR			
	11	2 scans	Pfannenber, 2010
OESOPHAGUS			
	21	2-4 scans	Yue, 2010
	22	? same patients	Han, 2010
	10		van Westreenen, 2005
	5		Dittmann, 2003
GASTRIC			
	45		Herrmann, 2007
COLORECTAL			
	26		Yamamoto, 2009
	15		Roel, 2008
	10		Francis, 2003
	11		Visvikis, 2004
	10	2 scans each	Wieder, 2007
GASTRIC			
	21		Kameyama, 2011
	45	2 scans each	Ott, 2011
	21		Kameyama, 2009
PANCREAS			
	46		Herrmann, 2012
	31 (10 benign)		Herrmann, 2008

CONFIDENTIAL

	5		Quon, 2008
HEPATOCELLULAR CARCINOMA			
<i>Cancer and benign</i>	18		Eckel, 2009
LUNG (NSCLC unless stated)			
	30	2 per patient	Kahraman, 2011
	51	3 per patient	Mileshkin, 2011
	9		Cheebsumon, 2011
	34	2 per patient	Zander, 2011
	22	2 or 3 per patient	Benz, 2011
	5	3 per patient	Everitt, 2009
	9	2 per patient	de Langen, 2009
	34		Yamamoto, 2008
	31	2 per patient	Sohn, 2008
<i>Cancer and benign</i>	55		Tian, 2008
	54 (? included above)		Yamamoto, 2008
	18		Yamamoto, 2007
<i>Cancer and benign</i>	22		Yap, 2006
	17		Muzi, 2005
<i>Pulmonary nodules</i>	47		Buck, 2005
	17		Cobben, 2004
<i>Cancer and benign</i>	20		Halter, 2004
	9		Dittmann, 2003
	26		Buck, 2003
	18		Vesselle, 2003
	10		Vesselle, 2002
Acute myeloid leukaemia			
	10		Buck, 2008
LYMPHOMA			
<i>Mantle lymphoma</i>	8		Herrmann, 2011
<i>NHL</i>	66		Herrmann, 2011
<i>HD and NHL</i>	48		Kasper, 2007
<i>Indolent lymphoma</i>	11		Wagner, 2003
<i>Indolent lymphoma</i>	7		Buchmann, 2004
Breast			
	20	2 scans each	Contractor, 2011
	21		Contractor, 2011
	13	2 scans each	Kenny, 2007
	14	2 scans each	Pio, 2006
	8		Been, 2006
	14	Breast cancer	Smyczek-Gargya, 2004
SARCOMA			
	20	2 scans each	Benz, 2011
	22		Buck, 2008
	19		Cobben, 2004
	2		Dittmann, 2003
MELANOMA			
	10		Cobben, 2003
RENAL			
	16	3 scans each	Liu, 2011

CONFIDENTIAL

	1		Dittmann, 2003
OVARIAN CANCER			
	6		Richard, 2011
Total number of patients	1623	601 repeat scans in these patients	

Table 1: Patients studies using PET [¹⁸F]-FLT reported in the literature: publications where it was thought the same patient group was republished have been omitted.

Note: There are additional studies by some of the authors which are believed to be duplicate studies and are included in the reference list at the end.

2.3 Investigational Medicinal Product: [¹⁸F]fluorodeoxyglucose ([¹⁸F]-FDG)

Full details of the the IMP [¹⁸F]-fluorodeoxyglucose, including pharmaceutical, clinical and preclinical information, is provided in the SmPC for MetaTrace FDG solution for injection.

2.4 Rational for Proposed Study

This exploratory phase II study seeks to identify whether PET functional imaging approaches using 2-[fluorine18]fluoro-2-deoxy-D-glucose (FDG) and 3'deoxy-3'-[¹⁸F]fluorothymidine (FLT) can be utilised alongside tumour derived biomarkers, including optical proteomic profiling, in patients with HER2+ve breast cancer to provide an in vivo assessment of response to standard neoadjuvant systemic therapy that is not constrained by the inherent time lag associated with MRI RECIST evaluation.

3 TRIAL DESIGN

3.1 Clinical Trial Objectives and Endpoints

3.1.1 PRIMARY OBJECTIVES AND ENDPOINTS

Primary Objective	Endpoint
To correlate PET imaging response in breast and axillary lymph nodes with residual cancer burden (RCB) at definitive surgery	Correlation of SUV response for each tracer with residual cancer burden(RCB) in breast and axilla

3.1.2 SECONDARY OBJECTIVES AND ENDPOINTS

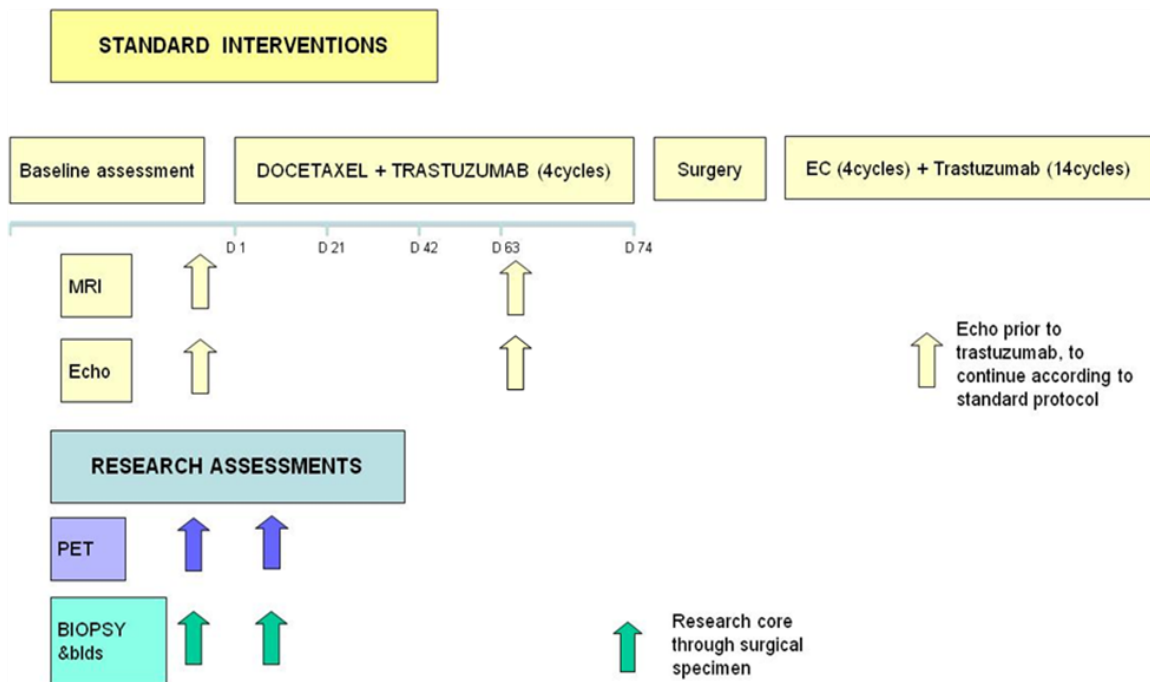
Secondary Objective	Endpoint
To evaluate optical proteomic profiling of HER2 and related protein interactions in primary tissue and circulating tumour cells as a method for predicting response to targeted treatment and chemotherapy	Correlation of outcome from optical proteomic profile with [¹⁸ F]-FLT and FDG, conventional MRI RECIST response criteria, RCB and pathological response to treatment from surgical specimen
To evaluate PET imaging using the tracers [¹⁸ F]-FLT and FDG as a method	Correlation of SUV response for each tracer with conventional

CONFIDENTIAL

for evaluating response to systemic therapy in HER2 positive breast cancer	MRI RECIST response assessment
To correlate PET imaging response with biopsy derived proliferation biomarkers	Correlation with % cell positive for proliferation markers ki 67 (MIB-1), geminin, mcms and mRNA expression markers of proliferation genes (if present)
Non invasive assessment of Ki and K1 from this dataset	The dynamic analyses will use an input function derived from the aorta of heart of both to derive rate constants Ki and K1, measurements transport and phosphorylation for both tracers
To obtain performance estimates for the ability of the tracers FDG and FLT to report MRI response	Evaluate the ability of FDG and FLT tracers to predict RCB
To assess nodal imaging response using PET imaging	Correlate with standard imaging response in nodes, SUV response in breast.
To assess the safety of fluorothymidine in patients with breast cancer.	Determining the causality of each adverse event to the two agents, and grading AE severity according to NCI CTCAE version 4.0.

3.2 Design of the Clinical Trial

3.2.1 STUDY SCHEMA



This is a multi-centre, non-therapeutic Phase II imaging trial study. Study participants will comprise 30 patients with ER negative HER2 positive breast cancer who require neoadjuvant chemotherapy and meet the eligibility criteria defined in section 4.

Patients will receive standard sequential chemotherapy with four cycles of T-H (taxane/ trastuzumab), prior to definitive surgery followed by four cycles of EC (epirubicin, cyclophosphamide). Chemotherapy will commence on D1 of each cycle, 21 days per cycle. All participants will have standard cross-sectional imaging response assessments using MRI after 3 cycles of treatment. Participants may also have USS and mammography as per local protocol wherever indicated.

In this proposed study, primary disease will be examined with FLT and FDG to assess the in vivo response characteristics. All patients will have standard diagnostic biopsy, and a research core biopsy taken prior to initiation of chemotherapy (D-14 to D0), a core biopsy after Day 17±3 PET scan, prior to cycle 2 chemotherapy and representative biopsies through the resection specimen from definitive surgery after completion of 4 cycles of primary chemotherapy. Tissue from these specimens will be analysed using the FRET/FLIM metastatic signature as well as other tissue derived biomarkers described in 3.4. Participants will undergo additional study interventions according to the diagram above.

CONFIDENTIAL**3.2.2 PATIENT RECRUITMENT**

30 patients with ER- HER2 positive breast cancer will be enrolled. Each patient will participate in the trial for approximately 16 weeks. Patients will be recruited from the breast cancer clinicians at Guy's and St. Thomas' NHS Foundation Trust Hospitals, and University College London NHS Trust Hospitals. Patient follow up will be performed through the local breast clinic.

The [¹⁸F]-Fluorodeoxyglucose and [¹⁸F]-fluorothymidine scans will be performed at the Guys and St Thomas' NHS Foundation Trust and KCL PET Imaging Centre. **Travel costs for patients from UCLH will be reimbursed for research visits for PET imaging.** Biopsies will be taken and fixed locally, and then sent to the central laboratory at the Breast Tissue Bank, Guy's Hospital for further processing. Surgical resection specimens may be retained at the local institution as long as a representative core biopsy is sent to the central laboratory. Patients will be asked to give consent to the biobanking of any biological material that is excess to requirements of the study for use in future research, subject to the approval of the research by a research ethics committee.

3. 3 Functional Imaging

Patients will be randomised to FLT or FDG to optimise the balance of tumour and patient factors that might affect performance assessment. In all patients baseline PET-CT scanning assessment will take place prior to commencing chemotherapy followed by a post cycle 1 chemotherapy scan on day 17(±3). Imaging will be performed using a GE Discovery VCT 64-slice PET-CT scanner.

3.3.1. PATIENTS ALLOCATED TO FDG PET-CT

Patients randomised to FDG tracer will have PET-CT imaging according to the following protocol.

Following a 6-hour fast, patients will receive intravenous injection of 200 MBq of [¹⁸F]FDG. A dynamic scan will be performed over the breast primary for 100 minutes and then two 10 minute local views over the whole breast and also incorporating the breast in the final scan. The first of these two scans will be at 120 to 130 min after FDG injection and the patient will remain on the couch for this scan. The second of these two scans will occur at 170-180 minutes and will require a further single bed position low dose CT scan and PET acquisition. In the first 10 patients allocated to this tracer, who give consent, a venous blood sample will be taken during the imaging study visit to record the radioactivity within the blood following injection of the FDG tracer and permit the analysis of metabolites for image data correction. These bloods samples may be taken via the patients indwelling chemotherapy venous access device where present, or via a second venous cannula inserted in the opposite arm and linked to a sterile cannula tubing.

This imaging time gives adequate count statistics for lesion localization, drawing of the region of interest and SUVmax determination. Acquired scans will be reconstructed with OSEM (ordered subset expectation maximization; 30 subsets, one iteration, 5.14 m post filter, 4.69 mm loop filter).

Scans will be evaluated qualitatively and semi-quantitatively using SUVmax and SUV peak. SUVmax is measured by a single operator hand-drawing a region of interest on the axial PET image using the CT component of the study to ensure the region corresponds to the tumour of interest. The SUVmax is derived as the highest SUV within the tumour and measured on all scans and displayed graphically against the time. Other volume processing

CONFIDENTIAL

of the uptake will be performed and the data will be used to test other offline processing methods. The dynamic images obtained will also have an input function derived by placing a region of interest over the aorta and over the heart cavity. From this input function a k_1 and K_i value for the tumour will be derived.

Following the FDG PET-CT scan patients will not require scheduled telephone follow up owing to the substantial clinical experience supporting absence of toxicity from this standard radiotracer as detailed in the SmPC.

3.3.2. PATIENTS ALLOCATED TO FLT PET-CT

Patients randomised to FLT tracer will have PET-CT imaging according to the following protocol.

Following a 6 hour fast, 200 MBq of FLT will be injected through a venous cannula whilst the patient is lying on the scanner couch. A dynamic scan will be performed for 100 minutes in a single position over the breast cancer. Semiquantitative imaging will be performed at 90 minutes using a static scan acquired from the dynamic imaging data set. Analysis of the static SUV measurements will be compared with histology and with the quantitative measurements. Quantitative imaging will be performed using the dynamic curves generated from the underlying aorta and heart.

In the first 10 patients allocated to this tracer, who give consent, 5 venous blood samples will be taken during their imaging studies to record the radioactivity within the blood following injection of the radioactive IMP and permit the analysis of metabolites (the glucuronide form of FLT) for image data correction. These blood samples may be taken via the patients indwelling chemotherapy venous access device where present, or via a second venous cannula inserted in the opposite arm and linked to a sterile cannula tubing. This will allow high performance liquid chromatography and a cartridge method will separate FLT from the FLT glucuronide on the 5 ml blood samples. These procedures allow a calibrated arterial input function, generated from the images of the aorta or the heart, corrected for decay and the presence of ^{18}F -labelled metabolites to be obtained.

Following their FLT PET-CT scan patients will have blood pressure and pulse check, and be telephoned the day after their scan to document any toxicities experienced.

Note: patients may have FLT and FDG-PET scans carried out on the same day as trastuzumab/Herceptin infusion in order to minimise patient visits. However, if this is the case, nursing staff who are pregnant may NOT administer trastuzumab due to risk to the foetus from radioactive tracer.

3.4 Biopsy & Blood Analyses

For all participants research-specific tumour tissue will be obtained pre and post treatment exposure and alterations in tissue characteristics correlated with change in FLT/FDG SUV. Material will include surplus tissue from the formalin-fixed, paraffin-embedded (FFPE) diagnostic core biopsy, an ultrasound guided pre-chemotherapy research core, an ultrasound guided research core biopsy performed following the day 17 PET-CT scan and a research core through the definitive surgical resection specimen. All research cores will be stored in both FFPE and fresh frozen format.

Immunohistochemical/immunofluorescent assessment will consist of FRET/FLIM metastatic signature, biomarkers of apoptosis (terminal transferase uridyl nick-end labelling assay, TUNEL), proliferation (MIB-1, the S-phase specific replication marker -geminin, MCM replication fork licensing factors) and glucose uptake biomarkers (Glut 1 receptor). Tumour genotype analysis will involve whole tumour genome sequencing techniques and use of

CONFIDENTIAL

specific tests to detect copy number change (e.g. neu/HER2), mutations (e.g. EGFR), DNA methylation status, changes in expression of known and as yet unknown oncogenes, tumour suppressor genes and mRNA expression markers of proliferation genes. These biomarker changes will be correlated with SUV and SUV change for both PET tracers.

Blood samples for assessment and harvest of CTCs will be taken prior to (day -14 to 0) and after 4 cycles of neoadjuvant chemotherapy. For the majority of patients at these time-points, routine bloods will be taken, e.g. prior to biopsy or surgical procedure. Hence, bloods for CTC will be taken at the same time. Presence of 5 or more CTCs per 7.5mls of blood has already been identified as a prognostic marker for metastatic breast cancer patients (Cristofalli et al.). Therefore, the number of CTCs per 7.5mls of whole blood will be measured pre and post treatment, as well as application of the FRET/FLIM metastatic signature described above.

Blood samples taken for CTC evaluation must be handled with the following restrictions:

- Blood should be taken by venepuncture or sterile collection from an indwelling catheter (e.g. PICC line or Hickman line) into a CellSave Preservative Tube only, and will be provided from the central laboratory (Prof Ng's lab at KCL) for each test required for each patient. These tubes are evacuated and are designed for use with standard blood collection systems.
- The Tube should be filled until blood flow stops, and then gently inverted 8 times in order to prevent coagulation.
- Tubes must be stored and transported at temperatures between 15-30 degrees (tubes crack if stored below 0 degrees)
- Samples may then be transported to the central lab for processing within 96 hours.

All analyses will be performed in collaboration with the bioinformatics, biostatistics and mathematics groups of the Comprehensive Cancer Imaging Centre and Breakthrough Breast Cancer Research Unit at KCL (Ton Coolen, Lars Holmberg and Tony Ng). At Guys hospital, the central radiology and pathology collaborators are Dr Jyothi Parikh, Professor Sarah Pinder and Dr Cheryl Gillett and our surgical collaborator is Prof Arnie Purushotham. All biopsy material will be taken and preserved locally according to standard operating procedures for FFPE or fresh frozen tissue. However, all study related material will be transported and stored for the purposes of the study in the HTA licensed Guys' and St Thomas' Breast Tissue and Data Bank. Patients will be asked to give consent to the biobanking of any biological material that is excess to requirements of the study for use in future research, subject to the approval of the research by a recognised research ethics committee.

4 PATIENT SELECTION**4.1 Eligibility Criteria**

Female patients with ER negative Her 2 positive breast cancer who will be treated with neoadjuvant chemotherapy should be considered for participation in accordance with the inclusion and exclusion criteria below.

4.1.1 INCLUSION CRITERIA:

- Female age \geq 18 years
- Women of childbearing potential must have documented negative pregnancy test

CONFIDENTIAL

within the 2 weeks prior to day 1 chemotherapy and agree to use a medically acceptable birth control during the duration of their chemotherapy.

- Stage II-III biopsy proven early breast cancer for whom primary chemotherapy is recommended. Staging performed in accordance to local criteria.
- All patients will have Her 2 positive tumours (IHC 3 or IHC 2 and FISH amplified)
- All patients will have ER negative primary tumours (Allred <3)
- ECOG PS of 0 or 1
- Primary tumour size >2cm
- Eligible for neoadjuvant chemotherapy according to departmental guidelines
- Adequate biochemistry for chemotherapy:
Laboratory values as follows
- ALT and AST $\leq 1.5X$ upper limit of normal [ULN];
- total bilirubin \leq upper limit of normal except in patients with document Gilbert's syndrome,
- Alkaline phosphatase $\leq 2.5 \times$ ULN
- Adequate haematology for chemotherapy. Laboratory values as follows
- Absolute neutrophil count (ANC) $\geq 1,500/\mu\text{l}$,
- Platelets count $\geq 100,000/\mu\text{l}$
- Haemoglobin $\geq 10\text{g/dL}$
- Adequate renal function for chemotherapy; creatinine clearance greater than 60 assessed by Cockcroft Gault calculation or EDTA.
- Adequate cardiac function with baseline left ventricular ejection fraction(LVEF) of >55% on echo/MUGA prior to treatment
- No prior malignancies other than CIN cervix or basal cell skin cancer
- Written informed consent

Able to comply with treatment plans, scheduled visits, all study PET imaging and biopsy procedures and follow-up

4.1.2 EXCLUSION CRITERIA:

- Any prior treatment for breast cancer
- Patients who are pregnant will be excluded. If there is any doubt about pregnancy a pregnancy test will be taken.
- Patients who are breast feeding
- Evidence of distant metastasis at diagnosis precluding neoadjuvant treatment
- Requirement for concurrent radiotherapy treatment
- Serious medical condition or concurrent medical illness likely to compromise ability to complete prescribed chemotherapy course.
- Anticoagulation requirement which would preclude serial biopsy
- Significant history of uncontrolled cardiac disease/clinically significant cardiac disease; i.e. unstable angina, recent myocardial infarction (within prior 6 months); NYHA Class III-IV heart failure, including pre-existing ventricular arrhythmia valvular dysfunction or conduction abnormality
- Any other problems that may make the patient unable to tolerate the PETCT scan or translational biopsies
- Investigational Medicinal Product in the previous 28 days

CONFIDENTIAL**4.2 Patient Registration**

All patients screened will be registered in the electronic data capture (EDC) system. A screening number will be automatically allocated during this process and will include any patients who are screen failures or those who decline participation.

All patients who give informed consent for the trial will be registered within the EDC system. The patient trial number and tracer allocation will be automatically allocated by the EDC system during the registration process. Patients must be registered in the EDC system within 7 days prior to first study specific procedure.

5 TREATMENT**5.1 PET Imaging**

A total of 30 patients will be scanned in this study using either FDG or FLT tracers.

5.1.1 RADIATION DOSE AND SCHEDULE15 patients scanned using FDG

PET component, 200 MBq of FDG: 4 mSv

CT component for dynamic and static PET scan: 2 mSv

CT component for second static PET scan: 2 mSv

Total effective dose per session: 8 mSv

Total effective dose for two sessions: 16 mSv

15 patients scanned using FLT

PET component, 200 MBq FLT: 6.5 mSv

CT component for dynamic and static PET scan: 2 mSv

Total effective dose per session: 8.5 mSv

Total effective dose for two sessions: 17 mSv

5.1.2 RISK ASSESSMENT

The total radiation dose to patients enrolled in this study is ~ 9 times the natural background radiation dose in the UK. The risk of inducing fatal cancer as a result of radiation exposure is less than ~0.05/Sv for the whole population and less for older age groups (1/5 of this value for patients over 60). The risks of fatal cancer associated with the exposures in this study are therefore up to ~ 1 in 1170. These are small compared to a natural lifetime risk of 1 in 4.

5.1.3 POST SCAN FOLLOW-UP

The post-imaging assessment will be scheduled as a telephone call on 24hours following PET scanning. If there are AEs that occurred while the patient was on study which are attributed (including possibly related AEs) to [¹⁸F]-thymidine and are still present at the post-imaging phone call the patient will be followed up monthly afterwards until resolution, to baseline or stabilisation of these events. Due to the short half life of FLT 30 day follow-up is not necessary and will not be performed.

Post-scan safety assessment is not required for participants randomised to FDG due to the known safety profile of this standard tracer and absence of any expected side effects.

CONFIDENTIAL

With respect to chemotherapy, follow-up will occur as normal for these standard chemotherapy in local oncology clinics after every cycle of chemotherapy. The end of study is defined at definitive surgery. The Off-Study visit will constitute a final clinic appointment after surgery whereby the patient will be seen by one of the Participating Investigators after surgical treatment.

Further details regarding follow-up can be found in Section 7.4.

5.1.4 REPLACEMENT OF PATIENTS

Any patient who does not have fully evaluable (for example due to scanner failure) PET-CT scans will be replaced.

5.1.5 MODIFICATIONS TO THE IMAGING SCHEDULE

The imaging schedule should be completed on the day allocated. If the schedule is not able to be completed on Day 1 the patient will be asked to return the following day. This may result from an isotope production failure. If the patient declines then the patient will be replaced in the total numbers to be recruited.

5.2 Chemotherapy**5.2.1 CHEMOTHERAPY DOSE AND DOSE MODIFICATIONS**

Chemotherapy is given as per SmPC protocol with 4 cycles of trastuzumab/taxane combination prior to surgery, followed by 4 cycles of anthracycline with cyclophosphamide, e.g. EC. These regimens are widely used and described on the South East London Cancer Network guidelines as outlined below. Dose modification should follow these or local guidelines:

(www.selcn.nhs.uk/content/load_document.asp?document_id=7877)

It is permitted to use docetaxel (100mg/m²) with trastuzumab followed by AC (doxorubicin 60mg/m² and cyclophosphamide 600mg/m²) or EC (epirubicin 90mg/m², cyclophosphamide 600mg/m²) as per local preference. Definitive surgery must occur between 3-6 weeks post cycle 4 of docetaxel/trastuzumab. Adjuvant anthracycline chemotherapy should be commenced at least 3 weeks after the last cycle of trastuzumab and once the patient is deemed to have recovered clinically post-op, pending review by treating physician and satisfactory LVEF assessment by echo/MUGA. Radiotherapy may be administered as indicated and per local guidelines after chemotherapy has been completed.

5.3 Trastuzumab/Herceptin dose and dose modifications

Trastuzumab should be given in accordance to local and national guidelines with appropriate LVEF monitoring, for example as per the South East London Cancer Network guidelines which have been adopted by Guy's and St. Thomas' Hospital, summarised below:

(www.selcn.nhs.uk/content/load_document.asp?document_id=8377)

Loading dose is given on Day 1 of the first day of cycle 1 at 8mg/kg as per normal practice with docetaxel administered on day 2. Following this first loading dose, 4 subsequent cycles will be administered at a dose of 6mg/kg concomitantly with docetaxel. Cardiac monitoring with an initial echo or MUGA (depending on local protocol), and a repeat echo or MUGA after 3 cycles of trastuzumab will be carried out as per normal protocol. After 4 cycles, trastuzumab will be stopped whilst the patient is undergoing definitive surgery, followed by adjuvant treatment with anthracycline and cyclophosphamide for 4 cycles. Following anthracycline treatment, a repeat echo or MUGA (depending on local protocol) will be

CONFIDENTIAL

required prior to re-loading with trastuzumab at 8mg/kg, followed by 13 cycles of trastuzumab will be administered, at maintenance dose (6mg/kg) with cardiac monitoring as per standard protocol.

5.4 Concomitant Medication and Treatment

Concomitant medication may be given as medically indicated. Details (including doses, frequency, route and start and stop dates) of the concomitant medication given must be recorded in the patient's medical records and the electronic Case Report Form (eCRF).

6 PHARMACEUTICAL INFORMATION**6.1 [¹⁸F]-fluorothymidine****6.1.1 SUPPLY OF [¹⁸F]-FLUOROTHYIMIDINE**

A conditional Qualified Person (QP) certificate including a 'use within' period must be provided for each batch of IMP, immediately following each synthesis, and prior to administration to the patient. A final QP certification must be provided for each batch of IMP once all of the data is available, and has been reviewed by the QP, following administration to the patient.

The PET Clinician will order the [¹⁸F]-fluorothymidine for each patient and the laboratory manager for the Radiochemistry facility will order the required precursor and any chemicals related to its production. The study drug [¹⁸F]-fluorothymidine will be supplied by:

**The PET Imaging Centre
St. Thomas' Hospital
London
SE1 7EH
UK**

MIA(IMP) No. 11387

Tel: 020-7188-4988
Fax: 020-7620-0790

The PET Imaging Centre, where the GMP manufacture of the tracer takes place, is a controlled area only accessible by authorised personnel, who are required to follow strict protocols (PET Imaging Centre SOPs) to minimise microbial contamination entering the facility and radioactive contamination being tracked outside.

6.1.2 FORMULATION OF [¹⁸F]-FLT

[¹⁸F]-FLT is prepared individually for each patient immediately prior to use. It is supplied as a sterile, pyrogen free and essentially particle free, intravenous solution for injection, containing [¹⁸F]-FLT. The final [¹⁸F]FLT drug product is supplied in a simple 10% ethanol solution, which is the eluent from the final column at the end of the drug substance manufacture. Due to the nature of the product no further formulation development has been undertaken. The final vial will contain a minimum of 500MBq with a volume of 1-10ml

CONFIDENTIAL**6.1.3 [¹⁸F]-FLT STORAGE AND LABELLING**

The [¹⁸F]-FLT must be used within a maximum of 3 hours after the end of synthesis. The actual expiry date and time for each individual batch of IMP will be dependent upon the radioactivity of each batch measured at the end of synthesis. The vials of IMP must be stored and transported within a lead pot or other suitable shielded container, in the absence of light. The IMP should be maintained at ambient temperature.

The vials of IMP and the lead pot container will be labelled according to Eudralex volume 4: Annex 13 'Investigational Medicinal Products' of the EU guide to GMP.

6.2 [¹⁸F]-fluorodeoxyglucose ([¹⁸F]-FDG)

The study drug [¹⁸F]-FDG will be MetaTrace FDG Solution for injection.

Marketing authorisation number: PL 27150/001
Marketing authorisation holder: Siemens PLC
Siemens House
Oldbury
Bracknell
Berkshire
RG12 8FZ
United Kingdom

The PET Clinician will order the MetaTrace FDG Solution for injection for each patient. Multidose vials will be labeled for clinical trial use and a separate stock maintained for the purpose of this trial. Storage, administration and disposal will be in accordance with the SmPC.

6.3 [¹⁸F]-FLT and [¹⁸F]-FDG tracer Administration

Aseptic technique must be employed when preparing the drug for administration. Both tracers are radioactive and must be handled to ensure the safety of the operators and patients. This will be achieved by adhering to the local rules and Ionising Radiation (Medical Exposure) Regulations (IRMER) requirements which define practice, and the IRR99 regulations which cover radiation doses to staff.

Metatrace FDG is delivered in multidose vials and tracer withdrawal will be performed under aseptic conditions in accordance with the SmPC. Each vial of [¹⁸F]-fluorothymidine is intended for single use only, and any unused portion of the product should be discarded.

The intravenous administration of allocated radiotracer will take place in the radionuclear imaging lab within the PET Imaging Centre. The radioactivity concentration of the tracer will be measured immediately prior to use. The exact volume of tracer drug product that will be administered to each patient will be dependent on the tracer concentration.

FDG tracer administration will be in accordance with the SmPC and patients will receive a maximum radioactivity dose of 200 MBq (-10%) [¹⁸F]-FDG

For FLT the clinical dose will contain a maximum of 50 µg of [¹⁸F]-FLT, and radioactivity concentration. The volume will be adjusted to account for the radioactive concentration of the product at the time of administration. Patients will receive a maximum radioactivity dose of 200 MBq (-10%) [¹⁸F]-FLT, equating to a maximum chemical dose of less than 50 µg [¹⁸F]-FLT.

CONFIDENTIAL

Before administration, the exact administered activity must be checked and documented by two independent operators within the PET Centre. Operators will be adequately trained and can be imaging technologists, radiologists or doctors. The IMP administration documentation must be available for the verification by representatives of the sponsor or regulatory authorities.

- Patients must fast starting 6 hours prior to tracer administration (Time = T_0), until after their scan (Time = T_{0+1}). Patients may drink water throughout this period of approximately 5 hours of fasting.
- Patients will be administered a single *i.v.* dose of [^{18}F]-FLT or [^{18}F]-FDG over a period of approximately 10 seconds. The tracer will be injected through a cannula with the patient lying in a supine position on the imaging couch. A three-way tap is used so that the cannula can be flushed with saline to check patency, prior to the tracer administration using one port. The tracer is then administered through a second port and the cannula again flushed with saline to ensure there is no tracer residue within the cannula. The administration site will be evaluated pre- and post-administration for any localised reaction.

6.4 IMP Accountability

Accurate records relating to the order for the IMP, dispensing of the IMP, and administration (including the exact date and time the IMP was administered) to the patient must be maintained. These records must be available for inspection at any time by representative of the sponsor or regulatory authorities. The IMPs employed for the imaging study are to be used in accordance with this protocol and under the supervision of the Investigators. Any discrepancies between the number of vials dispensed and the volumes administered to patients must be accounted for in the Radio-pharmacy records.

Unused [^{18}F]-FLT IMP manufactured at site or MetaTrace FDG will be destroyed by an authorised person following the local destruction policy for radiopharmaceuticals and the MetaTrace FDG SmPC. Returned IMP will not be retained for verification by the CRA due to the associated hazards of handling radiopharmaceuticals. Full documentation of all processed will be maintained for verification.

7 INVESTIGATIONS SCHEDULE

Please also refer to the tabulated Schedule of Assessments in Section 7.5.

In cases where a patient has investigations at a different hospital, for example a blood sample, then it is the Investigator's responsibility to ensure he/she receives and reviews the results. The results must be recorded in the eCRF and the reports from the other hospitals must be available for source data verification. Laboratory reference ranges, including effective dates, and evidence of laboratory accreditation must be obtained from all laboratories used. Details of all evaluations/ investigations, including relevant dates, required by the protocol must be recorded in the medical records.

7.1 Baseline- Pre Imaging Evaluations

The following must be performed/obtained prior to randomisation:

- Written informed consent (see Section 7.1.1 "Obtaining Written Informed

CONFIDENTIAL

Consent")

- Demographic details
- Medical History (including diagnosis, current signs and symptoms at time of consent)
- Histological confirmation of ER negative and HER2 positive breast cancer >2cm in diameter
- Concomitant diseases,
- Concomitant medication, treatment plan and Treatment History
- Physical Examination
- ECOG performance status
- Negative pregnancy test
- Echo/MUGA confirming adequate cardiac function with baseline left ventricular ejection fraction(LVEF) of >55%

After completion of these screening assessments, if the patient is eligible for the trial, the patient must then be registered

7.1.1 OBTAINING WRITTEN INFORMED CONSENT

- Written informed consent must be obtained from the patient before any protocol-specific procedures are carried out and within 28 days before administration of the IMP, [¹⁸F]-FLT or [¹⁸F]-FDG.
- The patient will be approached by their treating Oncologist/Clinician for an initial discussion of the study. If the patient is interested in participating, they will be given the patient information sheet to read. If the patient then decides to participate, they will be referred to the PET Imaging Centre where any further questions with regard to the radiation aspects of the trial will be discussed by the Clinical PET Specialists and any other aspects of the trial prior to their PET imaging. The patient will be able to withdraw consent at this time if they wish. The final signature will be obtained at least 24 hours after the initial discussion by the oncologist or the PET physician.
- Patients will be approached in order to obtain consent for extra biopsy material to be collected specifically for research prior to commencement of their standard chemotherapy and during therapy after cycle 1 as described in the protocol. Patients will be asked to give consent to the biobanking of any biological material which is excess to the requirements of this study for use in future research, subject to the approval of the research by a research ethics committee.

Only the Chief Investigator (CI) and those Sub-Investigator(s) delegated responsibility by the CI, and who have signed the 'Delegation of Duties & Authorised Signatures Form are permitted to obtain informed consent from patients and to sign the consent form. All signatures must be obtained before the occurrence of any medical intervention required by the protocol and at the same time.

The CI or the Sub-Investigators must inform the patient about the background to, and present knowledge of the normal management of their disease and the IMPs, and must also ensure that the patient is aware:

- Of the absence of known toxicity of the IMPs and the possibility of experiencing side-effects.
- The study is assessing the FLT and FDG IMP because it is not currently known if PET-CT imaging using these tracers offers an improvement on the use of standard imaging assessment of response.

CONFIDENTIAL

- The PET-CT scans performed for the study following start of chemotherapy will not be used by her oncologist/clinician to determine further treatment
- That she may refuse to participate either before, or at any time during the trial, without penalty or loss of benefits, to which he is otherwise entitled.
- Of whom to contact for answers to pertinent questions about the research and their rights, and also who to contact in the event of a research-related injury.
- A copy of the consent form and patient information sheet must be given to the patient to keep, and the original consent form and patient information sheet, must be filed in the Investigator Site File.

7.2. Evaluations During the Study**7.2.1 PRECHEMOTHERAPY STUDY IMAGING AND BIOPSY (D-10 TO D1)**

Randomisation to FLT or FDG tracer will take place after obtaining informed consent. All study specific pre-chemotherapy procedures will be completed within 10 days of randomisation. Day 1 of the study will be defined as the first study specific imaging procedure; this may be up to and including 10 days prior to first chemotherapy administration. Biopsy will take place following all pre-chemotherapy study imaging.

7.2.1.1 PET imaging

Baseline PET scans using the allocated tracer will be performed following completion of screening assessments prior to the first cycle of chemotherapy/trastuzumab.

FLT PET Group

Patients will fast prior to the PET scan for 6 hours. An intravenous injection of 200MBq (-10%) [¹⁸F]-fluorothymidine will be administered (Time = T₀) and imaged in accordance with section 3.3.2 and section 6.

Participant will receive a telephone call from one of the investigators on the day following completion of all baseline FLT PET scans to collect information to evaluate AEs experienced.

FDG PET Group

Patients will fast for 6 hours prior to their PET scan. An intravenous injection of 200 MBq (-10%) [¹⁸F]-fluorodeoxyglucose will be administered (Time = T₀) and imaged in accordance with section 3.3.1. Follow-up telephone call is not required due to the absence of side effects as described in the SmPC

7.2.1.2 Biopsy & research bloods

Histopathological material should be available for the purposes of this study from the routinely collected biopsy material and, in all patients, blocks from the original diagnostic core will be requested for baseline assessment of study biomarkers.

In all patients an ultrasound guided core biopsy will be collected using a 16 or 14 gauge needle specifically for research prior to commencement of their standard chemotherapy. This will be scheduled at the time of marker clip insertion where possible. This biopsy may be taken at any time between 24 hours after PET imaging and commencement of chemotherapy. Research bloods will be taken at the same time as the pre-research biopsy bloods and processed as outlined in section 3.4 for evaluation for circulating tumour cells.

All biopsy material and material from research bloods will be stored for the purposes of the study in the HTA licensed Guys' and St Thomas' Breast Tissue and Data Bank. Patients

CONFIDENTIAL

will be asked to give consent to the biobanking of any biological material which is excess to the requirements of this study for use in future research, subject to the approval of the research by a research ethics committee. Analyses will be performed in accordance with 3.4.

7.2.2 STUDY EVALUATIONS AFTER CYCLE 1 CHEMOTHERAPY/TRASTUZUMAB (DAY 17±3)

Participants will receive all pre-chemotherapy investigations, prescription and administration of their first cycle of chemotherapy/trastuzumab in accordance with SmPC guidelines and local protocols on the chemotherapy day unit, as outlined in section 5.2 and 5.3. The date of their first cycle will be recorded.

7.2.2.1 PET imaging

A post chemotherapy PET scan will be performed on day 17+/-3 after first chemotherapy. The tracer used will be according to allocated group

FLT PET Group

Patients will fast for 6 hours before the PET scan. An intravenous injection of 200 MBq (-10%) [¹⁸F]-fluorothymidine will be administered (Time = T₀) and imaged in accordance with section 3.3.2 and section 6.

Participants randomised to FLT group will receive a telephone call from one of the investigators on the day following completion of the day 17+/-3 scan to collect information to evaluate AEs or concomitant medications continuing from, or experienced since, Day 1.

FDG PET Group

Patients will fast for 6 hours prior to their PET scan. An intravenous injection of 200 MBq (-10%) [¹⁸F]-fluorodeoxyglucose will be administered (Time = T₀) and imaged in accordance with section 3.3.1. Follow-up telephone call is not required due to the absence of side effects as described in the SmPC

7.2.2.2 Biopsy& research bloods

All participants will have a pre-biopsy blood sample for analysis of haemoglobin, INR, white blood count (WBC) with differential count and platelets. The research blood test for evaluation of CTCs will be carried out at this point, and will be processed as described in section 3.4.

Unless technically impossible or laboratory results outside acceptable guidelines tumour biopsy will be performed under imaging guidance prior to commencing chemotherapy and following completion of day 17±3 study imaging (prior to the second cycle of treatment). This will be scheduled at a minimum of 24 hours following PET study imaging and will comprise one core to be formalin fixed and paraffin embedded and one core to be fresh frozen. Where possible this will be scheduled on the same day as other routine hospital appointments. All biopsy material and blood samples will be stored for the purposes of the study in the HTA licensed Guys' and St Thomas' Breast Tissue and Data Bank. Patients will be asked to give consent to the biobanking of any biological material which is excess to the requirements of this study for use in future research, subject to the approval of the research by a research ethics committee.

7.3 Cycle 2 to end of study

CONFIDENTIAL

Patients will complete their neoadjuvant chemotherapy (cycles 2-4) according to Guys and St Thomas' Breast Unit protocols or local protocols, and the SmPC. Dates of each cycle and the administered cytotoxic will be documented on the eCRF.

Response monitoring, including clinical assessment, magnetic resonance imaging tumour response measurements (RECIST and ADC) will be performed at any point after the third cycle of neoadjuvant chemotherapy according to standard practice.

7.3.1 DEFINITIVE SURGERY

Patients will proceed to definitive surgery according to usual practice at 3 to 6 weeks after their final chemotherapy. At definitive surgery, research cores will be taken through the resected surgical specimen for FFPE and fresh frozen processing. Although lymph node tissue will not be routinely required, we reserve the right to request access to this tissue at a later date. All biopsy material to be stored for the purposes of the study in the HTA licensed Guys' and St Thomas' Breast Tissue and Data Bank. Pathological evaluation of chemotherapy response on the resection specimen will incorporate residual cancer burden (RCB) assessment of the primary tumour and lymph nodes.

7.4 Post Study Follow-up

End of study is defined as day of post-surgery oncology clinic visit prior to commencing adjuvant anthracycline based chemotherapy.

All patients should have assessment of cardiac function by echo or MUGA depending on local protocol, at least 3 weeks after the last cycle of docetaxel/trastuzumab, prior to recommencing anthracyclines. All ongoing follow-up and any further treatment will be in accordance with Guys and St Thomas Breast Unit or local hospital protocols under the supervision of the clinical team.

CONFIDENTIAL

Schedule of Events

TIME in relations to scheduled breast cancer therapy	Baseline	pre therapy	Cycle 1		Cycle 2	Cycle 3		Cycle 4	Post therapy	Surgery	Post surgical follow up
	d-10 to d1		d1	d17 ±3	d1	d1	D17 ±3	D1		within 21 days final cycle	At least 3 weeks after cycle 4 chemo
Pregnancy test (where indicated)	X										
Consent	X										
Demographics	X										
Medical History	X										
Height	X										
Weight	X										
Physical Examination	X										
FBC	X			X							
Clotting	X			X							
Biochemistry	X										
Research bloods for CTC	X			X							
Echo/MUGA	X						X				X
FDG PET		X		X							
FLT PET		X		X							
Research Core Biopsy		X		X							
Chemotherapy & trastuzumab #			X		X	X		X			
Standard MRI#†	X						X				
Core biopsy through resected surgical specimen										X	

#neoadjuvant chemotherapy, and all associated monitoring including MRI at baseline, post cycle 3 and prior to definitive surgery will be supervised by the treating oncologist and performed in accordance with departmental protocols in all patients. DW sequences are incorporated as part of standard MRI acquisition sequences.

†PET and MRI imaging may be scheduled on the same day. If MRI is taking place after the PET scan this may be a minimum of 4 hours after completion of the PET imaging. MRI may be scheduled at any point after the third cycle of treatment, prior to surgery, as per local protocol.

∞ Telephone call for AE recording will take place 24 hours following FLT PET imaging

CONFIDENTIAL**8 ASSESSMENT OF SAFETY****8.1 Adverse Event Definitions****8.1.1 ADVERSE EVENT**

The Medicines for Human Use (Clinical Trials) Regulations 2004 and Amended Regulations (2006) gives the following definitions:

Adverse Event (AE): Any untoward medical occurrence in a subject to whom a medicinal product has been administered including occurrences which are not necessarily caused by or related to that product.

Adverse Reaction (AR): Any untoward and unintended response in a subject to an investigational medicinal product which is related to any dose administered to that subject.

Unexpected Adverse Reaction (UAR): An adverse reaction the nature and severity of which is not consistent with the information about the medicinal product in question set out in:

The summary of product characteristics (SmPC) for [¹⁸F]-FDG .

The Investigator's Brochure (IB) for [¹⁸F]-FLT

8.1.2 SERIOUS ADVERSE EVENTS (SAEs)**Serious adverse Event (SAE), Serious Adverse Reaction (SAR) or Unexpected**

Serious Adverse Reaction (USAR): Any adverse event, adverse reaction or unexpected adverse reaction, respectively, that

- Results in death;
- Is life-threatening;
- Required hospitalisation or prolongation of existing hospitalisation;
- Results in persistent or significant disability or incapacity;
- Consists of a congenital anomaly or birth defect.

8.2 REPORTING RESPONSIBILITIES

Guy's & St Thomas NHS Foundation Trust and King's College London as sponsor has delegated the delivery of the Sponsor's responsibility for Pharmacovigilance (as defined in Regulation 5 of the Medicines for Human Use (Clinical Trials) Regulations 2004 to the King's Health Partners Clinical Trials Office (KHPCTO).

All SAEs, SARs and SUSARs (excepting those specified in this protocol as not requiring reporting) will be reported immediately by the Chief Investigator to the (KHPCTO) in accordance with the current Pharmacovigilance Policy.

Death as a result of disease progression and other events that are primary or secondary outcome measures are not considered to be SAEs and should be reported in the normal way, on the appropriate CRF.

The KHPCTO will report SUSARs (Suspected Unexpected Serious Adverse

CONFIDENTIAL

Reactions) and other SARs to the regulatory authorities (MHRA, competent authorities of other EEA (European Economic Area) states in which the trial is taking place.

The Chief Investigator will report to the relevant ethics committees. Reporting timelines are as follows:

- SUSARs which are fatal or life-threatening must be reported not later than 7 days after the sponsor is first aware of the reaction. Any additional relevant information must be reported within a further 8 days.
- SUSARs that are not fatal or life-threatening must be reported within 15 days of the sponsor first becoming aware of the reaction.

The Chief Investigator and KHPCTO (on behalf of the co-sponsors), will submit a Development Safety Update Report (DSUR) relating to this trial IMP, to the MHRA and REC annually.

8.2.1 EVENTS EXEMPT FROM BEING REPORTED AS SAEs TO KHPCTO

Events specified in this section do not require reporting as SAEs in this trial.

SAE or SAR related to chemotherapy or targeted treatment - Any AE or SAR deemed related to chemotherapy or Trastuzumab as per the Guys and St Thomas Breast Unit Protocols or local Hospital Breast Unit Protocols, and the relevant SmPC does not require reporting.

Elective admissions – Elective admissions to hospital for procedures which were planned and documented in the medical records at the time of consent (e.g. planned surgical procedure chemotherapy administration) are not SAEs, and do not require SAE reporting.

8.3 Recording of adverse events and serious adverse events in eCRFs

AEs, including SAEs, must be recorded in the eCRF for that patient.

Patients who have received either IMP [¹⁸F]-FLT will have specific telephone assessment of AEs at 24 hours post scan. The IMP [¹⁸F]-FDG is the standard diagnostic radiotracer used in PET imaging and undesirable effects following its administration have not been observed to date. Therefore routine 24 hour telephone assessment following FDG PET imaging is not mandated by the study protocol.

All concomitant medications including herbal medications and supplements must be recorded. Any therapy used to treat the event must be recorded. The eCRF will be reconciled with the Safety Database during and at the end of the trial. Therefore it should be ensured the data entered on the SAE report and the data entered into the eCRF are consistent. The DDO Medical Advisor and the Investigator(s) will regularly review the safety data from both the Safety Database and the clinical database.

8.4 Follow-up of adverse events

Follow up will continue until all the necessary safety data for the event has been gathered and until the drug-related AE or SAE has either resolved, returned to baseline or stabilised (section 7.4).

Requested follow-up information should be reported to the KHPCTO in a timely manner and as soon as possible after receipt of the follow up request. For fatal or life-

CONFIDENTIAL

threatening cases, follow-up information should be reported to the KHPCTO as soon as possible.

8.5 Ethics and Regulatory approval

The trial will be conducted in compliance with the principles of the Declaration of Helsinki (1996), the principles of GCP and in accordance with all applicable regulatory requirements including but not limited to the Research Governance Framework and the Medicines for Human Use (Clinical Trial) Regulations 2004, as amended in 2006 and any subsequent amendments.

This protocol and related documents will be submitted for review to the Research Ethics Committee (REC), and to the Medicines and Healthcare products Regulatory Agency (MHRA) for Clinical Trial Authorisation

Subsequent protocol amendments will be submitted to the REC and Regulatory Authorities for approval. Annual progress and safety reports and a final report at conclusion of the trial will be submitted to the KHPCTO (on behalf of the Sponsors), the REC and the MHRA within the timelines defined in the Regulations

8.6 Pregnancy

The Investigator must make every effort to try and ensure that a clinical trial patient is not pregnant. This should be done as part of the consent process by explaining clearly to the patient the potential dangers of radiation if the patient is pregnant.

CONFIDENTIAL**9 ASSESSMENT OF IMAGING TECHNIQUES****9.1 Timing and Type of Imaging Assessments**

The timings of the dynamic sequence may require modification to achieve the highest possible quality study imaging data. This would not affect the overall radiation dose. The venous sampling times may also be modified but the total number of samples will not be changed.

9.1.1 BASELINE EVALUATIONS

A mammogram and MRI must be performed prior to entry into the study. Patients must have an identified HER2 positive ER negative breast cancer confirmed on biopsy. Patients must also have adequate assessment of cardiac function as described in eligibility criteria. If additional conventional imaging is available i.e. MRI or CT scans, this will be utilised for identification of the abnormal site.

9.1.2 INTERPRETATION OF IMAGING DATA

Images from the first patient will be analysed unblinded to the MRI or mammogram scan to assess whether the scanning equipment specifications and scanning methodology are effective, and to adapt them to ensure quality imaging data. The purpose is also to resolve any practical and logistical issues with the events schedule for future patients, such as patient discomfort or adjusting the timing of study assessments.

All PET CT scans will be analysed using SUV and a variety of image processing methods to analyse the dynamic data and the blood sampling. Example proforma scoring sheets are shown in Appendix 3.

Following scoring of all study scans, the results will be compared with the standard MRI cross-sectional imaging, biopsy and definitive surgical histology to assess whether the [¹⁸F]-fluorothymidine agrees with tumour proliferation index and clinical response.

The scans will be read and scored by two of the three reviewers Dr SF Barrington, Dr MJ O'Doherty, Dr V Warbey individually and by consensus. The dynamic data will be analysed by Physicists working with Dr P Marsden. The reporters will not know the histology or outcome measurements performed.

Patients who have not completed the imaging schedule will be replaced on the trial and their scans will not be included in the imaging analysis.

CONFIDENTIAL**10 PATIENT WITHDRAWAL BEFORE COMPLETION OF STUDY SCHEDULE**

The Investigator must make every reasonable effort to keep each patient on study for the whole duration of the trial (i.e. until a maximum of 7 days post IMP administration). However, if the Investigator removes a patient from the study, or if the patient declines further participation, final off-study assessments must be performed. This may be on the day the decision is made to withdraw, or should be as soon as possible thereafter. All the results of the evaluations and observations, together with a description of the reasons for study withdrawal, must be recorded in the medical records and eCRF.

Patients who are removed from the study due to AEs (clinical or laboratory) will be treated and followed according to accepted medical practice. All pertinent information concerning the outcome of such treatment must be recorded in the eCRF and SAE form where necessary.

The following are justifiable reasons for the Investigator to withdraw a patient from study:

1. Withdrawal of consent by patient
2. Withdrawal by the Investigator for clinical reasons not related to the IMPs [¹⁸F]-fluorothymidine
3. SAE preventing completion of imaging schedule
4. Unacceptable toxicity from IMPs [¹⁸F]-fluorothymidine
5. Serious violation of the study protocol (including persistent patient attendance failure and persistent non-compliance)

11 DEFINING THE END OF STUDY

The 'end of trial' is defined as the last visit of the last patient participating in the trial and is defined as the date of post-surgical follow up. Therefore, this will either be completion of the last patient's Off-Study visit after surgery if no IMP-related AEs have been seen, or until any IMP-related AE monthly follow-up visits have been completed.

It is the responsibility of the KHPCTO to inform the MHRA and the investigator to inform the Main REC within 90 days of the 'end of the trial' that the trial has closed.

In cases of early termination of the trial (e.g. due to a clear difference between the two agents at the interim analysis), the KHPCTO will notify the MHRA and the investigator will notify the Main REC within 15 days of the decision and a detailed, written explanation for the termination/halt will be given.

The entire trial will be stopped when:

1. The stated number of patients to be recruited is reached.
2. The stated objectives of the trial are achieved.

Regardless of the reason for termination, all data available for the patient at the time of discontinuation of follow-up must be recorded in the eCRF.

In terminating the trial, the Investigators must ensure that adequate consideration is given to the protection of the patient's interest.

CONFIDENTIAL**12 DATA ANALYSIS AND STATISTICAL CONSIDERATIONS****12.1 Randomisation**

Consenting patients who meet the study eligibility criteria will be randomised to one of the 2 PET tracer groups. Treatment allocation will be stratified for tumour nodal involvement (yes/no) and performed centrally via the electronic data capture system.

12.2 Sample size

The primary objective of the study (Parts A and B) is to correlate SUV change for each tracer with RCB. If this correlation is high (85% or higher) in this exploratory study then SUV change will be considered a good guide to the RCB. If the correlation is 60% or less then it would not be considered reliable. This would require a total of 30 patients randomised, 15 to each tracer, using an alpha of 10%, one sided and a power of 80%. Additional patients will be recruited if fully evaluable scans are not available for each patient.

The final analysis will be conducted after one of the following conditions is met:

1. The trial is terminated early (e.g. due to toxicity).
2. All patients have had the opportunity to complete the experimental and standard of care imaging schedule, definitive surgery and have completed their Off-Study visit.

Once one of the conditions is met, a data cut-off date will be established. All patient visits occurring on or before this date will be analysed and summarised in the final study report. Any data collected after this date will be summarised in a supplemental report.

12.3 Interim Assessment

An interim assessment will be performed to ensure that the data acquisition is optimal for the patients taking part in the study. This will be performed after the first patient willing to have dynamic imaging and blood sampling and conventional dynamic imaging without blood sampling. This will be reviewed by the imaging specialists and the CI.

12.3 Presentation of Data

Statistical analysis: This is an exploratory study. Therefore the statistical analysis will be predominantly descriptive in nature. The primary objective will be assessed using Pearson's correlation coefficient assuming normality of the change in SUV and % change in the sum of the longest dimensions of the tumour using MRI. If not, then Spearman's rank correlation will be considered. All evaluable patients will be analysed.

Secondary endpoints will be analysed using the relevant descriptive summary statistics, e.g. proportions with 95% confidence intervals or means with standard deviations and presented in tabular and graphical formats. As this is an exploratory study with a small sample size, no formal comparisons will be made between tracers for these endpoints.

Data will be presented in a descriptive fashion. Variables will be analysed to determine whether the criteria for the trial conduct are met. This will include a description of

CONFIDENTIAL

patients who did not meet all the eligibility criteria, an assessment of protocol violations, IMP accountability and other data that impact on the general conduct of the trial.

Baseline characteristics will be summarised for all enrolled patients. Patients who died or withdrew before treatment started or did not complete the required safety observations will be described and evaluated separately.

IMP administration and extent of completion of the imaging schedule will be described.

12.5 Toxicity

Patients who have received either IMP [¹⁸F]-fluorothymidine or [¹⁸F]-fluorodeoxyglucose will be assessed for toxicity by assessment of AEs. Basic safety variables will be summarised by descriptive statistics. All AEs including laboratory variables will be assessed for severity using the NCI CTCAE (Version 4.0).

13 ADMINISTRATION

13.1 Completion of the eCRF

An eCRF will be used to collect the data. The Investigator is responsible for ensuring the accuracy, completeness, clarity and timeliness of the data reported in the eCRFs.

Only the Investigator and those personnel who have signed the 'Delegation of Duties & Authorised Signatures Form and have been authorised by the Investigator should enter or change data in the eCRFs. Authorised users will be included on a Master User List in order to be provided access to the eCRF. All protocol required investigations must be reported in the eCRF. The Investigators must retain all original reports, traces and images from these investigations for future reference.

Data will be entered directly into electronic screens by authorised site personnel. Amendments to eCRF data will be made directly to the system and the system audit trail will retain details of the original value(s), who made the change, a date and time and a reason for the change.

Once an eCRF has been entered by the site personnel, the data is cleaned using manual and automated checks. Queries will be issued to the site electronically. Authorised personnel must answer the queries by making relevant amendments to data or providing a response. Answered queries will be closed or reissued as appropriate.

Once the patient is off study and the eCRF has been fully completed, the Investigator must provide an electronic signature to authorise the complete subject casebook.

At the end of the study all eCRFs are retained and archived and a PDF copy will be archived at site.

13.2 Quality Assurance

Monitoring of this trial to ensure compliance with Good Clinical Practice and scientific integrity will be managed by the King's Health Partners Clinical Trials Office Quality

CONFIDENTIAL

Team.

Investigator (s) and the institution (s) will permit trial-related monitoring, audits, REC review, and regulatory inspections (where appropriate) by providing the sponsor's representative direct access to source data and other documents (i.e. patients' case sheets, blood test reports, x-ray reports, histology reports etc).

13.3 Data Handling

The Chief Investigator will act as custodian for the trial data. The following guidelines will be strictly adhered to:

Patient data will be anonymised.

All anonymised data will be stored on a password protected computer.

All trial data will be stored and archived in line with the Medicines for Human Use (Clinical Trials) Amended Regulations 2006 as defined in the King's Health Partners Clinical Trials Office Archiving SOP.

13.4 Clinical Study Report

At appropriate intervals, interim data listings will be prepared to give the Chief Investigator the possibility to review the data and check the completeness of information collected. All clinical data will be presented at the end of the trial on final data listings. The report will be submitted by the Chief Investigator to the MHRA, REC and Sponsor.

13.5 Indemnity

This trial is being carried out under the auspices of Guy's and St Thomas' NHS Foundation Trust and University College London NHS Trust. Therefore injury to a patient caused by the compound under study will be covered by the NHS liability scheme. The NHS Trusts will provide patients with compensation for adverse side effects, in accordance with the principles set out in the Association of the British Pharmaceutical Industry (ABPI) guidelines on compensation for medicine-induced injury.

13.6 Publication Policy and Press Releases

The data from this study will be presented at conferences or research meetings and published in peer reviewed journals.

13.7 Finance

Funding for this trial has been provided by a grant awarded by the European Union FP7 entitled 'HER imaging and molecular interaction mapping in breast cancer (IMAGINT)' and through funding provided by the King's College London Comprehensive Cancer Imaging Centre.

CONFIDENTIAL

14 REFERENCES

Agool A, Schot BW, Jager PL, Vellenga E. 18F-FLT PET in hematologic disorders. *J Nucl Med* 2006; 47(10):1592-98.

Bading J, Shields A. Imaging of Cell Proliferation: status and prospects. *J. Nucl. Med* 2008; 49, Suppl 2. 64S – 80S.

Backes, H., R. Ullrich, et al. Noninvasive quantification of 18F-FLT human brain PET for the assessment of tumour proliferation in patients with high-grade glioma. European Journal of Nuclear Medicine and Molecular Imaging, Springer Berlin / Heidelberg. 2009 **36**: 1960-1967.

Baselga J, Bradbury I, Eidtmann H, Di Cosimo S, Aura C, De Azambuja E, Gomez H, Dinh P, Fauria K, Van Dooren V, Paoletti P, Goldhirsch A, Chang T-W, Lang I, Untch M, Gelber RD, Piccart-Gebhart M. Lapatinib with trastuzumab for HER2-positive early breast cancer (NeoALLTO): a randomised, open-label, multicentre, phase 3 trial. *Lancet* 2012 Jan 16.

Baselga J, Swain SM. CLEOPATRA: a phase III evaluation of pertuzumab and trastuzumab for HER2-positive metastatic breast cancer. *Clin Breast Cancer*. 2010 Dec 1;10(6):489-91

Basu S, Chen W, Tchou J, Mavi A, Cermik T, Czerniecki B, Schnall M, Alavi A. Comparison of triple-negative and estrogen receptor-positive/progesterone receptor-positive/HER2-negative breast carcinoma using quantitative fluorine-18 fluorodeoxyglucose/positron emission tomography imaging parameters: a potentially useful method for disease characterization. *Cancer*. 2008 Mar 1;112(5):995-1000.

Basu S, Mavi A, Cermik T, Houseni M, Alavi A. Implications of standardized uptake value measurements of the primary lesions in proven cases of breast carcinoma with different degree of disease burden at diagnosis: does 2-deoxy-2-[F-18]fluoro-D-glucose-positron emission tomography predict tumor biology? *Mol Imaging Biol*. 2008 Jan-Feb;10(1):62-6.

Basu S, Nair N, Thorat M, Shet T. Uptake characteristics of FDG in multiple juvenile cellular fibroadenomata of the breast: FDG-PET and histopathologic correlation. *Clin Nucl Med*. 2007 Mar;32(3):203-4.

Been LB, Elsinga P H. Positron emission tomography in patients with breast cancer using (18)F-3'-deoxy-3'-fluoro-l-thymidine ((18)F-FLT)-a pilot study. *Eur J Surg Oncol* 2006; 32(1): 39-43.

Been LB, Suurmeijer AJH, Elsinga PH, Jager PL, Ginkel RJV, Hoekstra HJ. 18F-fluorodeoxythymidine PET for evaluation the response to hyperthermic isolated limb perfusion for locally advanced soft-tissue sarcomas. *J Nucl Med* 2007; 48: 367-372.

Benz MR, J. Czernin, et al. "3'-deoxy-3'-[18F]fluorothymidine positron emission tomography for response assessment in soft tissue sarcoma." Cancer: 2012 Jun 15;118(12):3135-44.

CONFIDENTIAL

Benz, M. R., K. Herrmann, et al. "18F-FDG PET/CT for Monitoring Treatment Responses to the Epidermal Growth Factor Receptor Inhibitor Erlotinib." Journal of Nuclear Medicine; 2011 52(11): 1684-1689.

Boerner AR, Weckesser M, Herzog H, et al. Optimal scan time for fluorine-18 fluorodeoxyglucose positron emission tomography in breast cancer. *Eur J Nucl Med*. 1999; 26(3): 226-30.

Buchmann I, Neumaier Bernd, Schreckenberger M, Reske S. [18F] 3'-Deoxy-3'-fluorothymidine-PET in NHL Patients: whole-body biodistribution and imaging of lymphoma manifestations- a pilot study. *Cancer Biother Radiopharm* 2004; 19:436-442.

Buck AK, Schirrmeister H, Mattfeldt T, Reske SN. Biological characterisation of breast cancer by means of PET. *Eur J Nucl Med Mol Imaging*. 2004;31 Suppl 1:S80-7.

Buck AK, Bommer M, Stilgenbauer S, et al. Molecular Imaging of Proliferation in Malignant Lymphoma. *Cancer Res* 2006; 66:(22)11055-11061.

Buck AK, Schirrmeister H, Hetzel M, et al. 3-Deox-3-[18F] Fluorothymidine-Positron Emission Tomography for noninvasive assessment of proliferation in pulmonary nodules. *Cancer Research* 2002; 62:3331-3334.

Buck AK, Halter G, Schirrmeister H, et al. Imaging Proliferation in Lung Tumors with PET: 18F-FLT Versus 18F-FDG. *J Nucl Med* 2003; 44:1426-1431.

Buck AK and Hetzel M. Clinical relevance of imaging proliferative activity in lung nodules. *Eur J Nucl Med Mol Imaging* 2005; 32(5):525-33.

Buck AK, Hermann K, Buschenfelde CMZ, et al. Imaging bone and soft tissue tumors with the proliferation marker [18F] fluorodeoxythymidine. *Clin Cancer Res* 2008; 14(10): 2970 - 2977.

Buck AK, Bommer M, Juweid ME, et al. First Demonstration of leukemia imaging with the proliferation marker 18F-fluorothymidine. *J Nucl Med* 2008; 49(11): 1756 - 1762.

Buzdar, A. U., Ibrahim, N. K., Francis, D., Booser, D. J., Thomas, E. S., Theriault, R. L., Pusztai, L., Green, M. C., Arun, B. K., Giordano, S. H., Cristofanilli, M., Frye, D. K., Smith, T. L., Hunt, K. K., Singletary, S. E., Sahin, A. A., Ewer, M. S., Buchholz, T. A., Berry, D., Hortobagyi, G. N. Significantly higher pathologic complete remission rate after neoadjuvant therapy with trastuzumab, paclitaxel, and epirubicin chemotherapy: results of a randomized trial in human epidermal growth factor receptor 2-positive operable breast cancer. *J Clin Oncol* 2005; 23(16) 3676-85

Cardoso F, Piccart MJ, Durbecq V, Di Leo A. Resistance to trastuzumab: a necessary evil or a temporary challenge? *Clinical breast cancer*. 2002 Oct;3(4):247-57; discussion 58-9

Chambers AF, Groom AC, MacDonald IC. Dissemination and growth of cancer cells in metastatic sites. *Nat Rev Cancer*. 2002 Aug;2(8):563-72

Channing MA, Huang BX, Eckelman WC. Analysis of residual solvents in 2-[18F]FDG by GC. *Nuclear Medicine and Biology* 2001; 28: 469-471.

CONFIDENTIAL

Cheebsumon, P., F. H. P. van Velden, et al. "Effects of Image Characteristics on Performance of Tumor Delineation Methods: A Test-Retest Assessment." Journal of Nuclear Medicine; 2011 **52**(10): 1550-1558.

Chen W, Cloughesy T, et al. Imaging proliferation in brain tumors with 18F-FLT PET: comparison with 18F-FDG. *J Nucl Med* 2005; 46(6): 945-52.

Chen W, Delaloye S, Silverman DHS, et al. Predicting treatment response of malignant gliomas to bevacizumab and irinotecan by imaging proliferation with [18F] Fluorothymidine positron emission tomography. *J Clin Onc* 2007; 25(3): 4714 – 4721.

Choi SJ, Kim JS. [18F]3'-deoxy-3'-fluorothymidine PET for the diagnosis and grading of brain tumors. *Eur J Nucl Med Mol Imaging* 2005; 32(6): 653-9.

Cobben DCP, Elsinga PH, Suurmeijer AJH, et al. Detection and Grading of Soft Tissue Sarcomas of the Extremities with 18F-3'-Fluoro-3'-Deoxy-L-Thymidine. *Clinical Cancer Research* 2004; 10:1685-1690.

Cobben DCP, Jager PL, Elsinga PH, Maas B, Suurmeijer AJH, Hoekstra HJ. 3'-18F-Fluoro-3'-Deoxy-L-Thymidine. A new tracer for staging metastatic melanoma? *J Nucl Med* 2003; 44:1927-1932.

Cobben DCP, van der Laan BFAM, Maas B, et al. 18F-FLT PET for Visualization of Laryngeal Cancer: Comparison with 18F-FDG PET. *J Nucl Med* 2004; 45:226-231.

Contractor, K. B., L. Kenny, et al. Biological basis of [11C]choline-positron emission tomography in patients with breast cancer: comparison with [18F]fluorothymidine positron emission tomography. Nuc Med Commun; 2011 **32**(11): 997-1004.

Contractor, K. B., L. Kenny, et al. [18F]-3'-deoxy-3'-Fluorothymidine Positron Emission Tomography and Breast Cancer Response to Docetaxel. Clinical Cancer Research; 2011 published online doi:10.1158/1078-0432.CCR-11-0783.

Coudert, B. P., Largillier, R., Arnould, L., Chollet, P., Campone, M., Coeffic, D., Priou, F., Gligorov, J., Martin, X., Trillet-Lenoir, V., Weber, B., Bleuse, J. P., Vasseur, B., Serin, D., Namer, M. Multicenter phase II trial of neoadjuvant therapy with trastuzumab, docetaxel, and carboplatin for human epidermal growth factor receptor-2-overexpressing stage II or III breast cancer: results of the GETN(A)-1 trial. *J Clin Oncol* 2007 25(19): 2678-84

Cristofanilli M, Budd GT, Ellis MJ, et al.(2004) Circulating tumor cells, disease progression, and survival in metastatic breast cancer. *N Engl J Med* 351:781–791.

de Langen AJ, Klabbers B, Lubberink M, et al. Reproducibility of Quantitative 18F-3'-deoxy-3'-Fluorothymidine measurements using positron emission tomography. *Eur J Nucl Med Mol Imaging*. 2009; 36(3): 389 - 395.

Dittmann H, Dohmen BM, Kehlbach R, Bartusek G, Pritzkow M, Sarbia M, Bares R. Early changes in [(18)F]FLT uptake after chemotherapy: an experimental study. *Eur J Nucl Med Mol Imaging* 2002; 29(11):1462- 1469.

Dittmann H, Dohmen BM, Paulsen F, et al. [18F]FLT PET for diagnosis and staging of thoracic tumours. *European Journal of Nuclear Medicine Molecular Imaging* 2003; 30:1407 - 1412.

CONFIDENTIAL

Dreisbach RH and Robertson WO. Handbook of poisoning: prevention, diagnosis and treatment; 12th ed. p 171-4, Appleton and Lange Publ., Los Altos (CA), 1987.

Eckel, F., K. Herrmann, et al. Imaging of Proliferation in Hepatocellular Carcinoma with the In Vivo Marker 18F-Fluorothymidine
10.2967/jnumed.109.065896. Journal of Nuclear Medicine; 2009 **50**(9): 1441-1447.

Everitt, S., R. J. Hicks, et al. Imaging Cellular Proliferation During Chemo-Radiotherapy: A Pilot Study of Serial 18F-FLT Positron Emission Tomography/Computed Tomography Imaging for Non-Small-Cell Lung Cancer. International journal of radiation oncology, biology, physics; 2009 **75**(4): 1098-1104.

Faraj A, Fowler DA, Bridges EG, Sommadossi JP. Effects of 2',3'-dideoxynucleosides on proliferation and differentiation of human pluripotent progenitors in liquid culture and their effects on mitochondrial DNA synthesis. Antimicrobial Agent Chemother 1994; 38(5): 924-930.

FDA Guidance for Industry ICH Q3C—Tables and List (November 2003 Revision 1)

Flexner C, van der Horst C, Jacobson MA. Relationship between plasma concentrations of 3'-deoxy-3'-fluorothymidine (Alovudine) and antiretroviral activity in two concentration-controlled trails. J Infec Dis 1994; 170:1394-1403.

Francis DL, Freeman A, Visvikis D, et al. In vivo imaging of cellular proliferation in colorectal cancer using positron emission tomography. Gut 2003; 52: 1602-1606.

Francis DL, Visvikis D, Costa DC, et al. Potential impact of [18F]3'-deoxy-3'-fluorothymidine versus [18F]fluoro-2-deoxy-D-glucose in positron emission tomography for colorectal cancer. Eur J Nucl Med Mol Imag 2003; 30:988 - 994.

Fredriksson S, Dixon W, Ji H, Koong AC, Mindrinos M, Davis RW. Multiplexed protein detection by proximity ligation for cancer biomarker validation. Nature methods. 2007 Apr;4(4):327-9

Gaborit N, Larbouret C, Vallaghe J, Peyrusson F, Bascoul-Mollevi C, Crapez E, Azria D, Charde T, Poul M, Mathis G, Bazin H, Pelegrin A. Time-Resolved Fluorescence Energy Transfer (TR-FRET) to analyze the disruption of EGFR/HER2 dimers. Journal of Biological Chemistry Vol 286 NO 13, pp 11337-11345, Apr 1 2011

Galldiks, N., L. W. Kracht, et al. (2010). "Patient-tailored, imaging-guided, long-term temozolamide chemotherapy in patients with glioblastoma." Mol Imaging **9**(1): 40-60.

Ghosh R, Narasanna A, Wang S, Liu S, Chakrabarty A, Balko J, Gonzalez-Angulo A, Mills G, Penuel E, Winslow J, Sperinde J, Dua R, Pidaparathi S, Mukherjee A, Leitzel K, Kostler W, Lipton A, Bates M, Arteaga C. Trastuzumab has preferential activity against breast cancers driven by HER2 homodimers. Cancer Research; 71:1871-1882. Feb 15, 2011

Gianni L, Pienkowski T, Im YH, Roman L, et al. Efficacy and safety of neoadjuvant pertuzumab and trastuzumab in women with locally advanced, inflammatory, or early HER2-positive breast cancer (NeoSphere): a randomised multicentre, open-label, phase 2 trial. Lancet Oncol 2012 Jan; 13(1):25-32.

CONFIDENTIAL

Gianni, L., Eiermann, W., Semiglazov, V., Manikhas, A., Lluch, A., Tjulandin, S., Zambetti, M., Vazquez, F., Byakhov, M., Lichinitser, M., Climent, M. A., Ciruelos, E., Ojeda, B., Mansutti, M., Bozhok, A., Baronio, R., Feyereislova, A., Barton, C., Valagussa, P., Baselga, J. Neoadjuvant chemotherapy with trastuzumab followed by adjuvant trastuzumab versus neoadjuvant chemotherapy alone, in patients with HER2-positive locally advanced breast cancer (the NOAH trial): a randomised controlled superiority trial with a parallel HER2-negative cohort. *Lancet* 2010; 375 (9712): 377-84

Grierson JR and Shields AF. Radiosynthesis of 3'-deoxy-3'-[(18)F]fluorothymidine: [(18)F]FLT for imaging of cellular proliferation in vivo. *Nucl Med Biol* 2000; 27(2):143-56.

Halter G, Buck AK, Schirrmester H, et al. [18F] 3-deoxy-3'-fluorothymidine positron emission tomography: alternative or diagnostic adjunct to 2-[18f]-fluoro-2-deoxy--glucose positron emission tomography in the workup of suspicious central focal lesions? *J Thoracic and Cardiovasc Surg* 2004; 127 (4):1093-1099.

Han, D., J. Yu, et al. Comparison of 18F-Fluorothymidine and 18F-Fluorodeoxyglucose PET/CT in Delineating Gross Tumor Volume by Optimal Threshold in Patients With Squamous Cell Carcinoma of Thoracic Esophagus. *International journal of radiation oncology, biology, physics*; 2010 **76**(4): 1235-1241.

Hatakeyama T, Kawai N, Nishiyama Y, Yamamoto Y, Sasakawa Y, Ichikawa T, Tamiya T. 11C-methionine (MET) and 18F-Fluorothymidine (FLT) PET in patients with newly diagnosed glioma. *Eur J Nucl Med Mol Imaging* 2008; 35(11): 2009 - 2017.

Henderson, I. C. Berry, D. A., Demetri, G. D., Cirincione, C. T., Goldstein, L. J., Martino, S., Ingle, J. N., Cooper, M. R., Hayes, D. F., Tkaczuk, K. H., Fleming, G., Holland, J. F., Duggan, D. B., Carpenter, J. T., Frei, E., 3rd, Schilsky, R. L., Wood, W. C., Muss, H. B., Norton, L. Improved outcomes from adding sequential Paclitaxel but not from escalating Doxorubicin dose in an adjuvant chemotherapy regimen for patients with node-positive primary breast cancer. *J Clin Oncol.* 2003; 21(6): 976-83

Herrmann, K., A. K. Buck, et al. Predictive Value of Initial 18F-FLT Uptake in Patients with Aggressive Non-Hodgkin Lymphoma Receiving R-CHOP Treatment 10.2967/jnumed.110.084566." *Journal of Nuclear Medicine*; 2011 **52**(5): 690-696.

Herrmann, K., A. K. Buck, et al. A Pilot Study to Evaluate 3'-Deoxy-3'-18F-Fluorothymidine PET for Initial and Early Response Imaging in Mantle Cell Lymphoma. *Journal of Nuclear Medicine*; 2011 **52**(12): 1898-1902.

Herrmann, K., M. Erkan, et al. Comparison of 3'-deoxy-3'-[18F]fluorothymidine positron emission tomography (FLT PET) and FDG PET/CT for the detection and characterization of pancreatic tumours. *European Journal of Nuclear Medicine and Molecular Imaging*; 2012 Springer Berlin / Heidelberg: 1-6.

Herrmann K, Ott K, Buck AK, Lordick F, Wilhelm D, Souvatzoglou M, Becker K, Schuster T, Wester HJ, Siewert JR, Schwaiger M, Krause BJ. Imaging Gastric Cancer with PET and Radiotracers [18F]-FLT and [18F]-FDG. *J Nucl Med* 2007; 48:1945-1950.

Herrmann K, Wieder HA, Buck AK, et al. Early Response Assessment using 3'-Deoxy-3'-[18F] Fluorothymidine Positron Emission Tomography in high-grade Non-Hodgkin's lymphoma. *Clin Cancer Res* 2007; 13(12): 3552 - 3554.

CONFIDENTIAL

Herrmann K, Eckel F, Schmidt S, et al. In vivo characterization of proliferation for discriminating cancer from pancreatic pseudotumours. *J Nucl Med* 2008; 49:1437-1444.

Heys, S. D., Hutcheon, A. W., Sarkar, T. K., Ogston, K. N., Miller, I. D., Payne, S., Smith, I., Walker, L. G., Eremin, O. Neoadjuvant docetaxel in breast cancer: 3-year survival results from the Aberdeen trial. *Clin Breast Cancer*; 2002, 3 Suppl 2. S69-74

Holbro, T., et al., The ErbB2/ErbB3 heterodimer functions as an oncogenic unit: ErbB2 requires ErbB3 to drive breast tumor cell proliferation. *Proceedings of the National Academy of Sciences of the United States of America*, 2003. **100**(15): p. 8933-8938.

Hong, I. K., J. H. Kim, et al. Diagnostic usefulness of 3-deoxy-3-[¹⁸F]fluorothymidine positron emission tomography in recurrent brain tumour. *J Comput Assist Tomogr*; 2011 **35**(6): 679-84.

Hoshikawa, H., Y. Nishiyama, et al. Comparison of FLT-PET and FDG-PET for Visualization of Head and Neck Squamous Cell Cancers. *Molecular Imaging and Biology*, Springer New York. 2011 **13**: 172-177.

Jacobs AH and Thomas A. 18F-fluoro-L-thymidine and 11C-methylmethionine as markers of increased transport and proliferation in brain tumors. *J Nucl Med* 2005; 46(12):1948-1958.

Joensuu, H., Kellokumpu-Lehtinen, P. L., Bono, P., Alanko, T., Kataja, V., Asola, R., Utriainen, T., Kokko, R., Hemminki, A., Tarkkanen, M., Turpeenniemi-Hujanen, T., Jyrkkio, S., Flander, M., Helle, L., Ingalsuo, S., Johansson, K., Jaaskelainen, A. S., Pajunen, M., Rauhala, M., Kaleva-Kerola, J., Salminen, T., Leinonen, M., Elomaa, I., Isola, J. Adjuvant docetaxel or vinorelbine with or without trastuzumab for breast cancer. *New England Journal of Medicine*, 2006. **354**(8): p. 809-820.

Jung AL, Roan Y, Temple AR. Neonatal death associated with acute transplacental ethanol intoxication, *Am J Dis Child* 1980; 134: 419-20.

Kahraman, D., M. Scheffler, et al. Quantitative Analysis of Response to Treatment with Erlotinib in Advanced Non-Small Cell Lung Cancer Using 18F-FDG and 3'-Deoxy-3'-18F-Fluorothymidine PET 10.2967/jnumed.111.094458. *Journal of Nuclear Medicine*; 2011 **52**(12): 1871-1877.

Kameyama R, Yamamoto Y, Izuishi K, Takebayashi R, Masanobu H, Makiko M, Masato K, Haba R, Nishiyama Y. Detection of gastric cancer using 18F-FLT PET: comparison with 18F-FDG PET. *Eur J Nucl Med Mol Imaging* 2009; 36: 382-388.

Kameyama R, Yamamoto Y, et al "Correlation of 18F-FLT uptake with equilibrative nucleoside transporter-1 and thymidine kinase-1 expressions in gastrointestinal cancer." *Nucl Med Commun* 2011 32(6): 460-465.

Katlama Ch, Ghosn J, Tubiana R, et al. MIV-310 reduces HIV viral load in patients failing multiple antiretroviral therapy: results from a 4-week phase II study. *AIDS* 2004; 18:1299-1304.

Kasper B, Egerer G, Gronkowski M, et al.. Functional diagnosis of residual lymphomas after radiochemotherapy with positron emission tomography comparing FDG- and FLT PET. *Leukemia & Lymphoma*, 2007:48(4):746-753.

CONFIDENTIAL

Kelleher, M., F. Festy, T. Ng, C.E. Gillett, and P.A. Ellis. Breast cancer patient profiling using optical proteomics: novel applications to individualise prognosis and treatment. 2006 In San Antonio Breast Cancer Conference, San Antonio, Texas.

Kelleher, M., E. Shamil, F. Festy, K. Lawler, A. Coolen, G. Patel, G. Weitsman, G. Fruhwirth, L. Huang, P.R. Barber, B. Vojnovic, N. Woodman, C.E. Gillett, S. Pinder, E. Ofo, L. Fernandes, F. Fraternali, M. Beutler, S.M. Ameer-Beg, L. Holmberg, J. Condeelis, P.A. Ellis, and T. Ng. Imaging of the ezrin/protein kinase C/cofilin pathways yields a metastatic signature in breast cancer. 2012 to be submitted to PLOS medicine.

Kelleher, M.T., G. Fruhwirth, G. Patel, E. Ofo, F. Festy, P.R. Barber, S.M. Ameer-Beg, B. Vojnovic, C. Gillett, A. Coolen, G. Keri, P.A. Ellis, and T. Ng. The potential of optical proteomic technologies to individualize prognosis and guide rational treatment for cancer patients. *Target Oncol.* 2009 4:235 - 252.

Kenny LM and Vigushin DM. Quantification of cellular proliferation in tumor and normal tissues of patients with breast cancer by [18F]fluorothymidine-positron emission tomography imaging: evaluation of analytical methods. *Cancer Res* 2005; 65(21):10104-10112.

Kenny L, Coombes Ch, Vigushin DM, Sami Shousha AA, Aboagye EO. Imaging early changes in proliferation at 1 week post chemotherapy: a pilot study in breast cancer patients with 3'-deoxy-3'-[18F]Fluorothymidine positron emission tomography. *Eur J Nucl Med Mol Imaging* 2007; 34:1339-1347.

Koh Y, Keam B, Im S et al. Results of a 18F-FDG PET/CT after first cycle of neoadjuvant chemotherapy reflect tumour characteristics in breast cancer: possible value of SUV changes during chemotherapy in prediction of tumour biology and character. *Ann Oncol* 2008; 19 (Suppl 8):viii 63

Kong XB, Zhu QY, Vidal PM. Comparisons of anti-human immunodeficiency virus activities, cellular transport, and plasma intracellular pharmacokinetics of 3'-fluoro-3'-deoxythymidine and 3'-azido-3'-deoxythymidine. *Antimicrob Agents Chemo* 1992; 36(4):808-18.

Kupiecki FP and Coon MJ. Methylmalonic semialdehyde. *Biochem. Prep* 1960; 7: 69-71.

Langen P and Graetz H. Cell death resulting from inhibition by 3'-deoxy-3'-fluorothymidine, cytosine-arabinozide, 5-fluoro-2'-deoxyuridine, and hydroxyurea of DNA synthesis in cultured Ehrlich ascites carcinoma cells. *Studia Biophys* 1972; 31/32:359-366.

Langen P, Etzold G, Hintsche R, Kowollik G: 3'-Deoxy-3'-fluorothymidine, a new selective inhibitor of DNA synthesis. *Acta Biol Med Germ* 1969; 23:759-766.

Langen P, Kowollik G, Etzold G, Venner H, Reinhert H. The phosphorylation of 3'-deoxy-3'-fluorothymidine and its incorporation into DNA in a cell free system from tumor cells. *Acta Biol Med Germ* 1972; 29: 483-494.

Lee-Hoeflich S, Crocker L, Yao E, Pham T, Munroe X, Hoeflich K, Sliwkowski M, Stern H. A central role for HER3 in HER2-amplified breast cancer: implications for targeted therapy. *Cancer Research.* Jul 15, 2008 68(14):5878-87.

CONFIDENTIAL

Liu, G., R. Jeraj, et al. Pharmacodynamic Study Using FLT PET/CT in Patients with Renal Cell Cancer and Other Solid Malignancies Treated with Sunitinib Malate. *Clinical Cancer Research*; 2011 **17**(24): 7634-7644.

Liu MC, Shields PG, Warren RD, et al. Circulating tumor cells: A useful predictor of treatment efficacy in metastatic breast cancer. *J Clin Oncol* ; 2009 **27**:5153–5159.

Loo CE, Straver ME, Rodenhuis S, et al. Magnetic resonance imaging response monitoring of breast cancer during neoadjuvant chemotherapy: relevance of breast cancer subtype. *J Clin Oncol*. 2011 Feb 20;**29**(6):660-666

Lu L, Samuelsson L, Bergstrom M, Sato K, Fasth KJ, Langstrom B. Rat studies comparing ¹¹C-FMAU, ¹⁸F-FLT, and ⁷⁶Br-BFU as proliferation markers. *J Nucl Med* 2002; **43**(12):1688- 1698.

Lundgren B, Bottiger D, Ljungdahl-Stahle. Antiviral effects of 3'-fluorothymidine and 3'-azidothymidine in Cynomolgus monkeys infected with simian immunodeficiency virus. *J Acq Immunodef Synd* 1991; **4**(5): 489-498.

Mankoff DA, Shields AF, Graham MM et al. Kinetic analysis of 2-[¹¹C]thymidine PET imaging studies: compartmental model and mathematical analysis. *J Nucl Med* 1998; **39**: 1043-1055.

Matthes E, Lehmann Ch, Scholz D, Rosenthal HA and Langen P. Phosphorylation, anti-HIV activity and cytotoxicity of 3'-fluorothymidine. *Biochem Biophys Res Comm* 1998; **153**(2):825-831.

Matthes E, Lehmann Ch, Scholz D, et al. Inhibition of HIV-associated reverse transcriptase by sugar modified derivatives of thymidine 5'-triphosphate in comparison to cellular DNA polymerases. *Biochem Biophys Res Comm* 1987; **148**(1):78-85.

Mavi A, Cermik TF, Urhan M, Puskulcu H, Basu S, Yu JQ, Zhuang H, Czerniecki B, Alavi A. The effects of estrogen, progesterone, and C-erbB-2 receptor states on ¹⁸F-FDG uptake of primary breast cancer lesions. *J Nucl Med*. 2007; **48**(8):1266-72

Menda, Y., L. L. Boles Ponto, et al. Kinetic Analysis of 3'-Deoxy-3'-¹⁸F-Fluorothymidine (¹⁸F-FLT) in Head and Neck Cancer Patients Before and Early After Initiation of Chemoradiation Therapy. *Journal of Nuclear Medicine*; 2009 **50**(7): 1028-1035.

Menda Y, L. L. Boles Ponto, et al. Investigation of the pharmacokinetics of 3'-deoxy-3'-[¹⁸F]fluorothymidine uptake in the bone marrow before and early after initiation of chemoradiation therapy in head and neck cancer." *Nuclear medicine and biology* 2010 **37**(4): 433-438.

Mileshkin, L., R. J. Hicks, et al. Changes in ¹⁸F-Fluorodeoxyglucose and ¹⁸F-Fluorodeoxythymidine Positron Emission Tomography Imaging in Patients with Non-Small Cell Lung Cancer Treated with Erlotinib. *Clinical Cancer Research*; 2011 **17**(10): 3304-3315.

Mock BH, Winkle W, Vavrek MT. Technical Note: A Color Spot Test for the Detection of Kryptofix® [2.2.2] in [¹⁸F]FDG Preparations. *Nucl Med Biol* 1997; **24**:193-195.

CONFIDENTIAL

Muzi M, Vesselle H. Kinetic analysis of 3'-deoxy-3'-fluorothymidine PET studies: validation studies in patients with lung cancer. *J Nucl Med* 2005; 46(2):274-282.

Muzi M, Spence AM, O'Sullivan F, et al. Kinetic Analysis of 3' – Deoxy-3' – 18F-Fluorothymidine in patients with gliomas. *J Nucl Med* 2006; 47(10): 1612-21.

Oshida M, Uno K, Suzuki M, Nagashima T, Hashimoto H, Yagata H, Shishikura T, Imazeki K, Nakajima N. Predicting the prognoses of breast carcinoma patients with positron emission tomography using 2-deoxy-2-fluoro[18F]-D-glucose. *Cancer*. 1998 Jun 1;82(11):2227-34.

Ott, K., K. Herrmann, et al. Molecular Imaging of Proliferation and Glucose Utilization: Utility for Monitoring Response and Prognosis after Neoadjuvant Therapy in Locally Advanced Gastric Cancer. *Annals of Surgical Oncology*, Springer New York. 2011 **18**: 3316-3323.

Patel, G.S., T. Kiuchi, K. Lawler, E. Ofo, E. Shamil, M.T. Kelleher, G. Fruhwirth, R. Zhang, P. Selvin, M. Keppler, G. Santis, J. Spicer, N. Woodman, C. Gillett, A. Coolen, P.R. Barber, B. Vojnovic, G. Keri, V. Goh, M.J. O'Doherty, A. Tutt, P.A. Ellis, and T. Ng. 2010. The challenges of integrating molecular imaging into the optimization of cancer therapy. *Integrative Biology*: 2011 ; 6:603-31

Pfannenbergl, C., P. Aschoff, et al. "PET/CT with 18F-FLT: Does It Improve the Therapeutic Management of Metastatic Germ Cell Tumors?" *Journal of Nuclear Medicine*; 2010 **51**(6): 845-853.

Piccart-Gebhart, M.J., et al., Trastuzumab after adjuvant chemotherapy in HER2-positive breast cancer. *New England Journal of Medicine*, 2005. **353**(16): p. 1659-1672.

Pio BS, Park CK, Pietras R et al. Usefulness of 3'-[F-18]fluoro-3'-deoxythymidine with positron emission tomography in predicting breast cancer response to therapy. *Mol Imaging Biol* 2006; 8:36 - 42.

Price SJ, Fryer TD, Cleij MC, et al. Imaging regional variation of cellular proliferation in gliomas using 30-deoxy-30-[18F]fluorothymidine positron-emission tomography: an image-guided biopsy study. *Clinical Radiology* 2009; 64:52-63.

Quon A, Chang ST, Chin F, et al. Initial evaluation of [18F]-Fluorothymidine (FLT) PET/CT scanning for primary pancreatic cancer. *Eur J Nucl Med Mol Imaging* 2008; 35:527-531.

Rack B, Schindlbeck C, Andergassen U, et al. Prognostic role of circulating tumor cells in the peripheral blood of primary breast cancer patients. *Cancer Res*; 2010 70(suppl 24):93, abstr S6-5.

Rasey JS, Grierson JR, Wiens LW, Kolb PD, Schwartz JL. Validation of FLT uptake as a measure of thymidine kinase-1 activity in A549 carcinoma cells. *J Nucl Med*. 2002; 43(9):1210-1217.

Richard, S. D., B. Bencherif, et al. Noninvasive assessment of cell proliferation in ovarian cancer using [18F] 3'-deoxy-3'-fluorothymidine positron emission tomography/computed tomography imaging. *Nuclear medicine and biology*; 2011 **38**(4): 485-491.

CONFIDENTIAL

Roel, S., P. Slagmolen, et al. Biological image-guided radiotherapy in rectal cancer: is there a role for FMISO or FLT, next to FDG? *Acta Oncol*; 2008 **47**(7): 1237-1248.

Romond, E.H., et al., Trastuzumab plus adjuvant chemotherapy for operable HER2-positive breast cancer. *New England Journal of Medicine*, 2005. **353**(16): p. 1673-1684.

Saga T, Kawashima H, Araki N, et al. Evaluation of primary brain tumors with FLT-PET usefulness and limitation. *Clin Nucl Med* 31; 2006: 774- 780.

Sarah Roels, Pieter Slagmolen, Johan Nuyts, et al. Biological image-guided radiotherapy in rectal cancer. *Acta Oncologica*, 2008; 47: 1237-1248.

Schiepers, C., W. Chen, et al. 18F-fluorothymidine kinetics of malignant brain tumors. *European Journal of Nuclear Medicine and Molecular Imaging*, Springer Berlin / Heidelberg. 2007 **34**: 1003-1011.

Schiepers, C., M. Dahlbom, et al. Kinetics of 3'-Deoxy-3'-18F-Fluorothymidine During Treatment Monitoring of Recurrent High-Grade Glioma. *Journal of Nuclear Medicine*; 2010 **51**(5): 720-727.

Schubert W. Multiple antigen - mapping microscopy of human tissue. . In: Burger G, Oberholzer M, Vooijs GP, eds. *Adv Analyt Cell Pathol* Amsterdam: Elsevier 1990:97-8

Schubert W, Bonnekoh B, Pommer AJ, Philipsen L, Bockelmann R, Malykh Y, et al. Analyzing proteome topology and function by automated multidimensional fluorescence microscopy. *Nature biotechnology*. 2006 Oct;24(10):1270-8

Schwarz-Dose J, Untch M, Tiling R, Sassen S, Mahner S, Kahlert S, et al. Monitoring primary systemic therapy of large and locally advanced breast cancer by using sequential positron emission tomography imaging with [18F]fluorodeoxyglucose. *J Clin Oncol*. 2009 Feb 1;27(4):535-41

Schwarzenberg, J., J. Czernin, et al. (2012). 3'-Deoxy-3'-18F-Fluorothymidine PET and MRI for Early Survival Predictions in Patients with Recurrent Malignant Glioma Treated with Bevacizumab. *Journal of Nuclear Medicine*; 2012 **53**(1): 29-36.

Shaw G and Warrener RN. Purines, pyrimidines, and glyoxalines. Part VII. New syntheses of 2-thiouracils and 2-thiothymines *J. Chem. Soc*; 153-156, 1958

Shields AF, Grierson JR, Dohmen BM, et al. Imaging proliferation in vivo with [F-18]FLT and positron emission tomography. *Nat Med* 1998; 4(11):1334-1336.

Shields AF and Briston DA. A simplified analysis of [18F]3'-deoxy-3'-fluorothymidine metabolism and retention. *Eur J Nucl Med Mol Imaging* 2005; 32(11):1269-75.

Shields AF, Lawhorn-Crews JM, Briston DA, et al. Analysis and reproducibility of 3'-Deoxy-3'-[18F] Fluorothymidine in patients with non-small cell lung cancer. *Clin Cancer Res* 2008; 14(14): 4463 - 4468.

Smyczek-Gargya B, Fersis N, Dittmann H, et al. PET with [18F]fluorothymidine for imaging of primary breast cancer: a pilot study. *Eur J Nucl Med Mol Imaging* 2004; 31:720-724.

CONFIDENTIAL

Slamon DJ, Leyland-Jones B, Shak S, Fuchs H et al. Use of chemotherapy plus a monoclonal antibody against HER2 for metastatic breast cancer that over expresses HER2. *NEJM* 2001 Mar15;344(11) 783-92

Slamon, D., et al. Phase III randomized trial comparing doxorubicin and cyclophosphamide followed by docetaxel (AC (R) T) with doxorubicin and cyclophosphamide followed by docetaxel and trastuzumab (AC (R) TH) with docetaxel, carboplatin and trastuzumab (TCH) in HER2 positive early breast cancer patients: BCIRG 006 study. *JCO* 2005. San Antonio, TX: Springer. Vol27;5685-5692;FinHER

Sohn H-J, Yang Y-J, Ryu J-S, et al. [18F] Fluorothymidine positron emission tomography before and 7 days after gefitinib treatment predicts response in patients with advanced adenocarcinoma of the lung. *Clin Cancer Res* 2008; 14(22): 7159 - 60.

Sorlie T, Tibshirani R, Parker J, Hastie T, Marron JS, Nobel A, Deng S, Johnsen H, Pesich R, Geisler S, Demeter J, Perou CM, Lønning PE, Brown PO, Børresen-Dale AL, Botstein D. Repeated observation of breast tumor subtypes in independent gene expression data sets. *Proc Natl Acad Sci U S A*. 2003 Jul8;100(14):8418-23.

Spence A, Muzi M, Link J, Hoffman J, Eary J, Krohn K. NCI-Sponsored Trial for the evaluation of safety and preliminary efficacy of FLT as a marker of proliferation in patients with recurrent gliomas: safety studies. *Mol Imaging Biol*; 2008; 10: 271 - 280.

Spence, A., M. Muzi, et al. NCI-Sponsored Trial for the Evaluation of Safety and Preliminary Efficacy of 3-Deoxy-3[F]fluorothymidine (FLT) as a Marker of Proliferation in Patients with Recurrent Gliomas: Preliminary Efficacy Studies. *Molecular Imaging and Biology*, Springer New York. 2009 11: 343-355

Stemke-Hale, K., A.M. Gonzalez-Angulo, A. Lluch, R.M. Neve, W.L. Kuo, M. Davies, M. Carey, Z. Hu, Y. Guan, A. Sahin, W.F. Symmans, L. Pusztai, L.K. Nolden, H. Horlings, K. Berns, M.C. Hung, M.J. van de Vijver, V. Valero, J.W. Gray, R. Bernardis, G.B. Mills, and B.T. Hennessy. 2008. An integrative genomic and proteomic analysis of PIK3CA, PTEN, and AKT mutations in breast cancer. *Cancer research*. 2008 68:6084-6091.

Straver ME, Aukema TS, Olmos RA, Rutgers EJ, Gilhuijs KG, Schot ME, Vogel WV, Peeters MJ. Feasibility of FDG PET/CT to monitor the response of axillary lymph node metastases to neoadjuvant chemotherapy in breast cancer patients. *Eur J Nucl Med Mol Imaging*. 2010 Jun;37(6):1069-76.

Sundseth R, Joyner SS, Moore JT, Dornsife RE, Dev IK. The anti-human immunodeficiency virus agent 3'-fluorothymidine induces DNA damage and apoptosis in human lymphoblastoid cells. *Antimicrob Agents Chemother* 1996; 40(2):331-335.

Tchou J, Sonnad SS, Bergey MR, Basu S, Tomaszewski J, Alavi A, Schnell M. Degree of Tumor FDG Uptake Correlates with Proliferation Index in Triple Negative Breast Cancer. *Mol Imaging Biol*. 2009 Dec 12.

Tian J, Yang X, Yu L, et al. A multicenter clinical trial on diagnostic value of dual-tracer PET/CT in pulmonary lesions using 3'-Deoxy-3'-[18F]-Fluorothymidine and [18F]-FDG. *J Nucl Med* 2008; 49: 186 – 194.

CONFIDENTIAL

Tran A, Pio BS, Khatibi B, Czernin J, Phelps ME, Silverman DH. 18F-FDG PET for staging breast cancer in patients with inner-quadrant versus outer-quadrant tumors: comparison with long-term clinical outcome. *J Nucl Med*. 2005; 46(9):1455-9.

Troost, E. G. C., J. Bussink, et al. 18F-FLT PET/CT for Early Response Monitoring and Dose Escalation in Oropharyngeal Tumors. *Journal of Nuclear Medicine*; 2010 **51**(6): 866-874.

Troost EGC, Vogel WV, Merckx MAW, et al. 18F-FLT PET does not discriminate between reactive and metastatic lymph nodes in primary head and neck cancer patients. *J Nucl Med* 2007; 48(5):726-35.

Troost, E. G. C., J. Bussink, et al. Histopathologic Validation of 3'-Deoxy-3'-18F-Fluorothymidine PET in Squamous Cell Carcinoma of the Oral Cavity. *Journal of Nuclear Medicine*; 2010 **51**(5): 713-719.

Turcotte E, Wiens LW, Grierson JR, Peterson L, Wener MH, Vesselle H. Toxicology evaluation of radiotracer doses of 3'-deoxy-3'-[18F]fluorothymidine (18F-FLT) for human PET imaging: Laboratory analysis of serial blood samples and comparison to previously investigated therapeutic FLT doses. *BMC Nuc Med* 2007; 7: 3 - 9. .

Tzahar, E., et al., A hierarchical network of interreceptor interactions determines signal transduction by neu differentiation factor/neuregulin and epidermal growth factor. *Molecular and Cellular Biology*, 1996. **16**(10): p. 5276-5287.

Van Westreenen HL, Cobben DC. Comparison of 18F-FLT PET and 18F-FDG PET in esophageal cancer. *J Nucl Med* 2005; 46(3): 400- 404.

Ullrich R, Backes H, Li H, Kracht L, et al. Glioma proliferation as assessed by 3'-Fluoro-3'-Deoxy-L-Thymidine positron emission tomography in patients with newly diagnosed high-grade glioma. *Clin Cancer Res* 2008; 14(7): 2049 - 2055.

Untch M, Loibl S, Bischoff J, Eidtmann H et al. Lapatinib versus trastuzumab in combination with neoadjuvant anthracycline-taxane-based chemotherapy (GeparQuinto, GBG 44): a randomised phase 3 trial. [Lancet Oncol](#). 2012 Jan 16

Untch, M., Rezai, M., Loibl, S., Fasching, P. A., Huober, J., Tesch, H., Bauerfeind, I., Hilfrich, J., Eidtmann, H., Gerber, B., Hanusch, C., Kuhn, T., du Bois, A., Blohmer, J. U., Thomssen, C., Dan Costa, S., Jackisch, C., Kaufmann, M., Mehta, K., von Minckwitz, G. Neoadjuvant treatment with trastuzumab in HER2-positive breast cancer: results from the GeparQuattro study. *J Clin Onc* 2010 : 28(12) 2024-31

van Westreenen, H. L., D. C. P. Cobben, et al. Comparison of 18F-FLT PET and 18F-FDG PET in Esophageal Cancer. *J Nucl Med*; 2005 **46**: 400-404.

Vesselle H, Grierson J, Muzi M, et al. In vivo Validation of 3'deoxy-3'-[(18)F]fluorothymidine ([18F]FLT) as a proliferation imaging tracer in humans: Correlation of [18F]FLT uptake by positron emission tomography with Ki-67 immunohistochemistry and flow cytometry in human lung tumors. *Clin Cancer Res* 2002; 11: 3315-33123.

Vesselle H, Grierson J, Peterson LM, Mark Muzi M, Mankoff DA, and Krohn KA. 18F-fluorothymidine radiation dosimetry in human PET imaging studies. *J Nucl Med* 2003; 44:1482-1488.

CONFIDENTIAL

- Visvikis D, Francis D, Mulligan R, et al. Comparison of methodologies for the in vivo assessment of 18FLT utilisation in colorectal cancer. *Eur J Nucl Med Mollmaging* 2004; 31:169 - 178.
- Wagner M, Seitz U, Buck A, et al. 3'-[18F]Fluoro-3'-Deoxythymidine ([18F]-FLT) as positron emission tomography tracer for imaging proliferation in a murine B-Cell lymphoma model and in the human disease. *Cancer Research* 2003; 63: 2681-2687.
- Wardak, M., C. Schiepers, et al. Discriminant Analysis of 18F-Fluorothymidine Kinetic Parameters to Predict Survival in Patients with Recurrent High-Grade Glioma. *Clin Cancer Res*; 2011 **17**: 6553-6562.
- Wieder Hinrich A, Geinitz H, Rosenberg R, et al. PET imaging with [18F] 3'-deoxy-3'-fluorothymidine for prediction of response to neoadjuvant treatment in patients with rectal cancer. *Eur J Nucl Med Mol Imaging* 2007; 34: 878-883.
- Wobus AM. Clastogenic activity of cytosine arabinoside and 3'-deoxy-3'-fluorothymidine in Ehrlich acites tumor cells in vitro. *Mutation Res* 1976; 40:101-106.
- Yap, CS and Czernin J. Evaluation of thoracic tumors with 18F-Fluorothymidine and 18F-Fluorodeoxyglucose-positron emission tomography. *Chest* 2006; 129(2): 393-401.
- Yamamoto, Y., R. Kameyama, et al. Detection of colorectal cancer using 18F-FLT PET: comparison iwth 18F-FDG PET. *Nuc Med Commun*; 2009 **30**(11): 841-5.
- Yamamoto, Y., Y. Nishiyama, et al. Comparison of 18F-FLT PET and 18F-FDG PET for preoperative staging in non-small cell lung cancer. *European Journal of Nuclear Medicine and Molecular Imaging*, Springer Berlin / Heidelberg. 2008 **35**: 236-245.
- Yamamoto Y, Wong TZ, Turkington TG, Hawk TC, Reardon DA, Coleman RE. 3'-Deoxy-3'-[F-18]Fluorothymidine positron emission tomography in patients with recurrent glioblastoma multiforme: comparison with Gd-DTPA enhanced magnetic resonance imaging. *Mol Imaging Biol* 2006; 8:340-47.
- Yamamoto Y, Nishiyama Y, Ishikawa S, et al. Correlation of 18F-FLT and 18F-FDG uptake on PET with Ki-67 immunohistochemistry in non-small cell lung cancer. *Eur J Nucl Med Mol Imaging* 2007; 34:1610-1616.
- Yamamoto Y, Nishiyama Y, Kimura N, et al. Comparison of 18F-FLT PET and 18F-FDG PET for preoperative staging in non-small cell lung cancer. *Eur J Nuc Med Mol Imaging* 2008; 35:236-245.
- Yamamoto Y, Nishiyama Y, Ishikawa S, et al. 3'-Deoxy-3'-18F-Fluorothymidine as a proliferation imaging tracer for diagnosis of lung tumors: comparison with 2-deoxy-2-18F-fluoro-D-glucose. *Comput Assist Tomogr* 2008; 32(3): 432 - 7.
- Yap, C. S., J. Czernin, et al. Evaluation of thoracic tumours with 18F-fluorothymidine and 18F-fluorodeoxyglucose-positron emission tomography. *Chest*; 2006 **129**(2): 393-401.
- Yerushalmi R, Woods R, Ravdin PM, Hayes MM, Gelmon KA. Ki67 in breast cancer: prognostic and predictive potential. *Lancet Oncol*. 2010 Feb;11(2):174-83

CONFIDENTIAL

Yue, J., L. Chen, et al. Measuring Tumor Cell Proliferation with ¹⁸F-FLT PET During Radiotherapy of Esophageal Squamous Cell Carcinoma: A Pilot Clinical Study. *Journal of Nuclear Medicine*; 2010 **51**(4): 528-534.

Yun M, Oh SJ, Ha HJ, Ryu JS, Moon DH. High radiochemical yield synthesis of 3'-deoxy-3'-[¹⁸F]fluorothymidine using (5'-O-dimethoxytrityl-2'-deoxy-3'-O-nosyl-beta-D-threo pentofuranosyl)thymine and its 3-N-BOC-protected analogue as a labeling precursor. *Nucl Med Biol* 2003; 30(2):151-7.

Zander, T., M. Scheffler, et al. Early Prediction of Nonprogression in Advanced Non-Small-Cell Lung Cancer Treated With Erlotinib By Using [¹⁸F]Fluorodeoxyglucose and [¹⁸F]Fluorothymidine Positron Emission Tomography. *Journal of Clinical Oncology*; 2011 **29**(13): 1701-1708.

CONFIDENTIAL

15 APPENDICES

15.1 APPENDIX 1: WHO PERFORMANCE SCALE

Activity Performance Description	Score
Fully active, able to carry out all normal activity without restriction.	0
Restricted in physically strenuous activity but ambulatory and able to carry out work of a light or sedentary nature, e.g. light housework, office work.	1
Ambulatory and capable of all self-care, but unable to carry out any work activities. Up and about more than 50% of waking hours.	2
Capable of only limited self-care. Confined to bed or chair more than 50% of waking hours.	3
Completely disabled. Cannot carry out any self-care. Totally confined to bed or chair.	4

CONFIDENTIAL**15.2 APPENDIX 2: DECLARATION OF HELSINKI**

Recommendations guiding physicians in biomedical research involving human subjects

Adopted by the 18th World Medical Assembly, Helsinki, Finland, June 1964 amended by the 29th World Medical Assembly Tokyo, Japan, October 1975,

and
the 35th World Medical Assembly, Venice, Italy, October 1983

and
the 41st World Medical Assembly, Hong-Kong, September 1989

and
the 48th General Assembly, Somerset West, Republic of South Africa, October 1996

INTRODUCTION

It is the mission of the physician to safeguard the health of the people. His or her knowledge and conscience are dedicated to the fulfilment of this mission.

The Declaration of Geneva of the World Medical Association binds the physician with the words, "The health of my patient will be my first consideration", and the International Code of Medical Ethics declares that, "A physician shall act only in patient's interest when providing medical care which might have the effect of weakening the physical and mental condition of the patient".

The purpose of biomedical research involving human subjects must be to improve diagnostic, therapeutic and prophylactic procedures and the understanding of the aetiology and pathogenesis of disease.

In current medical practice most diagnostic, therapeutic or prophylactic procedures involve hazards. This applies especially to biomedical research.

Medical progress is based on research which ultimately must rest in part on experimentation involving human subjects.

In the field of biomedical research a fundamental distinction must be recognised between medical research in which the aim is essentially diagnostic or therapeutic for a patient, and medical research, the essential object of which is purely scientific and without implying direct diagnostic or therapeutic value to the person subjected to the research.

Special caution must be exercised in the conduct of research which may affect the environment, and the welfare of animals used for research must be respected.

Because it is essential that the results of laboratory experiments be applied to human beings to further scientific knowledge and to help suffering humanity, the World Medical Association has prepared the following recommendations as a guide to every physician in biomedical research involving human subjects. They should be kept under review in the future. It must be stressed that the standards as drafted are only a guide to physicians all over the world. Physicians are not relieved from criminal, civil and ethical responsibilities under the laws of their own countries.

CONFIDENTIAL**I - BASIC PRINCIPLES**

1. Biomedical research involving human subjects must conform to generally accepted scientific principles and should be based on adequately performed laboratory and animal experimentation and on a thorough knowledge of the scientific literature.
2. The design and performance of each experimental procedure involving human subjects should be clearly formulated in an experimental protocol which should be transmitted for consideration, comment and guidance to a specially appointed committee independent of the investigator and the sponsor provided that this independent committee is in conformity with the laws and regulations of the country in which the research experiment is performed.
3. Biomedical research involving human subjects should be conducted only by scientifically qualified persons and under the supervision of a clinically competent medical person. The responsibility for the human subject must always rest with a medically qualified person and never rest on the subject of the research, even though the subject has given his or her consent.
4. Biomedical research involving human subjects cannot legitimately be carried out unless the importance of the objective is in proportion to the inherent risk to the subject.
5. Every biomedical research project involving human subjects should be preceded by careful assessment of predictable risks in comparison with foreseeable benefits to the subject or to others. Concern for the interests of the subject must always prevail over the interests of science and society.
6. The right of the research subject to safeguard his or her integrity must always be respected. Every precaution should be taken to respect the privacy of the subject to minimise the impact of the study on the subject's physical and mental integrity and on the personality of the subject.
7. Physicians should abstain from engaging in research projects involving human subjects unless they are satisfied that the hazards involved are believed to be predictable. Physicians should cease any investigation if the hazards are found to outweigh the potential benefits.
8. In publication of the results of his or her research, the physician is obliged to preserve the accuracy of the results. Reports of experimentation not in accordance with the principles laid down in this Declaration should not be accepted for publication.
9. In any research on human beings, each potential subject must be adequately informed of the aims, methods, anticipated benefits and potential hazards of the study and the discomfort it may entail. He or she should be informed that he or she is at liberty to abstain from participation in the study and that he or she is free to withdraw his or her consent to participation at any time. The physician should then obtain the subject's freely given informed consent, preferably in writing.
10. When obtaining informed consent for the research project the physician should be particularly cautious if the subject is in a dependent relationship to him or her or may

CONFIDENTIAL

consent under duress. In that case the informed consent should be obtained by a physician who is not engaged in the investigation and who is completely independent of this official relationship.

11. In case of legal incompetence, informed consent should be obtained from the legal guardian in accordance with national legislation. Where physical or mental incapacity makes it impossible to obtain informed consent, or when the subject is a minor, permission from the responsible relative replaces that of the subject in accordance with national legislation.

12. The research protocol should always contain a statement of the ethical considerations involved and should indicate that the principles enunciated in the present Declaration are complied with.

**II - MEDICAL RESEARCH COMBINED WITH PROFESSIONAL CARE
(Clinical research)**

1. In the treatment of the sick person, the physician must be free to use a new diagnostic and therapeutic measure, if in his or her judgement it offers hope of saving life, re-establishing health or alleviating suffering.

2. The potential benefits, hazards and discomfort of a new method should be weighed against the advantages of the best current diagnostic and therapeutic methods.

3. In any medical study, every patient - including those of a control group, if any - should be assured of the best proven diagnostic and therapeutic method. This does not exclude the use of inert placebo in studies where no proven diagnostic or therapeutic method exists.

4. The refusal of the patient to participate in a study must never interfere with the physician-patient relationship.

5. If the physician considers it essential not to obtain informed consent, the specific reasons for this proposal should be stated in the experimental protocol for transmission to the independent Committee (1,2).

6. The physician can combine medical research with professional care, the objective being the acquisition of new medical knowledge, only to the extent that medical research is justified by its potential diagnostic or therapeutic value for the patient.

**III - NON-THERAPEUTIC BIOMEDICAL RESEARCH INVOLVING HUMAN SUBJECTS
(Non-clinical biomedical research)**

1. In the purely scientific application of medical research carried out on a human being, it is the duty of the physician to remain the protector of the life and health of that person on whom biomedical research is being carried out.

2. The subjects should be volunteers - either healthy persons or patients for whom the experimental design is not related to the patient's illness.

CONFIDENTIAL

3. The investigator or the investigating team should discontinue the research if in his/her or their judgement it may, if continued, be harmful to the individual.
4. In research on man, the interest of science and society should never take precedence over considerations related to the well-being of the subject.

CONFIDENTIAL

15.3 APPENDIX 3:

EXAMPLE PET REPORTING SCORING SHEETS FOR BREAST CANCER

PET Reporting [¹⁸F]-fluorothymidine

Subject no: / reader initials:

Mark axial slice number where possible

	<i>SUVmax</i>	<i>SUVpeak</i>	<i>SUVmean</i>	<i>Quantitative data</i>	<i>quantitative data</i>
Culprit lesion 1					
Culprit lesion 2					

PET Reporting [¹⁸F]-fluorothymidine Pre chemotherapy

Subject no: / reader initials:

Mark axial slice number where possible

	<i>SUVmax</i>	<i>SUVpeak</i>	<i>SUVmean</i>	<i>quantitative data</i>
Culprit lesion 1				
Culprit lesion 2				

PET Reporting [¹⁸F]-fluorothymidine post chemotherapy

Subject no: / reader initials:

Mark axial slice number where possible

	<i>SUVmax</i>	<i>SUVpeak</i>	<i>SUVmean</i>	<i>quantitative data</i>
Culprit lesion 1				

CONFIDENTIAL

Culprit lesion 2

MR Reporting

Subject no:

/

reader initials:

Mark axial slice number where possible

size

ADC

quantitative data

Culprit lesion 1

Culprit lesion 2
